Effect of deoxyribonuclease-deficiency on myeloid cells under homeostatic and inflammatory conditions

Doctoral thesis

to obtain a doctorate (PhD)

from the Faculty of Medicine

of the University of Bonn

Tatjana Reuter

from Bad Honnef, Germany

2022

Written with authorization of

the Faculty of Medicine of the University of Bonn

First reviewer: Prof. Dr. Eicke Latz

Second reviewer: Prof. Dr. Günter Mayer

Day of oral examination: 08.12.2022

From the Institute of Innate Immunity

Director: Prof. Dr. Dagmar Wachten, Prof. Dr. Eicke Latz, Prof. Dr. Felix Meissner

Table of Contents

List of abbreviations

AA	Amino acid
ACS	Apoptosis-associated speck-like protein containing a CARD
ADP	Adenosine diphosphate
AGS	Aicardi Goutières Syndrome
AIM2	Absent in melanoma 2
ANCA	Antineutrophil cytoplasmic antibodies
ANOVA	Analysis of variance
AP-1	Activator protein 1
APAF-1	Apoptotic peptidase-activating factor 1
ATP	Adenosine triphosphate
BAK	BCL2 antagonist/killer 1
BAL	Bronchoalveolar lavage
BAX	BCL2 associated X, apoptosis regulator
BCL-2	BCL2 apoptosis regulator
BCs	B cells
BID	BH3 interacting domain death agonist
BMDC	Bone marrow-derived dendritic cell
BMDM	Bone marrow-derived macrophage
bp	Base pair
CAD	Caspase-activated DNase
Ccl2	C-C motif chemokine ligand 2
Ccl5	C-C motif chemokine ligand 5
Ccr2	C-C chemokine receptor type 2
cDC	Conventional dendritic cell
cDNA	Complementary DNA
CD11b	Cluster of differentiation molecule 11B
cfDNA	Cell-free deoxyribonucleic acid
cGAMP	cyclic guanosine monophosphate-adenosine monophoshate
cGAS	Cyclic GMP-AMP synthase
CpG	5’-cytosine-phosphate-guanine-3’
CRISPR	Clustered regularly interspaced short palindromic repeats
Cxcl1	C-X-C motif chemokine ligand 1
Cx3cl1	C-X3-C motif chemokine ligand 1

Cx3cr1	C-X3-C motif chemokine receptor 1
DAH	Diffuse alveolar hemorrhage
DCs	Dendritic cells
DISC	Death-inducing signaling complex
DNA	Deoxyribonucleic acid
DNase1	Deoxyribonuclease 1
DNase1l1	Deoxyribonuclease 1 like 1
DNase1l2	Deoxyribonuclease 1 like 2
DNase1l3	Deoxyribonuclease 1 like 3
DOTAP	1,2-Dioleoyl-3-trimethylammonium propane
dsDNA	Double-stranded deoxyribonucleic acid
dsRNA	Double-stranded ribonucleic acid
EDTA	Ethylenediaminetetraacetic acid
ELISA	Enzyme-linked immunosorbent assay
ER	Endoplasmic reticulum
FACS	Fluorescence-activated cell sorting
FADD	Fas associated via death domain
FAS	Fas cell surface death receptor
FBS	Fetal bovine serum
FCL	Familial chilblain lupus
FSC	Forward scatter
F4/80	EGF-like module-containing mucin-like hormone receptor-like 1
gDNA	Genomic deoxyribonucleic acid
GM-CSF	Granulocyte-macrophage colony-stimulating factor
GPI	Glycosylphosphatidylinositol
gRNA	Guide RNA
GSDMD	Gasdermin D
HEK293	Human embryonic kidney 293 cells
HMGB1	High mobility group box protein 1
HSC	Hematopoietic stem cells
ICAD	DNA fragmentation factor subunit alpha
IFI16	Interferon gamma inducible protein 16
IFN	Interferon
Ifnar1	Interferon alpha and beta receptor subunit 1
IgG, IgM	Immunoglobulin G, immunoglobulin M

IL-1β	Interleukin 1β
IMCs	Immature myeloid cells
IMs	Interstitial macrophages
IRF	Interferon regulatory factor 3
KO	Knockout
LL37	Cathelicidin Antimicrobial Peptide
LXR	Liver X receptor
Ly6C	Lymphocyte antigen 6 complex locus C1
Ly6G	Lymphocyte antigen 6 complex locus G6D
MCL-1	Induced myeloid leukemia cell differentiation protein Mcl-1
MCSF	Macrophage colony stimulating factor 1
MDA5	Melanoma differentiation-associated protein 5
MDSCs	Myeloid-derived suppressor cells
MHC class II	Major histocompatibility complex class II
MLKL	Mixed lineage kinase domain like
MOMP	Mitochondrial outer membrane permeabilization
mtDNA	Mitochondrial deoxyribonucleic acid
MYD88	Myeloid differentiation primary response protein 88
NA	Nucleic acid
NET	Neutrophil extracellular trap
NF-κB	Nuclear factor kappa B
NK1.1	Killer cell lectin-like receptor subfamily B member 1C
NLRP3	Nucleotide-binding domain leucine-rich repeat containing family, pyrin domain containing 3
NOS2	Nitric oxide synthase 2
NR4A1	Nuclear receptor subfamily 4 group A member 1
ODN	Oligodeoxynucleotide
Ogg1	Oxoguanisine glycolase 1
OH	Hydroxyl
PBS	Phosphate-buffered saline
PCR	Polymerase chain reaction
pDC	Plasmacytoid dendritic cell
PEI	Polyethylenimine
Pld3/4	Phospholipase D 3/4
PO	Phosphate

PRR	Pattern recognition receptor
RBC	Red blood cell
RIG-I	Retinoic acid inducible gene 1
RIPK1	Receptor-interacting serine-threonine kinase 1
RIPK3	Receptor-interacting serine-threonine kinase 3
RNA	Ribonucleic acid
RNA-seq	Ribonucleic acid sequencing
rRNA	Ribosomal ribonucleic acid
SAVI	Sting-associated vasculopathy with onset in infancy
SD	Standard deviation
SEM	Standard error of the mean
Slc29a3	Solute carrier family 29 member 3
SLE	Systemic lupus erythematosus
SNP	Single-nucleotide polymorphism
SSC	Side scatter
ssDNA	Single-stranded deoxyribonucleic acid
ssRNA	Single-stranded ribonucleic acid
Sting	Stimulator of interferon response cGAMP interactor 1
S100a8	S100 calcium binding protein A 8
Tank	TRAF family member associated NFKB activator
TBK1	Tank-binding kinase 1
TCs	T cells
TFAM	Transcription factor A, mitochondrial
TGF-β	Transforming growth factor beta
TLR	Toll-like receptor
TNF	Tumor necrosis factor
Tnip1	TNFAIP3 interacting protein 1
Trex1	Three prime repair exonuclease 1
TRIF	TIR domain containing adaptor molecule 1
TUNEL	Terminal deoxynucleotidyl transferase dUTP nick end labeling
Unc93b1$^{3d/3d}$	Unc-93 homology B1, TLR signaling regulator; H412R mutation
WBC	White blood cell

1 Introduction

1.1 Innate immune sensors of deoxyribonucleic acid

Nucleic acids (NA) are essential buildings blocks of life yet pose shattering danger to the host (Bartok and Hartmann 2020). Detection of invading foreign genetic material is essential to host defense whereas compartmentalization and availability of self-NA must be stringently regulated to suppress their immunogenicity. Immune sensors that discriminate self- from non-self-NA evolved in various kingdoms of life ranging from bacteria to animals, illustrating the significance of the principle (Cohan et al. 2019, Doron et al. 2018). In animals, such ancient NA-sensing receptors can be classified into two major groups according to their subcellular localization. Cytosolic NA sensors including RIG-I, MDA5 and cGAS, are broadly expressed in nucleated cells enabling theoretically any nucleated cell to sense cell-intrinsic infections (Bartok and Hartmann 2020). RIG-I and MDA5 recognize foreign (ds)RNA structures (Andrejeva et al. 2004, Gitlin et al. 2006, Yoneyama et al. 2004), while cytosolic DNA derived from dsDNA viruses, retroviruses or host-derived self-dsDNA is primarily sensed by cGAS (cyclic GMP-AMP synthase) (Gao et al. 2013a, Li et al. 2013a, Sun et al. 2013, Wu et al. 2013).

cGAS preferentially binds DNA fragments equal to or longer than 36 bp via the ribose-phosphate backbone of dsDNA in a sequence-independent manner with its carboxyl terminus (Li et al. 2013b, Zhang et al. 2014). In addition, dsDNA of more than 200 bp can activate cGAS via U-turn structures organized by proteins including HMGB1 (high mobility group box protein 1) and TFAM (mitochondrial transcription factor A) (Andreeva et al. 2017). Upon ligand binding, cGAS dimerizes and synthesizes the cyclic dinucleotide 2’3’ c[GAMP] (cyclic GMP-AMP) which serves as a second messenger to stimulate STING (stimulator of interferon genes). STING activates TBK1 (TANK-binding kinase 1) which in turn phosphorylates the transcription factor IRF3 (interferon regulatory factor 3) and induces NF-κB (nuclear factor-κB) signaling, leading to an antiviral cellular state via type I interferon (IFN) and proinflammatory cytokine gene transcription (Abe and Barber 2014, Ablasser et al. 2013, Gao et al. 2013 b, Motwani et al. 2019). In addition, STING itself serves as cytosolic immune sensor of bacterial cyclic dinucleotides including 3’3’ c[GAMP], c[di-GMP] and c[di-AMP] (Burdette et al. 2011, Gao et al. 2013 c).

Accumulation of cytosolic DNA also initiates the assembly of DNA-sensing inflammasomes including AIM2 (absent in melanoma 2), AIM2-like receptors like IFI16, as well as NLRP3 secondary to STING-mediated cell lysis and K^+ release (Bartok and Hartmann 2020). AIM2 is the major cytosolic dsDNA sensor promoting inflammasome assembly in mice and can be activated by mitochondrial DNA (mtDNA), nuclear DNA leaking into the cytosol due to nuclear envelop disruption, and self-DNA transferred by extracellular vesicles of endosomal origin (Bartok and Hartmann 2020, Dan et al. 2017, Kalluri and LeBleu 2020, Lugrin and Martinon 2017). Its ligand binding is sequence-independent but relies on size with a minimal fragment length of 80 bp and optimal response to ~ 200 bp (Hornung et al. 2009, Jin et al. 2012, Kumar 2021, Matyszewski et al. 2018, Wang and Yin 2017). Upon DNA recognition, AIM2 inflammasome assembly is initiated including ASC adaptor nucleation that activates caspase-1 to produce mature proinflammatory cytokines (IL-1β and IL18) and induces pyroptosis (Bürckstümmer et al. 2009, Fernandes-Alnemri et al. 2009, Hornung et al. 2009, Lu et al. 2014, Morrone et al. 2015).

Endosomal NA sensors including the Toll-like receptors (TLRs) 3, 7, 8, 9, and 13 are highly expressed in phagocytic immune cells and strategically placed to sense endocytosed NAs and their degradation products in the endolysosomal compartment. TLR3 recognizes ~ 40 bp long dsRNA fragments, whereas TLR7 and TLR8 are activated by short ssRNA and its degradation products (Alexopoulou et al. 2001, Diebold et al. 2004, Judge et al. 2005, Jurk et al. 2002, Leonard et al. 2008, Liu et al. 2008). Although TLR7 and TLR8 share various structural and functional similarities, critical differences have been identified. While TLR7 is widely expressed and functional in humans and mice, the role of murine Tlr8 remains uncertain (Heil et al. 2004). Both receptors bind short di- or trinucleotides, however TLR7 preferentially recognizes guanosine, while TLR8 is activated by uridine (Shibata et al. 2016, Tanji et al. 2015, Zhang et al. 2016a). In contrast, Tlr13 is a murine-specific receptor of bacterial 23S rRNA that is not present in humans (Li and Chen 2012, Oldenburg et al. 2012). Although numerous RNA-sensing TLRs are known, TLR9 is the only endolysosomal DNA sensor and was the first immune NA sensor identified. More than twenty years ago, Hiroaki Hemmi and colleagues identified the mouse *Tlr9* gene and characterized Tlr9 as the receptor for cytosine-phosphate-guanine (CpG)-rich unmethylated DNA motifs (CpG

DNA), which are less frequent in eukaryotic compared to bacterial genomes that have highly conserved stimulatory CpG fragments in 16S and 23S ribosomal DNA sequences (Coch et al. 2009, Hartmann and Krieg 2000, Hemmi et al. 2000, Krieg et al. 1995, Liu et al. 2020). TLR9 has two binding pockets, one binds ssDNA with an unmethylated CpG motif while the second site prefers short 5'-hydroxyl ssDNA with a cytosine at the second position (5'-xCx DNA) (Ohto et al. 2018). When both DNA molecules are bound, TLR9 dimerizes and is activated. Upon NA recognition, endosomal TLRs orchestrate complex transcriptional responses that include NF-κB and AP-1 regulated inflammatory cytokine and chemokine secretion as well as IRF (interferon regulatory factors) 3/5/7-mediated type I IFN production leading to an inflammatory state of infected and bystander cells (Bartok and Hartmann 2020, Heinz et al. 2020).

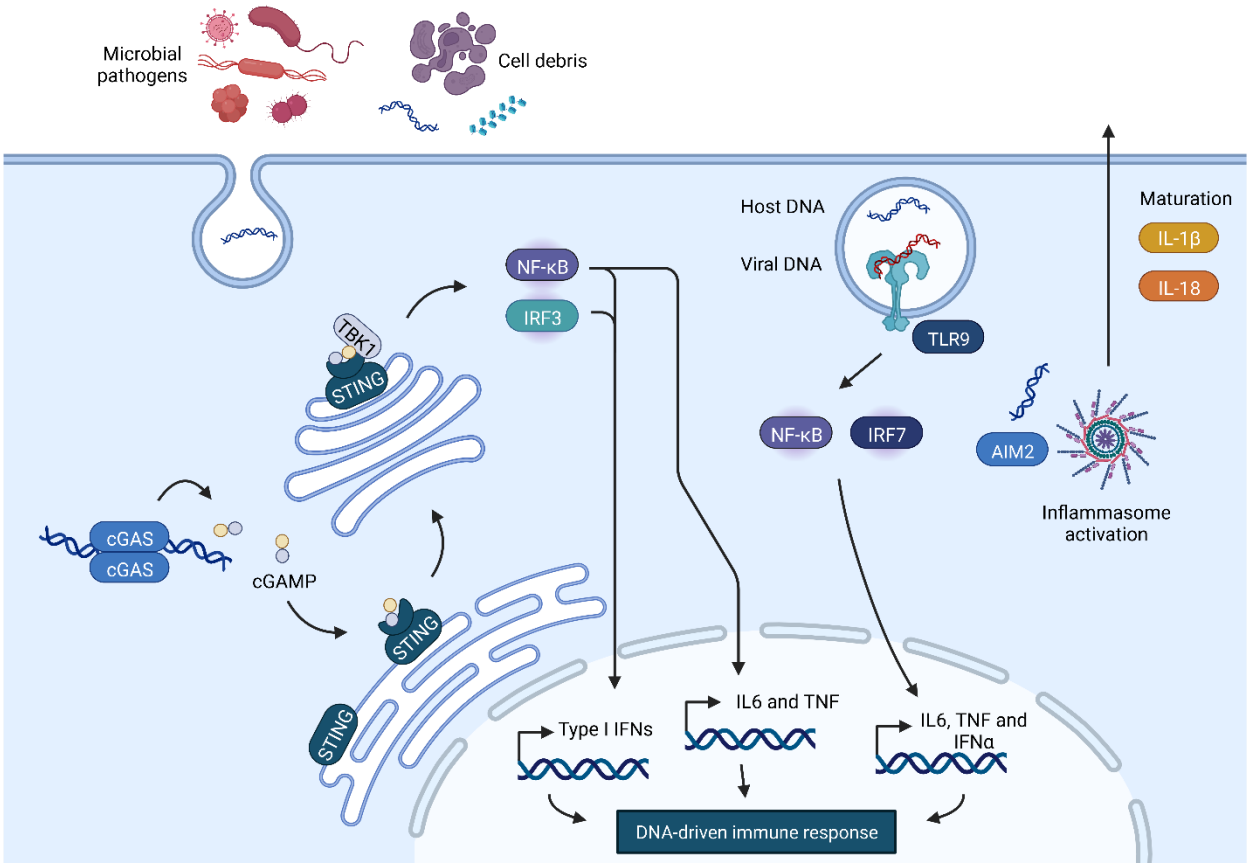

Fig. 1 DNA-sensing receptors. The three major DNA sensors that regulate immune responses to foreign and self-DNA are cGAS (cyclic GMP-AMP synthase), TLR9 (Toll-like receptor 9) and AIM2 (absent in melanoma 2). In the cytosol, AIM2 recognizes dsDNA, leading to the assembly of the AIM2 inflammasome, which initiates caspase-1-mediated maturation of the proinflammatory cytokines IL-1β and IL18, and ultimately pyroptosis. Besides, cytosolic DNA drives cGAS-dependent generation of cGAMP

(cyclic GMP-AMP) which binds to STING (stimulator of interferon genes), leading to the activation of TBK1 (TANK-binding kinase 1), IRF3 (interferon regulator factor 3) and NF-κB (nuclear factor-κB), resulting in the expression of type I interferons and proinflammatory cytokines such as IL6 and TNF (tumor necrosis factor). Finally, endosomal TLR9 binds CpG hypomethylated DNA and activates the transcription factors NF-κB and IRF7, leading to the transcription of proinflammatory cytokines and interferons, respectively. This figure was created with BioRender.com.

1.2 Role of Toll-like receptors in cell expansion and differentiation

Following infection, leukocytes proliferate in the bone marrow, lymphocytes clonally expand in secondary lymphoid tissues and long-term survival of memory cells is induced (Li et al. 2010). Cell proliferation and survival are critical to mammalian defense but also development, tissue regeneration and repair, while uncontrolled expansion leads to the life-threatening disease cancer. Many tumor cells express a certain repertoire of TLRs, pointing to a role in the regulation of excessive cell growth (Huang et al. 2008). Indeed, TLRs directly regulate cell proliferation and survival in various biological contexts including tumorigenesis by suppressing apoptosis, preventing cell cycle arrest, inducing proto-oncogene expression and upregulating growth factor secretion (Jiang et al. 2005, Naugler et al. 2007, Rakoff-Nahoum et al. 2004, Rakoff-Nahoum and Medzhitov 2007). For example, TLR signaling stimulates cell cycle entry and progression in fibroblasts and promotes survival of multiple myeloma cells (Bohnhorst et al. 2006, Hasan et al. 2005, Jego et al. 2006). Upon Tlr activation, multipotent hematopoietic stem cells (HSC) enter the cell cycle and their developmental potential is shifted towards myelopoiesis rather than lymphopoieses (Nagai et al. 2006). Common lymphoid progenitors from mice infected with herpes simplex virus differentiate into dendritic cells instead of B cells in a Tlr9-dependent manner (Welner et al. 2008).

Chronic activation of Tlr7 promotes the differentiation of Ly6C^{high} monocytes into specialized phagocytes that internalize red blood cells and drive anemia and thrombocytopenia (Akilesh et al. 2019). These inflammatory hemophagocytes are also found in experimental murine anemia caused by chronic Tlr9 signaling (Akilesh et al. 2019). Recently, a link between excessive lysosomal nucleoside storage and histiocytosis was revealed. Histiocytosis describes a group of disorders that are characterized by the excessive expansion of dendritic cells, monocyte-derived cells and

macrophages which can result in the formation of tumors and severe systemic inflammation (Cai et al. 2017, Haroche et al. 2017, Hsu et al. 2012). In endolysosomal compartments, nucleic acids are degraded into nucleosides which are shuttled to the cytoplasm by the nucleoside transporter Slc29a3 for further metabolization (Baldwin et al. 2005). Human mutations of SLC29A3 are associated with multiple diseases that are characterized by histiocytosis including H syndrome, Faisalabad Histiocytosis and familial Rosai-Dorfman disease (Molho-Pessach et al. 2008, Morgan et al. 2010). Tlr7 resides in endolysosomal compartments and binds uridine-containing ssRNAs and guanosine or 2'-deoxyguanosine (Jurk et al. 2002, Shibata et al. 2016, Zhang et al. 2016a), suggesting a potential link between histiocytosis and Tlr7 activation. Indeed, in *Slc29a3*$^{-/-}$ mice, guanosine and deoxyguanosine derived from phagocytosed cell corpse accumulate in lysosomes and drive the expansion of patrolling monocytes in a Tlr7-dependent manner (Shibata et al. 2019). These findings show that endosomal Tlrs influence proliferation and activation of monocytes under sterile conditions.

1.3 DNA sensors and programmed cell death

On the one hand, NA-sensing receptors mediate cell survival and proliferation, while on the other hand they can activate programmed cell death pathways as ultimate defense in response to infection (Bedoui et al. 2020, Ketelut-Carneiro and Fitzgerald 2022). Cell death obstructs replication of pathogens by eliminating the infected cell and boosts the release of cytokines and inflammatory mediators, but it also plays an important role in several noninfectious pathologies. In general, programmed cell death pathways can be grouped into two major types: lytic versus non-lytic.

Lytic forms of cell death, such as necroptosis and pyroptosis, result from the disruption of the plasma membrane integrity by forming pores or other lesions ultimately leading to the release of intracellular content such as nucleic acids, proteins, lipids or pathogenic material into the extracellular space, where they activate bystander cells and neighboring macrophages (Bedoui et al. 2020, Green 2019, Ketelut-Carneiro and Fitzgerald 2022, Rock and Kono 2008). The initiating event in pyroptosis is the activation of multiprotein complexes, termed inflammasomes, by intracellular sensors such as NLRP3 and AIM2. Inflammasomes assemble via the key adaptor protein ASC (apoptosis-associated speck-like protein) that in turn associates with pro-caspase-1

which undergoes autocatalytic cleavage and is released in its activated state (Boucher et al. 2018). Active caspase-1 promotes the conversion of the precursors of the pro-inflammatory cytokines, pro-IL-1β and pro-IL18, into their bioactive forms, and targets gasdermin D (GSDMD) by cleaving it into N-terminal and C-terminal fragments (Aglietti et al. 2016, Ding et al. 2016, Liu et al. 2016). Unleashed N-terminal GSDMD fragments are recruited to the cell membrane, where they organize transmembrane pores that allow potassium efflux and water influx, thereby destabilizing the plasma membrane potential and resulting in cellular rupture. Necroptosis can be induced by multiple innate immune receptors including RIG-I-like receptors, death receptors and TLRs, that mediate the phosphorylation and activation of the necroptotic kinase RIPK3 (receptor-interacting serine-threonine kinase 3) which in turn phosphorylates MLKL (mixed lineage kinase domain like) (Newton and Manning 2016). Phosphorylated MLKL undergoes conformational changes that allow its translocation to the plasma membrane, where it promotes membrane permeabilization (Khan et al. 2014) (Fig. 2).

A non-lytic form of programmed cell death is apoptosis which leads to the regulated disintegration of dying cells into smaller units, termed apoptotic bodies that ensure the containment of potentially harmful intracellular content (Bedoui et al. 2020). Cellular processes involved in cell demolition include DNA fragmentation by DNases, chromatin condensation and membrane blebbing (Kerr et al. 1972, Segawa et al. 2014). Two distinct pathways can initiate apoptosis: the intrinsic/mitochondrial and the extrinsic pathway. The intrinsic apoptotic pathway is triggered by various stressors including endoplasmic reticulum stress, DNA damage or diverse cytotoxic agents (Bedoui et al. 2020, Ketelut-Carneiro and Fitzgerald 2022). It involves the increased expression of pro-apoptotic BH3-only proteins that indirectly activate the effector proteins, Bax and Bak, by neutralizing pro-survival proteins such as Bcl-2 and Mcl-1 that keep the effectors in inactive state in healthy cells (Czabotar et al. 2014, Singh et al. 2019). Upon unleashing, Bax and Bak assemble into structures that perforate the outer mitochondrial membrane inducing MOMP (mitochondrial outer membrane permeabilization), thereby releasing mitochondrial content including cytochrome c. Cytochrome c binds Apaf-1 (apoptotic peptidase-activating factor 1) and initiates the formation of the apoptosome which in turn activates caspase-9 (Cosentino and García-Sáez 2017, O'Neill et al. 2016, Salvesen and Dixit 1999). Active caspase-9 proteolytically unleashes the effector caspases-3 and

-7, thereby promoting internucleosomal DNA cleavage by caspase-activated DNase (CAD) and chromatin condensation as well as actomyosin-driven membrane blebbing (Bedoui et al. 2020). Following MOMP mtDNA can leak into the cytosol, where it activates cGas (Rongvaux et al. 2014, White et al. 2014). Caspase-3 and -7 can also be activated by the extrinsic death receptor-induced apoptosis pathway. Such signaling cascade can be triggered by the activation of death receptors, such as FAS by FAS ligand interaction, and leads to the recruitment of pro-caspase-8 via the adaptor protein FADD (FAS associated via death domain), resulting in the assembly of the so-called DISC (death-inducing signaling complex), which catalyzes the activation of caspase-8 (Boatright and Salvesen 2003, Itoh et al. 1991, Kischkel et al. 1995). Active caspase-8 induces cell death, either directly by cleaving effector caspases-3 and-7 or indirectly, through proteolytically activating pro-apoptotic protein BID, thereby nurturing the intrinsic apoptotic pathway (Billen et al. 2009).

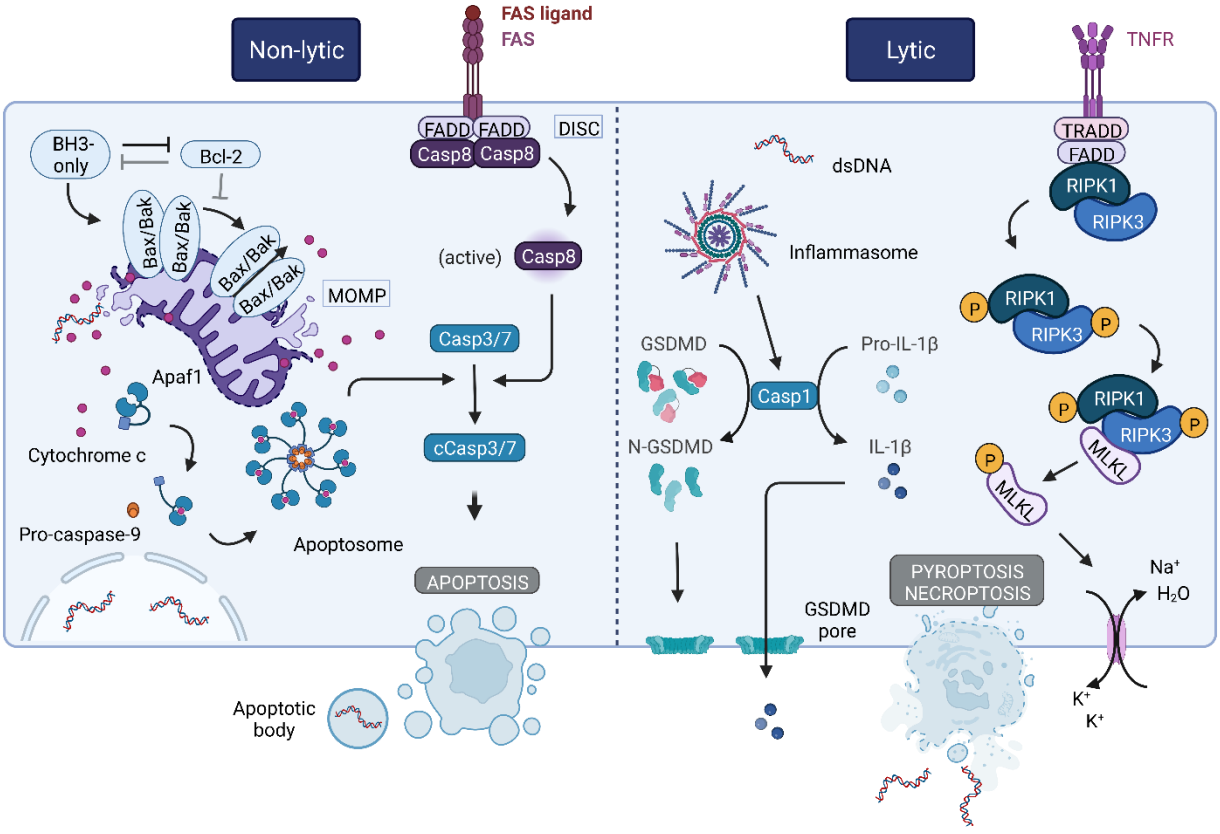

Fig. 2 Molecular mechanisms of non-lytic and lytic cell death. In the intrinsic non-lytic (apoptosis) pathway, pro-survival Bcl-2 proteins are blocked by pro-apoptotic BH3-only proteins liberating Bax and Bak, which become activated and assemble into complexes causing mitochondrial outer membrane permeabilization (MOMP).

Cytochrome c is released, binds Apaf-1 and initiates the assembly of the apoptosome, which in turn activates a cascade of caspase activation steps starting with caspase-9. Caspase-9 activates the effector caspases-3 and -7. In the extrinsic non-lytic pathway, ligand recognition by FAS recruits pro-caspase-8 through the intracellular adaptor protein FADD forming DISC which activates caspase-8. Active caspase-8 induces apoptosis by stimulating effector caspases-3 and -7 which promote apoptotic morphology including membrane blebbing, formation of apoptotic bodies, DNA condensation and fragmentation. Lytic pyroptotic cell death is initiated upon inflammasome assembly and activation of caspase-1. Active caspase-1 cleaves GSDMD and produces a N-terminal pore-forming fragment that drives pyroptosis, which is characterized by the loss of membrane integrity, release of cytosolic content, cell swelling and lysis. Lytic necroptotic cell death can occur when RIPK1 is not ubiquitinated and caspase-8 is blocked. Deubiquitination of RIPK1 promotes dissociation of TRADD and RIPK1 from the TNF receptor 1 complex to either trigger apoptosis or necroptosis. In necroptosis, RIPK1 activates RIPK3 which phosphorylates MLKL. Activated MLKL undergoes conformational changes allowing MLKL to translocate to the plasma membrane and disrupt the integrity (possibly by forming pores). Consequently, efflux of potassium (K^+) and influx of water and sodium (Na^+) lead to disruption of membrane potential, cell swelling and eventually cell lysis. This figure was created with BioRender.com.

1.4 Trashing DNA during non-lytic cell death

Cells in the human body die at any time by non-lytic cell death. To prevent autoimmune reactions, emerging cellular waste must be broken down and the cells replenished. In general, two groups of nucleases are involved in the degradation of cellular DNA during non-lytic cell death: i) cell-autonomous nucleases that cleave DNA within the dying cell and ii) waste-management nucleases that originated somewhere other than the dying cell, which means that they are either secreted into the extracellular space or compartmentalized in lysosomes of neighboring phagocytes (Samejima and Earnshaw 2005). During apoptosis, CAD, which is the main cell-autonomous nuclease, is activated and induces DNA fragmentation; and the formation of apoptotic bodies begins (Widlak and Garrard 2005). Usually, cellular components including DNA are compartmentalized within apoptotic cells until their engulfment and lysosomal disposal by phagocytes. The main lysosomal waste-management nuclease is DNase2a expressed by macrophages (Kawane et al. 2001, Krieser et al. 2002). DNase2a cleavage generates 5'OH termini products which may be further processed by the exonucleases Pld3 and Pld4 because both enzymes degrade ssDNA substrates with 5'OH terminus (Bartok and Hartmann 2020). Taken together, non-lytic cell death mediates compartmentalization of

fragmented DNA into vesicles that are subsequently engulfed by phagocytes, in which DNA undergoes DNase2a-mediated lysosomal degradation. If, however, the membrane integrity is disrupted during this process, DNA can be released into the extracellular space. Such circulating cell-free DNA (cfDNA) is further processed by the waste-management nucleases DNase1 and DNase1l3. After the release of cfDNA, DNase1l3 chops long DNA substates (> 250 bp), that originate from CAD-mediated DNA cleavage, into fragments that display a peak length of ~ 165 bp. Part of this fragment fraction is further broken down by DNase1 into smaller pieces (< 150 bp). Thus, plasma cfDNA shows a peak frequency at ~ 165 bp and minor populations of longer (600-2000 bp) and relative short (20-120 bp) DNA fragments (Han et al. 2020, Samejima and Earnshaw 2005, Serpas et al. 2019).

1.5 Sources of self-DNA and its immunogenic potential

Endogenous DNA is present in various forms of genomic (gDNA) and mitochondrial DNA (mtDNA) in the circulation of healthy and diseased individuals (Santa et al. 2021). It can be cell-free, associated with proteins or integrated into extracellular vesicles. Cell-free DNA contains both genomic and mitochondrial DNA and mostly originates from dying hematopoietic cells, including granulocytes and lymphocytes (Lui et al. 2002, Moss et al. 2018). Genomic cfDNA is thought to originate from apoptotic cells due to its predominant fragment length of ~ 160-170 bp, resembling the size of nucleosome (nucleosomes + linker histone)-bound DNA (Giacona et al. 1998, Snyder et al. 2016). Besides, short (35-80 bp) cfDNA fragments have been identified directly foot printing the occupancy of DNA-bound transcription factors (Snyder et al. 2016). In contrast, mitochondrial cfDNA shows higher fragmentation and 56-fold greater abundance than genomic cfDNA (Burnham et al. 2016, Chiu et al. 2003). While genomic cfDNA is mostly inert and shows low immunostimulatory capacities, mtDNA shares characteristics with bacterial DNA including increased frequency of unmethylated immunostimulatory CpG motifs which can activate Tlr9 (Oka et al. 2012, Stacey et al. 2003, Zhang et al. 2010). Such immunogenic potential is further increased when cfDNA is associated with proteins like HMGB1 (high mobility group box 1) and TFAM (mitochondrial transcription factor A), binding gDNA and mtDNA, respectively, that promote the transport into intracellular compartments containing Tlrs and facilitate secondary structures capable of activating cGas (Andreeva et al. 2017, Julian et al. 2012, Tian et al. 2007). While circulating DNA

mostly arises from apoptotic cells in healthy individuals, DNA can also be released from neutrophils in form of neutrophil extracellular traps (NETs) during infection (Delgado-Rizo et al. 2017). Such NETs facilitate trapping of bacteria and consist of genomic and mitochondrial DNA that can be protected from degradation when oxidized or bound by antimicrobial-peptide LL37 (Lande et al. 2007). Besides, the extruded DNA is highly immunogenic and induces type I IFNs in a Tlr9- and cGas-dependent manner (Caielli et al. 2016, Garcia-Romo et al. 2011, Lood et al. 2016). In addition to circulating NAs, intracellular DNA has the potential to stimulate DNA sensors when segregation fails. Cell stress and death mediate release of mtDNA into the cytoplasm where unmodified mtDNA initiates the cGas-Sting signaling, while oxidized mtDNA can stimulate the Nlrp3 (NLR family pyrin domain containing 3) inflammasome (Gehrke et al. 2013, Oka et al. 2012, Rongvaux et al. 2014, Shimada et al. 2012, White et al. 2014). Besides, autophagy-mediated transport of mtDNA into endolysosomal compartments triggers Tlr9 activation when lysosomal nucleic acid degradation is perturbed (Oka et al. 2012).

1.6 Degradation and processing of DNA by deoxyribonucleases

Regulation of the abundance, size and modifications of DNA is critical to control its immunogenic potential. The main nucleases degrading extracellular DNA are DNase1 and DNase1l3 which compose together with DNase1l1 and DNase1l2 the deoxyribonuclease (DNase)-1 family (Keyel 2017, Santa et al. 2021). All four members are structurally comparable (51 % homology) and share common features including DNase domain, ER trafficking signal sequence that also inhibits DNase activity, dependency on divalent cations (Ca^{2+}/Mg^{2+}); and they leave 3'hydroxy/5'phophor (3'-OH/5'-P) ends after cleavage (Shiokawa and Tanuma 2001). After removal of the signal sequence, DNase1 and DNase1l3 are secreted, whereas DNase1l1 remains at the plasma membrane through a glycosylphosphatidylinositol (GPI) anchor (Napirei et al. 2005, Shiokawa et al. 2007, Sisirak et al. 2016). Consistent with their extracellular localization, DNase1, DNase1l1 and DNase1l3 function optimally at neutral pH, whereas DNase1l2 degrades its substrates optimally at an acidic pH (Shiokawa and Tanuma 2001).

1.6.1 DNase1

DNase1 is expressed primarily in kidneys, salivary glands, gut, pancreas and secreted into the circulation, where it degrades naked DNA, DNA originating from NETs or chromatin of necrotic cells after removal of DNA-bound proteins by serum serine proteases like plasmin or thrombin (Chitrabamrung et al. 1981, Hakkim et al. 2010, Jiménez-Alcázar et al. 2017, Napirei at el. 2000, Napirei et al. 2004a, Napirei et al. 2005, Napirei et al. 2009). Its endonuclease activity allows degradation of high and low molecular weight fragments and does not exhibit preferences towards certain nucleotide sequences or bases. However, since DNase1 interacts with the minor groove of B-form DNA, the conformation of the DNA double helix is essential (Lahm and Suck 1991, Suck and Oefner 1986, Suck 1994). Hydrolysis of the double helix depends on the width and depth of the minor grove as well as rigidity of its structure. DNase1 introduces one to multiple single strand breaks into both DNA strands which are slightly displaced by several nucleotides and cleaves double-stranded DNA 100-500 times more efficiently than ssDNA (Baranovskii et al. 2004, Drew 1984).

It was assumed for a long time that low DNASE1 activity is associated with the autoimmune disease systemic lupus erythematosus (SLE) since patients with SLE complications showed reduced enzymatic activity (Hakkim et al. 2010, Sallai et al. 2005). In addition, mixed 129sv-C57BL/6 *DNase1*$^{-/-}$ mice spontaneously develop SLE-like syndromes including anti-nucleosome as well as anti-dsDNA autoantibodies and eventually glomerulonephritis (Napirei et al. 2000). However, these results could not be reproduced in pure 129SV and C57BL/6 *DNase1*$^{-/-}$ mice and it was shown that the mixed 129sv-C57BL/6 background predispose these mice to autoimmunity (Bygrave et al. 2004, Napirei et al. 2004b). Besides, the significance of DNASE1 in human SLE pathogenesis remains uncertain. Heterozygous non-sense mutations and single nucleotide polymorphisms (SNP) in *DNASE1* were associated with SLE, however follow-up studies failed to clarify the role of mutations in multiple cohorts of SLE patients (Balada et al. 2002, Bodaño et al. 2007, Chakraborty et al. 2003, Mohammadoo-Khorasani et al. 2016, Shin et al. 2004, Simmonds et al. 2002, Tew et al. 2001, Yasutomo et al. 2001). In addition, treatment of SLE patients with recombinant human DNASE1 failed to show clinical benefits (Davis et al. 1999). Interestingly, the serum ability to eliminate chromatin from NETs, primary or secondary necrotic cells is

decreased in a large fraction of SLE patients, however when used on naked DNA no significant alterations compared to healthy controls were found, suggesting that not the enzyme activity *per se* is decreased but rather the access to DNA might be impaired, potentially by hindering anti-dsDNA antibodies that are generated as the disease progresses (Leffler et al. 2015, Sallai et al. 2005). Thus, DNase1-deficiency might not be a predisposing factor of SLE but rather a consequence of the autoimmune response likely further fueling pathological manifestations. In line with this, the inability of SLE patients to degrade NETs was mostly reversible within several months and correlated with titers of nuclear autoantibodies and disease activity (Leffler et al. 2013). Additionally, loss of renal DNase1 expression in (NZBxNZW)F1 mice and human SLE patients is acquired during transformation from mild to severe membranoproliferative lupus nephritis (Seredkina and Rekvig 2011, Zykova et al. 2010).

1.6.2 DNase1l3

DNase1l3 is the major nuclease eliminating endogenous DNA released by dying cells and is highly expressed in dendritic cells and macrophages (Sisirak et al. 2016, Wilber et al. 2002). Similar to DNase1, DNase1l3 is able to degrade naked DNA and NETs although less efficiently than DNase1 (Hakkim et al. 2010, Jiménez-Alcázar et al. 2017, Napirei et al. 2009). However, DNase1l3 has the unique ability to cleave DNA encapsulated in liposomes or microvesicles which relies on its C-terminal domain that is highly hydrophobic and positively charged (Santa et al. 2021, Sisirak et al. 2016, Wilber et al. 2002). Contrary to *DNase1*$^{-/-}$ mice, deletion of DNase1l3 causes the accumulation of circulating microvesicle-associated DNA and long poly-nucleosomal DNA as well as aberrations of end-motif frequencies in plasma DNA (Serpas et al. 2019, Shiokawa et al. 2007, Sisirak et al 2016). Consistently, deficiency of DNASE1l3 is associated with the development of childhood-onset SLE and SLE-associated diseases in humans (Al-Mayouf et al. 2011, Belot et al. 2020, Carbonella et al. 2017). Aberrantly activated autoimmune responses were also observed in *DNase1l3*$^{-/-}$ mice which developed anti-DNA and anti-nucleosome antibodies that resulted in minor kidney pathology primarily in 129 but not C57BL/6 *DNase1l3*$^{-/-}$ mice (Santa et al. 2021, Sisirak et al. 2016). Pathogenic activation of these immune responses was independent of Sting but relied on Tlr9 as well as Tlr7, and involved autoreactive B cell responses as well as production of type I IFNs by plasmacytoid DCs (Sisirak et al. 2016, Soni et al. 2020). In addition to

its well-established extracellular role, DNase1l3 is thought to be involved in internucleosomal DNA fragmentation in cells undergoing apoptosis and necrosis (Shiokawa et al. 1997, Shiokawa and Tanuma 1998, Shiokawa and Tanuma 2001, Shiokawa et al. 2002, Shiokawa et al. 2003, Yakovlev et al. 2000).

1.6.3 DNase1l1

DNase1l1 is highly expressed in skeletal muscle, cardiomyocytes as well as macrophages and is capable of digesting DNA complexed with transfection reagents (Shiokawa et al. 2005, Shiokawa et al. 2007). However, the natural substrate and function remains unknown. In human studies, inconsistent results were found associating SNPs in *DNASE1l1* with the development of Pompe's disease, a disorder characterized by myopathy and respiratory weakness (Lichtenbelt et al. 2006, Malferrari et al. 2001, Ueki et al. 2014). *DNase1l1*$^{-/-}$ mice showed signs of muscle damage and fatigue more rapidly during running (Rashedi 2018). Conversely, others suggested that dysfunctional human DNASE1l1 may be connected to type 1 diabetes, ANCA-associated vasculitis and schizophrenia (Brumpton and Ferreira 2016). In macrophages and monocytes, GPI-anchored DNASE1l1 serves as a receptor for the tick-borne intracellular bacterial pathogen *Ehrlichia chaffeensis* suggesting a rather important role of DNASE1l1 since pathogens often target essential molecules (Keyel 2017, Mohan Kumar et al. 2013). Besides, macrophages can form podosomes that recruit membrane-bound DNase1l1 to degrade extracellular double-stranded bacterial DNA on surfaces (Pal et al. 2021).

1.6.4 DNase1l2

DNase1l2 features a unique trait due to its optimal enzymatic activity at acidic pH which potentially points to an endolysosomal or autophagosomal localization (Santa et al. 2021, Shiokawa and Tanuma 2001). This enzyme is highly expressed in keratinocytes and acts intracellularly during differentiation when the cells lose their nuclear material and store keratin (Fischer et al. 2007). During this process the cytosol is acidified, and organelle disruption occurs which allows DNase1l2 to access the nucleus (Fischer et al. 2007, Naeem et al. 2015). Together with DNase2a and Trex2, DNase1l2 degrades nuclear DNA in skin and lingual keratinocytes, respectively (Fischer et al. 2011, Fischer et al. 2017, Manils et al. 2017). However, no signs of epithelial tissue inflammation are

observed in these double knockout mouse models, despite the accumulation of DNA. In contrast, human studies associate SNPs in *DNASE1l2* with psoriasis and reduced DNASE1l2 expression with inflamed psoriatic skin suggesting a regulatory role of DNASE1l2 (Fischer et al. 2007, Ueki et al. 2015). In keratinocytes, TNFα and IL-1β induce DNASE1l2 expression via NF-κB signaling, further pointing to the involvement of DNASE1l2 in skin autoimmunity (Shiokawa et al. 2004). In humans, DNASE1l2 is expressed at low levels in multiple tissues and a short product of the enzyme is expressed by peripheral blood leukocytes showing the same enzymatic properties (Shiokawa and Tanuma 2001, Shiokawa et al. 2004). In contrast to its intracellular function and biochemical properties, overexpression systems suggest extracellular secretion of DNASE1l2 which however may not be physiologically relevant (Shiokawa and Tanuma 2001).

1.6.5 DNase2

The DNase2 family consists of three members including DNase2a, DNase2b and L-DNaseII which do not require divalent cations, function at an acidic pH and generate 3'phophates after dsDNA cleavage (Keyel et al. 2017). DNase2a and L-DNaseII are widely distributed across tissues and highly expressed in macrophages and in case of L-DNaseII also in neutrophils, while DNase2b is primarily detected in the lens of the eye, salivary glands and lung (Cordonnier and Bernardi 1968, Kawane et al. 2001, Krieser et al. 2001, Nishimoto et al. 2003, Padron-Barthe et al. 2007). DNase2a and -b share structural similarities including signal sequences enabling their lysosomal trafficking (Nakahara et al. 2007, Sleat et al. 2006). Besides, they feature phospholipase D (PLD) signature motifs in their catalytic domain and are considered to be part of the phospholipase D superfamily just as Pld3/4 (Cymerman et al. 2005, Schafer et al. 2007). DNase2a is indispensable for definitive erythropoiesis in the mouse fetal liver, where macrophages destroy engulfed nuclear DNA that is expelled from erythroid precursor cells during their maturation into erythrocytes (Bessis and Breton-Gorius 1962, Kawane et al. 2001). In DNase2a-deficienct mice, large DNA-containing bodies, derived from improper digestion of engulfed apoptotic cell corpses, accumulate in multiple organs and induce severe anemia, inflammation and defects in the diaphragm that ultimately mediate lethality at an early stage of life (Kawane et al. 2001, Krieser et al. 2002). Embryonic lethality is also associated with the excessive production of type I IFNs since

DNase2a$^{-/-}$ *Ifnar1*$^{-/-}$ mice survived for at least 2 months post birth (Kawane et al. 2006, Yoshida et al. 2005). Such aberrant production of IFNs was fully dependent on sensing DNA via the cGas-Sting pathway and independent of endosomal Tlrs (Ahn et al. 2012, Gao et al. 2015, Okabe et al. 2005). Interestingly, *DNase2a*$^{-/-}$ *Ifnar1*$^{-/-}$ mice manifest different abnormalities suggesting that DNase2a regulates the activation of various nucleic acid sensing receptors. Firstly, *DNase2a*$^{-/-}$ *Ifnar1*$^{-/-}$ mice develop TNFα-driven rheumatoid arthritis that is mediated by cGas-Sting signaling but also Aim2 inflammasome activation (Baum et al. 2015, Kawane et al. 2010). Secondly, these mice show elevated levels of anti-nuclear autoreactive antibodies as they age, and this production is fully dependent on endosomal Tlrs (Baum et al. 2015). Thirdly, *DNase2a*$^{-/-}$ *Ifnar1*$^{-/-}$ mice were used to show that DNase2a processes bacterial DNA and is required for the generation of Tlr9 ligands from complex natural substrates, including the release of ssDNA from genomic dsDNA and production of 5'OH termini for the second binding pocket of Tlr9 (Chan et al. 2015). In human studies, SNPs in *DNASE2A* are linked to rheumatoid arthritis and patients with null mutations in *DNASE2A* develop severe non-regenerative anemia and deforming arthropathy accompanied by elevated TNFα levels and upregulation of interferon-stimulated genes (Rodero et al. 2017, Rossol et al. 2009).

1.6.6 Pld3 and Pld4

Pld3 and Pld4 belong to the phospholipase D family and were recently characterized as endolysosomal 5'-exonucleases that are involved in the removal of ssDNA and small ssRNAs (Gavin et al. 2018, Gavin et al. 2021). They function both at neutral and acidic pH and contain a N-terminal transmembrane domain mediating their localization in endolysosomes (Gavin et al. 2018, Gonzalez et al. 2018, Otani et al. 2011). Pld3 is expressed in most tissues by macrophages, whereas Pld4 is highly expressed in bone marrow, spleen and lymphoid tissue by dendritic cells (Gavin et al. 2018). Genome-wide association studies connect *PLD4* polymorphisms with rheumatoid arthritis, system lupus erythematosus and systemic sclerosis, while PLD3 dysfunction is linked with Alzheimer's disease (Chen et al. 2017, Cruchaga et al. 2014, Okada et al. 2012, Santa et al. 2021, Terao et al. 2013, Zhang et al. 2016b). *Pld4*$^{-/-}$ mice show signs of chronic inflammation including elevated plasma levels of interferon-γ (IFN-γ), splenomegaly and aberrant immune cell activation (Gavin et al. 2018). Abnormally increased numbers of blood monocytes and hepatic CD68^{+} macrophages as well as splenomegaly are

dependent on Tlr9. *Pld3*$^{-/-}$ *Pld4*$^{-/-}$ mice develop lethal liver inflammation in early stages of life which is driven by both endosomal Tlrs and a Sting-dependent nucleic acid-sensing pathway (Gavin et al. 2018, Gavin et al. 2021). Thus, Pld3 and Pld4 prevent activation of multiple endolysosomal and cytosolic nucleic acid sensors and exhibit functional redundancy.

1.6.7 Trex1

Trex1, also called DNase3, is a ubiquitously expressed cytosolic 3' -> 5' exonuclease that eliminates ssDNA derived from retroelements, micronuclei and dsDNA (Lindahl et al. 1969, Mazur and Perrino 1999). In steady state, Trex1 is attached to the ER via a C-terminal transmembrane domain while the N-terminal domain harbors the exonuclease activity (Lindahl et al. 2009, Mazur and Perrino 1999, Orehaugh et al. 2013). In humans, mutated TREX1 is associated with Aicardi Goutières Syndrome (AGS), which is characterized by encephalitis, infiltration of lymphocytes in the central nervous system and type I IFN signature. Furthermore, mutations affecting the human exonuclease are linked to familial chilblain lupus (FCL), which is an inflammatory disease, causing ulcerating lesions of the skin, retinal vasculopathy with cerebral leukodystrophy and systemic lupus erythematosus (SLE) (Lee-Kirsch et al. 2007a, Lee-Kirsch et al. 2007b, Namiou et al. 2011, Rice et al. 2007). Most of the genetic alterations associated with AGS, FCL and SLE target the N-terminal exonuclease domain of TREX1, suggesting a crucial role of the cytosolic nuclease in the removal of immunostimulatory endogenous DNA (Gray et al. 2015, Santa et al. 2021). In mice, Trex1-deficiency leads to severe myocarditis, systemic inflammation and familial chilblain lupus-like syndromes including elevated titers of autoantibodies, ultimately causing premature death (Crow et al. 2006, Stetson et al. 2008). Deletion of the cGas-Sting pathway prevented fatal autoimmunity in *Trex1*$^{-/-}$ mice (Gall et al. 2012, Gao et al. 2015, Hasan et al. 2013).

1.6.8 CAD

CAD (Caspase-activated DNase), also called DFFB, is a cytoplasmic and nuclear endonuclease that is ubiquitously expressed, functions at neutral pH, requires Mg^{2+} as cofactor and is exclusively activated during apoptosis (Sameijima and Earnshaw 2005, Widlak and Garrard 2005, Zhang et al. 1999). Upon activation of apoptotic signaling cascades, caspase-3, caspase-7 and/or granzyme B can cleave the inhibitory

chaperone ICAD and release CAD (Enari et al. 1998, Liu et al. 1997, Sakahira et al. 1998, Thomas et al. 2000, Wolf et al. 1999). Active CAD has a scissors-like structure, forms homodimers or oligomers and becomes immobilized within apoptotic nuclei potentially preventing its release into the extracellular space (Lechardeur et al. 2004, Sameijima and Earnshaw 2005, Woo et al. 2004). CAD cleaves dsDNA at positions within the internucleosomal linker, degrades chromatin almost as efficiently as naked DNA and is assumed to be sequence non-selective (Sameijima and Earnshaw 2005, Widlak et al. 2000). Studies of apoptotic cells that are deficient in components of the CAD system show either no or strongly decreased amounts of internucleosomal DNA fragmentation, incomplete chromatin condensation and fail to form discrete apoptotic bodies (McIlroy et al. 2000, Samejima et al. 2001, Sameijima and Earnshaw 2005, Zhang et al. 1998). Additionally, *CAD*$^{-/-}$ mice show defects in apoptotic DNA degradation, however, pathological consequences of the deficiency are mild (Kawane et al. 2003, Keyel et al. 2017, Zhang et al. 1998).

1.7 When nucleic acid clearance fails: Systemic lupus erythematosus

Failed clearance of nucleic acids has long been associated with an autoimmune disease termed systemic lupus erythematosus (SLE), which is characterized by global loss of self-tolerance and systemic inflammation affecting multiple regions including neurological, pleural, renal and musculoskeletal tissues (Kaul et al. 2016). Especially women of childbearing age and Hispanic, Asian or African origin have a high risk of developing SLE with an estimated female to male sex ration of 9 to 1 (Kaul et al. 2016, Lim et al. 2014, Yee et al. 2015). Patients with SLE report decreased quality of life owing to disease manifestations, treatments as well as secondary conditions including anxiety, fatigue, depression, and eventually suffer from an increased mortality risk (Kaul et al. 2016). One of the primary sites of tissue damage is the kidney, the inflammation of which is referred to as lupus nephritis. Lupus nephritis results from glomerular deposition of immune complexes, autoantibodies and complement fixation that initiates recruitment and activation of tissue-infiltrating monocytes/macrophages which promote uncontrolled inflammatory as well as repair responses damaging the tissue (Bethunaickan et al. 2011, Choi et al. 2012, Kaul et al. 2016).

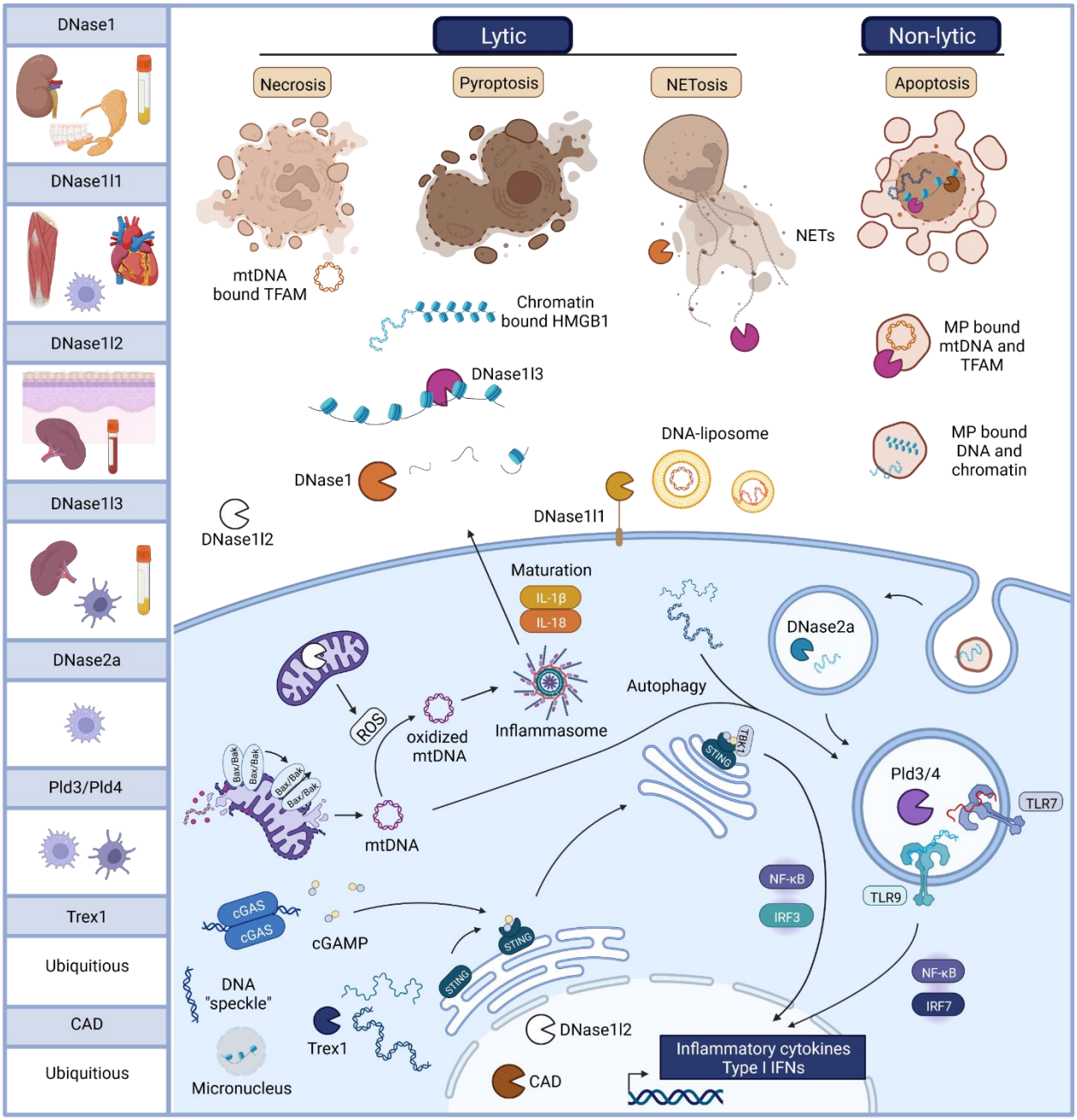

Fig. 3 Deoxyribonucleases process NAs in extra- and intracellular compartments. At the head are presented extracellular sources of NAs that originate from dying cells in multiple forms including cell-free DNA, chromatin, mtDNA, neutrophil extracellular trap (NET-) and microparticle (MP-)associated DNA. Lytic cell death leads to the exposure of NAs, while apoptosis mediates CAD-regulated fragmentation and compartmentalization of DNA. Circulating DNase1 (orange) and DNase1l3 (pink) process chromatin, cell-free DNA, NETs and microparticle-associated DNA, whereas membrane-bound DNase1l1 (yellow) digests DNA-liposomes. Below are presented extracellular NAs that are internalized into endolysosomes where they are cleaved by DNase2a (light blue), Pld3 or Pld4 (purple) and recognized by Toll-like receptors (Tlr9/7), which activate NF-κB and Irf7 transcription factors that upon their translocation to the nucleus promote the production of inflammatory cytokines and type I interferons. Cytoplasmic DNA originates

for instance from mitochondria and can be oxidized in the presence of ROS (reactive oxygen species) acquiring the ability to initiate inflammasome assembly, which drives caspase-1-mediated processing of pro-IL-1β and -IL18 into active IL-1β and IL18. mtDNA can also stimulate cGas. On binding dsDNA, cGas dimerizes resulting in the enzymatic activation and synthesizes of 2'3' cGAMP (cyclic GMP-AMP) that in turn binds to Sting dimers localized at the endoplasmic reticulum (ER) membrane and triggers translocalization to the Golgi where Sting recruits Tbk1 and promotes the activation of Irf3 and NF-κB transcription factor cascades. Upon autophagy, cytoplasmic DNA can gain access to endolysosomal compartments and stimulate Tlr9. Extracellular NET-associated DNA, mtDNA and microparticle can be internalized, gain access to the cytosol and activate cGas. Nuclear DNA can be released into the cytosol upon stress in forms of micronuclei and "speckles". Cytosolic DNA is exposed to Trex1 (dark blue) digestion. On the left tissue or cell specificity of individual deoxyribonucleases are presented. This figure was created with BioRender.com.

Several environmental factors can trigger disease onset and progression including apoptotic or necrotic cell debris and nucleic acids. These stressors can activate Tlrs and promote plasmacytoid dendritic cell (pDC) survival and type I IFN production (Barrat et al. 2005, Lovgren et al. 2004). Type I IFNs are central to the activation and regulation of the innate immune system by promoting the capacity of antigen presenting DCs to effectively present (self-)antigens to T cells. The stimulation of T cells leads to the production of cytokines and drives B cell differentiation and production of autoantibodies directed against endogenous nucleic acids and binding proteins (Kaul et al. 2016).

Although pDCs are the main source of type I IFNs, other cell types such as neutrophils are involved in amplifying IFN signaling (Kaul et al. 2016). Neutrophils exposed to increased IFNα level or engulfing circulating immune complexes are primed to undergo NETosis and extrude DNA in form of neutrophil extracellular traps (NETs) that might (i) facilitate the trafficking of DNA-containing immune complexes to the TLR-containing intracellular endosome, (ii) induce the production of type I IFNs by pDCs, (iii) serve as a source of self-antigens for presentation to T lymphocytes and (iv) mediate vascular damage and thrombosis (Brinkmann et al. 2004, Garcia-Romo et al. 2011, Haul et al. 2016, Kaplan 2011, Lande et al. 2011, Mahajan et al. 2016, Villanueva et al. 2011).

Studies of kidney infiltrating cells have identified patrolling monocyte populations that contribute to immune-mediated pathology in SLE patients and lupus-prone mouse models (Bethunaickan et al. 2011, Kuriakose et al. 2019). In the Yaa mouse model of

lupus, Tlr7 is hyperactivated due to its gene duplication leading to lupus-associated monocytosis (Amano et al. 2005, Pisitkun et al. 2006, Subramanian et al. 2006). Amelioration of lupus nephritis could be achieved in B6.Sle1yaa and *Tnip1*$^{-/-}$ mice by preventing the maturation of patrolling monocytes due to the deletion of the monocytic master transcription factor Nr4a1 (Kuriakose et al. 2019). In NZBWF1 mice, lupus nephritis is associated with an increase of patrolling monocytes, and administration of anti-TLR7 but not anti-TLR9 antibodies protected NZBWF1 mice from nephritis by reducing the production of autoantibodies directed against RNA-associated antigens and abolishing infiltration of patrolling monocytes into glomeruli (Murakami et al. 2021).

Although renal damages are more common, pulmonary manifestations including diffuse alveolar hemorrhage (DAH) are severe clinical complications of SLE. DAH is considered as a rare complication with 1-5 % prevalence, but mortality rates of 30-80 % were reported (Andrade et al. 2016, de Prost et al. 2010, Kamen and Strange 2010, Kazzaz et al. 2015, Zamora et al. 1997). The disorder is characterized by a disruption of the alveolar capillary basement membrane (BM) integrity resulting in the accumulation of red blood cells in the alveolar space (Park et al. 2013). The BM is a fusion of the alveolar and capillary basement membrane leading to a single sheet of specialized extracellular matrix that closely connects alveolus and capillaries facilitating efficient gas exchange. Upon BM disruption, focal and bland pulmonary hemorrhages occur that eventually lead to respiratory failure. In human lupus-associated DAH, neutrophil-predominant infiltration, hemosiderin-laden macrophages and fibrinoid necrosis of vessel walls, which is associated with endothelial damage, deposition of serum proteins in the vessel walls and fibrin polymerization, occur (Park et al. 2013, Zhuang et al. 2017). Treatment of patients with DAH typically includes high doses of immunosuppressive drugs including steroids and plasmapheresis. In > 50 % of cases of SLE-associated DAH, mechanical ventilation is necessary (Badsha et al. 2004). Further studies focusing on the development and prevention of DAH are required and involve studies with model systems since the acquisition of pulmonary material from human patients is inapplicable.

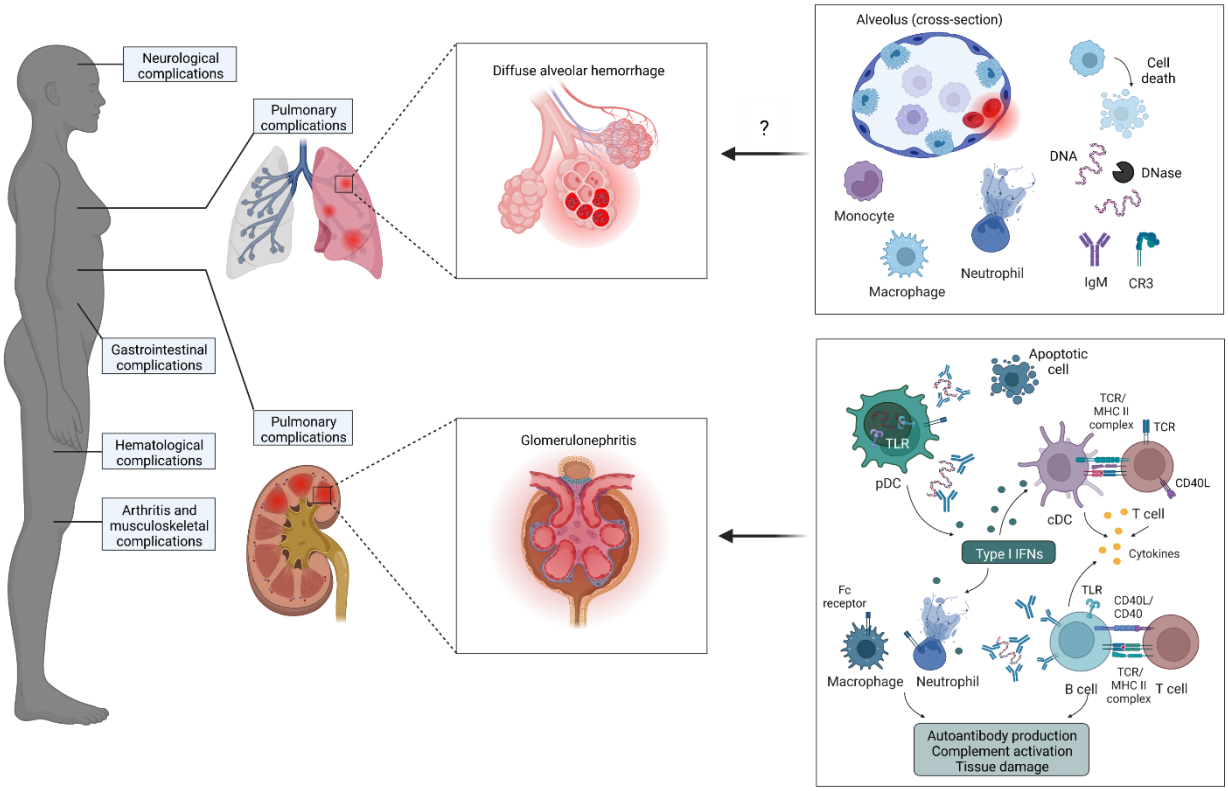

Fig. 4 Clinical heterogeneity of systemic lupus erythematosus. Pathological complexity is shown by the number of different organs that can be affected. Renal complications that manifest as lupus nephritis are common in comparison to diffuse alveolar hemorrhage. Involved innate and adaptive immune cells driving glomerulonephritis as well as factors mediating diffuse alveolar hemorrhage are represented. This figure was created with BioRender.com.

1.7.1 Chemically induced diffuse alveolar hemorrhage

The naturally occurring isoprenoid alkane (2,6,10,14-tetramethylpentadecane) commonly known as pristane is widely used to induce a lupus-like disease in BALB/c and SJL mice characterized by the generation of a broad spectrum of autoantibodies that are associated with systemic lupus erythematosus (SLE) including anti-U1RNP/Sm, -Su, -dsDNA, and -chromatin autoantibodies (Satoh and Reeves 1994, Satoh et al. 1995, Satoh et al. 1996). Syndromes also include immune complex-mediated glomerulonephritis and arthritis. Although most of these characteristics can also be investigated in several genetic models of SLE, pristane has the unique ability to induce diffuse alveolar hemorrhage in C57BL/6 (B6) mice (Barker et al. 2011, Chowdhary et al.

2007, Lee et al. 2008a, Lee et al. 2008b, Lee et al. 2009, Nacionales et al. 2006, Satoh et al. 2000).

In B6 mice, pulmonary hemorrhage starts three days after peritoneal pristane injection in form of small distinct foci that are uniformly distributed in all lobes. After seven days, complete hemorrhage can occur in some individuals and peaks after 14 days with an incidence of ~ 80 %. Perivascular neutrophilic and mononuclear cell infiltrates as well as hemosiderin-laden macrophages can be found within alveoli. Although endothelial activation was suggested, it is reported that the alveolar basement membrane remains primarily intact and no immune complexes either in the alveolar BM or endothelial cells are detected. In addition, sera from pristane treated mice are negative for anti-neutrophil cytoplasm antibody (ANCA) (Baker et al. 2001, Chowdhary et al. 2007, Zhuang et al. 2017).

Lipophilic alkanes like pristane are practically immiscible with aqueous media. However, when withdrawn from the peritoneal cavity it is emulsified which is probably facilitated by fatty acids, phospholipids or proteins that are abundantly present in an inflammatory environment (Janz and Shacter 1991). Pristane is incorporated into fixed inflammatory tissues so-called “lipogranuloma” that are seen in peritoneum, spleen, liver and kidney and it remains over a prolonged period in the peritoneal fluid (Nacionales et al. 2006). Due to some sort of emulsification, it is comprehensible that pristane may be distributed systemically. Indeed, it is shown that pristane reaches the lung and bone marrow where it exacerbates cell death (Zhuang et al. 2014, Zhuang et al. 2017). Interestingly, lipogranuloma occur in several organs embedded in the peritoneum but vasculitis was only observed in the lung (Baker et al. 2001). The bronchoalveolar lavage (BAL) fluid of pristane-injected mice is highly cellular with granulocytes, lymphocytes and especially macrophages that are positively stained for lipoid material like pristane indicating its take up (Chowdhary et al. 2007). TUNEL (terminal deoxynucleotidyl transferase dUTP nick end labeling) staining of lung sections from pristane treated mice revealed that DNA fragmentation mainly occur in large, vacuolated cells, indicating their late stage of apoptosis. These cells are located in alveoli and reminiscent of alveolar macrophages (Zhuang et al. 2017).

To identify the effector cells that drive alveolar damage, various genetically or pharmacologically ablated mouse models were examined showing their prevalence of DAH or resistance to pristane treatment. B6 *Rag1*$^{-/-}$ mice, that are deficient in both B and T cells, show partially reduced prevalence of pulmonary hemorrhages, indicating that both populations are not absolutely required but may accelerate the development of DAH. To dismantle the role of the individual cell populations, B6 *Tcr*$^{-/-}$ and B6 *Igμ*$^{-/-}$ mice which lack T cells or B cells, respectively, were investigated. T cell deficient mice develop DAH with a prevalence comparable to wild-type controls, whereas B6 *Igμ*$^{-/-}$ are mainly resistant to pristane treatment and reconstitution with wild-type B cells strikingly increase the rate of DAH. Interestingly, infusion of mouse IgG does not restore the susceptibility to pristane but conventional mouse serum and human IgM i.v. do. However, pristane treatment is associated with a reduction of B and T lymphocytes, while CD11b^{+} myeloid cells make up the majority of infiltrating immune cells in the lung. Neutrophils, Ly6C^{high} inflammatory monocytes, and Ly6C^{low} patrolling monocytes strikingly increase following pristane injection. In addition, expansion of these populations and depletion of alveolar macrophages correlate with the severity of DAH. Interestingly, several groups have studied the role of neutrophils in pristane-induced DAH using antibody-mediated depletion in mice and observed no marked differences in the severity of DAH. In contrast, liposome-mediated depletion of monocytes and alveolar macrophages greatly reduce the frequency of DAH. Mice with genetic ablations leading to deficient monocyte development or trafficking are greatly protected from the development of DAH. In *Irf8*$^{-/-}$ mice, monocytes are largely absent in the bone marrow due to defective development whereas neutrophil differentiation is enhanced. Following pristane injection ~ 7 % of B6 *Irf8*$^{-/-}$ mice developed DAH, whereas ~ 80 % of wild-type B6 were affected. Egress of Ly6C^{high} monocytes from the bone marrow into the blood stream and migration to the site of inflammation depends on Ccr2/Ccl2 signaling. In pristane treated *Ccr2*$^{-/-}$ mice, the incidence of DAH was greatly diminished to ~ 20 %. Besides, development of DAH was restored in *Ccr2*$^{-/-}$ mice by infusion of wild-type Ly6C^{high} monocytes. Cx3cr1/Cx3cl1 signaling is linked to the homing of patrolling Ly6C^{low} monocytes. *Cx3cr1*$^{-/-}$ mice showed a significant depletion of lung monocytes and reduced prevalence of DAH by ~ 50 % (Barker et al. 2011, Lee et al. 2019, Zhuang et al. 2017). These results strongly suggest a crucial role of monocytes in the development of

DAH and lead to the question how these cells contribute to the pulmonary tissue damage.

It would be conceivable that myeloid cells are activated by an antigen-antibody-dependent mechanism since pristane administration leads to the generation of a broad spectrum of autoantibodies. Such immune complexes bind Fc receptors and modulate innate and adaptive immune responses. For instance, crosslinking of Fc-γ receptors (FcγR) by binding IgG proteins within immune complexes are known to activate myeloid cells by stimulating phagocytosis and cytokine release. Interestingly, alveolar macrophages and non-classical lung monocytes highly express the high-affinity FcγR1 (CD64). However, *FcγR1*$^{-/-}$ mice show a similar incidence of DAH as wild-type controls after pristane administration which is consistent with the observation that not IgG but IgM is required for DAH development. SLE-like manifestations are associated with accelerated cell death combined with insufficient clearance of dead or dying cells that potentially release damage-associated molecules including DNA. Such stressors activate PRRs like endosomal Tlrs but also inflammasomes that induce the release of highly pro-inflammatory cytokines IL-1β and IL18. Upon activation, pro-IL-1β and pro-IL18 are converted to their biologically active forms by caspase-1 or caspase-11. Interestingly, neither mice deficient in Tlr7, Tlr9, Myd88, Trif, nor caspase-1/11 or IL-1β, show significantly changed incidences of DAH. Although pristane-induced renal complications are dependent on type I IFN production, mice deficient in type I IFN signaling remain susceptible to DAH. In addition, lack of classical proinflammatory macrophage mediators such as TNFα and NOS2 (nitric oxide synthase 2) has no effect on the prevalence of alveolar hemorrhage. In contrast, genetic ablations of the central complement component C3 and CD18 which is a component of the C3b receptors CR3/4 prevent DAH. In addition, deficiency of IL10 accelerates the development of DAH, suggesting IL10 has a protective function (Barker et al. 2011, Lee et al. 2019, Schyns et al. 2019, Zhuang et al. 2017). Taken together, it remains unclear how exactly myeloid cells contribute to the development of DAH and which molecular mechanisms are involved.

1.8 Aim of this thesis

Innate nucleic acid-sensing receptors have contrasting functions. On the one hand, their activation can result in cell death, but on the other they transmit pro-survival signals leading to complex clinical manifestations when errors occur. An abnormal increase in the number of monocyte-derived cells, macrophages and dendritic cells, which are also termed histiocytes, indicates a cancer-like condition termed histiocytosis. In histiocytosis, proliferating histiocytes may form tumors and can be intensely activated damaging several parts of the body. Both Tlr7 and Tlr9 were found to be associated with symptoms similar to those of certain forms of histiocytosis. Disrupted removal of DNA degradation products from lysosomal compartments can lead to chronic activation of Tlr7 resulting in the excessive expansion of patrolling-like monocytes, which accumulate primarily in blood and spleen. DNases function upstream or within these waste-management compartments, preprocessing the DNA of cells to be disposed of. Thus, the loss of DNases may mediate the accumulation of DNA degradation products, which could influence the development of myeloid cells, and provide insights into the role of endogenous DNA-derived ligands in the fate of myeloid cells.

Part one of this work was to investigate whether the loss of individual members of the DNase1 family leads to changes in myeloid cell populations. The recently discovered exonuclease Pld3, which is highly expressed by macrophages and monocyte-derived cells, was selected as a comparative group. A systematic analysis of myeloid cells in blood and spleen, which serves as a reservoir of monocytes, was performed using flow cytometry.

Part two of this thesis was to gain insights into the physiological relevance of the DNase-deficiency mediated alterations of myeloid cell populations. Therefore, a common but unresolved disease model, reflecting the life-threatening pulmonary complications of systemic lupus erythematosus, was chosen in which a single intraperitoneal injection of mineral oil leads to increased cell death, chronic inflammation and lung damage involving monocyte-derived cells. Wild-type, *DNase1*$^{-/-}$, *DNase1l1*$^{-/-}$, *DNase1l2*$^{-/-}$, *DNase1l3*$^{-/-}$ und *Pld3*$^{-/-}$ mice were examined for pulmonary damages and cellular immune responses using flow cytometry. Part of this section was also to investigate which DNA sensors are involved in the development of pristane-induced lung pathology.

2 Methods

2.1 Materials

Table 1 List of antibodies including manufacturer and identifier.

Material	Source	Identifier
Antibodies		
APC/Cyanine7 anti-mouse CD45.2	BioLegend	109824
Brilliant Violet 785 anti-mouse/human CD11b	BioLegend	101243
PE/Cyanine7 anti-mouse CD11c	BioLegend	117318
Anti-Mouse F4/80 Antigen PerCp.Cyanine5.5	TONBObioscience	65-4801-U100
FITC anti-mouse Ly-6C	BioLegend	128006
Brilliant Violet 421 anti-mouse Ly-6G	BioLegend	127628
BV510 Rat anti-mouse I-A/I-E	BD OptiBuild	742893
Brilliant Violet 421 anti-mouse NK-1.1	BioLegend	108741
APC anti-mouse CD16.2 (FcgRIV)	BioLegend	149506
PerCP/Cyanine5.5 anti-mouse CD3e	BioLegend	25-0031-81
PE anti-mouse CD3e	BioLegend	100308
Anti-Mo CD3e, eBioscience PE-Cyanine7	Invitrogen	25-0031-81
BV421 Rat anti-mouse CD45R/B220	BD Horizon	562922
Anti-Hu/Mo CD45R (B220), PE	Invitrogen	12-0452-82
FITC anti-mouse/human CD45R/B220	BioLegend	103206
Anti-Mouse CD8a FITC	eBioscience	11-0081-85
BV421 Rat Anti-Mouse CD8a	BD Horizon	563898
PE CD4 Monoclonal Antibody	eBioscience	12-0042-82
Brilliant Violet 785 anti-mouse CD4	BioLegend	100552
PE anti-mouse CD69	BioLegend	104508
FITC anti-mouse CD317 (Bst2, PDCA-1)	BioLegend	127008
APC anti-mouse CD103	BioLegend	121414
PE anti-rat CD2	BioLegend	201305
PE Mouse Anti-Mouse CD289 (TLR9)	BD Pharmingen	565640

Table 2 List of materials, instruments and sources. Includes cell culture reagents, stimuli, kits, enzymes, commercial assays, instruments, equipment, chemicals as well as other reagents, software and databases.

Material	Source
Cell culture reagents and stimuli	
CELLect Fetal Bovine Serum	MP Biomedicals
Pen Strep Glutamine (100x)	Gibco Life Technologies Corporation
2-Mercaptoethanol	Nacalai Tesque
RPMI 1640 medium	Nacalai Tesque

DMEM (High Glucose) medium	Nacalai Tesque
D-PBS(-) 1x sterile	Nacalai Tesque
M-CSF 100 ug/ml	Peprotech
GM-CSF 10 ug/ml	Peprotech
Blasticidin 10 mg/ml	InvivoGen
Puromycin 10 mg/ml	InvivoGen
Neomycin (G418) 300 mg/ml	Nacalai Tesque
Opti-MEM reduced serum medium	Gibco Life Technologies Corporation
DOTAP Liposomal Transfection Reagent	Roche
Lipofectamine 2000	Invitrogen
FuGENE 6 Transfection Reagent	Promega
Pristane synthetic >=98% (GC)	Sigma
Dimethyl Sulfoxide (DMSO)	Nacalai Tesque
Sterile/Endotoxin free water	InvivoGen
Lipid A, DIPHOSPHORYL	Sigma
CpGB 1826	InvivoGen
CpGB 1668	InvivoGen
CpGA 1585	InvivoGen
CpGA ODN 2216	InvivoGen
CpGB ODN 2006	InvivoGen
2’3’cGAMP	InvivoGen
Pam3csk4	InvivoGen
Sa19	InvivoGen
dsDNA E.Coli	InvivoGen
PolyI:C	InvivoGen
Poly-U	InvivoGen
Flagellin	InvivoGen
R848	InvivoGen
Fsl-1	InvivoGen

Kits, enzymes and other commercial assays	
GenteMACS™ C Tubes	MACS Miltenyi Biotec
MACS SmartStrainers (100 um)	MACS Miltenyi Biotec
Lung Dissociation Kit, mouse	MACS Miltenyi Biotec
Debris Removal Solution	MACS Miltenyi Biotec
RBC Lysis Buffer	BioLegend
ELISA Ready-SET-Go! Anti-Mouse IL6	eBioscience
ELISA Ready-SET-Go! Anti-Mouse IL12p40	eBioscience
ELISA DuoSet Mouse CCL5/RANTES	R&D Systems
ELISA POD Substrate TMB Kit	Nacalai Tesque
RNeasy Plus Mini Kit	QIAGEN

ReverTra Ace qPCR RT Master Mix	TOYOBO
SYBR Green Realtime PCR Master Mix -Plus-	TOYOBO
DNA-1000 Reagent Kit for MultiNA	SHIMADZU Corporation
DNA-500 Reagent Kit for MultiNA	SHIMADZU Corporation
GelStar Nucleic Acid Gel Stain	LONZA
pUC19 DNA/ MspI (HpaII), 23	Thermo Scientific
100 bp DNA Ladder	TaKaRa
TKs Gflex DNA polymerase	TaKaRa
2x Glex PCR Buffer (Mg2+, dNTP plus)	TaKaRa
KOD OneTM PCR Master Mix -blue-	TOYOBO
NEBuilder HiFi DNA Assembly Master Mix M5520AA	New England Biolabs
Quick ligase M2200L	New England Biolabs
2x Quick Ligase Reaction Buffer B2200S	New England Biolabs
FastDigest NotI	Thermo Scientific
FastDigest XhoI	Thermo Scientific
CutSmart Buffer	New England Biolabs
Gene Ladder Fast 2	NIPPON GENE
Gene Ladder Wide 1	NIPPON GENE
6x Loading Buffer	TaKaRa
NucleoSpin Plasmid QuickPure	Macherey-Nagel
QIAquick Gel Extraction Kit/ QIAquick PCR & Gel Cleanup Kit	QIAGEN
Wizard SV Gel and PCR Clean-Up System	Promega
Ampicillin	Sigma
LB broth	Sigma

Instruments and equipment	
GentleMACS Octo Dissociator with Heaters	MACS Miltenyi Biotec
BD LSRFortessa X-20	BD Biosciences
Spectral Cell Analyzer ID7000	Sony
Brightfield Cell Counter CellDrop BF	DeNovix
Countess II FL	Invitrogen
Automated Hematology Analyzer CellTacA MEK-6558	NIHON KOHDEN
CO2 Cell Incubator	Sanyo
Plate washer Hydrospeed	TECAN Austria GmbH
MultiMode Microplate Reader GloMax Explorer	Promega
Automated Vacuum Tissue Processor LEICA ASP200	Leica
EVOS FL Auto Imaging System	Life Technologies

MultiNA	SHIMADZU Corporation
BioShaker BR-32FM	TAITEC
Gel Documentation System ATTO AE-6932GXES	ATTO
Mastercycler nexus GSX1	Eppendorf
Mastercycler nexus GX2	Eppendorf
Submarine electrophoresis system Mupid-exU	ADVANCE
QuantStudio 3	Thermo Fisher Scientific
StepOnePlus (Real-Time PCR System)	Thermo Fisher Scientific
Spectrophotometer NANODROP 2000c	Thermo Scientific
Incubator IC-300A	AS ONE corporation
Laminar Flow Hood	AS ONE corporation
Micro blood collection tube EDTA-2KA U-type	Erma Tokyo
Needle 27G x 3/4”	TERUMO
Needle 26G x 1/2” (0.45x13mm)	TERUMO
Needle 23G x 1 1/4” (0.60x32mm)	TERUMO
Needle 21G x 1 1/2” (0.80x38mm)	TERUMO
Syringe 1 ml	TERUMO
Syringe 5 ml	TERUMO
Syringe 10 ml	TERUMO
Tubes 1.5 ml	AXYGEN
Microtubes (2 ml)	AXYGEN
Tubes 5.0 ml	AXYGEN
D200 Diamond ECO-PACK 2-200 µl	GILSON
10 µl clear Tips	WATSON Bio Lab
D1200 Diamon TIPACK	GILSON

Chemicals and other reagents	
BD FACSFlow optimized sheath fluid for use on flow cytometry instruments	BD Biosciences
20 % Formalin Neutral Buffer Solution for tissue fixation	WAKO FUJIFILM
Pure Eosin Solution	MUTO PURE Chemicals Co. LTD
Mayer’s Hematoxylin Solution	WAKO FUJIFILM
Xylene	WAKO FUJIFILM
99.5 % Ethanol	Nacalai Tesque
Agarose for >= 1kbp fragment	Nacalai Tesque
Ethidium Bromide Solution (0.44 mg/ml)	Nacalai Tesque

Software and databases	
Excel	Microsoft
SnapGene Viewer	Dotmatics
Genetyx	GENETYX CORPORATION
Prism 9	GraphPad Software
FlowJo	BD Biosciences
CRISPRdirect	https://crispr.dbcls.jp/
CCDS Database	https://www.ncbi.nlm.nih.gov/projects/CCDS/CcdsBrowse.cgi
BioGPS	http://biogps.org/#goto=welcome
The Human Protein Atlas	https://www.proteinatlas.org/
Immunological Genome Project (ImmGen)	https://www.immgen.org/

Table 3 List of self-made solutions including ingredients.

Self-made solutions	Ingredients
Lysis Buffer (ES)	10mM Tris pH7.4, 10 mM EDTA, 10 mM NaCl, 0.5 % Sarcosyl
FACS buffer	1x PBS, 2.5 % FCS, 0.1% NaN3
Detachment buffer	0.1 % Tripsin, 0.02% EDTA, PBS, 1% chicken serum, 0.1 % D-Glucose
PBS-Tween	0.05 % Tween 20, 1x PBS

2.2 Mice

Mice were maintained in specific pathogen-free facilities at the Institute of Medical Science, The University of Tokyo (IMSUT) and all animal experiments were approved by the Institutional Animal Care and Use Committee of the IMSUT.

2.3 Generation of genome edited mice

C57BL/6 *DNase1* knockout (*DNase1*$^{-/-}$), *Tlr9* knockout (*Tlr9*$^{-/-}$) and *Tmem173* knockout (*Sting*$^{-/-}$) mice were gifts from Dr. Takuma Shibata (The Institute of Medical Science, The University of Tokyo, Japan), Dr. Ryutaro Fukui (The Institute of Medical Science, The University of Tokyo, Japan) and Dr. Ryota Sato (The Institute of Medical Science, The University of Tokyo, Japan), respectively. *DNase1l1* knockout (*DNase1l1*$^{-/-}$), *DNase1l2* knockout (*DNase1l2*$^{-/-}$), *DNase1l3* knockout (*DNase1l3*$^{-/-}$) and *Pld3* knockout (*Pld3*$^{-/-}$) were generated using a CRISPR/Cas9 system. Highly specific gRNA target sites of *DNase1l1*, *DNase1l2*, *DNase1l3* and *Pld3* genes were identified using CRISPRdirect software (https://crispr.dbcls.jp/) and used to generate chimeric genome edited mice in

the Laboratory of Reproductive Systems Biology, Center for Experimental Medicine and Systems Biology of The Institute of Medical Science (The University of Tokyo, Japan). Briefly, pronuclear zygotes from C57BL/6 mice were microinjected with gRNA and Cas9 protein and subsequently transferred to the oviducts of pseudopregnant female mice. Chimeric candidates of *DNase1l1*$^{-/-}$, *DNase1l2*$^{-/-}$, *DNase1l3*$^{-/-}$ and *Pld3*$^{-/-}$ mice were determined by analyzing polymerase chain reaction products generated with primer pairs flanking the targeted genomic sites using MCE-202 MultiNA Microchip Electrophoresis System for DNA/RNA Analysis (table 4). Genomic alterations were confirmed by DNA sequencing (FASMAC) and promising mutant mice were backcrossed with wild-type C57BL/6 mice. Heterozygous offspring was used to generate knockout mice.

Table 4 Generation of *DNase1l1*$^{-/-}$, *DNase1l2*$^{-/-}$, *DNase1l3*$^{-/-}$ and *Pld3*$^{-/-}$ mice. Sequences of gRNA target sites and primer pairs flanking the targeted genomic region.

Target	gRNA target sequence (5‘->3‘)	Flanking Primer Forward (5‘->3‘)	Flanking Primer Reverse (5‘->3‘)
DNase1l1	GATGCACACATAGCAATGCG	CAGAAGTTGAAATACGTTCC	TCCTTTATGGTCAGGCAG
DNase1l2	AGCACGAGTACGGCTTTGTG	GTGCATCTGTGGGTTTTC	GCAGTATCAACTCACCAC
DNase1l3	TATGTGATTAGTTCTCGACT	GGGAATGCGGAGGCAGATGC	CTCTCACTAGCCTAACACC
Pld3	CGAGGTGTAAAGGTTCGCAT	TTCTTAGGGGGCGCCCGTGG	AGACCTGGGTCAGCGACCGC

2.4 Pristane-induced diffuse alveolar hemorrhage and single-cell preparation

To induce diffuse alveolar hemorrhage in mice (female and male) at the age of 8-10 weeks, 0.5 ml of pristane (Sigma) was administered i.p. and eleven days later mice were analyzed. Controls were left untreated. Peripheral blood was collected in EDTA-containing collection tubes (Erma Tokyo). After euthanizing mice, the peritoneal cavity was flushed with 10 ml RPMI1640 (Nacalai Tesque). Spleens were collected, minced with slide glasses and pipetted several times to disperse the cells in RPMI1640 medium. Splenocyte suspensions were filtered through nylon meshes to remove debris. Lung tissues were harvested at the indicated time points and weights were measured. Single-cell suspensions were obtained using the Lung dissociation Kit (MACS Miltenyi Biotec) and gentleMACS dissector (MACS Miltenyi Biotec) according to the manufacturer’s

instructions with a minor adjustment. Briefly, lungs were transferred into gentleMACS C Tubes containing 2.4 ml 1 x buffer S and chopped into small pieces before adding enzyme P (100 µl) and enzyme A (15 µl) and running program m_LDH_37. The samples were filtered through 100 µm strainers, tubes were washed twice with 2 ml PBS and samples were centrifuged at 300 g for 10 min. Tissue debris was removed by using Debris removal Kit (MACS Miltenyi Biotec) according to the manufacturer's instructions. Briefly, 15 ml falcons containing 4 ml of ice-cold PBS were prepared and stored on ice until used. Cells were resuspended in 8 ml of debris removal solution and transferred to ice-cold PBS-containing tubes using glass Pasteur pipettes to overlay the cell suspension with PBS. Samples were centrifuged at 3000 g for 10 min and supernatants were removed. All samples were stored on ice and treated with RBC lysis buffer (BioLegend) to remove red blood cells before obtaining absolute cell numbers using Countess II FL automated cell counter (Thermo Fisher Scientific) and subjecting to flow cytometry analysis.

2.5 Lung histology

Lungs were collected, shortly washed with PBS to remove superficial blood traces and fixed in 4 % paraformaldehyde for at least 24 h. The fixed lung tissues were embedded in paraffin, cut into 5 µm sections and stained with hematoxylin (WAKO FUJIFILM) and eosin (MUTO PURE Chemicals Co. LTD).

2.6 Murine white blood cell (WBC) and platelet counts

Blood was freshly collected into EDTA-coated tubes and directly subjected to total WBC and platelets counting using the hematology cell counter, Celltac α (Nihon Kohden).

2.7 Plasmid, primer and transformation

Overexpression plasmids were constructed using Gibson assembly-mediated integration (NEBuilder HiFi DNA Assembly Master Mix, New England Biolabs) of target sequences into XhoI/NotI cut pMX4 (with neomycin resistance gene). Firstly, the target sequence was PCR amplified using a cDNA library or genomic DNA as template, secondly extended by overhangs (~ 20 nt complementary to XhoI/NotI cut pMX4 ends) via PCR and subsequently gel purified using the QIAquick Gel Extraction Kit/ QIAquick PCR & Gel Cleanup Kit (QIAGEN). Gibson assembly was performed according to manufacturer's recommendation and mixture was directly heat shock transformed into

competent DH5α *E. Coli*. Suitable clones were identified by colony PCR and plasmid sequence was confirmed by DNA sequencing. Plasmids with correct sequences were used as templates to generate guide-RNA resistant constructs. The pLCV2 (with puromycin resistance gene) plasmid was used to integrate hCAS9 and guide RNA into target cells, whereas pKLV (containing fluorescence marker) was used to express additional guide RNAs when required. Specific guide RNA sequences were designed using the target consensus sequence (obtained from CCDS) and CRISPRdirect (https://crispr.dbcls.jp/). Sequences were extended by overhangs complementary to BamHI cut pLCV2/pKLV ends and synthesized by FASMAC. Complementary oligos were annealed and integrated into plasmids using T4 ligase (Quick Ligation Kit, New England Biolabs).

Table 5 List of primers used for constructing overexpression plasmids

Amplification primer (5'->3')
DNase1l3 Fw: ATGTCCCTGCACCCAGCTTC
DNase1l3 Rv: GGAGCGATTGCCTTTTTTTCTC
DNase1l3 gR resist Fw: CAACTACGTGATCAGCTCCCGGCTGGGAAGAAACACGTACAAAGAG
DNase1l3 gR resist Rv: CTTCCCAGCCGGGAGCTGATCACGTAGTTGTATGTTGTGCTTCTTC
Integration primer (5'->3')
GA DNase1l3 Fw: CTAGCTAGTTAATTAAGGATCTCGAGATGTCCCTGCACCCAGCTTCCCCAC
GA Dnase1l3 pMX IRES Rv: GGGCGGAATTTACGTAGCGGCCGCCTAGGAGCGATTGCCTTTTTTTCTC
Plasmid
pMX4n mDNase1l3 IRES rCD2

Table 6 List of used gRNA oligos, flanking primers and primers integrating edited genomic target sequences into plasmids.

gRNA oligos (5'->3')
DNase1l1 gRNA1 Fw: CACCGATGCACACATAGCAATGCG
DNase1l1 gRNA1 Rv: AAACCGCATTGCTATGTGTGCATC
DNase1l2 gRNA1 Fw: CACCGCACAAAGCCGTACTCGTGCT
Dnase1l2 gRNA1 Rv: AAACAGCACGAGTACGGCTTTGTGC
DNase1l3 gRNA1 Fw: CACCGTATGTGATTAGTTCTCGACT
Dnase1l3 gRNA1 Rv: AAACAGTCGAGAACTAATCACATAC

Pld3 gRNA1 Fw: CACCGATGCGAACCTTTACACCTCG
Pld3 gRNA 1 Rv: AAACCGAGGTGTAAAGGTTCGCATC
Sting gRNA Fw: CACCGCCTCTGGGCCGTGGGATGGC
Sting gRNA Rv: AAACGCCATCCCACGGCCCAGAGGC
Tlr9 gRNA2 Fw: CACCGTCAGCTGCCGCAGGTTGGAC
Tlr9 gRNA2 Rv: AAACGTCCAACCTGCGGCAGCTGAC

Flanking primers (5'->3') to amplify edited genomic region
DNase1l1 gRNA1 check Fw new: CAGAAGTTGAAATACGTTCC
Dnase1l1 gRNA1 check Rv: TCCTTTATGGTCAGGCAG
Dnase1l2 gRNA1 check Fw: GTGCATCTGTGGGTTTTC
Dnase1l2 gRNA1 check Rv: GCAGTATCAACTCACCAC
DNase1l3 gRNA1 check Fw new: GGGAATGCGGAGGCAGATGC
Dnase1l3 gRNA1 check Rv: CTCTCACTAGCCTAACACC
Pld3 gRNA 1 check Fw3: TTCTTAGGGGGCGCCCGTGG
Pld3 gRNA 1 check Rv3: AGACCTGGGTCAGCGACCGC
Sting gRNA check Fw: AGTATTCTCCTGGTACTTCG
Sting gRNA check Rv: AGGCAGGCGCGCACAGCCTT
Tlr9 gRNA2 check Fw: TCTCACAGGTTCTCCGTCGAAGG
Tlr9 gRNA2 check Rv: CACATCAAGTACTCGAAGGGAGG

Integration primers (5'->3')
GA DNase1l1 gR1 check Fw:
CTAGCTAGTTAATTAAGGATCTCGAGGATGAAAAAGCTCTGCCG
GA mDNase1l1 gR1 check Rv:
AGGTCGACCACTGTGCTGGCGGCCGCTCCTTTATGGTCAGGCAG
GA mDNase1l2 gR1 check Fw:
CTAGCTAGTTAATTAAGGATCTCGAGGTGCATCTGTGGGTTTTC
GA mDNase1l2 gR1 check Rv:
AGGTCGACCACTGTGCTGGCGGCCGCGCAGTATCAACTCACCAC
GA mDNase1l3 gR1 check Fw:
CTAGCTAGTTAATTAAGGATCTCGAGGAGACCAGCCTAGTCTAC
GA mDNase1l3 gR1 check Rv:
AGGTCGACCACTGTGCTGGCGGCCGCCTCTCACTAGCCTAACACC
GA mPld3 gRNA1 Fw3 new:
CTAGCTAGTTAATTAAGGATCTCGAGTTCTTAGGGGGCGCCCGTGG
GA mPld3 gRNA1 Rv3 new:
AGGTCGACCACTGTGCTGGCGGCCGCAGACCTGGGTCAGCGACCGC
GA check Sting Fw:
CTAGCTAGTTAATTAAGGATCTCGAGAGTATTCTCCTGGTACTTCG

GA check Sting Rv:
AGGTCGACCACTGTGCTGGCGGCCGCAGGCAGGCGCGCACAGCCTT
GA check TLR9 gR2 Fw:
CTAGCTAGTTAATTAAGGATCTCGAGTCTCACAGGTTCTCCGTCGAAGG
GA check TLR9 gR2 Rv:
AGGTCGACCACTGTGCTGGCGGCCGCCACATCAAGTACTCGAAGGGAGG

2.8 Virus production, retro- and lentiviral transduction

For retroviral overexpression of target cDNA, retroviruses were produced in Plat-E cells ($2x10^5$/500 µl/24-well) by transfecting pMX4 plasmid (200 ng) with FuGene6 (Promega) (0.6 µl) in serum-free Opti-MEM (Gibco Life Technologies Corporation) (20 µl) after 15 min incubation at room temperature. Lentivirus transduction was used to overexpress gRNA and hCAS9. HEK293T ($3x10^5$/500µl/24-well) cells were transfected with pLCV2 plasmid (300 ng), ViraPower Packaging Mix (Thermo Fisher) (200 ng) and PEI (1.2 µl) in serum-free Opti-MEM (total 100 µl). Lentiviral plasmid and PEI were separately incubated in Opti-MEM for 5 min. Following this, both mixtures were combined and incubated for 20-30 min until transfection. Medium was changed the next day and on day 3 supernatants were harvested and centrifuged to pellet any virus producing cells. Virus transduction was conducted immediately by mixing virus supernatant with target cells ($5x10^4$/50 µl/24-well) and DOTAP (Roche) (2-3 µl). In case of non-adherent cells, mixture was centrifuged at 2000 rpm for 60 min. After 24 h and 48 h the supernatant was replaced by fresh cell culture medium. On day 3 transduced cells were analyzed for target gene/marker expression by FACS and afterwards sorted. In case of J774, transduced cells were selected with puromycin (InvivoGen) or neomycin (Nacalai Tesque) until non-transduced control cells were dead. If required monoclonal cell populations were isolated by limiting dilution.

2.9 Cell culture

Cell lines were grown at 37 °C in the presence of 5 % CO_2. J774 mouse macrophages and HEK293T cell lines were maintained in RPMI1640 medium (Nacalai Tesque) supplemented with 10 % fetal bovine serum (MP Biomedicals), 1 x Penicillin-Streptomycin-Glutamine (Gibco Life Technologies Corporation) and 50 µM β-Mercaptoethanol (Nacalai Tesque) in tissue culture plates and collagen-coated tissue culture plates, respectively. Plat-E cells were cultured in DMEM (high glucose) medium

(Nacalai Tesque) with 10 % fetal bovine serum, 1 x Penicillin-Streptomycin-Glutamine (Gibco Life Technologies Corporation), 50 µM β-Mercaptoethanol (Nacalai Tesque), 1 µg/ml puromycin (InvivoGen) and 10 µg/ml blasticidin (InvivoGen) in collagen-coated tissue culture plates. For cell passaging, cells were washed once with 10 ml PBS before detachment with either 2 mM EDTA-PBS (J774) or trypsin/EDTA (HEK293T, Plat-E). EDTA and trypsin were neutralized by adding fresh cell culture medium and removed.

2.10 Flow cytometry and cell sorting

Staining of single-cell suspension from peripheral blood, peritoneal cavity, spleens and lungs were performed in FACS buffer (0.1 % NaN_3, 2.5 % FBS in PBS). To block Fc receptors, cell suspensions were incubated with rat anti-mouse CD16/CD32 mAB (clone: 2.4G2) diluted (500 x) in FACS buffer for 15 min. Then cells were stained by fluorescein-conjugated antibodies for 15-20 min, washed and analyzed using LSRFortessa X-20 (BD Bioscienes) flow cytometry system or sorted by the FACSAria flow cytometer (BD Biosciences). All data were analyzed using FlowJo software (BD Bioscienes).

Table 7 Antibody clones and concentrations used for flow cytometry

Antibody	Clone	Dilution
APC/Cyanine7 anti-mouse CD45.2	104	500
Brilliant Violet 785 anti-mouse/human CD11b	M1/70	2500
PE/Cyanine7 anti-mouse CD11c	N418	1500
Anti-Mouse F4/80 Antigen PerCp.Cyanine5.5	BM8.1	1000
FITC anti-mouse Ly-6C	HK1.4	1000
Brilliant Violet 421 anti-mouse Ly-6G	1A8	1000
BV510 Rat anti-mouse I-A/I-E	M5/114.15.2	1000
Brilliant Violet 421 anti-mouse NK-1.1	PK136	1000
APC anti-mouse CD16.2 (FcgRIV)	9E9	1000
PerCP/Cyanine5.5 anti-mouse CD3e	145-2C11	500
PE anti-mouse CD3e	145-2C11	500
Anti-Mo CD3e, eBioscience PE-Cyanine7	145-2C11	500
BV421 Rat anti-mouse CD45R/B220	RA3-6B2	1000
Anti-Hu/Mo CD45R (B220), PE	RA3-6B2	1000
FITC anti-mouse/human CD45R/B220	RA3-6B2	1000
Anti-Mouse CD8a FITC	53-6.7	500
BV421 Rat Anti-Mouse CD8a	53-6.7	500
PE CD4 Monoclonal Antibody	RM4-5	800

Brilliant Violet 785 anti-mouse CD4	RM4-5	800
PE anti-mouse CD69	H1.2F3	1000
FITC anti-mouse CD317 (Bst2, PDCA-1)	927	800
APC anti-mouse CD103	2E7	500
PE anti-rat CD2	OX-34	1000
PE Mouse Anti-Mouse CD289 (TLR9)	J15A7	200

2.11 *In vitro* cell stimulation and cytokine analysis

To analyze cytokine production, J774 macrophages (5×10^4) and bone marrow-derived cells (1×10^5) were plated in 96-well plates and stimulated with the indicated ligands at indicated concentrations for 24 h. Supernatants were collected, diluted and subjected to ELISA to determine the concentration of mouse CCL5, IL6 and IL12p40 using Mouse CCL5/RANTES DuoSet ELISA Kit (R&D Systems), Mouse IL6 Ready-Set-Go! ELISA Kit (eBioscience) and Mouse IL12p40 Ready-Set-Go! ELISA Kit (eBioscience).

2.12 Quantitative real-time polymerase chain reaction (qPCR)

Total RNA was extracted using RNeasy Mini Kit (QIAGEN) and reverse-transcribed to cDNA using ReverTra Ace qPCR RT Master Mix (TOYOBO). Real-time quantitative PCR ($\Delta\Delta C_T$) was performed using SYBR Green Realtime PCR Master Mix -Plus- (TOYOBO) and StepOnePlus Realtime PCR System (Thermo Fisher Scientific) or Quantstudio 3 (Thermo Fisher Scientific). Expression of target genes was normalized to Hprt.

Table 8 Quantitative real-time PCR primer

Forward primer (5'->3')	Reverse primer (5'->3')
mHprt qPCR Fw: CCCAGCGTCGTGATTAGCGATGA	mHprt qPCR Rv: CCTGTCCATAATCAGTCCATGAG
mIL1b qPCR Fw: TGCCACCTTTTGACAGTGATG	mIL1b qPCR Rv: ATGTGCTGCTGCGAGATTTG
mCxcl1 qPCR Fw: CAAACCGAAGTCATAGCCACA	mCxcl1 qPCR Rv: CCGTTACTTGGGGACACCTTT
mS100a8 qPCR Fw: GTCCTCAGTTTGTGCAGAATATAAA	mS100a8 qPCR Rv: TTTGTGAGATGCCACACCCA

2.13 Generation of bone marrow-derived macrophages and dendritic cells

Bone marrow (BM) was collected from tibiae and femora of wild-type, *DNase1l1*$^{-/-}$, *DNase1l2*$^{-/-}$, *DNase1l3*$^{-/-}$ and *Pld3*$^{-/-}$ mice by flushing bones with RPMI1640, pipetting several times to disperse cells and filtering through nylon mesh to remove debris. Red blood cell lysis was performed using RBC Lysis Buffer (BioLegend). To prepare BM-derived macrophages (BMDMs), 1 x 10^7 cells were cultured in 10 cm non-tissue culture polystyrene petri dishes and differentiated in RPMI1640 (Nacalai Tesque) supplemented with 10 % FBS (MP Biomedicals), 1x Penicillin-Streptomycin-Glutamine (Gibco Life Technologies Corporation), 50 µM β-Mercaptoethanol (Nacalai Tesque) and 100 ng/ml recombinant murine macrophage colony stimulating factor (M-CSF, PreproTech) for 6 days. For BM-derived dendritic cell (BMDCs) generation, 1 x 10^7 cells were cultured in 10 cm tissue culture dishes and differentiated in RPMI1640 supplemented with 10 % FBS, 1x Penicillin-Streptomycin-Glutamine, 50 µM β-Mercaptoethanol (Nacalai Tesque) and 10 ng/ml recombinant murine granulocyte-macrophage colony stimulating factor (GM-CSF, PreproTech) for 7 days. Half of the medium was replaced every other day for BMDMs and on day 3 and 6 for BMDCs.

2.14 Data analysis and statistics

Data were analyzed with Genetyx (GENETYX CORPORATION), FlowJo (BD Biosciences), Microsoft Excel (Microsoft) and GraphPad Prism 9 (Graph Pad Software Inc.). Statistical parameters including the value of n, precision measures (mean ± SEM or SD), methods used to calculate statistical significance and statistical significance are reported in the figures. Data have been statistically analyzed in GraphPad Prism 9 and are considered to be statistically significant when $p < 0.05$. In figures asterisks indicate statistical significance (* $p < 0.05$, ** $p < 0.01$, *** $p < 0.001$, **** $p < 0.0001$).

3 Results

3.1 Characterization of genome edited C57BL/6 mice

To investigate the effect of disturbed self-DNA clearance on myeloid cell populations, their composition and activation state, deoxyribonuclease-deficient C57BL/6 mice were generated. The focus was on members of the DNase1 family and one of the recently discovered lysosomal exonucleases (Pld3) as comparative control. Genomic editing of *DNase1l1*, *DNase1l2*, *DNase1l3* and *Pld3* genes was achieved using a CRISPR/Cas9 system resulting in either a 10 nt deletion in *DNase1l1*, 50 nt deletion in *DNase1l2*, 14 nt insertion in *DNase1l3* or 43 nt deletion in *Pld3* gene (Fig. 5 A-D). Due to these alterations frameshifts occur and premature stop codons can be predicted. In the case of CCDS30223:c.52_61del (*DNase1l1*$^{-/-}$), the deletion of 10 nt in exon 2 results in a change of the amino acid (AA) sequence after 17 AA and a premature stop codon after 47 AA. Predicted active sites of DNase1l1 are located at amino acid position 113 and 164. The 50 nt deletion in *DNase1l2* covers an intronic region including a splice site 10 nt upstream of CCDS37489:c.204 (exon 4) and likely leads to a truncation upstream of the predicted active sites at AA position 99 and 150. The insertion of 14 nt in exon 3 of *DNase1l3* initiates a frameshift and changed the AA sequence that alters the predicted active sites and results in a premature stop codon after 122 AA. In case of CCDS21025:c.434_476del, the missing sequence of 43 nt in exon 8 of *Pld3* results in an altered AA sequence and premature stop codon after 150 AA. Thus, alterations are upstream of predicted active sites at position 199, 201 and 206. Mice that were homozygous for the described mutations were viable, fertile, normal in size and did not display any gross behavioral abnormalities.

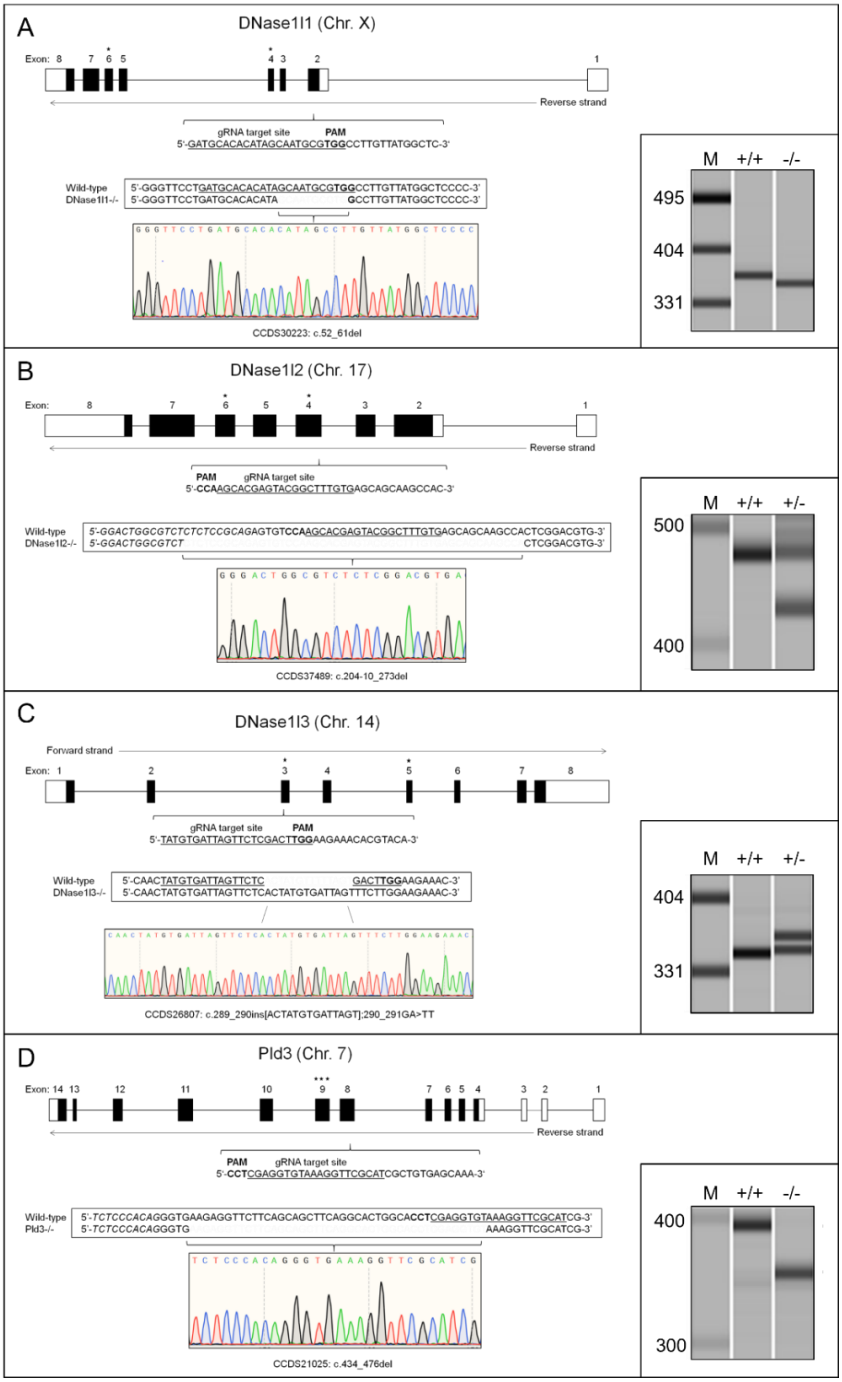

Fig. 5 Generation of *DNase1l1*$^{-/-}$, *DNase1l2*$^{-/-}$, *DNase1l3*$^{-/-}$ and *Pld3*$^{-/-}$ mice. Depiction of the genomic regions of *DNase1l1*, *DNase1l2*, *DNase1l3* and *Pld3* harboring gRNA target sites. Introduction of CRISPR/Cas9-mediated mutations targeting exon 2 of *DNase1l1*, exon 4 of *DNase1l2*, exon 3 of *DNase1l3* and exon 8 of *Pld3* gene. Black boxes represent exons, white boxes highlight untranslated regions and asterisks indicate predicted active sites. The PAM sequence is shown in bold and gRNA target site is underlined. Sequencing results of wild-type and mutated genomic target sites are depicted. Microchip electrophoresis of wild-type and mutant PCR products flanking gRNA target sites show structural changes of genomic regions due to deletions in *DNase1l1*, *DNase1l2* and *Pld3* or an insertion in *DNase1l3*. M: Marker.

3.2 Influence of deoxyribonuclease-deficiency on myeloid cells and their activation state

3.2.1 Profiling of immune cells in spleen and blood

Bone marrow progenitors give rise to myeloid cells in the circulation including neutrophils and monocytes. Monocytes act as circulating sensors that respond to environmental changes and differentiate into macrophages and monocyte-derived dendritic cells (Robinson et al. 2021). Two major populations of monocytes are present in mouse and humans, termed classical and patrolling/non-classical. Classical Ly6C^{high} monocytes are formed primarily in the bone marrow and are released into the circulation where they differentiate into patrolling monocytes or are recruited to tissues by specific chemoattractants. Neutrophils, classical monocytes, monocyte-derived dendritic cells and patrolling monocytes can be discriminated by their expression profiles of Ly6G, CD11b, CD11c, Ly6C, FcγRIV and MHC class II (IA/IE) as previously described (Sato et al. 2020). Here, flow cytometry analysis of isolated cells from peripheral blood (Fig. 6) or spleen (Fig. 7) was used to profile murine myeloid cells and lymphocytes from deoxyribonuclease-deficient mice.

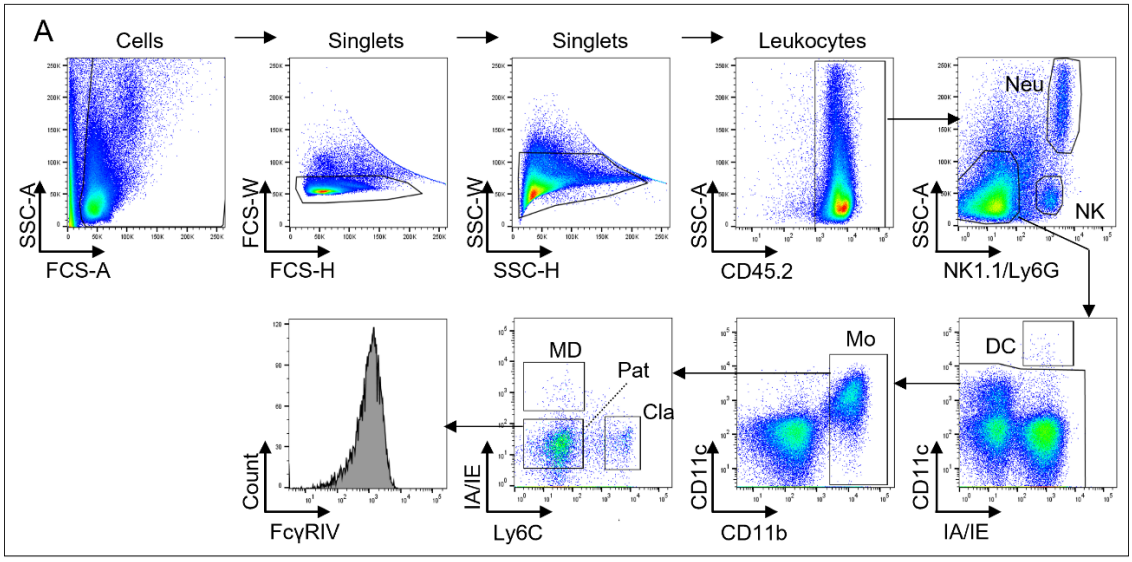

Fig. 6 Gating strategy used to classify myeloid cells in blood. (A) Representative scheme for flow cytometry analysis of isolated cells from peripheral blood after red blood cell lysis showing single-cell leukocytes which were separated into various cell populations including neutrophils (SSC^{high} Ly6G^{+} CD11b^{+}, Neu), NK cells (SSC^{low} NK1.1^{+}, NK), dendritic cells (Ly6G/NK1.1^{-} CD11c^{high} IA/IE^{high}, DC) and monocytes (Ly6G/NK1.1^{-} CD11c^{low} CD11b^{+}, Mo) which were divided into classical (Ly6C^{high} IA/IE^{low}, Cla), patrolling (Ly6C^{low} IA/IE^{low} FcγRIV^{high}, Pat) and monocyte-derived dendritic cells (Ly6C^{low} IA/IE^{high}, MD).

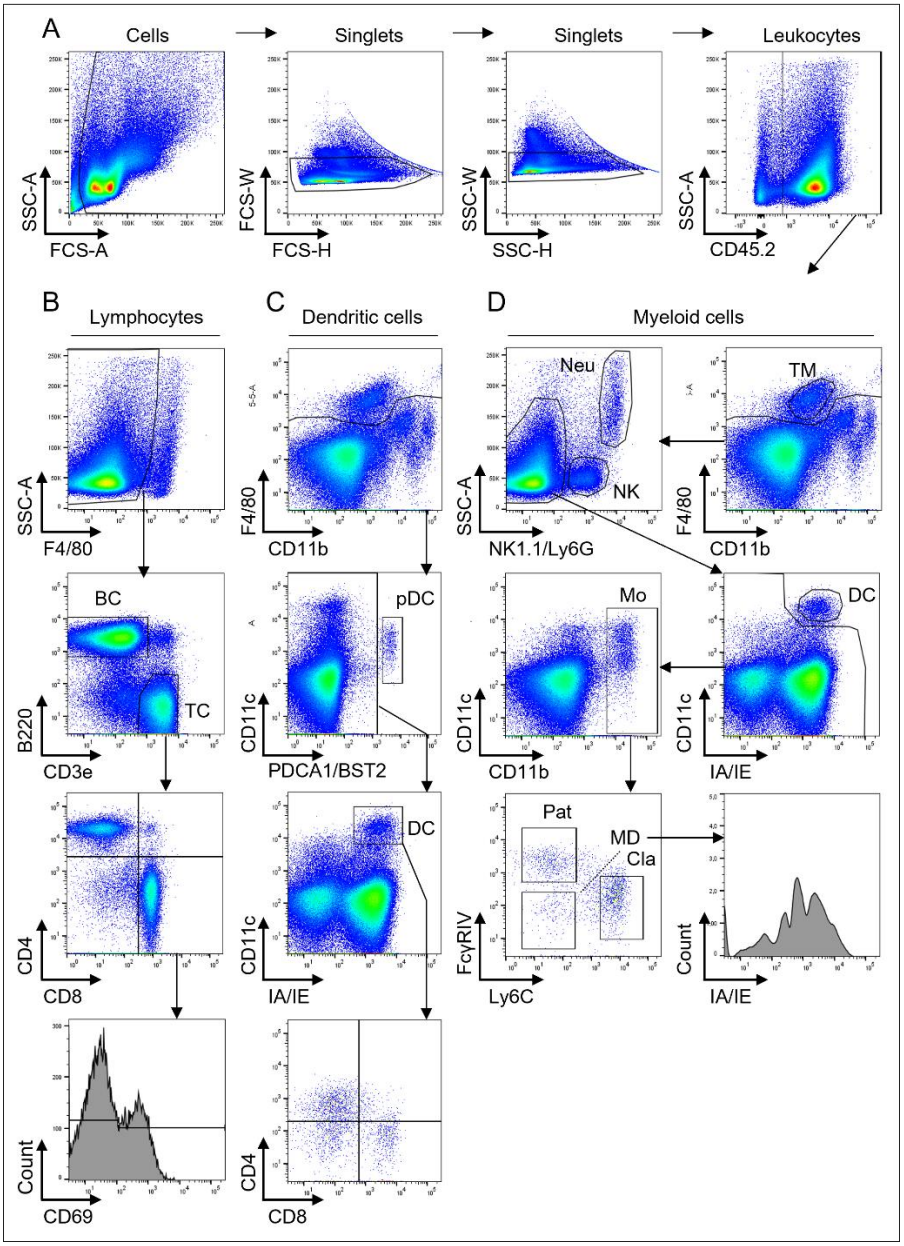

Fig. 7 Gating strategy used to classify myeloid cells and lymphocytes in spleen. (A-D) Representative scheme for flow cytometry analysis of isolated cells from minced spleen tissue. (A) Shared scheme to identify single-cell leukocytes. (B) Strategy to exclude tissue-resident macrophages (F4/80^{+}) and separate B cells (B220^{+}, BC) and T cells (TC, CD3e^{+}). T cells are divided into CD4^{-} CD8^{-}, CD4^{+}, CD8^{+} and CD4^{+} CD8^{+} T cells. Expression of activation marker CD69 was analyzed for individual T cell subsets. (C) Scheme to detect plasmacytoid (PDCA1/BST2^{high} CD11c^{int}, pDC) and conventional (IA/IE^{high} CD11c^{high}, DC) dendritic cells which were further divided into subpopulations depending on their expression of CD4 and CD8. (D) Strategy to identify multiple myeloid cells including tissue-resident macrophages (F4/80^{+} CD11b^{int}, TM), neutrophils (SSC^{high} Ly6G^{+} CD11b^{+}, Neu), NK cells (SSC^{low} NK1.1^{+}, NK), conventional dendritic cells (Ly6G/NK1.1^{-} CD11c^{high} IA/IE^{high}, DC) and monocytes (Ly6G/NK1.1^{-} CD11c^{low} CD11b^{+}, Mo) which were divided into classical (Ly6C^{high} FcγRIV^{low}, Cla), patrolling (Ly6C^{low} FcγRIV^{high}, Pat) and monocyte-derived dendritic cells (Ly6C^{low} FcγRIV^{low} IA/IE^{high}, MD).

3.2.2 DNase1-deficiency has minor effects on immune cells in spleen

To test whether the deficiency of DNase1 influences the frequency and number of immune cell populations in the spleen, four to eight months old male and female C57BL/6 mice were analyzed. *DNase1*$^{-/-}$ mice showed no significant increase in spleen weight and number of splenocytes (Fig. 8 A). Moreover, no significant changes were observed regarding the frequency and total number of tissue-resident macrophages (F4/80^{+} CD11b^{int}), neutrophils (CD11b^{+} Ly6G^{+}), monocytes (Ly6G^{-} CD11b^{+}), patrolling monocytes (Ly6C^{low} FcγRIV^{high}), monocyte-derived dendritic cells (Ly6C^{low} IA/IE^{high}), conventional dendritic cells (CD11c^{high} IA/IE^{high}), plasmacytoid dendritic cells (PDCA-1^{+} CD11c^{int}) and B cells (B220^{high}) (Fig. 8 B-D, F-J). In contrast, the frequency of classical/inflammatory monocytes (Ly6C^{high}) and T cells (CD3e^{+}) seemed significantly decreased compared to wild-type controls, however, such alterations were not confirmed by total cell numbers (Fig. 8 E, K). Thus, DNase1 deficiency did not affect immune cell populations in the spleen of aged (4-8 months) C57BL/6 mice extensively.

3.2.3 DNase1-deficiency mediates expansion of blood monocytes in Tlr9-dependent manner

Although rather negligible alterations of splenic immune cells were observed in DNase1-deficient mice, significant perturbations of myeloid cell populations were identified in peripheral blood. Higher frequencies of Ly6G^{-} CD11b^{+} monocytes, especially FcγRIV^{high} patrolling monocytes were detected (Fig. 9 F, H). In contrast, fractions of classical monocytes (Ly6C^{high}), monocyte-derived dendritic cells (Ly6C^{high} IA/IE^{high}), CD11b^{+} Ly6G^{+} neutrophils, NK cells (NK1.1^{+}), dendritic cells (CD11c^{high} IA/IE^{high}) as well as numbers of platelets and leukocytes (WBC) were unaltered (Fig.9 A-E, G, I).

DNase1 is a secreted nuclease that is thought to be a critical gatekeeper of tolerance by eliminating cell-free DNA that harbors the potential to activate innate immune sensors. Consequently, one would expect that its deficiency leads to the build-up of circulating DNA. Phagocytes take up debris including nucleic acids and shuttle the material to endolysosomal compartments. One could hypothesize that the deficiency of DNase1 results in increased amounts of DNA in endolysosomal compartments where the DNA sensor Tlr9 is localized. Thus, increased activation of Tlr9 might mediate cellular alterations in *DNase1*$^{-/-}$ mice.

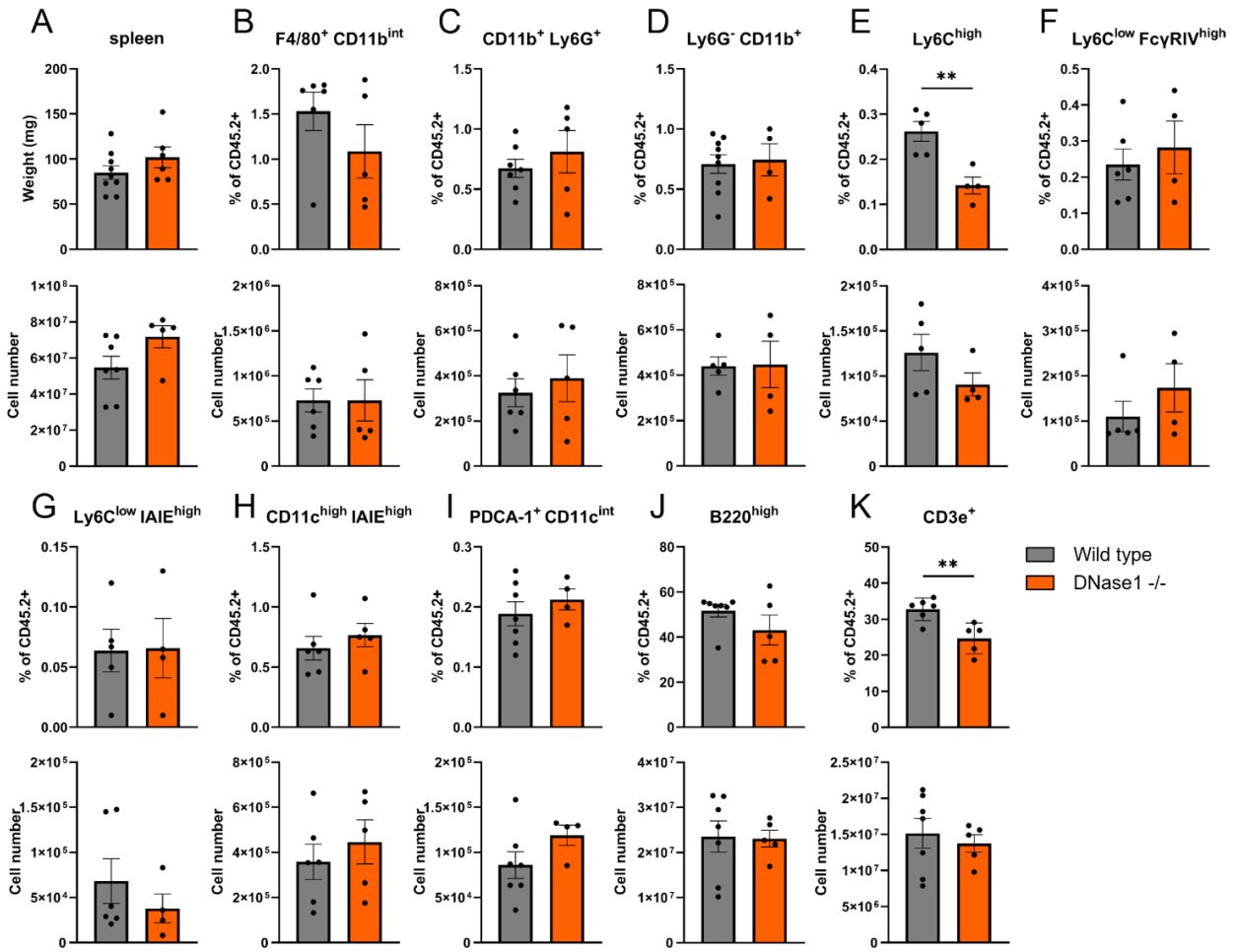

Fig. 8 Splenic immune cell populations in wild-type and *DNase1*$^{-/-}$ mice. (A) Quantitative comparison of spleen weight and total number of spleen cells from wild-type and *DNase1*$^{-/-}$ mice (n = 5-8 per group, means + SEM). (B-K) Quantitative comparison of fractions and total numbers of spleen lymphocytes and myeloid cells from wild-type and *DNase1*$^{-/-}$ mice (n = 5-8 per group, means + SEM) based on flow cytometry analysis. Data are pooled from 3 independent experiments. Statistical analysis was performed using unpaired Student's *t* test. *p < 0.05, **p < 0.01, ***p < 0.001, ****p < 0.0001

To test whether the elimination of Tlr9 signaling leads to the loss of *DNase1*$^{-/-}$-dependent manifestations, *DNase1*$^{-/-}$ mice were crossed with *Tlr9*$^{-/-}$ (C57BL/6) individuals and double deficient mice were bred. As expected, *DNase1*$^{-/-}$ *Tlr9*$^{-/-}$ mice did not manifest expanded fractions of (patrolling) monocytes. Besides, *Tlr9*$^{-/-}$ mice displayed the same cellular composition as wild type (Fig. 9 F, H). Thus, one might conclude that DNase1 prevents Tlr9-dependent expansion of patrolling monocytes in the circulation.

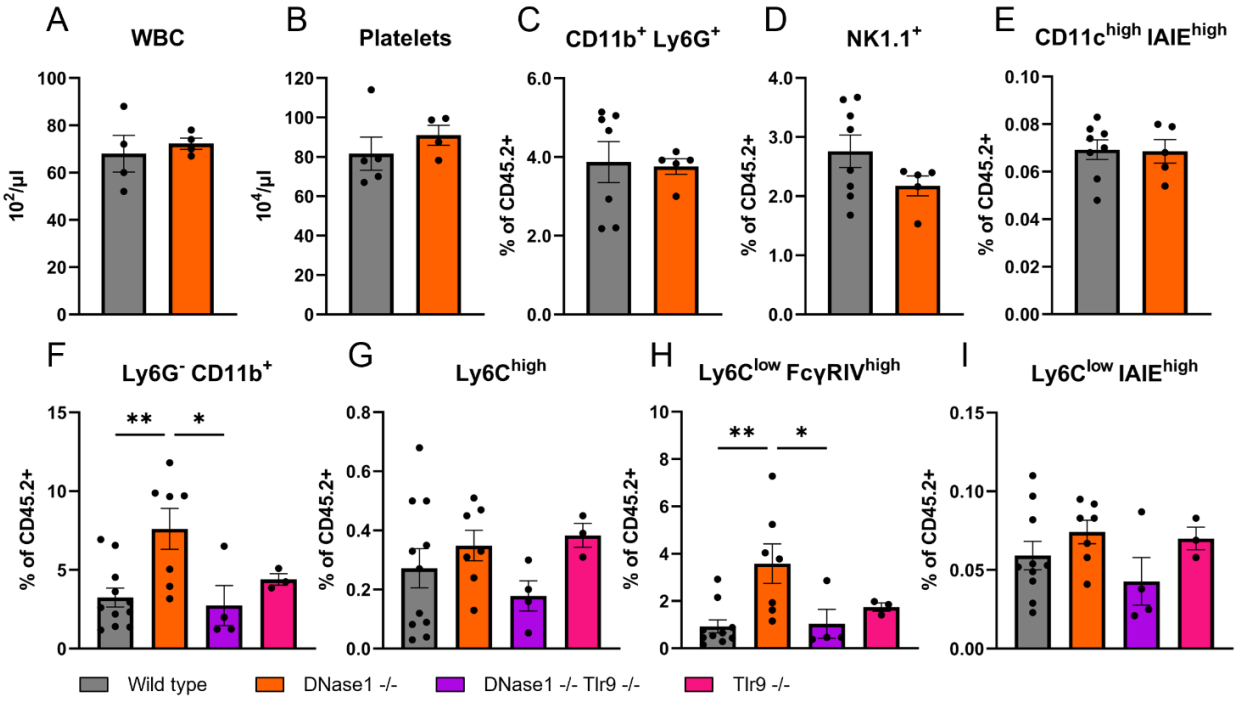

Fig. 9 Myeloid cells in the peripheral blood of *DNase1*$^{-/-}$ and wild-type mice. (A-B) Concentration of white blood cells (leukocytes) (n = 4 per group, means + SEM) and platelets (n = 4-5 per group, means + SEM) in wild-type and *DNase1*$^{-/-}$ mice. (C-E) Quantitative comparison of blood myeloid populations from wild-type and *DNase1*$^{-/-}$ mice (n = 5-7 per group, means + SEM) based on flow cytometry analysis. Data are pooled from 3 independent experiments. (F-I) Quantitative comparison of blood myeloid cells from wild-type, *DNase1*$^{-/-}$, *DNase1*$^{-/-}$ *Tlr9*$^{-/-}$ and *Tlr9*$^{-/-}$ (n = 3-9 per group, means + SEM) based on flow cytometry analysis. Data are pooled from 3 independent experiments. Statistical analysis was performed using unpaired Student's *t* test (A-E) and one-way ANOVA with p values corrected for multiple comparison using Tukey (F-I). *p < 0.05, **p < 0.01, ***p < 0.001, ****p < 0.0001

3.2.4 Expansion of monocyte-derived cells in *DNase1l1*$^{-/-}$ mice

DNase1l1 is a GPI-anchored DNase expressed by monocytes/macrophages that is capable of digesting liposome-coated DNA *in vitro* but its function *in vivo* remains uncertain (Keyel 2017). Here, C57BL/6 *DNase1l1*$^{-/-}$ mice were analyzed regarding potential perturbations of myeloid cell populations in spleen and blood. Firstly, minor expansion of the spleen size and total number of splenocytes was observed, although not significantly changed compared to wild type (Fig. 10 A). Splenic B and T cells, macrophages, monocytes and conventional as well as plasmacytoid dendritic cells were unaltered in frequency and total number (Fig. 10 B, D, H-K). However, a decrease in

neutrophils ($CD11b^+$ $Ly6G^+$) and $Ly6C^{high}$ monocytes accompanied by an increase of $Ly6C^{low}$ IA/IE^{high} monocyte-derived cells was observed (Fig. 10 E, G). Additionally, $Ly6C^{low}$ IA/IE^{high} monocyte-derived cells showed a significantly increased cell number in contrast to other analyzed cell populations (Fig. 10 G).

Interestingly, manifested expansion of $Ly6C^{low}$ IA/IE^{high} monocyte-derived cells was not restricted to the spleen. In peripheral blood, monocytic fractions showed an increasing tendency with a significant enhancement of $Ly6C^{low}$ IA/IE^{high} monocyte-derived cells (Fig. 11 F-I). Frequencies of neutrophils, $NK1.1^+$ or $CD11c^{high}$ IA/IE^{high} cells were not significantly changed (Fig. 11 C-E). Dysregulated numbers of leukocytes and platelets were not observed (Fig. 11 A, B). These results may suggest that DNase1l1-deficiency influences the development of monocyte-derived cells potentially by driving the differentiation of classical monocytes into monocyte-derived dendritic cells. However, DNase1l1-deficient bone marrow-derived macrophages (BMDMs) and dendritic cells (BMDCs) stimulated with various nucleic acid-derived ligands released similar amounts of Ccl5 and IL12p40 compared to wild-type controls. (Fig. 11 J, K). In contrast, DNase1l1-deficient J774 cells released significantly higher amounts of Ccl5 in response to *E. coli* dsDNA complexed with DOTAP (Fig. 11 L). Taken together, DNase1l1-deficiency might influence the development of monocyte-derived cells *in vivo* and the activation state of certain cell types. It is conceivable that cell-specific expression of other DNases influences the proinflammatory response to DNA-derived ligands.

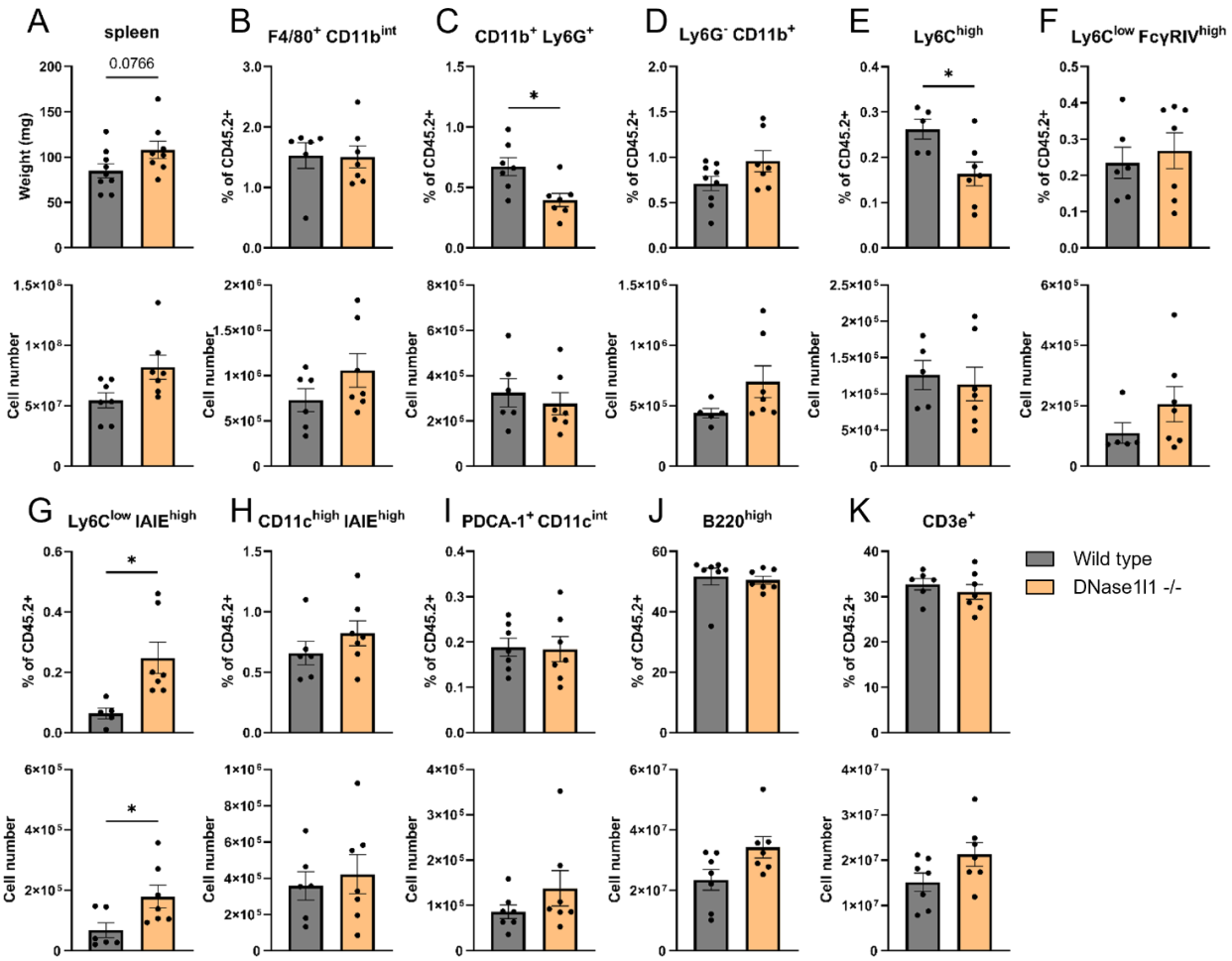

Fig. 10 Splenic immune cell populations in wild-type and *DNase1l1*$^{-/-}$ mice. (A) Quantitative comparison of spleen weight and total number of spleen cells from wild-type and *DNase1l1*$^{-/-}$ mice (n = 7-8 per group, means + SEM). (B-K) Quantitative comparison of fractions and total numbers of spleen lymphocytes and myeloid cells from wild-type and *DNase1l1*$^{-/-}$ mice (n = 5-8 per group, means + SEM) based on flow cytometry analysis. Data are pooled from 3 independent experiments. Statistical analysis was performed using unpaired Student's *t* test. *$p < 0.05$, **$p < 0.01$, ***$p < 0.001$, ****$p < 0.0001$

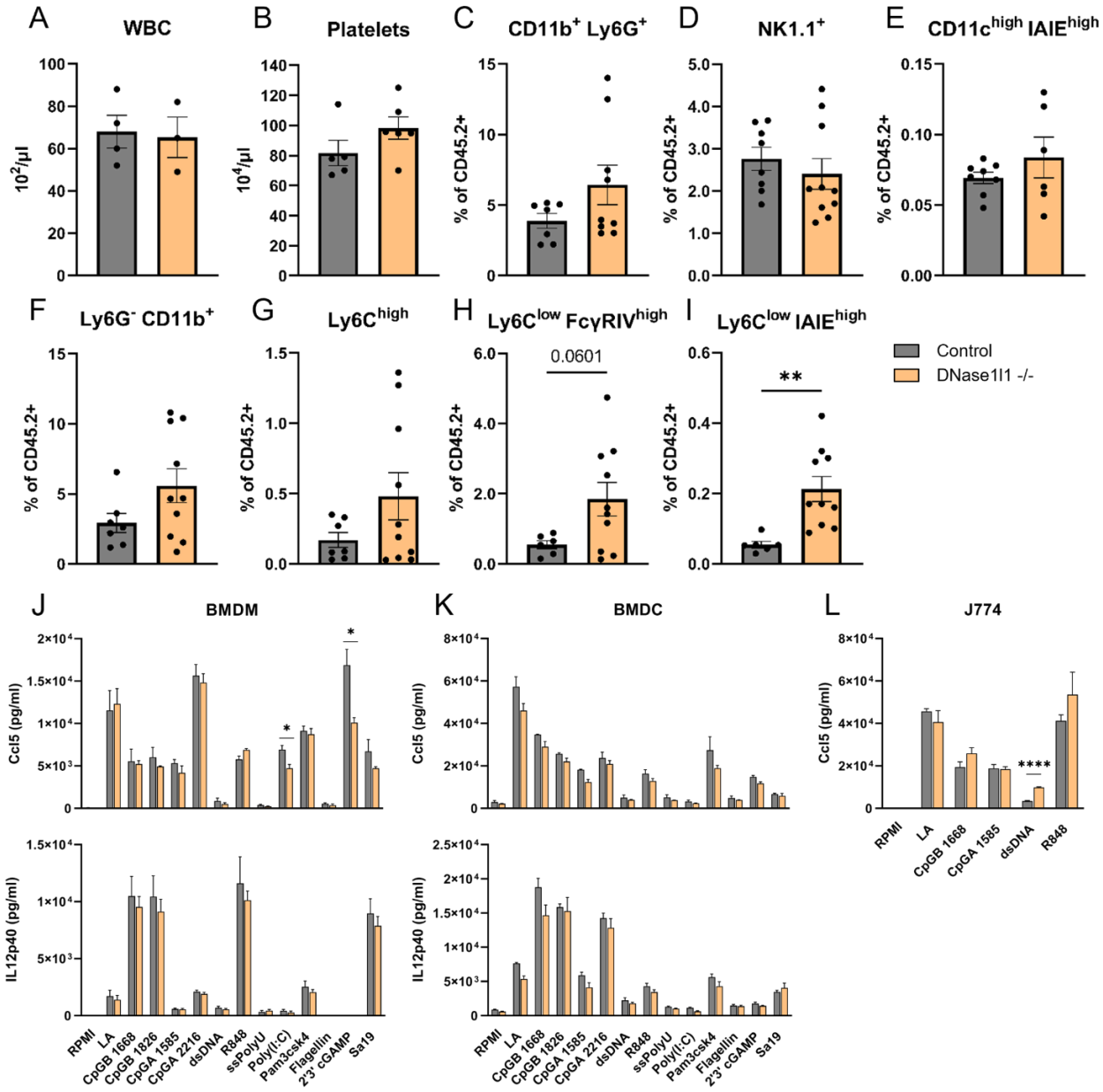

Fig. 11 Myeloid cells in the peripheral blood of *DNase1l1*$^{-/-}$ and wild-type mice. (A-B) Concentration of white blood cells (leukocytes) (n = 3-4 per group, means + SEM) and platelets (n = 5-6 per group, means + SEM) in wild-type and *DNase1l1*$^{-/-}$ mice. (C-I) Quantitative comparison of blood myeloid populations from wild-type (control) and *DNase1l1*$^{-/-}$ mice (n = 7-9 per group, means + SEM) based on flow cytometry analysis. Data are pooled from 3 independent experiments. (J-K) Cytokine secretion of wild-type (control) and *DNase1l1*$^{-/-}$ bone marrow-derived macrophages (BMDM) and dendritic cells (BMDC) stimulated with 100 ng/ml lipid A (LA), 50 nM CpGB 1668, 50 nM CpGB 1826, 1 µg/ml CpGA 1585 + DOTAP, 1 µg/ml CpGA 2216 + DOTAP, 1 µg/ml *E. coli* dsDNA + DOTAP, 50 nM R848, 5 µg/ml ssPolyU, 1 µg/ml Poly(I:C), 1 µg/ml Pam3csk4, 100 ng/ml Flagellin, 7 µg/ml 2'3' cGAMP + lipofectamine 2000 and 1 µg/ml Sa19 (n = 3 per group, means + SEM). One experiment representative of 3 is shown. (L) Cytokine secretion of control (empty vector) and DNase1l1-deficient J774 cells stimulated with

100 ng/ml lipid A, 20 nM CpGB 1668, 1 µg/ml CpGA 1585 + DOTAP, 0.5 µg/ml *E. coli* dsDNA + DOTAP and 100 nM R848 (means + SD of triplicate wells are shown). One representative experiment of more than 3 is presented. Statistical analysis was performed using unpaired Student's *t* test. *$p < 0.05$, **$p < 0.01$, ***$p < 0.001$, ****$p < 0.0001$

3.2.5 Increase of patrolling monocytes in *DNase1l2*$^{-/-}$ mice

Here, the cellular composition of myeloid cells and lymphocytes in spleen as well as blood was examined to gain more insights into potential functions of DNase1l2 in secondary lymphoid tissues. In *DNase1l2*$^{-/-}$ mice, the fraction of monocytes as well as their total number was expanded in the spleen (Fig. 12 D). Further analysis revealed an increase of Ly6C^{low} FcγRIV^{high} patrolling monocytes without significant alterations of other monocytic cell populations (Fig. 12 E-G). The spleen size and total number of splenocytes was not significantly changed under the established criteria ($p = 0.0578$, Fig. 12 A) but showed an increasing trend. Consequently, the number of B cells, T cells, conventional as well as plasmacytoid dendritic cells was increased although not significantly changed in *DNase1l2*$^{-/-}$ (Fig. 12 H-K). Tissue-resident macrophages and neutrophils did not show any alterations in cellular fraction or total number of cells (Fig. 12 B, C).

Expansion of patrolling monocytes was also detected in peripheral blood samples of *DNase1l2*$^{-/-}$ mice, while the fraction of monocytes was unaltered (Fig. 13 F, H). Thus, DNase1l2-deficiency influences accumulation of patrolling monocytes in spleen and blood. *DNase1l2*$^{-/-}$ J774 cells showed an increased release of Ccl5 upon stimulation with DNA ligands including CpGA (1585) and *E. coli* dsDNA both transfected with DOTAP but also upon treatment with naked dsRNA ligand polyI:C (TLR3 agonist) (Fig. 13 L). In addition, *DNase1l2*$^{-/-}$ BMDCs displayed stronger responses towards transfected Tlr9 agonists CpGA (2216) and *E. coli* dsDNA compared to wild-type controls (Fig. 13 K). Bone marrow-derived macrophages seemed to be unaffected by DNase1l2-deficiency since analyzed cytokine secretion was not perturbed (Fig. 13 J). These results suggest that DNase1l2 might limit availability of immunogenic DNA in certain cell types and subsequently dampens endosomal Tlr signaling.

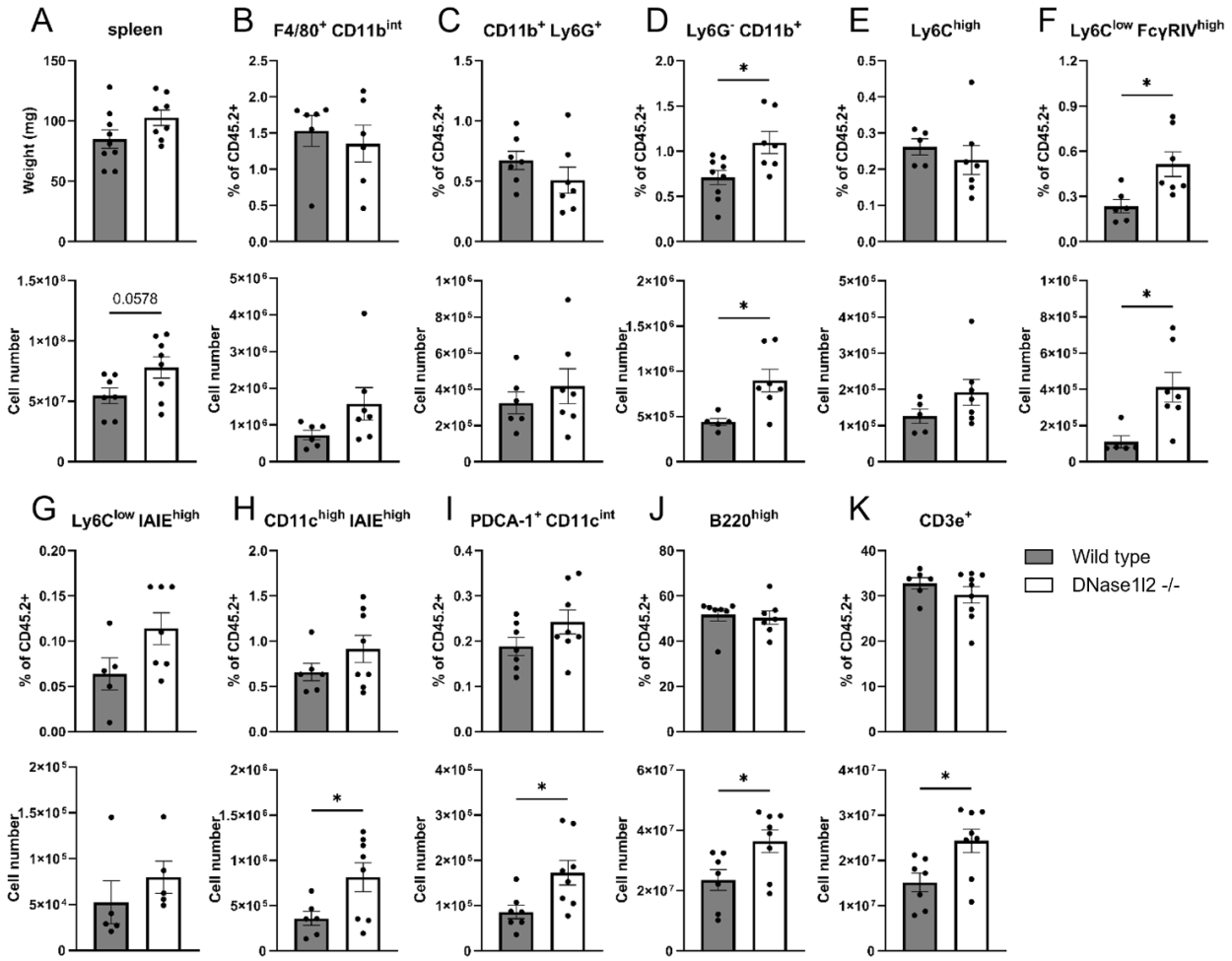

Fig. 12 Splenic immune cell populations in wild-type and *DNase1l2*$^{-/-}$ mice. (A) Quantitative comparison of spleen weight and total number of spleen cells from wild-type and *DNase1l2*$^{-/-}$ mice (n = 7-8 per group, means + SEM). (B-K) Quantitative comparison of fractions and total numbers of spleen lymphocytes and myeloid cells from wild-type and *DNase1l2*$^{-/-}$ mice (n = 5-8 per group, means + SEM) based on flow cytometry analysis. Data are pooled from 3 independent experiments. Statistical analysis was performed using unpaired Student's *t* test. *p < 0.05, **p < 0.01, ***p < 0.001, ****p < 0.0001

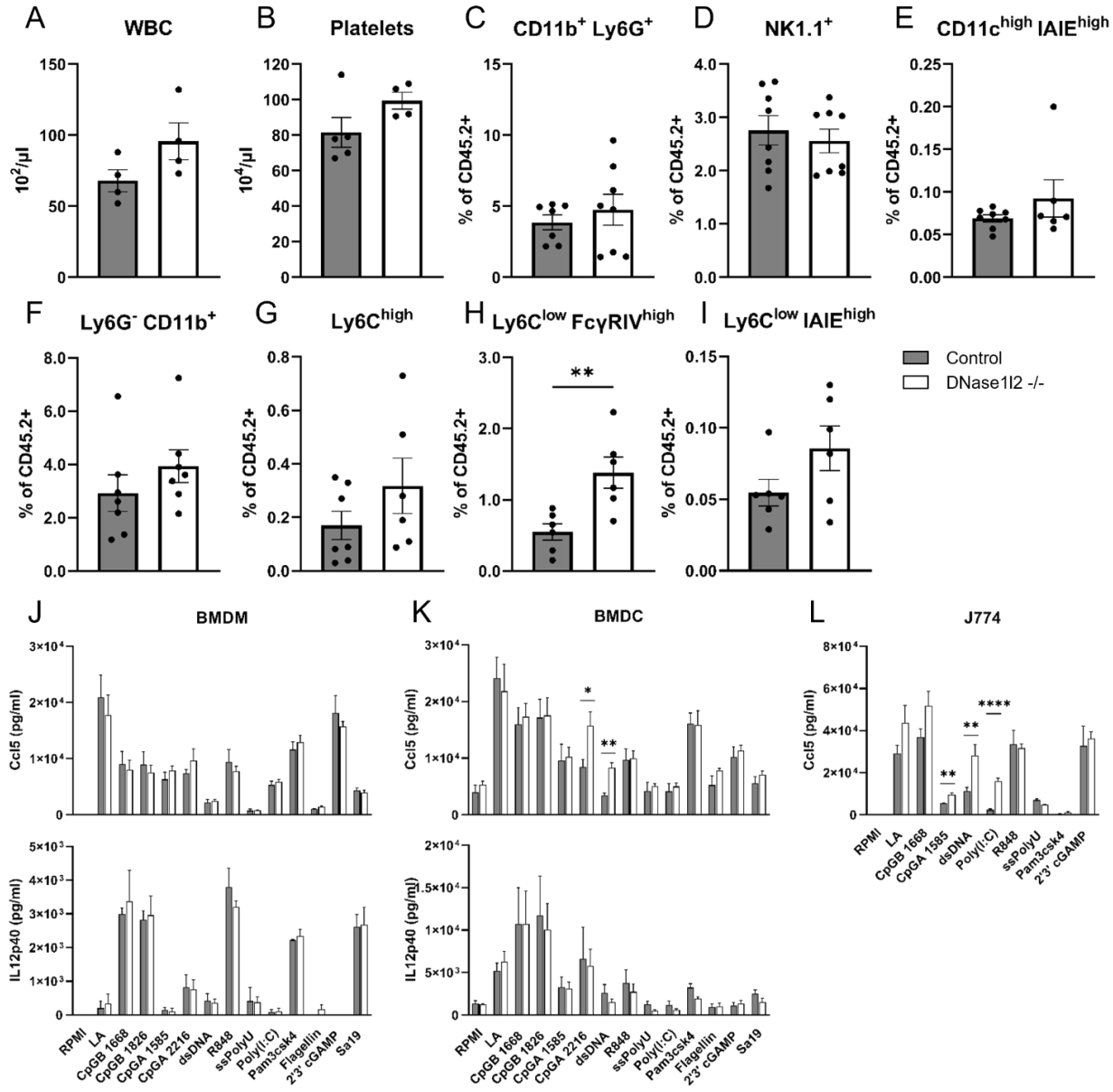

Fig. 13 Myeloid cells in the peripheral blood of *DNase1l2*$^{-/-}$ and wild-type mice. (A-B) Concentration of white blood cells (leukocytes) (n = 4 per group, means + SEM) and platelets (n = 4-5 per group, means + SEM) in wild-type and *DNase1l2*$^{-/-}$ mice. (C-I) Quantitative comparison of blood myeloid populations from wild-type (control) and *DNase1l2*$^{-/-}$ mice (n = 7-8 per group, means + SEM) based on flow cytometry analysis. Data are pooled from 3 independent experiments. (J-K) Cytokine secretion of wild-type (control) and *DNase1l2*$^{-/-}$ bone marrow-derived macrophages (BMDM) and dendritic cells (BMDC) stimulated with 100 ng/ml lipid A (LA), 50 nM CpGB 1668, 50 nM CpGB 1826, 1 µg/ml CpGA 1585 + DOTAP, 1 µg/ml CpGA 2216 + DOTAP, 1 µg/ml *E. coli* dsDNA + DOTAP, 50 nM R848, 5 µg/ml ssPolyU, 1 µg/ml Poly(I:C), 1 µg/ml Pam3csk4, 100 ng/ml Flagellin, 7 µg/ml 2'3' cGAMP + lipofectamine 2000 and 1 µg/ml Sa19 (n = 3 per group, means + SEM). One experiment representative of 3 is shown. (L) Cytokine secretion of control (empty vector) and DNase1l2-deficient J774 cells stimulated with

100 ng/ml lipid A, 20 nM CpGB 1668, 1 µg/ml CpGA 1585 + DOTAP, 1 µg/ml *E. coli* dsDNA + DOTAP, 1 µg/ml Poly(I:C), 50 nM R848, 5 µg/ml ssPolyU, 1 µg/ml Pam3csk4 and 7 µg/ml 2'3' cGAMP + lipofectamine 2000 (means + SD of triplicate wells are shown). One representative experiment of more than 3 is presented. Statistical analysis was performed using unpaired Student's *t* test. *$p < 0.05$, **$p < 0.01$, ***$p < 0.001$, ****$p < 0.0001$

3.2.6 Increased frequency of monocyte-derived cells in *DNase1l3*$^{-/-}$ mice

DNase1l3 is a secreted nuclease that is highly expressed by conventional dendritic cells, macrophages and enriched in lymphoid tissue, bone marrow as well as liver. Recently, it was shown that DNase1l3 digests extracellular microparticle-associated chromatin and loss of this waste-management process contributes to lupus-like manifestations in mice including anti-DNA responses, expansion of monocyte populations in peripheral blood and splenomegaly (Sisirak et al. 2016).

In *DNase1l3*$^{-/-}$ mice used here, increased but not significantly altered spleen weights and numbers of splenocytes were detected (Fig. 14 A). Cellular compositions of splenocytes were mostly comparable to wild-type animals. Fractions and total cell numbers of macrophages, neutrophils, dendritic cells and B cells did not significantly differ from controls (Fig. 14 B, C, H-J). Rates of CD3e^{+} T cells were unchanged but total cell numbers were slightly though significantly increased in comparison to wild-type controls, presumably due to the overall expansion of splenocytes in *DNase1l3*$^{-/-}$ mice (Fig. 14 A, K). Besides, composition of T cell subsets and activation state were unaltered in spleen (Fig. 18 B, C). In contrast, the percentage of monocytes including Ly6C^{low} IA/IE^{high} monocyte-derived dendritic cells was clearly elevated (Fig. 14 D, G).

In peripheral blood, platelet concentrations and fractions of neutrophils, NK1.1^{+} cells, dendritic cells and monocytes including classical and patrolling subsets were not significantly changed (Fig. 15 B-H). However, rates of Ly6C^{low} IA/IE^{high} monocyte-derived cells were significantly expanded in blood as well as spleen from *DNase1l3*$^{-/-}$ mice (Fig. 15 G, 14 I). These results might suggest that DNase1l3-deficiency promotes the generation of Ly6C^{low} MHC class II expressing monocyte-derived cells.

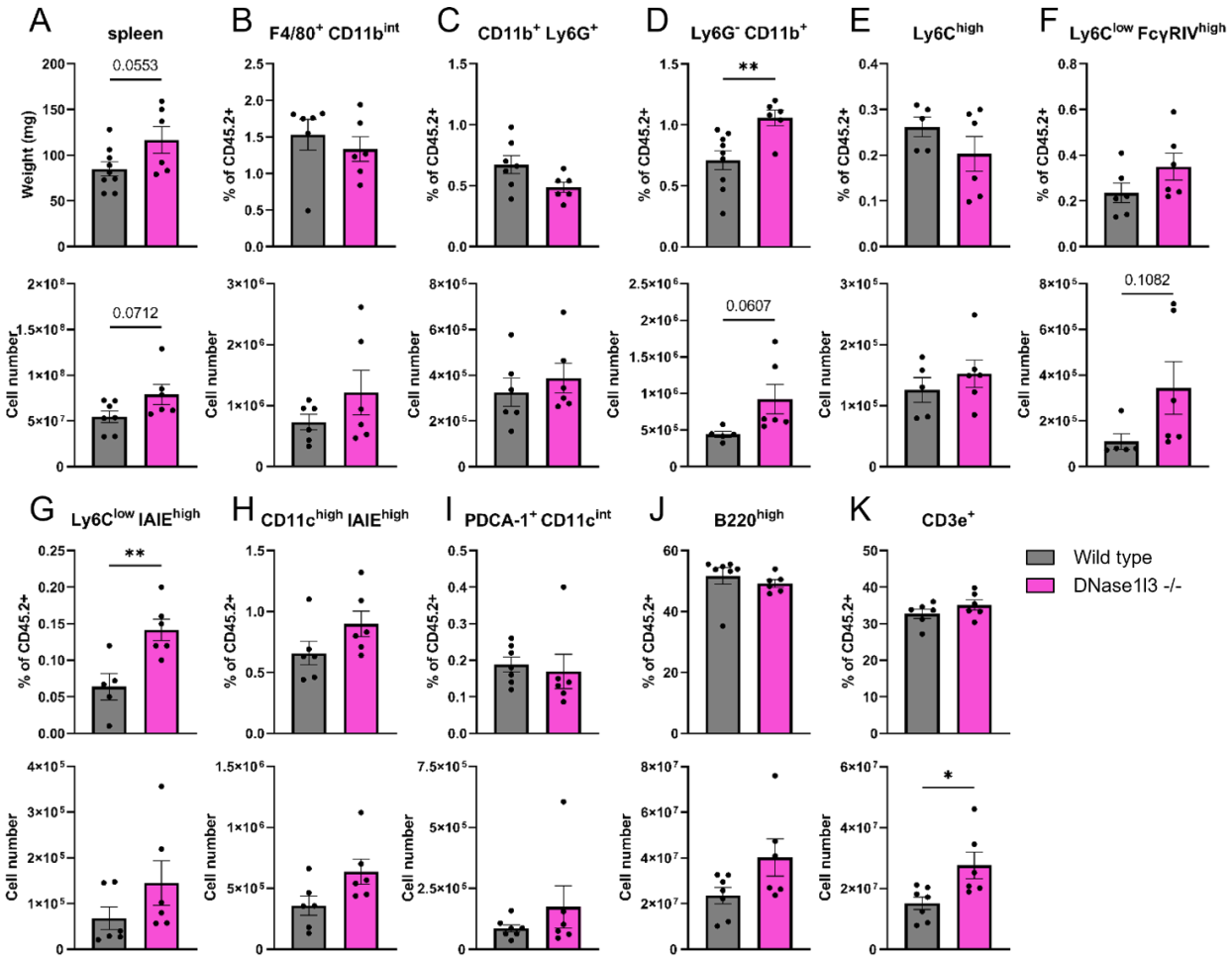

Fig. 14 Splenic immune cell populations in wild-type and *DNase1l3*$^{-/-}$ mice. (A) Quantitative comparison of spleen weight and total number of spleen cells from wild-type and *DNase1l3*$^{-/-}$ mice (n = 6-7 per group, means + SEM). (B-K) Quantitative comparison of fractions and total numbers of spleen lymphocytes and myeloid cells from wild-type and *DNase1l3*$^{-/-}$ mice (n = 5-8 per group, means + SEM) based on flow cytometry analysis. Data are pooled from 3 independent experiments. Statistical analysis was performed using unpaired Student's *t* test. *$p < 0.05$, **$p < 0.01$, ***$p < 0.001$, ****$p < 0.0001$

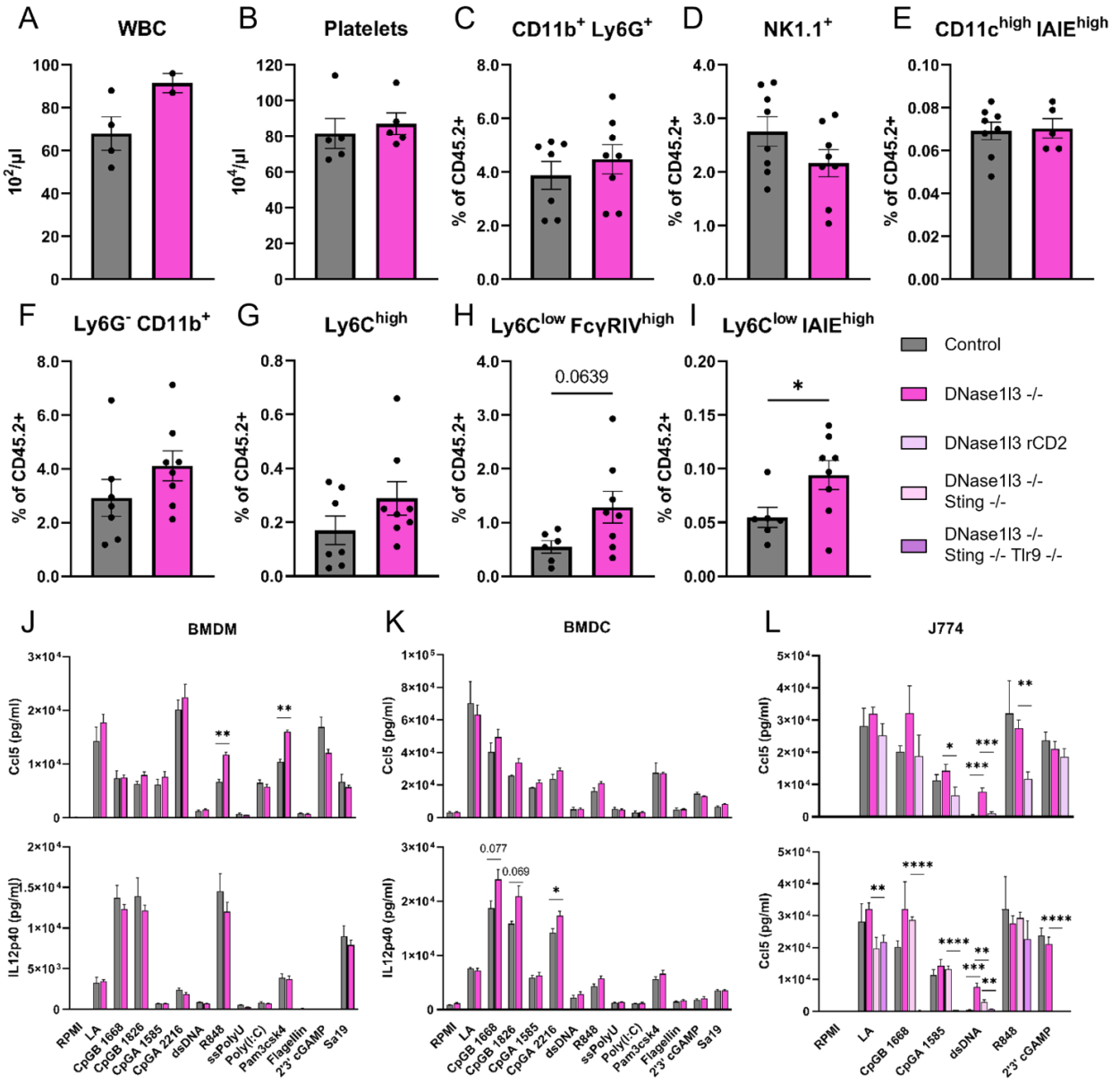

Fig. 15 Myeloid cells in the peripheral blood of *DNase1l3*$^{-/-}$ and wild-type mice. (A-B) Concentration of white blood cells (leukocytes) (n = 3-4 per group, means + SEM) and platelets (n = 5 per group, means + SEM) in wild-type and *DNase1l3*$^{-/-}$ mice. (C-I) Quantitative comparison of blood myeloid populations from wild-type (control) and *DNase1l3*$^{-/-}$ mice (n = 7-8 per group, means + SEM) based on flow cytometry analysis. Data are pooled from 3 independent experiments. (J-K) Cytokine secretion of wild-type (control) and *DNase1l3*$^{-/-}$ bone marrow-derived macrophages (BMDM) and dendritic cells (BMDC) stimulated with 100 ng/ml lipid A (LA), 50 nM CpGB 1668, 50 nM CpGB 1826, 1 µg/ml CpGA 1585 + DOTAP, 1 µg/ml CpGA 2216 + DOTAP, 1 µg/ml *E. coli* dsDNA + DOTAP, 50 nM R848, 5 µg/ml ssPolyU, 1 µg/ml Poly(I:C), 1 µg/ml Pam3csk4, 100 ng/ml Flagellin, 7 µg/ml 2'3' cGAMP + lipofectamine 2000 and 1 µg/ml Sa19 (n = 3 per group, means + SEM). One experiment representative of 3 is shown. (L) Cytokine secretion of control (empty vector), *DNase1l3*$^{-/-}$, *DNase1l3*$^{-/-}$ reconstituted with murine CRISPR/Cas9 resistant DNase1l3 (DNase1l3 rCD2), *DNase1l3*$^{-/-}$ *Sting*$^{-/-}$ and *DNase1l3*$^{-/-}$

Sting$^{-/-}$ *Tlr9*$^{-/-}$ J774 cells stimulated with 100 ng/ml lipid A, 20 nM CpGB 1668, 1 µg/ml CpGA 1585 + DOTAP, 1 µg/ml *E. coli* dsDNA + DOTAP, 50 nM R848 and 7 µg/ml 2'3' cGAMP + lipofectamine 2000 (means + SD of triplicate wells are shown). One representative experiment of more than 3 is presented. Statistical analysis was performed using unpaired Student's *t* test (A-K) and one-way ANOVA with p values corrected for multiple comparison using Tukey (L). *p < 0.05, **p < 0.01, ***p < 0.001, ****p < 0.0001

DNase1l3 is highly expressed by dendritic cells and macrophages, thus one might expect altered proinflammatory responses of bone marrow-derived myeloid cells upon DNA sensor stimulation. However, bone marrow-derived dendritic cells from wild-type and *DNase1l3*$^{-/-}$ animals responded to endosomal and cytoplasmic DNA sensor ligands mostly similarly, only upon stimulation with Tlr9 ligand CpGA (2216) significantly increased release of IL12p40 was detected (Fig. 15 K).

Additionally, DNase1l3-deficient J774 cells displayed an elevated response towards transfected bacterial dsDNA that was rescued by overexpressing CRISPR/Cas9 resistant murine DNase1l3 (DNase1l3 rCD2), and potentially mediated by both Tlr9- and cGas-Sting-signaling (Fig. 15 L). In contrast, *DNase1l3*$^{-/-}$ BMDMs secreted similar amounts of Ccl5 compared to wild-type controls upon transfection of bacterial dsDNA, while enhanced responses towards Tlr7 ligand R848 and Tlr2/1 ligand Pam3csk4 were observed (Fig. 15 J). Taken together, lack of DNase1l3 provides a milieu favoring the generation of monocyte-derived cells expressing MHC class II (IA/IE).

3.2.7 Expansion of monocytes and splenomegaly in *Pld3*$^{-/-}$ mice

Pld3 is highly expressed in murine macrophages among other immune cells and can be detected in various organs including brain, bone marrow and lymphoid tissues in mice and humans according to The Human Protein Atlas and BioGPS databases. In contrast to the endonuclease DNase 1 family members, Pld3 has recently been identified as a single-stranded acid 5'-exonuclease that primarily functions in endolysosomal compartments by degrading nucleic acids and thereby dampening Tlr signaling (Gavin et al. 2018).

Here, *Pld3*$^{-/-}$ C57BL/6 mice were generated and examined regarding changes in the composition of immune cells in spleen and blood. Firstly, it is shown that splenomegaly

can occur in *Pld3*$^{-/-}$ mice from the age of 5 months, since spleen weight and total cell numbers were significantly increased compared to wild-type controls (Fig. 16 A). Cellular fractions of macrophages, neutrophils, dendritic cells, B cells and T cells were unaffected, while total cell numbers were elevated in case of cDC, B cells and T cells in *Pld3*$^{-/-}$ spleens (Fig. 16 B, C, H, J, K). Total cell numbers of monocytes including patrolling and monocyte-derived dendritic cells (MoDCs) were significantly enhanced, whereas only the percentage of MoDCs was clearly expanded (Fig. 16 D, F, G). In addition, fractions of both CD4^{+} and CD8^{+} T cells seemed to be activated in Pld3$^{-/-}$ spleens since increased proportions of CD69^{+} T cells were measured (Fig. 18 C).

In peripheral blood samples from *Pld3*$^{-/-}$ mice, elevated concentrations of platelets were detected and both classical as well as patrolling monocytes but not Ly6C^{low} IA/IE^{high} cells accumulated (Fig. 17 B, F-I). These results may suggest a systemic expansion of monocytes and augmented differentiation of monocytes into monocyte-derived cells in certain microenvironments. In addition, *Pld3*$^{-/-}$ BMDMs and J774 cells showed elevated cytokine responses upon stimulation with various Tlr9 and Tlr7 ligands (Fig. 17 J, L). Macrophages derived from Pld3-deficient bone marrow secreted higher amounts of both Ccl5 and IL12p40 after CpGA (2216) and *E. coli* dsDNA stimulation, whereas Tlr7 agonist R848 lead solely to an increased release of Ccl5 (Fig. 17 J). In Pld3-deficient J774 cells, activation of Tlr9 signaling by bacterial dsDNA, CpGB (1668) and CpGA (1585) lead to an elevated secretion of both Ccl5 and IL6 (Fig. 17 L). In addition, Tlr7 stimulation by R848 and ssPolyU resulted in an enhanced level of IL6 released by *Pld3*$^{-/-}$ J774 cells in comparison to control cells. In contrast, *Pld3*$^{-/-}$ bone marrow-derived dendritic cells seemed to respond to Tlr9 (CpGB 1668,1826) and Tlr7 (R848) ligands with similar or lower intensity in case of IL12p40 compared to wild-type BMDCs (Fig. 17 K).

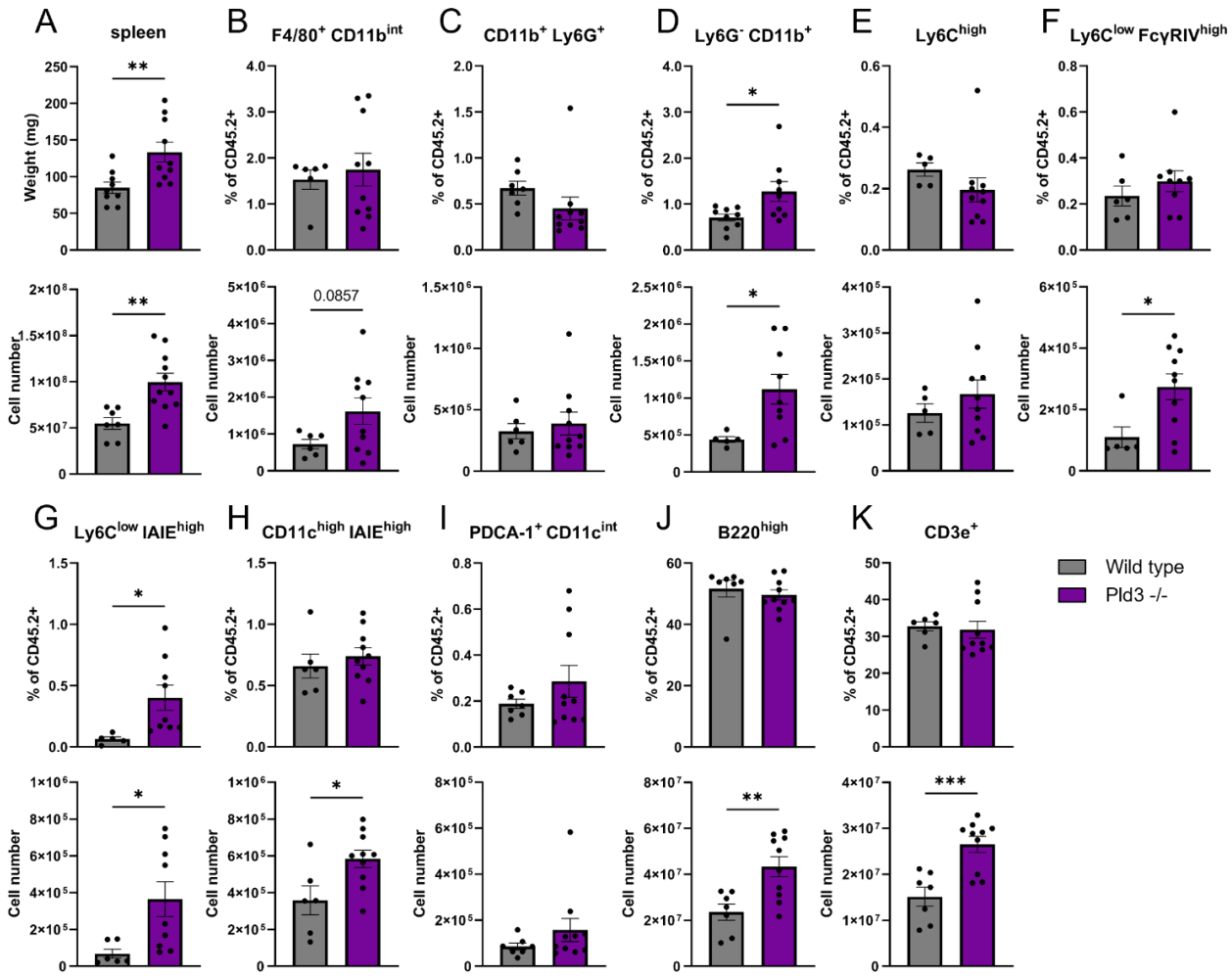

Fig. 16 Splenic immune cell populations in wild-type and *Pld3*$^{-/-}$ mice. (A) Quantitative comparison of spleen weight and total number of spleen cells from wild-type and *Pld3*$^{-/-}$ mice (n = 7-10 per group, means + SEM). (B-K) Quantitative comparison of fractions and total numbers of spleen lymphocytes and myeloid cells from wild-type and *Pld3*$^{-/-}$ mice (n = 7-10 per group, means + SEM) based on flow cytometry analysis. Data are pooled from 3 independent experiments. Statistical analysis was performed using unpaired Student's *t* test. *p < 0.05, **p < 0.01, ***p < 0.001, ****p < 0.0001

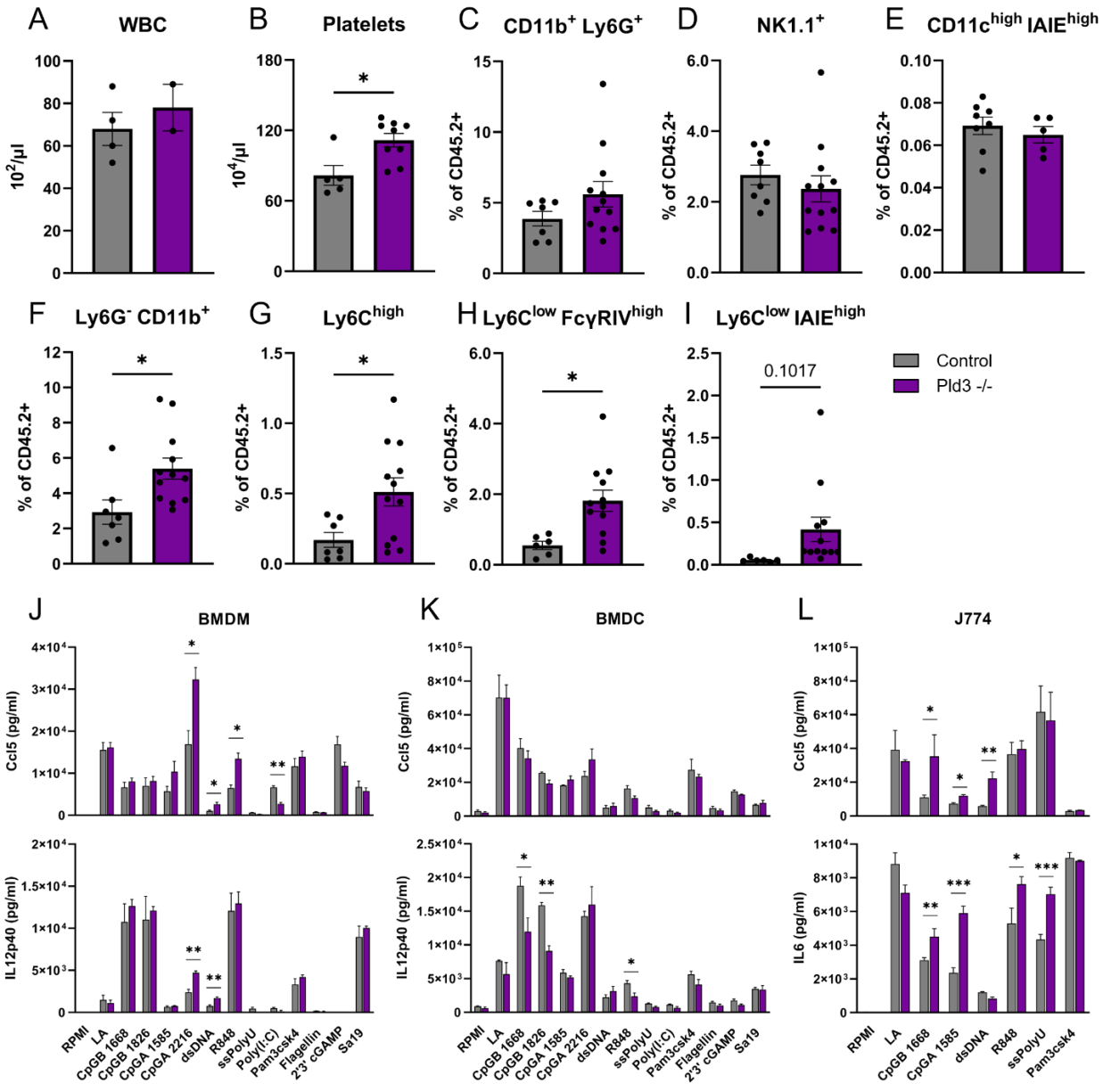

Fig. 17 Myeloid cells in the peripheral blood of *Pld3*$^{-/-}$ and wild-type mice. (A-B) Concentration of white blood cells (leukocytes) (n = 3-4 per group, means + SEM) and platelets (n = 5-9 per group, means + SEM) in wild-type and *Pld3*$^{-/-}$ mice. (C-I) Quantitative comparison of blood myeloid populations from wild-type (control) and *Pld3*$^{-/-}$ mice (n = 7-12 per group, means + SEM) based on flow cytometry analysis. Data are pooled from 4 independent experiments. (J-K) Cytokine secretion of wild-type (control) and *Pld3*$^{-/-}$ bone marrow-derived macrophages (BMDM) and dendritic cells (BMDC) stimulated with 100 ng/ml lipid A (LA), 50 nM CpGB 1668, 50 nM CpGB 1826, 1 µg/ml CpGA 1585 + DOTAP, 1 µg/ml CpGA 2216 + DOTAP, 1 µg/ml *E. coli* dsDNA + DOTAP, 50 nM R848, 5 µg/ml ssPolyU, 1 µg/ml Poly(I:C), 1 µg/ml Pam3csk4, 100 ng/ml Flagellin, 7 µg/ml 2'3' cGAMP + lipofectamine 2000 and 1 µg/ml Sa19 (n = 3 per group, means + SEM). One experiment representative of 3 is shown. (L) Cytokine secretion of control (empty vector) and Pld3-deficient J774 cells stimulated with 100 ng/ml lipid A,

20 nM CpGB 1668, 1 µg/ml CpGA 1585 + DOTAP, 1 µg/ml *E. coli* dsDNA + DOTAP, 50 nM R848, 5 µg/ml ssPolyU and 1 µg/ml Pam3csk4 (means + SD of triplicate wells are shown). One representative experiment of more than 3 is presented. Statistical analysis was performed using unpaired Student's *t* test. *p < 0.05, **p < 0.01, ***p < 0.001, ****p < 0.0001

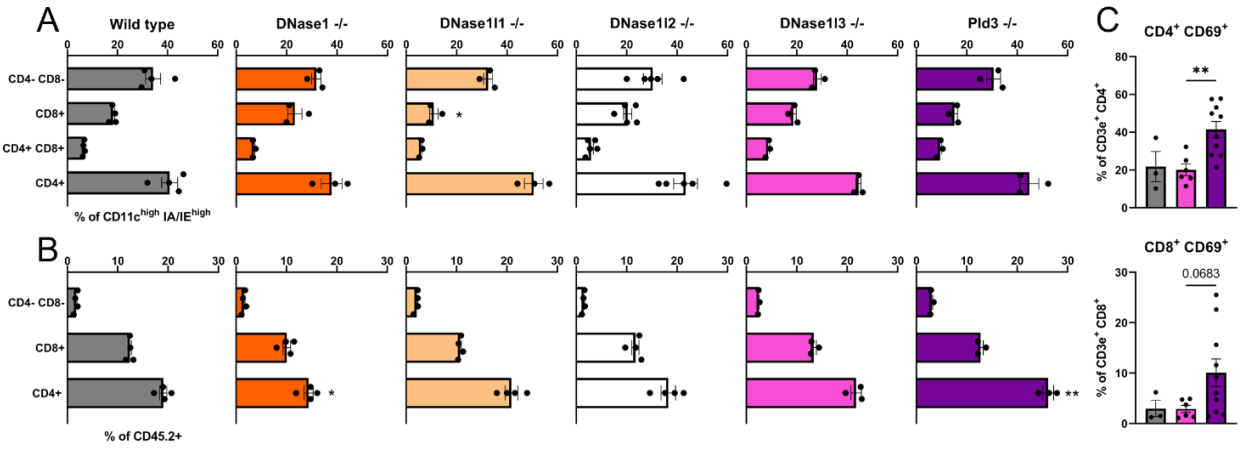

Fig. 18 Splenic subsets of conventional dendritic cells and T cells in wild-type and DNase-deficient mice. (A) Quantitative comparison of cellular fractions of $CD4^-$ $CD8^-$, $CD8^+$, $CD4^+$ $CD8^+$ and $CD4^+$ dendritic cells in wild-type, *DNase1*$^{-/-}$, *DNase1l1*$^{-/-}$, *DNase1l2*$^{-/-}$, *DNase1l3*$^{-/-}$ and *Pld3*$^{-/-}$ mice (n = 3-5 per group, means + SEM) based on flow cytometry analysis. (B) Quantitative comparison of cellular fractions of $CD4^-$ $CD8^-$, $CD8^+$ and $CD4^+$ T cells in wild-type, *DNase1*$^{-/-}$, *DNase1l1*$^{-/-}$, *DNase1l2*$^{-/-}$, *DNase1l3*$^{-/-}$ and *Pld3*$^{-/-}$ mice (n = 3-4 per group, means + SEM) based on flow cytometry analysis. (C) Quantitative comparison of cellular fractions of $CD4^+$ $CD69^+$ and $CD8^+$ $CD69^+$ T cells in wild-type (grey), *DNase1l3*$^{-/-}$ (pink) and *Pld3*$^{-/-}$ (purple) mice (n = 3-10 per group, means + SEM) based on flow cytometry analysis. Data are pooled from 3 independent experiments. Statistical analysis was performed using ANOVA with p values corrected for multiple comparison using Dunnett (A-B) and Tukey (C). *p < 0.05, **p < 0.01, ***p < 0.001, ****p < 0.0001

3.3 Pristane-induced diffuse alveolar hemorrhage in DNase-deficient mice

Multiple knockout mice targeting various DNases involved in the clearance of circulating and intracellular NAs were developed. These mice did not display any gross physical or behavioral abnormalities but manifested alterations in myeloid cell compositions. Since myeloid cells contribute to various SLE-associated complications, *Dnase1*$^{-/-}$, *DNase1l1*$^{-/-}$, *DNase1l2*$^{-/-}$, *DNase1l3*$^{-/-}$ and *Pld3*$^{-/-}$ as well as control wild-type mice were subjected to pristane treatment. On the C57BL/6 background, pristane induces diffuse alveolar

hemorrhage (DAH) which is a life-threatening complication of SLE. Here, it was intended to examine how the lack of deoxyribonucleases as well as the perturbation of myeloid cell populations influence the progression of DAH.

To investigate this issue, 2-month-old mice were i.p. injected with 500 µl pristane and sacrificed on day 11 to analyze systemic inflammation and lung pathology (Fig. 19). As expected, wild-type animals manifested severe alveolar hemorrhages which filled up alveolar spaces and extended over the whole organ resulting in heavy swelling and increase of tissue weight (Fig. 20 A, B, D). Similar pathological responses were observed in *DNase1l1*$^{-/-}$, *DNase1l2*$^{-/-}$ and *Dnase1l3*$^{-/-}$ mice after pristane injection (Fig. 20 D). Unexpectedly, *DNase1*$^{-/-}$ mice displayed significantly less severe lung damage depicted by a profound remission of hemorrhagic areas and organ swelling indicated by lung weight (Fig. 20 A-E). Additionally, significantly decreased prevalence of DAH was detected in *DNase1*$^{-/-}$ mice compared to wild-type controls (Fig. 20 C). Prevalence was categorized into no, partial and complete hemorrhage based on the gross lung pathology as previously described by others (Barker et al. 2011) (Fig. 19, 20 C). In addition, the blood-air barrier seemed to be intact in *DNase1*$^{-/-}$ mice since alveolar spaces were clear of fluid and erythrocytes (Fig. 20 B). However, few *DNase1*$^{-/-}$ individuals were observed that developed severe DAH like wild-type mice, indicating that DNase1-deficiency is not completely protective but rather attenuates pathological manifestations of DAH after pristane treatment (Fig. 19, 20 D, E). In contrast, all *Pld3*$^{-/-}$ mice treated with pristane developed severe DAH and showed significantly increased tissue swelling indicated by lung weight (Fig. 20 D, E). Thus, Pld3-deficiency seemed to exacerbate pristane-induced DAH.

As previously observed by others (Lee et al. 2019), severity of lung pathology, here indicated by lung weight, positively correlates with the cell number of pulmonary CD11b^{+} cells, here divided into neutrophils (CD11b^{+} Ly6G^{+}) and monocytes (Ly6G^{-} CD11b^{+}) (Fig. 20 F). Results from wild-type and knockout mice were pooled for this analysis. In addition, a link between increasing lung weights and decreasing cell numbers of tissue-resident macrophages (F4/80^{+} CD11b^{int}) was observed (Fig. 20 F).

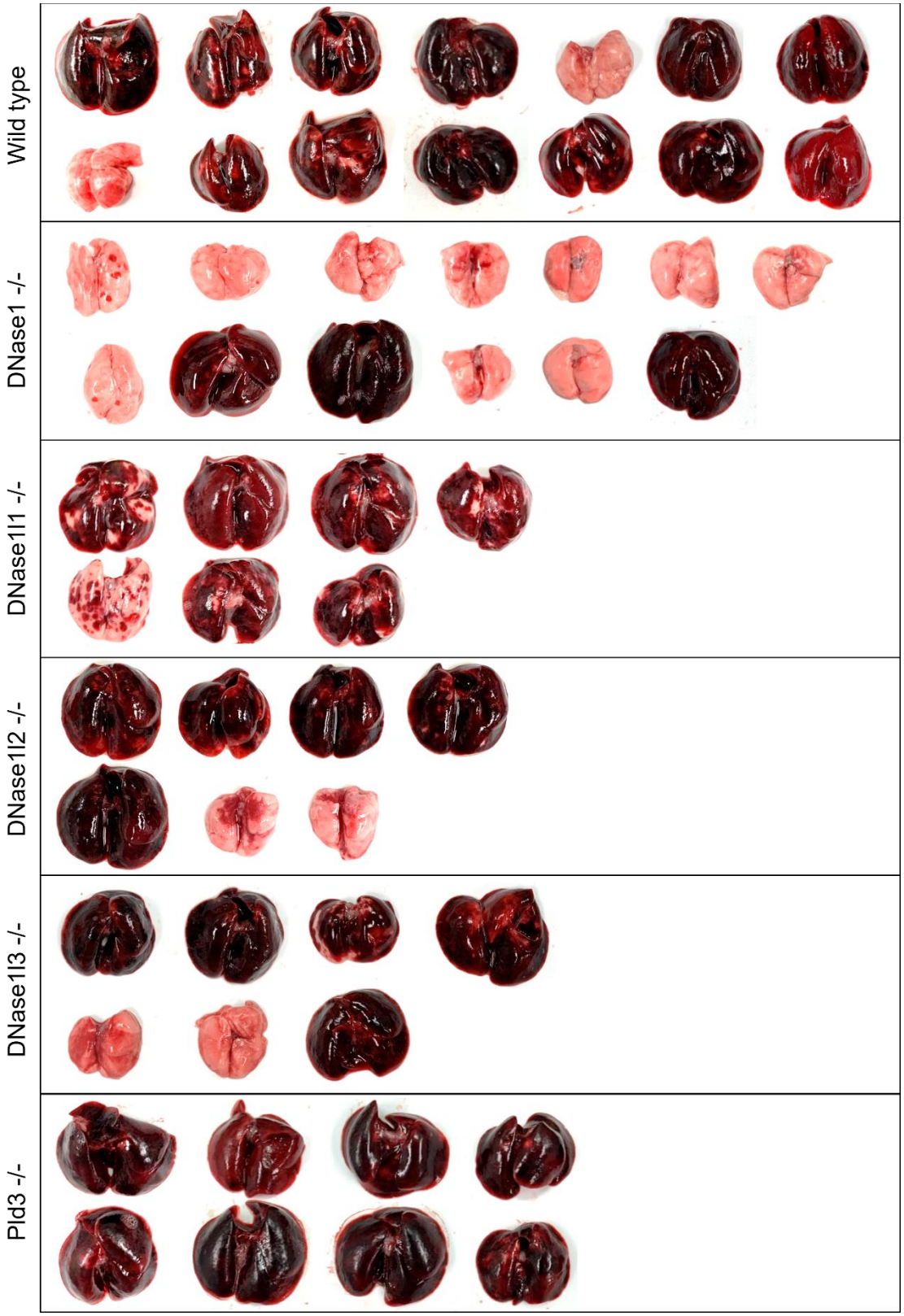

Fig. 19 Gross lung pathology of pristane-induced diffuse alveolar hemorrhage in wild-type, *DNase1*$^{-/-}$, *DNase1l1*$^{-/-}$, *DNase1l2*$^{-/-}$, *DNase1l3*$^{-/-}$ and *Pld3*$^{-/-}$ mice. Age-matched female and male mice received a single i.p. injection of pristane and were sacrificed 11 days later for further analysis.

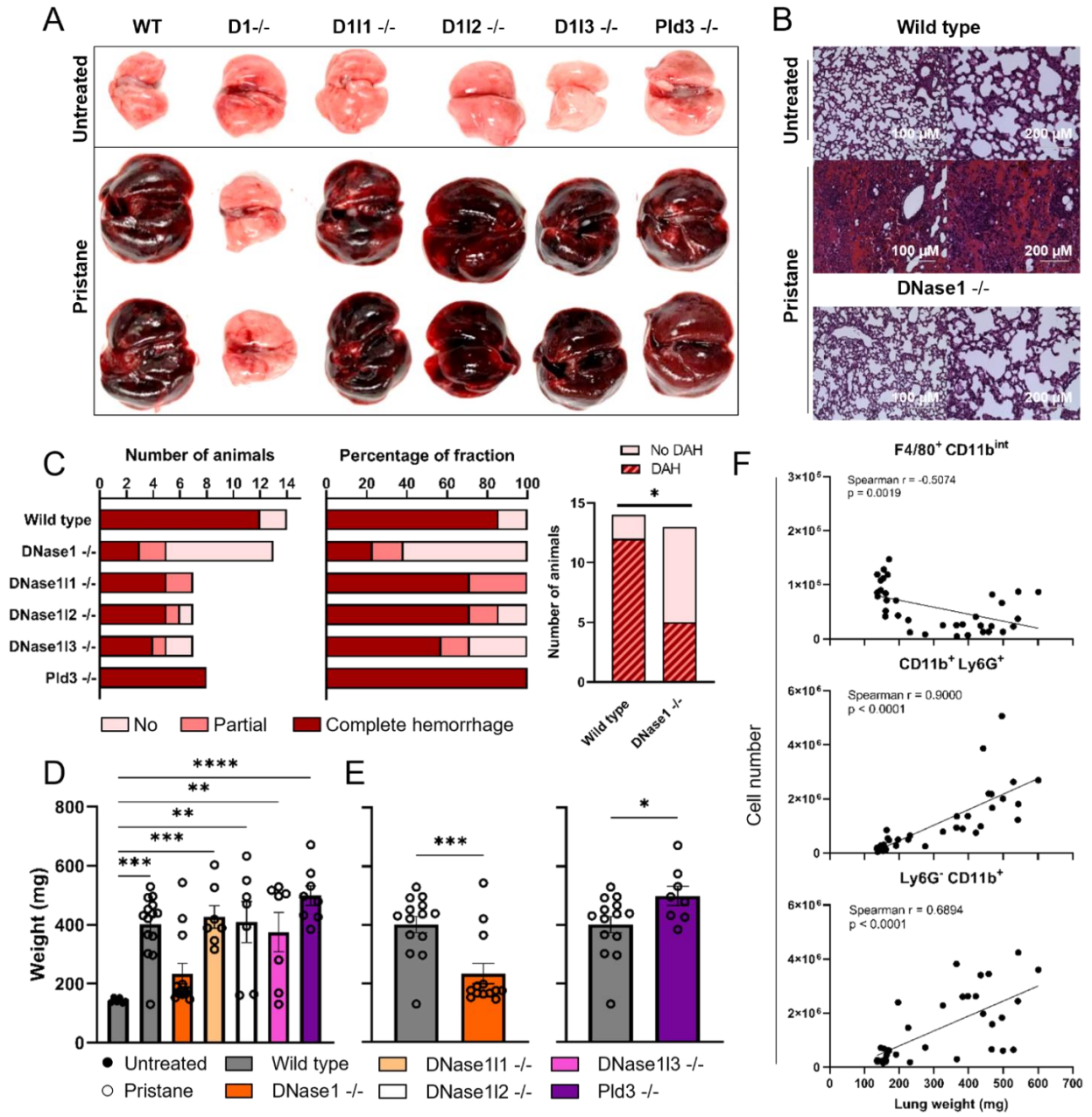

Fig. 20 Lung pathology of pristane-induced diffuse alveolar hemorrhage (DAH). (A) Wild-type, *DNase1*$^{-/-}$, *DNase1l1*$^{-/-}$, *DNase1l2*$^{-/-}$, *DNase1l3*$^{-/-}$ and *Pld3*$^{-/-}$ were treated with pristane or left untreated, and lungs were examined 11 days later. Gross lung pathology of representatives is shown. (B) Representative images of hematoxylin and eosin staining of lung tissue from untreated wild-type and pristane-treated wild-type and *DNase1*$^{-/-}$ mice are presented. (C) Incidence and types of gross pathology classified into no, partial and complete hemorrhage in wild-type, *DNase1*$^{-/-}$, *DNase1l1*$^{-/-}$, *DNase1l2*$^{-/-}$, *DNase1l3*$^{-/-}$ and *Pld3*$^{-/-}$ mice are presented as total numbers of animals and percentage. Comparison of prevalence of diffuse alveolar hemorrhage (DAH) including partial and complete hemorrhagic samples from wild-type and *DNase1*$^{-/-}$ mice after pristane administration (n = 13-14 per group). (D) Comparison of lung weight from untreated wild-type and pristane-treated wild-type, *DNase1*$^{-/-}$, *DNase1l1*$^{-/-}$, *DNase1l2*$^{-/-}$, *DNase1l3*$^{-/-}$ and

Pld3$^{-/-}$ mice (n = 7-14 per group, mean + SEM). (E) Comparison of lung weight from pristane-treated wild-type, *DNase1*$^{-/-}$ and *Pld3*$^{-/-}$ mice (n = 8-14 per group, mean + SEM). (F) Correlation of lung macrophage (F4/80^{+} CD11b^{int}) depletion or expansion of neutrophils (CD11b^{+} Ly6G^{+}) and monocytes (Ly6G^{-} CD11b^{+}) with lung weight. (C-F) Pooled data from 4-5 independent experiments. Statistical analysis was performed using Fisher's exact test (C), one-way ANOVA with p values corrected for multiple comparison using Dunnett (D), unpaired Student's *t* test (E) and Spearman's correlation (F). *p < 0.05, **p < 0.01, ***p < 0.001, ****p < 0.0001. D1: DNase1, D1l1: DNase1l1, D1l2: DNase1l2, D1l3: DNase1l3.

3.4 Manifestations of pristane-induced peritonitis in DNase-deficient mice

Peritoneal cell populations were examined to investigate whether altered immune responses occur at the injection site of the mineral oil, thus the initial site of inflammation. Firstly, total cell numbers were determined to ascertain that all tested mice displayed peritoneal cell infiltration after treatment. Secondly, cells were isolated from the peritoneal lavage and subsequently processed for flow cytometry analysis. Representatives of pristane-induced cellular alterations in the peritoneum are depicted in Fig. 21 D. In case an animal displayed no increase of peritoneal cell number, decrease of tissue-resident macrophages or infiltration of neutrophils and monocytes, the injection was considered as unsuccessful, and results were excluded.

Wild-type, *DNase1*$^{-/-}$, *DNase1l1*$^{-/-}$, *DNase1l2*$^{-/-}$, *DNase1l3*$^{-/-}$ and *Pld3*$^{-/-}$ showed comparable levels of infiltrating cells (Fig. 22 I). Further signs of inflammation, such as loss of tissue-resident macrophages (F4/80^{high} CD11b^{high}) and monocyte-derived cells (Ly6C^{low} IA/IE^{high}) became clear both in terms of the cellular proportions and total numbers of cells (Fig. 22 A, F). In addition, neutrophils (CD11b^{+} Ly6G^{+}) and monocytes (Ly6G^{-} CD11b^{+}) including inflammatory (Ly6C^{high}) and patrolling monocytes (Ly6C^{low} FcγRIV^{+}) accumulated in the peritoneum of all analyzed mice, although to varying scale (Fig. 22 B-E). In case of *DNase1*$^{-/-}$ significant increases of neutrophils and monocytes in percentage and total cell number were detected. Besides, increasing rates of dendritic cells (CD11c^{high} IAIE^{high}) were observed in the peritoneal lavage, especially in *DNase1*$^{-/-}$, *DNase1l1*$^{-/-}$ and *DNase1l2*$^{-/-}$ cellular fractions were significantly elevated (Fig. 22 G).

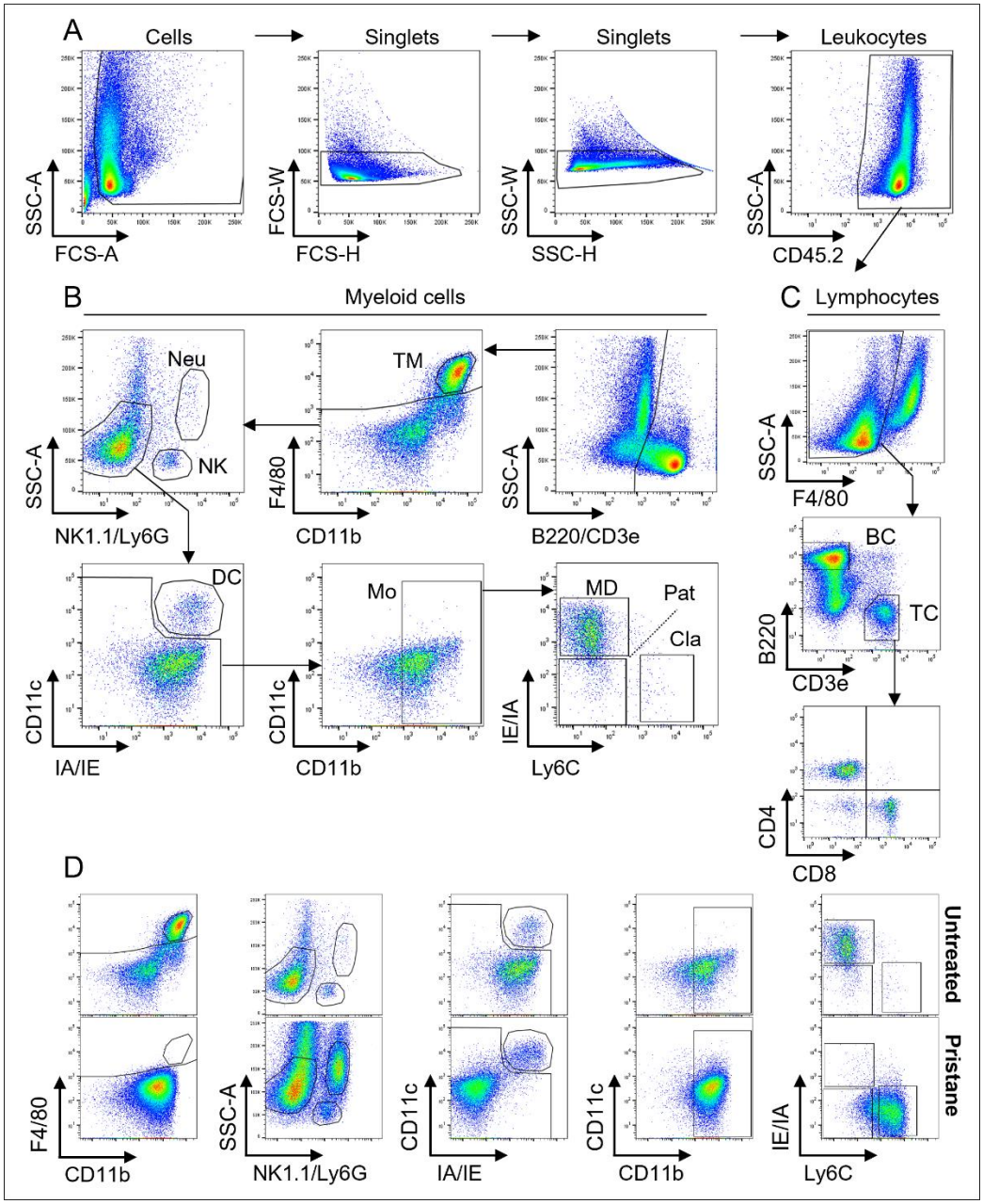

Fig. 21 Gating strategy used to detect myeloid cells and lymphocytes in peritoneal lavage. (A-C) Representative scheme for flow cytometry analysis of isolated cells from peritoneal lavage. (A) Shared scheme to identify single-cell leukocytes. (B) Scheme showing exclusion of B220^{+} and CD3e^{+} lymphocytes and subsequent identification of multiple myeloid cells including tissue-resident macrophages (F4/80^{high} CD11b^{high}, TM), neutrophils (SSC^{high} Ly6G^{+} CD11b^{+}, Neu), NK cells (SSC^{low} NK1.1^{+}, NK), conventional dendritic cells (Ly6G/NK1.1^{-} CD11c^{high} IA/IE^{high}, DC) and monocytes (Ly6G/NK1.1^{-} CD11c^{low} CD11b^{+}, Mo) which were divided into classical (Ly6C^{high} IA/IE^{low}, Cla), patrolling (Ly6C^{low} IA/IE^{low} FcγRIV^{high}, Pat) and monocyte-derived cells (Ly6C^{low} IA/IE^{+}, MD). (C) Strategy to exclude tissue-resident macrophages (F4/80^{+}) and separate B cells (B220^{+}, BC) and T cells (CD3e^{+}, TC). T cells are divided into CD4^{-} CD8^{-}, CD4^{+}, CD8^{+} and CD4^{+} CD8^{+} T cells. (D) Representative of flow cytometry analysis of cellular alterations after a single injection i.p. of pristane.

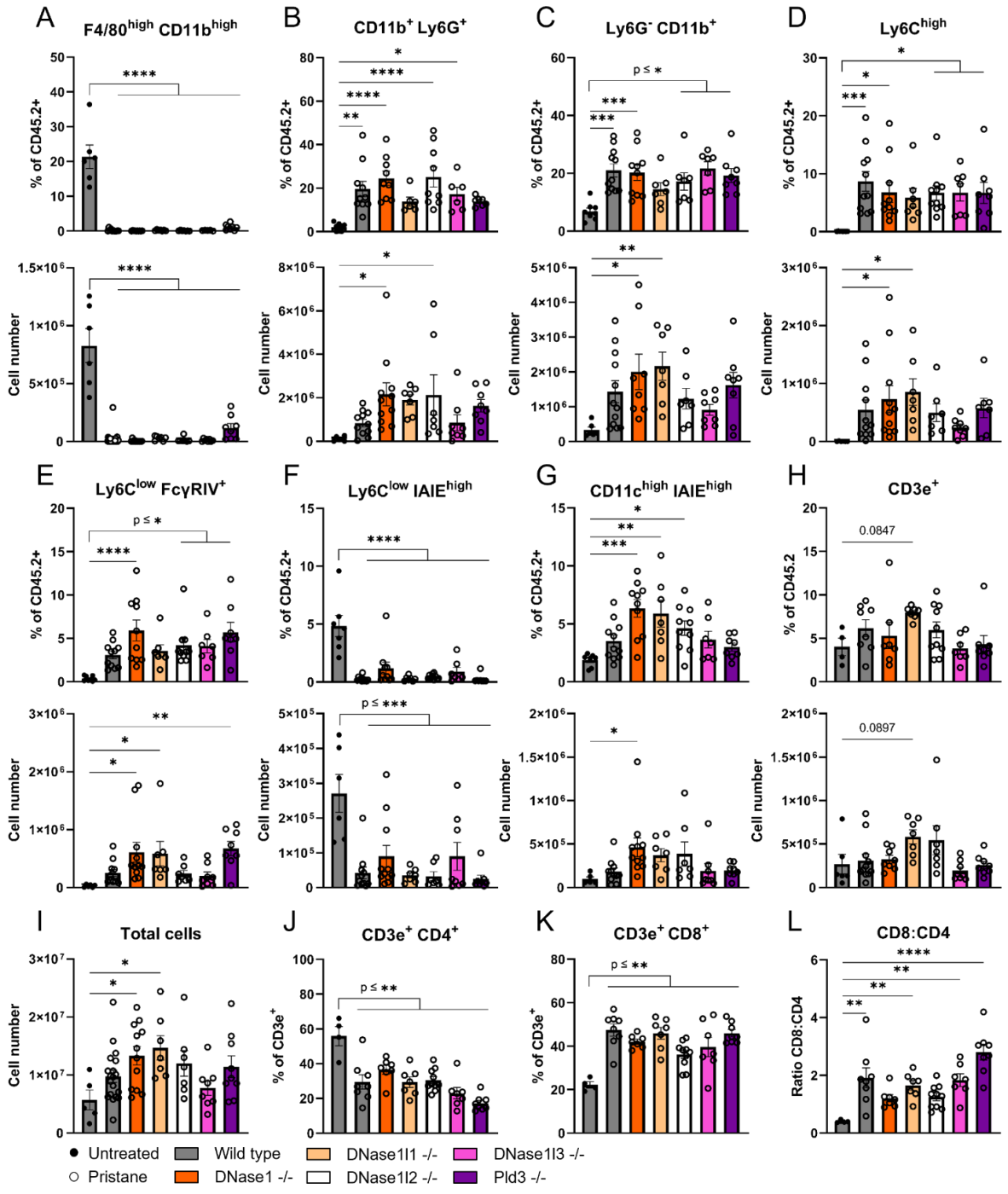

Fig. 22 Immune cell populations in peritoneal lavage from wild-type and DNase-deficient mice after pristane administration. (A-H) Quantitative comparison of cellular fractions and total number of peritoneal myeloid cells and lymphocytes from untreated wild-type and pristane-treated wild-type, *DNase1*$^{-/-}$, *DNase1l1*$^{-/-}$, *DNase1l2*$^{-/-}$, *DNase1l3*$^{-/-}$ and *Pld3*$^{-/-}$ mice (n = 7-14 per group, means + SEM) based on flow cytometry analysis. (I) Quantitative comparison of total numbers of cells in peritoneal lavage. (J-K) Comparison of cellular fractions of CD4^{+} and CD8^{+} T cells in peritoneal lavage. (L) Ratio of CD8^{+} versus CD4^{+} T cells in peritoneal lavage. Data are pooled from 4-5 independent

experiments. Statistical analysis was performed using one-way ANOVA with p values corrected for multiple comparison using Dunnett. *p < 0.05, **p < 0.01, ***p < 0.001, ****p < 0.0001

Frequency and total cell number of CD3e$^+$ T cells were mildly affected and showed no significant differences compared to untreated controls (Fig. 22 H). However, the proportions of CD4$^+$ and CD8$^+$ T cells changed after pristane administration. A significant reduction in CD4$^+$ accompanied by an increase in CD8$^+$ T cells was detected in all tested nuclease knockout and wild-type mice (Fig. 22 J-L). In untreated controls, CD4$^+$ T cells predominate, the average ratio of CD8$^+$ versus CD4$^+$ (CD8:CD4) cells is 0.5. In contrast, pristane treated wild-type mice displayed a shift towards CD8$^+$ T cells resulting in a CD8:CD4 ratio of ~ 2 on average. In *DNase1l1*$^{-/-}$, *DNase1l3*$^{-/-}$ and *Pld3*$^{-/-}$ comparable ratios were determined, whereas *DNase1*$^{-/-}$ and *DNase1l2*$^{-/-}$ mice did not manifest significantly shifted fractions of CD4$^+$ and CD8$^+$ T cells (Fig. 22 L). As expected, injection of the mineral oil led to the recruitment of granulocytes, inflammatory monocytes as well as perturbed balance of T cell populations in favor of CD8$^+$ T cells. Taken together, the presented results suggest that pristane-mediated peritonitis manifests in wild-type, *DNase1*$^{-/-}$, *DNase1l1*$^{-/-}$, *DNase1l2*$^{-/-}$, *DNase1l3*$^{-/-}$ and *Pld3*$^{-/-}$ mice to a similar extent.

3.4.1 Comparison of peritoneal inflammation in wild-type, *DNase1*$^{-/-}$ and *Pld3*$^{-/-}$ mice

To gain insights into the possible association between peritoneal inflammation and lung pathology, findings of pristane-treated wild-type, *DNase1*$^{-/-}$ and *Pld3*$^{-/-}$ mice were compared. Firstly, total numbers of cells in peritoneal lavage were similarly elevated (Fig. 23 L). Loss of resident macrophages was less severe in *Pld3*$^{-/-}$ mice, although such deprivation was tremendous in all mice, decreasing from ~ 20 % in untreated controls to ≤ 1 % in treated animals on average (Fig. 23 A). Equal proportions of granulocytes were found in wild type, *DNase1*$^{-/-}$ and *Pld3*$^{-/-}$, however, the total number of neutrophils was slightly increased in *DNase1*$^{-/-}$ compared to wild type (Fig. 23 B). In addition, frequency and total number of conventional dendritic cells (CD11c^{high} IA/IE^{high}) were enhanced in *DNase1*$^{-/-}$ compared to wild type or *Pld3*$^{-/-}$ (Fig. 23 G). In contrast, no significant deviations were found between wild type, *DNase1*$^{-/-}$ and *Pld3*$^{-/-}$ regarding monocytic populations (Fig. 23 C-F). Total number and cellular fraction of CD3e$^+$ T cells were

steady, while the balance between $CD4^+$ and $CD8^+$ T cells was shifted towards $CD8^+$ cells in wild-type and especially *Pld3*$^{-/-}$ (Fig. 23 H, K). In *DNase1*$^{-/-}$, the CD8:CD4 ratio of T cells was not significantly altered in comparison to untreated controls (Fig. 23 K). Thus, the cellular immune response to pristane is similar in wild type, *DNase1*$^{-/-}$ and *Pld3*$^{-/-}$ at the initial site of inflammation suggesting that occurrence of pulmonary hemorrhages potentially is not directly linked to peritonitis.

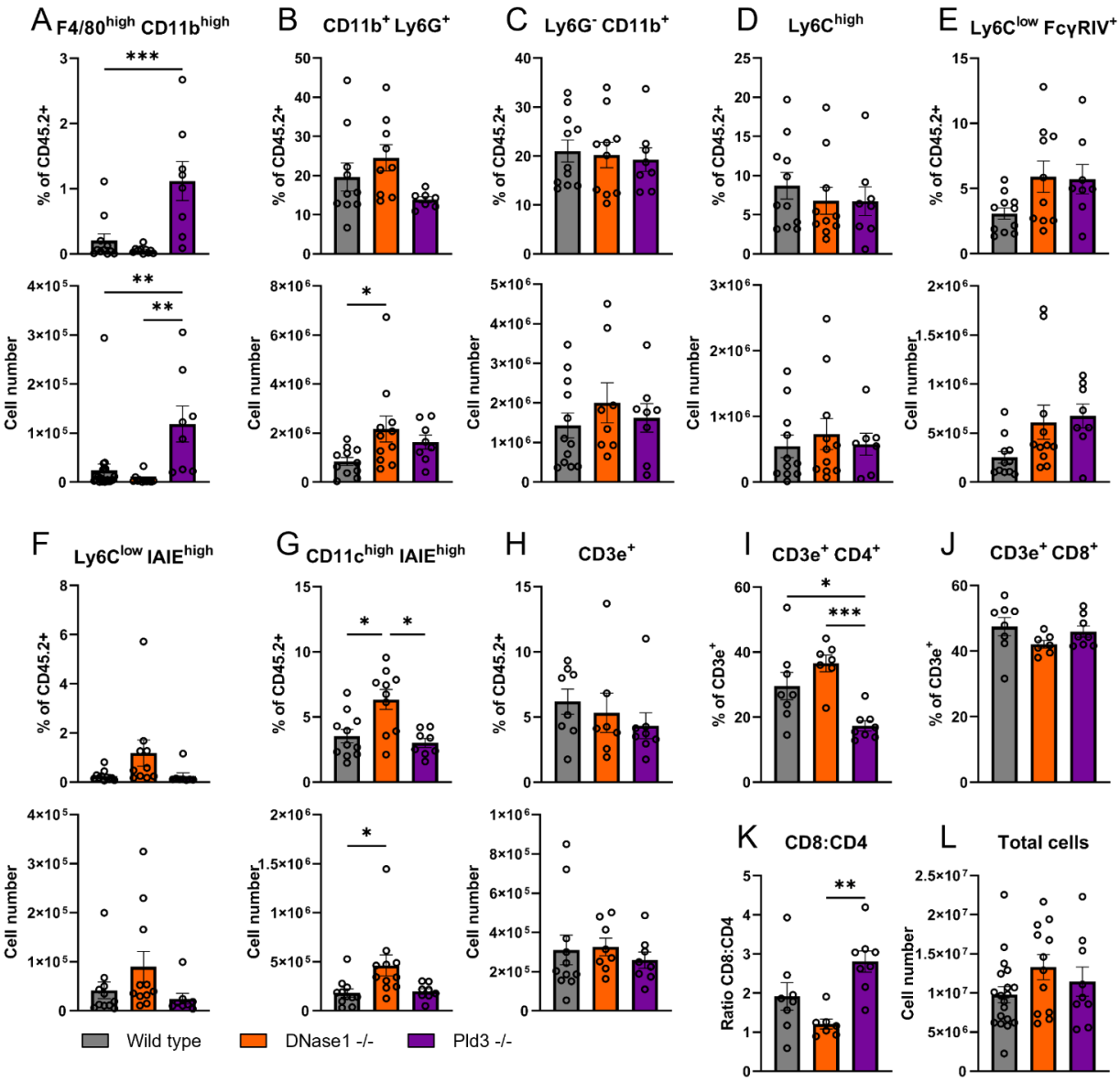

Fig. 23 Comparison of immune cell populations in peritoneal lavage from wild-type, *DNase1*$^{-/-}$ and *Pld3*$^{-/-}$ mice after pristane administration. (A-H) Quantitative comparison of cellular fractions and total number of myeloid cells and lymphocytes in peritoneal lavage from pristane-treated wild-type, *DNase1*$^{-/-}$ and *Pld3*$^{-/-}$ mice (n = 8-11 per group, means + SEM) based on flow cytometry analysis. (I-J) Quantitative

comparison of cellular fractions of $CD4^+$ and $CD8^+$ T cells. (K) Ratio of $CD8^+$ versus $CD4^+$ T cells in peritoneal lavage. (L) Total number of cells in peritoneal lavage. Data are pooled from 3 independent experiments. Statistical analysis was performed using one-way ANOVA with p values corrected for multiple comparison using Tukey. *p < 0.05, **p < 0.01, ***p < 0.001, ****p < 0.0001

3.5 Comparison of tissue-specific alterations in wild type and *DNase1*$^{-/-}$

3.5.1 Immune cells in spleen, blood and bone marrow

Pristane is known to mediate chronic inflammation which has been characterized by the continuous recruitment of lymphocytes, neutrophils and monocytes/macrophages to the peritoneal cavity and the spleen, where leukocyte infiltration is accompanied by reduction of resident B and T cells (Li et al. 2017).

Here, immune cell populations in spleen were analyzed in untreated and pristane-treated *DNase1*$^{-/-}$ and wild-type mice. In accordance with the data described before, no significant differences in splenic immune cell populations could be determined between untreated wild-type and *DNase1*$^{-/-}$ animals (Fig. 8 A-K, 24 A-J). Intraperitoneal injection of pristane did not clearly alter total numbers of splenocytes or tissue-resident macrophages, although an increasing trend in macrophage numbers may be observed (Fig. 24 A, B). In contrast, total numbers of neutrophils were clearly increased, whereas monocyte counts were elevated but not significantly altered in both wild-type and *DNase1*$^{-/-}$ under the given conditions (Fig. 24 C, D). However, elevated numbers of potentially inflammatory $Ly6C^{high}$ monocytes were observed in both after pristane administration, as well as slightly decreased monocyte-derived dendritic cell counts accompanied by an increase of $Ly6C^{low}$ $FcγRIV^{high}$ monocytes (Fig. 24 E-G). Populations of dendritic cells seemed to be rather unaffected by pristane, while the treatment led to reduced numbers of B cells and T cells in wild-type mice (Fig. 24 H-J). In *DNase1*$^{-/-}$, numbers of B and T lymphocytes were unaffected by the administration of pristane (Fig. 24 I, J). Examination of blood and bone marrow of pristane-treated wild-type and DNase1-deficient mice did not show significant perturbations (Fig. 24 K, L). However, an increasing trend of monocyte frequencies, especially patrolling monocytes were observed in *DNase1*$^{-/-}$ samples which is in line with results shown before (Fig. 9 F, H, 24 K).

Taken together, pristane induces inflammation in multiple organs including spleen in both wild type and *DNase1*$^{-/-}$. Total numbers of splenocytes were slightly elevated potentially due to the clear expansion of neutrophils and monocytes. B cells and T cells were slightly decreased in wild-type but not *DNase1*$^{-/-}$ mice. Thus, wild-type and *DNase1*$^{-/-}$ animals displayed comparable immune responses to pristane in multiple organs including peritoneal cavity, bone marrow and spleen.

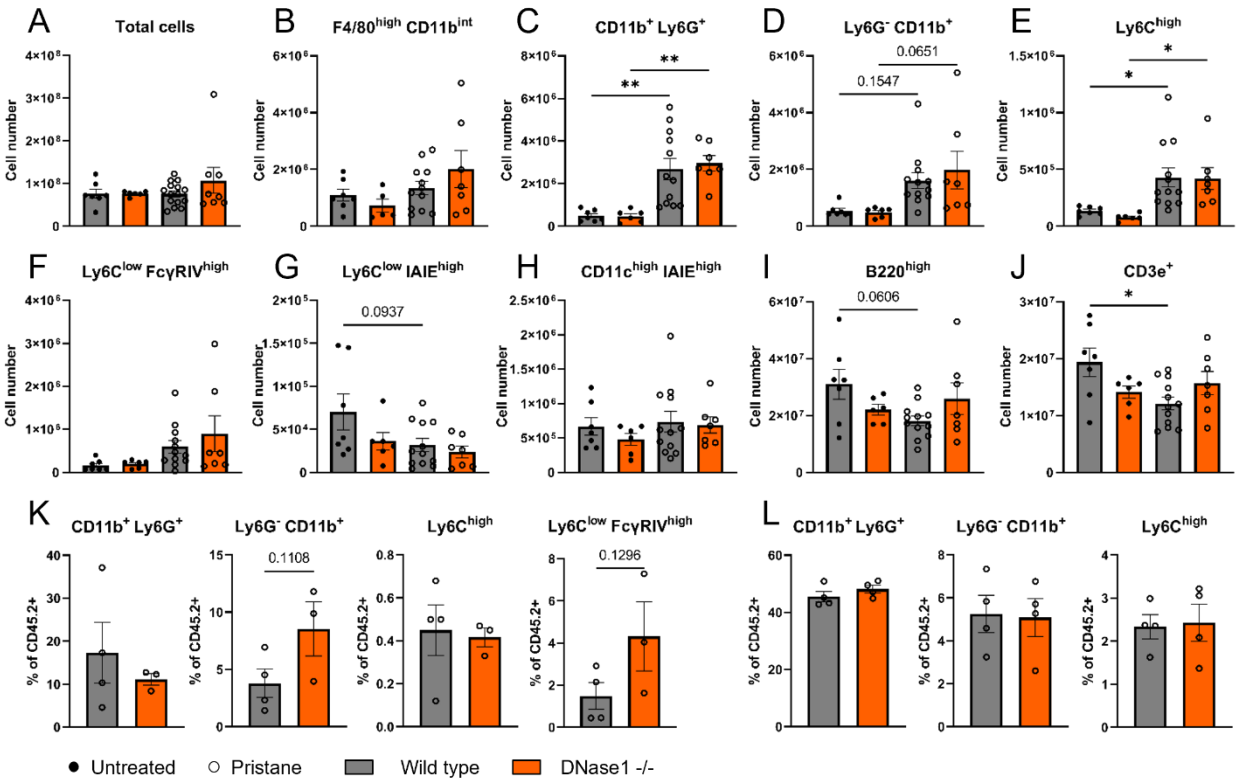

Fig. 24 Myeloid cells and lymphocytes in spleen, blood and bone marrow from wild-type and *DNase1*$^{-/-}$ mice. (A-J) Quantitative comparison of total number of myeloid cells and lymphocytes in spleen from untreated as well as pristane-treated wild-type and *DNase1*$^{-/-}$ mice (n = 6-10 per group, means + SEM) based on flow cytometry analysis. Data are pooled from 3 independent experiments. (K-L) Comparison of cellular fractions of myeloid cells in blood and bone marrow from pristane-treated wild-type and *DNase1*$^{-/-}$ mice (n = 3-4, means + SEM). Statistical analysis was performed using one-way ANOVA with p values corrected for multiple comparison using Tukey (A-J) and Student's *t* test (K-L). *p < 0.05, **p < 0.01, ***p < 0.001, ****p < 0.0001

3.5.2 Pulmonary accumulation of myeloid cells

The mineral oil pristane induced comparable inflammatory responses at the initial site of inflammation in both wild-type and *DNase1*$^{-/-}$ mice, but severe pulmonary hemorrhages

occurred only in wild type. These results suggest that independent inflammatory responses may appear. In line with this presumption, previous results emphasized pristane is systemically distributed and arrives in bone marrow and lung where it triggers cell death (Zhuang et al. 2017). So, the question arose whether DNase1-deficiency influenced the local pulmonary response to pristane and to what extent that reaction may differ from wild type. Therefore, flow cytometry analysis was used to profile pulmonary immune cells (Fig. 25).

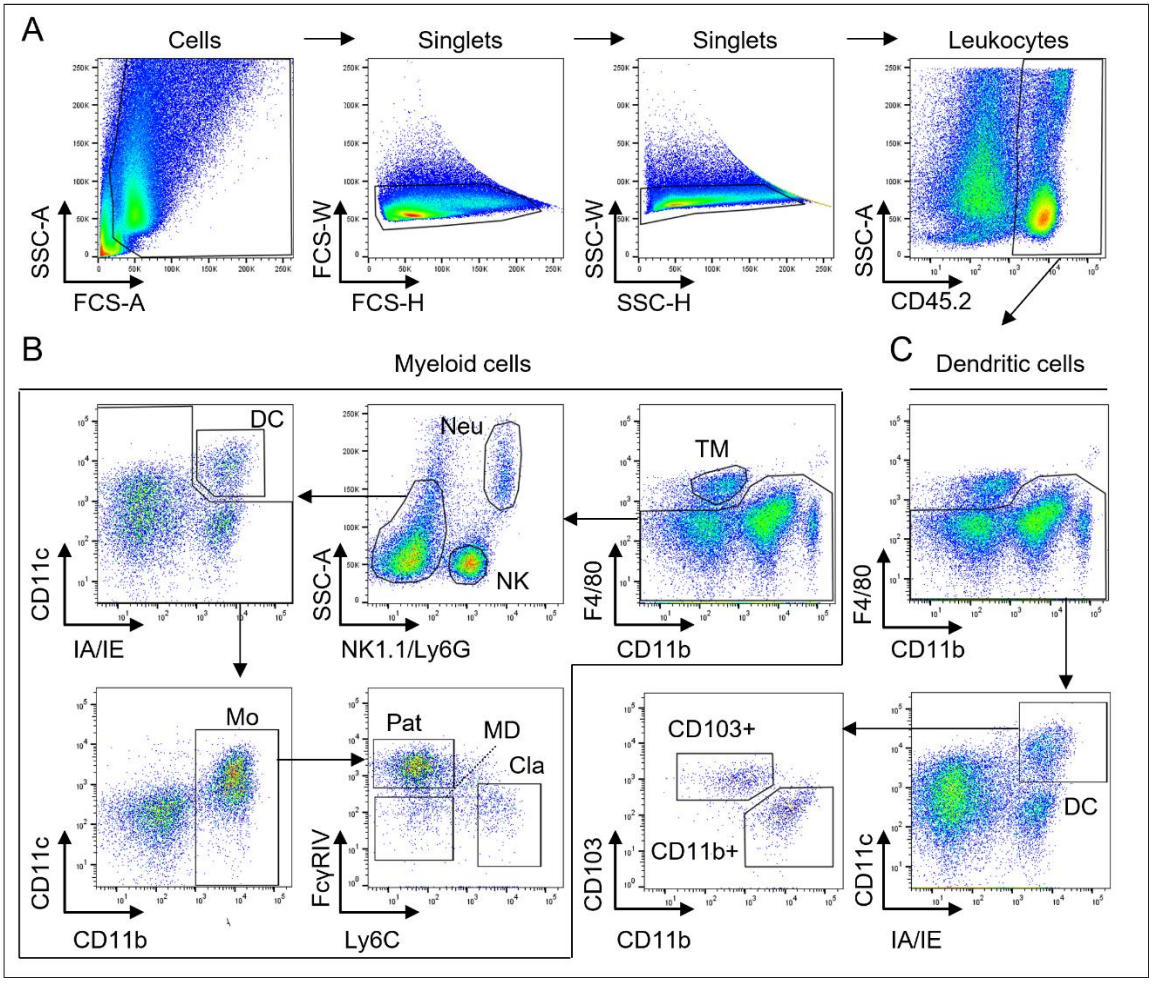

Fig. 25 Gating strategy used to detect myeloid cells in lung. (A-C) Representative scheme for flow cytometry analysis of isolated cells from lung tissue. (A) Shared scheme to identify single-cell leukocytes. (B) Scheme to identify multiple myeloid cells including tissue-resident macrophages (F4/80^{+} CD11b^{int}, TM), neutrophils (SSC^{high} Ly6G^{+} CD11b^{+}, Neu), NK cells (SSC^{low} NK1.1^{+}, NK), conventional dendritic cells (Ly6G/NK1.1^{-} CD11c^{high} IA/IE^{high}, DC) and monocytes (Ly6G/NK1.1^{-} CD11c^{low} CD11b^{+}, Mo) which were divided into classical (Ly6C^{high} FcγRIV^{low}, Cla), patrolling (Ly6C^{low} FcγRIV^{high}, Pat) and monocyte-derived cells (Ly6C^{low} FcγRIV^{low} IA/IE^{+}, MD). (C) Strategy to exclude tissue-resident macrophages (F4/80^{+} CD11b^{int}) and detect dendritic cells (F4/80^{low} CD11c^{high} IA/IE^{high}, DC) which were separated into CD11b^{+} and CD103^{+} DCs.

In line with previous work, pristane injection led to pulmonary accumulation of leukocytes ($CD45.2^+$) which was more prominent in wild-type mice with severe alveolar hemorrhage (Fig. 26 A). Invasion of leukocytes was accompanied by the loss of tissue-resident macrophages ($F4/80^+$ $CD11b^{int}$) in wild-type mice (Fig. 26 B). Pristane-treated *DNase1*$^{-/-}$ mice also showed reduced cellular fractions and cell counts of macrophages but less pronounced (Fig. 26 B). $CD11b^+$ myeloid cells made up the largest proportion of leukocytes found in lungs which is in line with previous work (Lee et al. 2019). Here, $CD11b^+$ $Ly6G^+$ neutrophils accounted for about 20 % of the accumulating immune cells in both wild-type and *DNase1*$^{-/-}$ mice (Fig. 26 C). However, total numbers of neutrophils were significantly less in *DNase1*$^{-/-}$ compared to wild-type lungs (Fig. 26 C). In addition, buildups of $Ly6G^-$ $CD11b^+$ monocytes were observed in pristane treated animals which is evident from the increase in total numbers of cells, but these expansions were not significant under the given conditions (wild type $p = 0.16552$, *DNase1*$^{-/-}$ $p = 0.0629$) (Fig. 26 D). However, the fraction of monocytes was significantly increased in lungs of pristane-treated *DNase1*$^{-/-}$ compared to untreated *DNase1*$^{-/-}$ and treated wild-type controls (Fig. 26 D).

Since monocytes are believed to be key drivers of pristane-induced DAH, the question arose whether *DNase1*$^{-/-}$ monocytes responded proinflammatorily to pristane. Therefore, $Ly6G^-$ $CD11b^+$ monocytes were isolated from treated wild-type and *Dnase1*$^{-/-}$ lungs and purified via fluorescence-activated cell sorting. RNA was isolated and the expression of inflammatory mediators including TGF-β, Cxcl1, S100a8 and IL1b was analyzed by qPCR. These targets were selected based on previous studies, indicating that monocytes strongly upregulate these target genes after pristane administration in contrast to PBS injection (Lee et al. 2019). Here, relative fold expression of TGF-β, Cxcl1, S100a8 and IL-1β were not significantly altered comparing monocytes from wild-type individuals with severe pulmonary hemorrhage and treated *DNase1*$^{-/-}$ mice without DAH (Fig. 26 H).

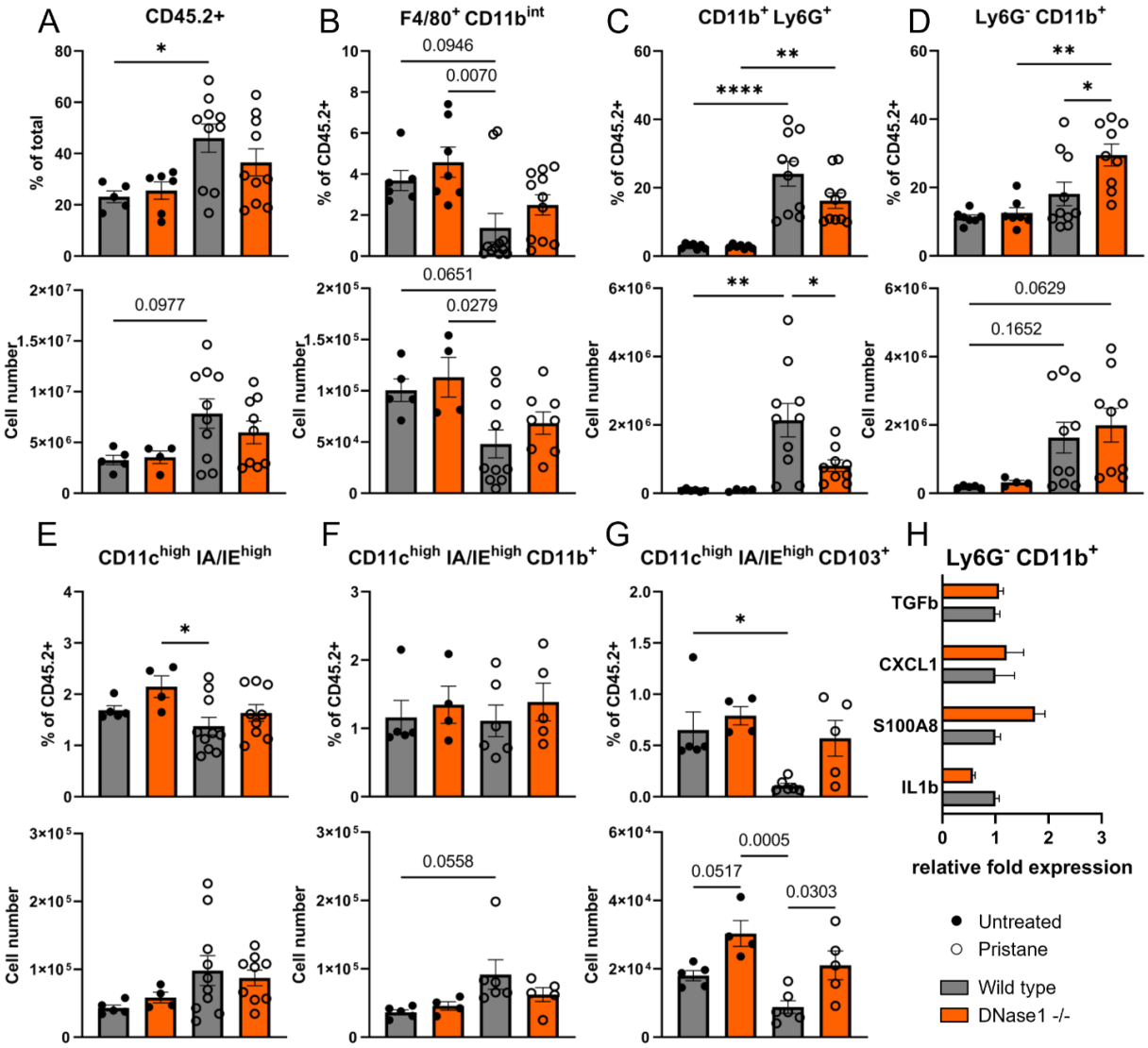

Fig. 26 Myeloid cells in lungs from wild-type and *DNase1*$^{-/-}$ mice. (A-G) Quantitative comparison of cellular fractions and total number of myeloid cells in lung from untreated and pristane-treated wild-type and *DNase1*$^{-/-}$ mice (n = 5-10 per group, means + SEM) based on flow cytometry analysis. Data are pooled from 3 independent experiments. (H) Cytokine expression of pulmonary monocytes (Ly6G^{-} CD11b^{+}) from pristane-treated wild-type mice with DAH and DNase1$^{-/-}$ mice without DAH (n = 2 per group, mean + SEM). One experiment representative of 2 is shown. Statistical analysis was performed using one-way ANOVA with p values corrected for multiple comparison using Tukey (A-G) and Student's *t* test (H). *p < 0.05, **p < 0.01, ***p < 0.001, ****p < 0.0001

Efforts to profile monocyte subpopulations were attempted. However, in severely injured lungs, consistent division into inflammatory (Ly6C^{high} FcγRIV^{low}) and patrolling monocytes (Ly6C^{low} FcγRIV^{high}) was challenging due to the occurrence of an

intermediate population that showed a broad expression of Ly6C and low levels of FcγRIV (Fig. 27 A). This observation was made in mice with severe DAH regardless of genotype. In contrast, two clearly separated monocyte subsets could be detected in mildly injured or intact lungs where one population resembled patrolling monocytes which were also found in untreated controls and the other Ly6C^{high} inflammatory monocytes (Fig. 27 A). High expression of Ly6C in pulmonary monocytes from *DNase1*$^{-/-}$ could indicate myeloid-derived suppressor cell (MDSC) origin since MDSCs are characterized by their high expression of Ly6C and low expression of F4/80 (Gabrilovish and Nagaraj 2009). However, compared to inflammatory monocytes present in peritoneal lavage from pristane-treated wild-type mice, the level of Ly6C did not appear to be greatly elevated and F4/80 expression was unaltered (Fig. 27 A). Taken together, monocytes found in pristane-treated wild-type and *DNase1*$^{-/-}$ lungs displayed distinct marker profiles but similar cytokine/chemokine expression, suggesting that *DNase1*$^{-/-}$ monocytes differ from common myeloid-derived suppressor cells.

In the lung, two major populations of DCs expressing CD11b or CD103 can be found. CD11b^{high} DCs reside beneath the lung epithelium in the lamina propria, while CD103^{+} DCs express langerin and are closely associated with the epithelium or can be found within in epithelial layer. CD11b^{high} DCs patrol pulmonary vessel walls and sample blood borne pathogens, whereas CD103^{+} DCs capture antigens from the airway lumen. Both DC subsets can migrate to regional lymph nodes, so called mesenteric lymph nodes (MLNs) and present antigens to T cells. Under inflammatory conditions, monocytes can give rise to so-called inflammatory CD11b^{high} CD11c^{high} DCs in the lung, which express high levels of Ly6C and inflammatory mediators (GeurtsvanKessel and Lambrecht 2008).

Here, pristane treatment did not lead to significant changes in the frequency or number of pulmonary DCs (CD11c^{high} IA/IE^{high}) neither in wild-type nor *DNase1*$^{-/-}$ mice although increasing cell numbers were observed (Fig. 26 E). Besides, wild-type and DNase1-deficient CD11c^{high} IA/IE^{high} DCs showed similar expression level of Ly6C and CD11b (Fig. 27 B). In contrast, the fraction of CD103^{+} DCs was significantly reduced in treated wild-type lungs, whereas no significant alteration was observed in *DNase1*$^{-/-}$ (Fig. 26 G). The loss of CD103^{+} DCs could be due to epithelial damage or indicate migration of

CD103^{+} DCs to regional lymph nodes. Taken together, the data shown here suggest that pristane induces pulmonary inflammation in wild-type and *DNase1*$^{-/-}$ mice. Major differences include reduced accumulation of neutrophils, increased frequencies of monocytes and preservation of alveolar macrophages and CD103^{+} DCs in *DNase1*$^{-/-}$ compared to wild-type mice.

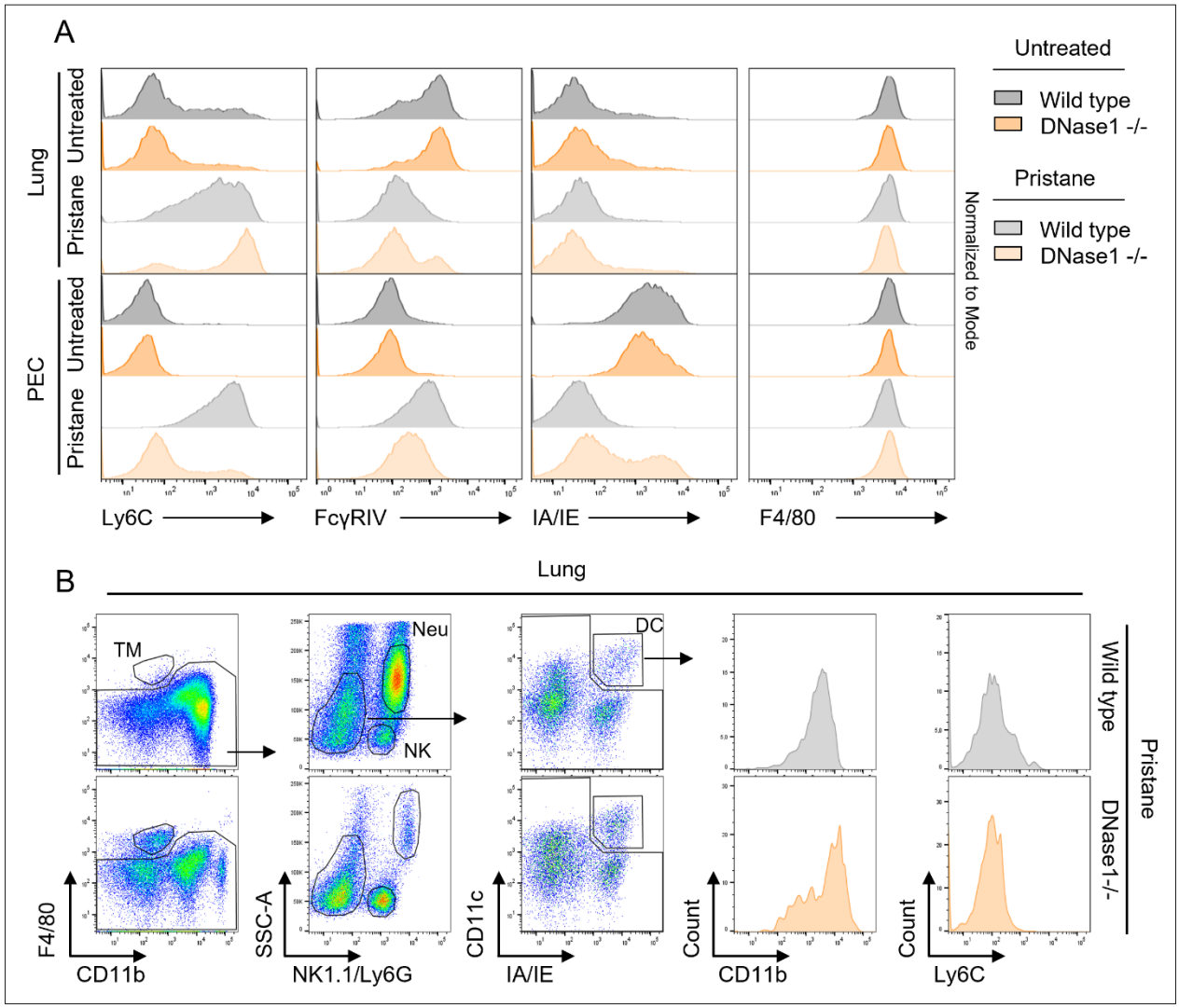

Fig. 27 Pristane-mediated altered phenotypes of pulmonary and peritoneal monocytes and dendritic cells. (A) Representative of marker expression profiles of monocytes in peritoneal lavage and lung from untreated and pristane treated wild-type and *DNase1*$^{-/-}$ mice. (B) Representative of strategy used to detect expression profiles of common inflammatory dendritic cell markers in lungs from pristane-treated wild-type and *DNase1*$^{-/-}$ mice.

3.6 Pristane-mediated pathological manifestations in wild-type, *DNase1*$^{-/-}$ and *DNase1*$^{-/-}$ *Tlr9*$^{-/-}$ mice

It is a widely accepted concept that deoxyribonucleases degrade and eliminate DNA to prevent autoimmune responses. For example, DNase2a-deficient mice die as embryos due to failed removal of nuclear DNA expelled from erythroid precursor cells leading to severe anemia (Kawane et al. 2001, Krieser et al. 2002). In contrast, DNase2a is also required to process CpG type A oligonucleotides and bacterial genomic DNA into short ligands that then activate Tlr9 signaling in plasmacytoid DCs (Chan et al. 2015). These observations imply two opposite functions of DNA nucleases: DNA degradation versus DNA processing. If this concept is applied to the observations in pristane-treated *DNase1*$^{-/-}$ mice, it would be possible that either defective DNA degradation occurs and stimulatory ligands accumulate, or stimulatory DNA is not generated due to the lack of DNase1. Accumulation of DNA, for example originating from NETs, contributes and exacerbates SLE manifestations (Jarrot et al. 2019, Tumurkhuu et al. 2022). Therefore, one would expect tremendous pulmonary injuries in mice lacking circulating DNA-degrading enzymes. However, *DNase1*$^{-/-}$ mice show the opposite of the expected response. *DNase1*$^{-/-}$ animals were not more severely affected but protected from pulmonary injuries.

Another possibility might be that anti-inflammatory DNA ligands accumulate in the absence of DNase1, which then induce protective mechanisms that prevent severe DAH. For example, it was shown that Tlr9-deficiency leads to accelerated renal disease and myeloid lineage abnormalities in pristane-induced murine lupus which suggests that Tlr9 has a protective function (Bossaller et al. 2016). If such a mechanism would also function in *DNase1*$^{-/-}$ mice, loss of Tlr9 should prevent protective signaling and severe DAH would occur. To test this hypothesis, *DNase1*$^{-/-}$ *Tlr9*$^{-/-}$ mice were bred, pristane was administered and peritoneal inflammation as well as pulmonary damage were investigated.

3.6.1 Peritoneal inflammation

Pristane injection resulted in elevated cell numbers in the peritoneal lavage of wild-type, *DNase1*$^{-/-}$ and *DNase1*$^{-/-}$ *Tlr9*$^{-/-}$ mice, although such increases were primarily significant in *DNase1*$^{-/-}$ (Fig. 28 A). The majority of infiltrating immune cells were neutrophils and

monocytes comprising together ~ 40 % of leukocytes (Fig. 28 C, D). Comparing *DNase1*$^{-/-}$ and *DNase1*$^{-/-}$ *Tlr9*$^{-/-}$, frequencies of neutrophils and monocytes were not significantly changed (Fig. 28 C, D). Prior results showed that DNase1-deficiency led to increased numbers of neutrophils in the peritoneal lavage (Fig. 22 B). Such elevation might partially be mediated by Tlr9 since a decreasing trend of cell numbers were observed in *DNase1*$^{-/-}$ *Tlr9*$^{-/-}$ (Fig. 28 C). The fraction of monocytes was similarly increased in wild-type, *DNase1*$^{-/-}$ and *DNase1*$^{-/-}$ *Tlr9*$^{-/-}$ mice after receiving pristane (Fig. 28 D). Percentage and cell number of inflammatory Ly6C^{high} monocytes were unaltered, whereas the fraction of patrolling monocytes was increased in *DNase1*$^{-/-}$ compared to wild type and *DNase1*$^{-/-}$ *Tlr9*$^{-/-}$ (Fig. 28 E, F).

Loss of monocyte-derived cells (Ly6C^{low} IA/IE^{high}) occurred in all groups tested (Fig. 28 G). In addition to infiltrating neutrophils and monocytes, elevated numbers of dendritic cells were detected in the peritoneal lavage (Fig. 28 H). DNase1-deficiency resulted in significantly increased numbers of DCs compared to wild-type or *DNase1*$^{-/-}$ *Tlr9*$^{-/-}$ mice suggesting Tlr9 activation may be involved in such expansion.

Under homeostatic conditions, the majority of cells in the peritoneal cavity highly express B220 which is primarily expressed by B cells. Pristane administration leads to loss of B220^{high} cells potentially due to cell death. Here, B220^{high} cells were similarly reduced in wild type, *DNase1*$^{-/-}$ and *DNase1*$^{-/-}$ *Tlr9*$^{-/-}$ (Fig. 28 I). Interestingly, frequency and number of T cells (CD3e^{+}) were unaffected in wild type and *DNase1*$^{-/-}$ but significantly increased in *DNase1*$^{-/-}$ *Tlr9*$^{-/-}$ (Fig. 28 J). CD4^{+} T cells were most severely reduced in *DNase1*$^{-/-}$ *Tlr9*$^{-/-}$, however, such decrease was not compensated by an increase of CD8^{+} TCs suggesting another population of T cells might be expanded (Fig. 28 K, L). Taken together, lack of Tlr9 signaling did not perturb peritoneal inflammation in *DNase1*$^{-/-}$ mice, since *DNase1*$^{-/-}$ *Tlr9*$^{-/-}$ did not resemble all cellular alterations seen in wild-type mice after pristane administration, but rather influences other potentially harmful processes.

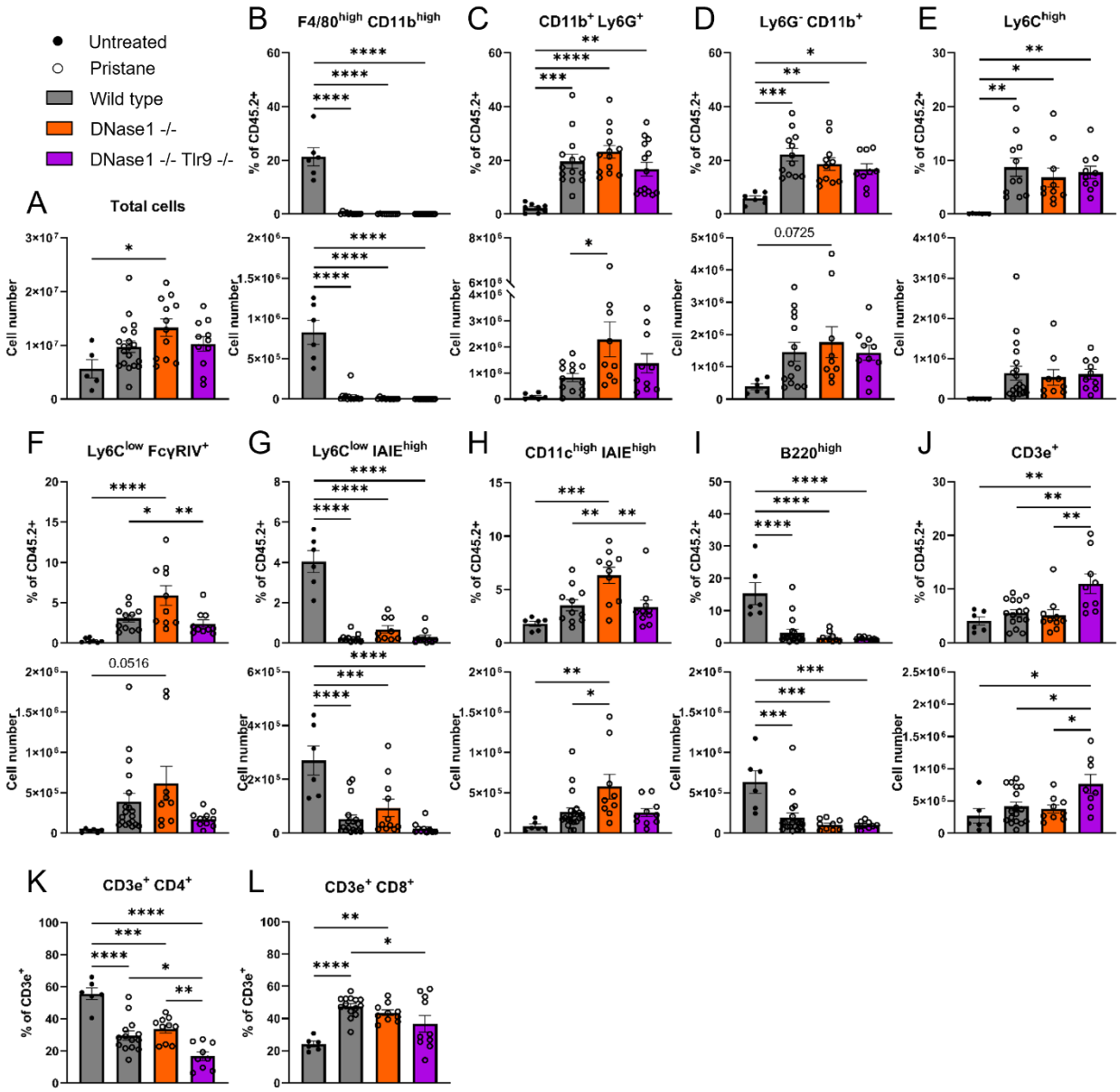

Fig. 28 Immune cell populations in peritoneal lavage from wild-type, *DNase1*$^{-/-}$ and *DNase1*$^{-/-}$ *Tlr9*$^{-/-}$ mice after pristane administration. (A-J) Quantitative comparison of cellular fractions and total number of peritoneal myeloid cells and lymphocytes from untreated wild-type and pristane-treated wild-type, *DNase1*$^{-/-}$ and *DNase1*$^{-/-}$ *Tlr9*$^{-/-}$ mice (n = 6-13 per group, means + SEM) based on flow cytometry analysis. (K-L) Comparison of cellular fractions of CD4^{+} and CD8^{+} T cells in peritoneal lavage. Data are pooled from 4 independent experiments. Statistical analysis was performed using one-way ANOVA with p values corrected for multiple comparison using Tukey. *p < 0.05, **p < 0.01, ***p < 0.001, ****p < 0.0001

3.6.2 Pulmonary inflammation and diffuse alveolar hemorrhage

Contrary to the hypothesis that DNase1-deficiency leads to the activation of protective mechanisms involving Tlr9 signaling, there was no significantly aggravated development of DAH in *DNase1*$^{-/-}$ *Tlr9*$^{-/-}$ mice after pristane injection (Fig. 30 A, 29 A). Cell count and fraction of pulmonary leukocytes seemed to be reduced in treated *DNase1*$^{-/-}$ *Tlr9*$^{-/-}$ compared to wild type (Fig. 30 B). Frequency and cell number of tissue-resident macrophages, neutrophils and dendritic cells including both subsets, CD11b^{+} and CD103^{+}, were unaltered comparing pristane-treated *DNase1*$^{-/-}$ and *DNase1*$^{-/-}$ *Tlr9*$^{-/-}$ mice (Fig. 30 C, D, F-H). However, in contrast to *DNase1*$^{-/-}$, the injection of pristane did not lead to an increased accumulation of monocytes in *DNase1*$^{-/-}$ *Tlr9*$^{-/-}$ lungs suggesting Tlr9 signaling might be involved in the increased buildup of monocytes in *DNase1*$^{-/-}$ (Fig. 30 E). These observations are consistent with previously presented results showing Tlr9-dependent accumulation of monocytes in blood from *DNase1*$^{-/-}$ mice (Fig. 9 F). Taken together, lack of DNase1 prevents severe DAH probably without major involvement of Tlr9 signaling.

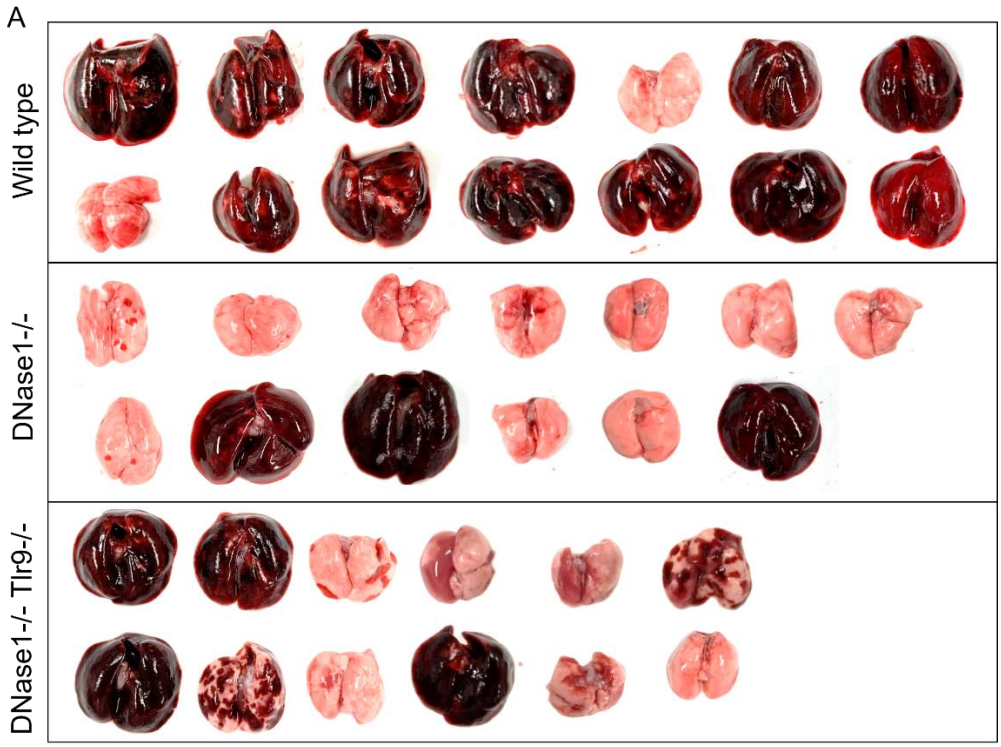

Fig. 29 Gross lung pathology after pristane administration in wild-type, *DNase1*$^{-/-}$ and *DNase1*$^{-/-}$ *Tlr9*$^{-/-}$ mice. (A) Mice received a single injection of pristane i.p. and development of diffuse alveolar hemorrhage was documented after 11 days (n = 12-14). Data are pooled from 3 independent experiments.

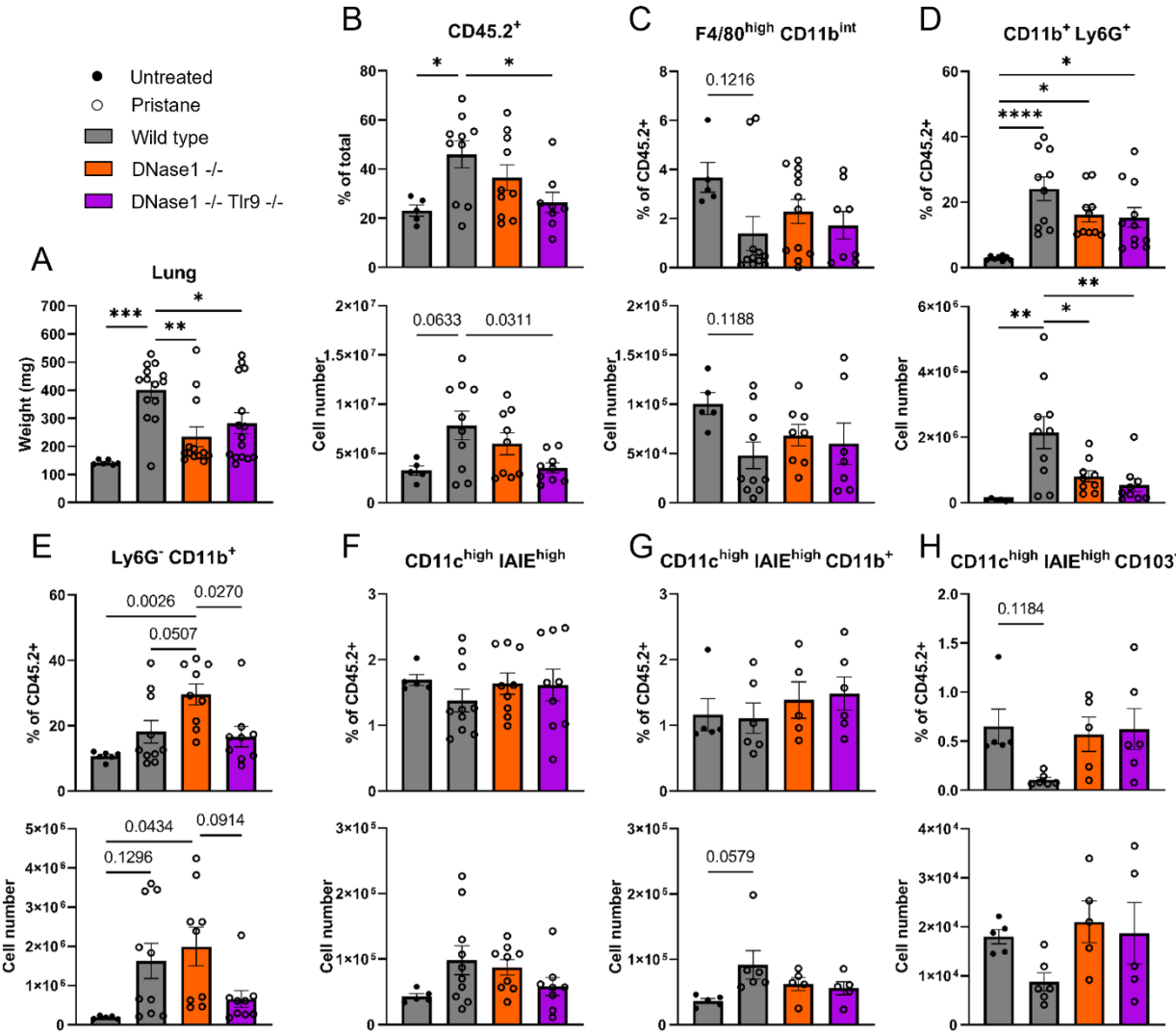

Fig. 30 Immune cell populations in lung from wild-type, *DNase1*$^{-/-}$ and *DNase1*$^{-/-}$ *Tlr9*$^{-/-}$ mice after pristane administration. (A) Comparison of lung weight from untreated wild-type and pristane-treated wild-type, *DNase1*$^{-/-}$ and *DNase1*$^{-/-}$ *Tlr9*$^{-/-}$ mice. (B-H) Quantitative comparison of cellular fractions and total number of myeloid cells from untreated wild-type and pristane-treated wild-type, *DNase1*$^{-/-}$ and *DNase1*$^{-/-}$ *Tlr9*$^{-/-}$ mice (n = 5-10 per group, means + SEM) based on flow cytometry analysis. Data are pooled from 3 independent experiments. Statistical analysis was performed using one-way ANOVA with p values corrected for multiple comparison using Tukey. *p < 0.05, **p < 0.01, ***p < 0.001, ****p < 0.0001

3.7 Involvement of endosomal and cytoplasmic DNA sensors in pristane-mediated peritonitis and DAH

Various studies were conducted pointing to adverse effects of DNA in developing SLE. Here, endosomal as well as cytoplasmic DNA receptor knockout mice were used to decipher the role of two major DNA sensor signaling pathways in developing DAH. Firstly, manifestations of peritonitis were analyzed in wild-type, *Tlr9*$^{-/-}$ and *Sting*$^{-/-}$ mice. Total number of cells within the peritoneal lavage was increased in wild-type and *Tlr9*$^{-/-}$ mice, while Sting-deficient mice showed barely cellular infiltrates after pristane administration (Fig. 31 A). However, peritoneal macrophages (F4/80^{high} CD11b^{high}) were severely affected by pristane in all tested mouse models (Fig. 31 B). In addition, cellular fractions of neutrophils (CD11b^{+} Ly6G^{+}), monocytes (Ly6G^{-} CD11b^{+}) and dendritic cells (CD11c^{high} IA/IE^{high}) were similarly increased in the peritoneal cavity in response to pristane (Fig. 31 C-E).

Tlr9-deficiency partially reduced lung swelling indicated by decreased tissue weight, while the lack of Sting attenuated severe pulmonary damage (Fig. 31 F). In wild-type and *Tlr9*$^{-/-}$ mice, leukocytes (CD45.2^{+}) accumulated, while Sting-deficiency prevented the cellular buildup (Fig. 31 G). Loss of tissue-resident macrophages (F4/80^{high} CD11b^{int}) was observed in wild-type and *Tlr9*$^{-/-}$ but not *Sting*$^{-/-}$ lungs (Fig. 31 H). Besides, the frequency of neutrophils was significantly reduced in *Sting*$^{-/-}$ mice compared to wild-type controls (Fig. 31 I). Cellular fraction of monocytes was primarily increased in *Tlr9*$^{-/-}$ mice (Fig. 31 J). Taken together, both endolysosomal and cytoplasmic recognition of DNA seem to contribute to the development of DAH. However, Sting-dependent DNA sensing might be crucial and involved in leukocyte recruitment to the lung as well as loss of pulmonary macrophages. These results suggest an important role of tissue-resident macrophage death and neutrophil accumulation in the manifestation of pristane-induced severe alveolar hemorrhages.

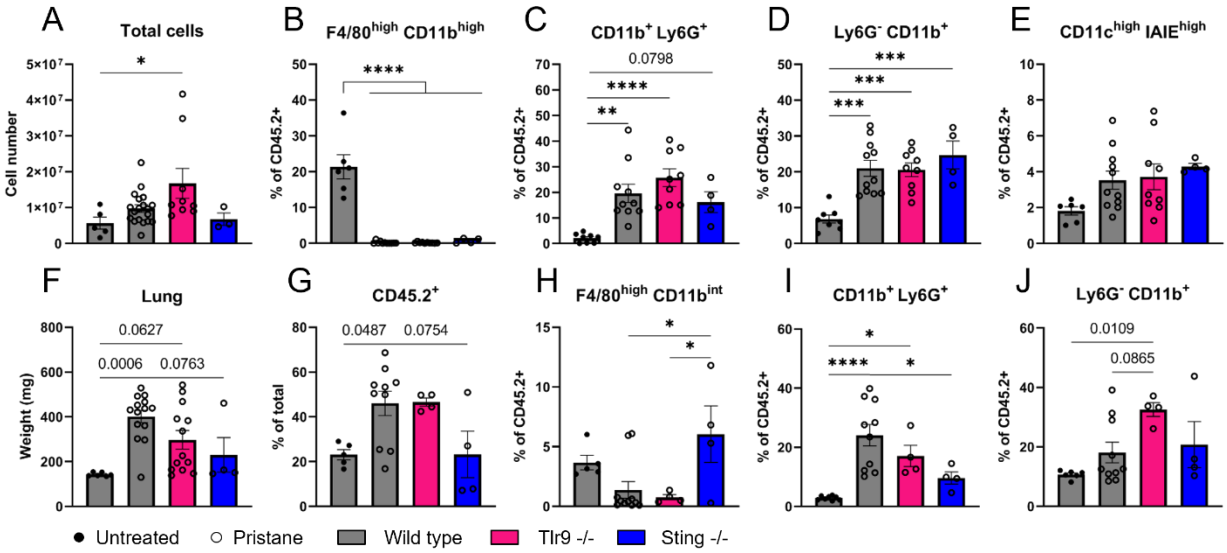

Fig. 31 Pristane induced inflammation in peritoneum (top) and lung (bottom) from wild-type, *Tlr9*$^{-/-}$ and *Sting*$^{-/-}$ mice. (A) Comparison of total cell numbers in peritoneal lavage from untreated wild-type and pristane-treated wild-type, *Tlr9*$^{-/-}$ and *Sting*$^{-/-}$ mice. (B-E) Quantitative comparison of cellular fractions of myeloid cells in peritoneal lavage from untreated wild-type and pristane-treated wild-type, *Tlr9*$^{-/-}$ and *Sting*$^{-/-}$ mice (F) Comparison of lung weights from untreated wild-type and pristane-treated wild-type, *Tlr9*$^{-/-}$ and *Sting*$^{-/-}$ mice. (G-H) Quantitative comparison of pulmonary leukocytes and myeloid cells from untreated wild-type and pristane-treated wild-type, *Tlr9*$^{-/-}$ and *Sting*$^{-/-}$ mice (n = 4-10 per group, mean + SEM) based on flow cytometry analysis. Data are pooled from 2 independent experiments. Statistical analysis was performed using one-way ANOVA with p values corrected for multiple comparison using Tukey. *p < 0.05, **p < 0.01, ***p < 0.001, ****p < 0.0001

4 Discussion

4.1 Loss of deoxyribonucleases alters monocyte profiles and priming

Monocytes function as circulating sensors that encounter environmental and endogenous stressors. Postnatal Ly6C^{high} monocytes are formed primarily in the bone marrow from differentiating hematopoietic stem cells, and are subsequently released into the circulation. During homeostasis, classical Ly6C^{high} monocytes differentiate into Ly6C^{low} patrolling monocytes which scan the vasculature, clear dying endothelial cells, and protect vessel health or replenish certain tissue-resident macrophages. Upon infection, tissue damage or inflammation, monocytes are recruited to tissues where they can differentiate into a variety of monocyte-derived cells to promote inflammatory responses, or resolution of inflammation in response to niche-specific signals. Factors like cytokines, pattern recognition receptors including Tlrs and others can influence the development of monocytes in the bone marrow or tissues (Robinson et al. 2021).

Recent findings uncovered a mechanism by which chronic activation of Tlr7 and Tlr9 defined monocyte fate and drove the development of a specialized population of phagocytes that originated from Ly6C^{high} monocytes and internalized red blood cells leading to anemia and thrombocytopenia (Akilesh et al. 2019). Additionally, a potential link between the expansion of patrolling monocytes and the accumulation of RNA- and DNA-derived nucleosides were found (Morgan et al. 2010, Shibata et al. 2019). Deficiency of lysosomal nucleoside transporter Slc29a3 led to the buildup of guanosine and especially deoxyguanosine primarily in spleen and monocytes. Comparing monocytic subsets, patrolling monocytes displayed the highest concentration of (deoxy)guanosine. Interestingly, expansion of patrolling monocytes and splenomegaly were rescued in the absence of Tlr7, suggesting that the accumulation of nucleosides activated Tlr7 signaling (Shibata et al. 2019). Although Tlr7 is often considered as ssRNA receptor, it was demonstrated that deoxyguanosine, which is one of the four deoxyribonucleosides DNA is composed of, functions as Tlr7 agonist (Davenne et al. 2020). A variety of nucleic acid receptors including endosomal Tlrs as well as cytosolic Aim2 and cGAS are expressed in monocytes influencing cell fate.

One aim of this thesis was to investigate whether the lack of deoxyribonucleases, which regulate degradation and processing of DNA, influences monocytic cell populations

under homeostatic or inflammatory conditions. In aged *DNase1*$^{-/-}$ and *DNase1l2*$^{-/-}$ mice, elevated levels of patrolling monocytes (Ly6C^{low} FcγRIV^{high}) were detected in blood and spleen, respectively. Expansion of patrolling monocytes seemed to be dependent on Tlr9 in *DNase1*$^{-/-}$ mice. Whether monocytic alterations depend on DNA sensors in *DNase1l2*$^{-/-}$ mice needs to be investigated. However, these results may further support the view that Tlr7 and Tlr9 function similarly since previous studies showed that chronic signaling of both Tlrs drove monocyte differentiation into specialized phagocytes (Akilesh et al. 2019). In contrast, loss of DNase1l1 and DNase1l3 resulted in elevated numbers of monocyte-derived cells expressing MHC class II (IA/IE), whereas *Pld3*$^{-/-}$ mice manifested splenomegaly as well as elevated levels of both Ly6C^{low} FcγRIV^{high} and Ly6C^{low} IA/IE^{high} monocytes, suggesting that the investigated nucleases do not only have redundant functions but also influence specific developmental routes of monocytes.

Circulating DNase1l3 prevents autoimmunity by digesting extracellular microparticle-associated chromatin released from apoptotic cells. Accordingly, DNase1l3-deficient mice as well as human SLE patients show elevated DNA concentrations in circulating microparticles. Loss of DNase1l3-mediated tolerance leads to the development of SLE-like characteristics including anti-DNA and anti-nucleosome autoantibodies and IgG deposition in kidneys of both 129 and B6 *DNase1l3*$^{-/-}$ mice. In addition, it is demonstrated that peripheral blood of DNase1l3-deficient mice harbors a progressively increasing fraction of CD11b^{+} Ly6C^{-} monocytes. By almost one year of age, KO mice develop splenomegaly with an increased fraction of germinal center B cells and activated CD4^{+} T cells (Sisirak et al. 2016, Soni et al. 2020).

As part of this dissertation, *DNase1l3*$^{-/-}$ mice were examined at the maximal age of 8 months. Up to this age, no significant increase in spleen weight ($p = 0.0553$) compared to age-matched wild-type controls was observed. In line with this, numbers of splenocytes were not significantly altered ($p = 0.0712$). Here, increasing but not significantly altered fractions of monocytes were observed in the circulation of DNase1l3-deficient mice. In contrast, clear differences were detected in *DNase1l3*$^{-/-}$ spleens compared to wild-type controls. Cellular fractions of monocytes (Ly6G^{-} CD11b^{+}) were elevated in *DNase1l3*$^{-/-}$. Especially Ly6C^{low} IA/IE^{high} monocyte-derived cells seemed to be significantly increased in circulation and spleen. This is contrary to the

previously described monocyte marker profile that were IA/IE (MHC class II) negative. In addition, increased frequencies of activated $CD4^+$ T cells ($CD4^+$ $CD44^+$ $CD45RB^-$) among $CD4^+$ T cells were observed (Sisirak et al. 2016, Soni et al. 2020). Here, CD69 was used as indicator of the activation status of T cells. Proportions of $CD4^+$ $CD69^+$ cells among $CD4^+$ T cells were unaltered in DNase1l3-deficient spleens compared to wild-type controls. Loss of DNase1l3 did not affect frequencies of total B cells in spleens of B6 mice (Sisirak et al. 2016), which is in line with results presented here. *DNase1l3*$^{-/-}$ bone marrow-derived macrophage and dendritic cells as well as J774 cells were treated with various ligands to determine inflammatory cytokine responses. Although *DNase1l3*$^{-/-}$ BMDCs showed a small but significant increase of IL12p40 release after Tlr9 stimulation, overall alterations compared to wild-type cells were rather insignificant which might be due to the low expression of DNase1l3 in the bone marrow. Publicly available RNA-seq data indicate that DNase1l3 is mainly expressed in spleen and lymphoid nodes. In the spleen, cDC highly express DNase1l3 compared to pDC or red pulp macrophages. Consistent with this, Sisirak et al. detected the highest expression of DNase1l3 in splenic cDC and in a fraction of macrophages (Sisirak et al. 2016). Taken together, DNase1l3-deficient mice described in this thesis showed some alterations similar to previously characterized B6 *DNase1l3*$^{-/-}$ mice (*Dnase1l3*$^{LacZ/LacZ}$ KO). Varying results are presumably due to age differences.

Pld3 and Pld4 are endolysosomal proteins whose function was obscure for a long time until recently Gavin et al. showed that these enzymes mediate the lysosomal degradation of single-stranded nucleic acids. It was shown that Pld3-deficient macrophages and Pld4-deficient dendritic cells are more sensitive to Tlr9 ligands. Notably, Pld3-deficient thioglycolated-elicited peritoneal macrophages released more IL6 in response to Tlr9 agonist 2216PS (an A-type CpG oligodeoxynucleotide primarily designed to activate human TLR9 which is partially modified by phosphorothioate linkages) than did wild-type controls or *Pld4*$^{-/-}$ cells, while responses to the Tlr4 ligand lipopolysaccharide were unperturbed. Interestingly, responses to the B-type CpG ODN 1668PS, which is fully modified by phosphorothioate (PS) linkages, or Tlr7 agonist R848 were unaltered (Gavin et al. 2018).

Here, Pld3-deficient J774 cells released more IL6 and Ccl5 in response to multiple Tlr9 ligands including CpGB 1668PS, CpGA 1585 and bacterial dsDNA, while responses to Tlr7 stimulation with R848 or Poly-U resulted in increased IL6 secretion. Tlr4 or Tlr2/Tlr1 heterodimer activation by lipid A or Pam3csk4 were unaltered compared to controls. These results were consistent with responses of bone marrow-derived macrophages stimulated with CpG 2216PS, bacterial dsDNA and R848 releasing higher amounts of Ccl5.

Pld4$^{-/-}$ splenic DCs were found to secrete more IL12p70 and IL6 in response to two Tlr9 ligands VACV70 as well as 2216PS. VACV70 is an unmodified double-stranded oligonucleotide containing CpG motifs which can also elicit IFN-λ responses through Sting-dependent cytoplasmic DNA-sensing pathway. *In vivo*, deficiency of Pld4 led to an inflammatory disorder characterized by elevated levels of IFNγ and splenomegaly which was traced to altered responsiveness of *Pld4*$^{-/-}$ dendritic cells to Tlr9 ligands. Compared to Pld4-sufficient controls, *Pld4*$^{-/-}$ mice displayed altered immune cell subsets including fewer natural killer cells, peritoneal B lymphocytes and platelets but increased numbers of splenic B cells and blood monocytes. In addition, peritoneal macrophages showed elevated expression of MCH class II. Pld3-deficient mice lacked these characteristics observed in *Pld4*$^{-/-}$ mice (Gavin et al. 2018).

In contrast to previously published data, *Pld3*$^{-/-}$ animals analyzed here developed splenomegaly and showed significantly increased splenocyte numbers. Although the proportions of splenic B cell, T cell and dendritic cells were unaltered, total cell numbers expanded in *Pld3*$^{-/-}$ mice compared to wild-type controls. Additionally, frequencies and cell numbers of monocytic cells in spleen and blood increased. The fraction of splenic monocytes highly expressing MHC class II was significantly increased, whereas the frequencies of all monocyte subsets were elevated in the circulation. Besides, levels of platelets were increased, whereas NK cells lacking Pld3 seemed to be unaffected. Thus, loss of Pld3 resulted in characteristics that mostly resemble but also exceed previous observations. *Pld3*$^{-/-}$ mice manifested splenomegaly which was previously only detected in case of Pld4-deficient animals. Therefore, Pld3 and Pld4 may share redundant functions but their loss manifests differently presumably due to distinct expression profiles. Interestingly, pathological manifestations in Pld4-deficient mice including

splenomegaly and elevated numbers of monocytes were rescued in *Pld4*$^{-/-}$ *Tlr9*$^{-/-}$ mice (Gavin et al. 2018). In contrast, endolysosomal accumulation of nucleosides activated Tlr7-dependent expansion of monocytes in Slc29a3-deficient mice (Shibata et al. 2019). Since Pld3 and Pld4 are proposed to degrade both ssDNA and ssRNA (Gavin et al. 2021), it remains to be clarified whether Tlr9 or Tlr7 drive cellular abnormalities in *Pld3*$^{-/-}$ mice.

In summary, one aim of this work was to investigate how the loss of DNA-degrading enzymes affects myeloid cells, especially monocytes, under homeostatic conditions. It was shown that the lack of individual DNases leads to specific alterations in the fate of monocytes, although there may be functional overlaps potentially due to redundant substrate specificity. Interestingly, murine blood monocyte subsets display distinct expression profiles of endolysosomal nucleic acid receptors. While classical monocytes express both Tlr7 and Tlr9, patrolling monocytes downregulate Tlr9 whereas monocyte-derived dendritic cells show reduced expression of Tlr7 (Sato et al. 2020). Both receptors can be activated by DNA degradation products and appear to have mutually opposing, pathogenic or protective, impacts in certain context (Bossaller et al. 2016, Fukui et al. 2009, Fukui et al. 2011). Perhaps, the investigation of Tlr-bound ligands in DNase-deficient cells could lead to the identification of specific endogenous ligands influencing the activation of Tlr9 and Tlr7 and thus the fate of monocytes. It is conceivable that there is an accumulation of activating ligands in DNase-deficient individuals, but also that, for instance, Tlr9-inhibiting DNA fragments are generated under homeostatic conditions, which could promote hyperresponsiveness of Tlr7. Insights might be gained if, for example, monocytes from DNase-deficient mice were isolated, Tlr9 crosslinked with bound ligands, immunoprecipitated and ligands subsequently sequenced.

4.2 Role of deoxyribonucleases in spontaneous and chemically induced SLE-like complications

4.2.1 Role of DNase1

Loss of DNase1 function has long been associated with systemic lupus erythematosus including renal complications (lupus nephritis) in humans and mice, however, increasing evidence indicate that DNase1 activity is not *per se* impaired. Instead, autoantibodies

directed against nucleic acids shield DNA and sterically hinder serum nucleases from degrading their substrates. Although sera from patients with SLE exhibit impaired ability to degrade chromatin from either NETs or necrotic cells, degradation of naked DNA proceeds unhindered (Leffler et al. 2015). In lupus prone (NZBNZW)F1 mice, DNase1 mRNA and enzyme activity in liver, spleen and serum samples were unaltered throughout different states of lupus nephritis, whereas expression of DNase1 and its activity was dramatically reduced in kidneys of mice with severe nephritis. Other nucleases including DNase1l1, DNase1l2, DNase1l3, CAD and DNase2a were not affected. Despite the acquired renal loss of DNase1 activity, serum activity was unaltered (Seredkina and Rekvig 2011). In spontaneous mouse models of lupus including MRL/lpr and (NZBNZW)F1, no coding mutations were found in *DNase1*, whereas both MRL/lpr and (NZBNZW)F1 mice harbor a missense mutation in *DNase1l3* which decreases its nuclease activity against naked and liposome complexed DNA (Wilber et al. 2003). Taken together, decreased serum DNase1 activity is not a predisposing factor but most likely further boosting disease pathology, whereas loss of DNase1l3 seems to play a crucial role in the development lupus nephritis.

Although loss of DNase1 may not be enough to trigger the development SLE-associated kidney damage, the question remains how DNase1 influences disease progression in other tissues. Here, a common model chemically inducing SLE-like autoimmune syndromes in non-autoimmune prone mice strains was used. After a single i.p. injection of pristane, especially BALB/c and SJL/J mice develop multiple characteristics of human SLE including various autoantibodies, as well as immune complex-mediated glomerulonephritis (Satoh and Reeves 1994, Satoh et al. 1995, Satoh et al. 1996). Compared to most genetic models of SLE, pristane has the unique ability to induce type I interferons and diffuse alveolar hemorrhage in C57BL/6 mice (Barker et al. 2011, Chowdhary et al. 2007, Lee et al. 2008a, Lee et al. 2008b, Lee et al. 2009, Nacionales et al. 2006, Satoh et al. 2000). Therefore, the chemical treatment is suitable for investigating autoantibody production as well as pulmonary and renal complications. Since SLE is associated with defective degradation of nucleic acids, it may be a promising tool to uncover the effects of dysfunctional nucleases under inflammatory conditions that are driven by DNA release. Here it was used to investigate the effect of DNA-degrading enzymes on pristane-induced diffuse alveolar hemorrhage.

Interestingly, evidence was found that contradict the widely held theory that the loss of DNase1 contributes to the development of SLE-associated complications. Surprisingly, milder progression and reduced occurrence of alveolar hemorrhages was observed in *DNase1*$^{-/-}$ mice after pristane challenge. Although wild-type, *DNase1*$^{-/-}$ and other DNase knockout mice responded similarly to the harmful mineral oil at the site of injection, amelioration of pulmonary inflammation was observed in mice lacking DNase1. At cellular level, this was reflected in the reduced loss of alveolar macrophages and CD103^{+} cDC as well as decreased number of neutrophils in the lung.

4.2.1.1 Contribution of neutrophil extracellular traps as source of DNA

It is conceivable that the reduced number of pulmonary neutrophils in *DNase1*$^{-/-}$ plays an important role. Activated neutrophils can release chromatin fibers, so-called neutrophil extracellular traps (NETs) which contain autoantigens including proteinase-3 (PR3) and myeloperoxidase (MPO) (Brinkmann et al. 2004). Such autoantigen-DNA complexes were found in the circulation as well as inflamed kidneys, and are proposed to trigger small-vessel vasculitis which is a chronic autoinflammatory condition leading to necrotic inflammation of small-sized blood vessels (Kessenbrock et al. 2008). Recently, Jarrot et al. proposed that NETs are associated with the pathogenesis of pristane-induced DAH. The authors suggested that pristane promotes NETs formation *in vitro* and *in vivo* and that the treatment of mice with recombinant human DNASE1 inhalations removed NETs and reduced lung injury leading to increased survival rates (Jarrot et al. 2019). In addition, Tumurkhuu et al. proposed that neutrophils contribute to ER stress in lung epithelial cells (Tumurkhuu et al. 2022). In contrast, previous work showed that neutrophil depletion using anti-Ly6G monoclonal antibody had no effect on the prevalence of pristane-induced DAH, although the number of neutrophils was massively decreased (Lee et al. 2019, Zhuang et al. 2017). Interestingly, monocyte/macrophage depletion using clodronate liposomes significantly decreased the prevalence of DAH (Zhuang et al. 2017). In addition, genetic deletion of *Irf8*, *Ccr2* or *Cx3cr1* leading to severely reduced monocyte numbers in mice, prevented the development of DAH after pristane challenge (Lee et al. 2019). Replenishment of circulating monocytes in *Ccr2*$^{-/-}$ mice with wild-type monocytes restored the incidence of DAH. Thus, comprehensive evidence suggest that monocytes are essential for pristane-induced DAH, while neutrophils presumably boost disease progression by NETs formation.

4.2.1.2 Profiling of potential myeloid-derived suppressor cells

Fractions of pulmonary monocytes were increased and altered in *DNase1*$^{-/-}$ compared to wild-type mice. While wild-type monocytes showed intermediate Ly6C expression levels, DNase1-deficient monocytes highly expressed Ly6C which could indicate myeloid-derived suppressor cell features. Myeloid-derived suppressor cells (MDSCs) contribute to the negative regulation of immune responses by suppressing T cells or modulating cytokine production of macrophages during cancer and autoimmune disorders including systemic lupus erythematosus and rheumatoid arthritis-associated interstitial lung disease which is characterized by the replacement of normal lung parenchyma with fibrotic tissue. It is anticipated that increased numbers of MDSCs might correlate with positive clinical outcomes and decreased disease severity in autoimmune disorders. MDSCs with monocytic morphology are CD11b^{+} Ly6G^{-} Ly6C^{high} and can be distinguished from tumor-associated macrophages by their high expression of Ly6C and by their low expression of F4/80. Besides, MDSCs originate from immature myeloid cells (IMCs) which are part of the normal process of myelopoiesis. Normally, IMCs migrate to various peripheral organs and differentiate into macrophages, dendritic cells or granulocytes. However, IMCs are also recruited to sites of acute or chronic infection, trauma or sepsis and tumor microenvironments, where their differentiation is prevented, and activation induced. These cells are known as MDSCs and exhibit immunosuppressive functions. The accumulation and activation of MDSCs is regulated by several factors including cytokine receptor signaling and Myd88-dependent Tlr pathways which initiate the upregulation of arginase 1, inducible nitric oxide synthase (iNOS) and suppressive cytokines including TGF-β and IL10 (Gabrilovish and Nagaraj 2009, Kim et al. 2009, Veglia et al. 2021). Here, DNase1-deficient monocytes seemed to highly express both Ly6C and F4/80 and did not upregulate TGF-β compared to wild-type monocytes. Thus, *DNase1*$^{-/-}$ monocytes did not display typical phenotypic similarities with MDSCs but it is possible that they are functionally similar to MDSCs and act immunosuppressively, for instance, by secreting anti-inflammatory cytokines such as IL10.

4.2.1.3 Protective potential of interstitial macrophages and IL10

Alveolar exposure to CpG but no other Tlr ligand leads to the recruitment of splenic monocytes that differentiated into regulatory lung interstitial macrophages (IMs) which

protect the host from allergen induced airway inflammation. IM-mediated protection involves IL10, given that *IL10*$^{-/-}$ IMs lack immunosuppressive effects (Sabatel et al. 2017). Schyns et al. identified two populations of interstitial macrophages, CD206^{+} and CD206^{-} IMs. CD206^{+} IMs exhibit tolerogenic profiles constitutively producing high levels of chemokines and immunosuppressive cytokines including IL10, while CD206^{-} IMs have an antigen-presenting cell profile and populate the alveolar interstitium. Additionally, a discrete population of extravasating non-classical monocytes which arise from intravascular Ly6C^{low} patrolling monocytes was found in murine lungs. A fraction of these non-classical monocytes also express IL10 (Schyns et al. 2019). Notably, *IL10*$^{-/-}$ mice have a significantly increased mortality rate due to pristane-induced DAH, suggesting that IL10 is protective against alveolar hemorrhages (Zhuang et al. 2017). Based on these data, one could hypothesize that the protection of *DNase1*$^{-/-}$ mice against DAH involves IL10. Since Ly6C^{low} patrolling monocytes expanded in *DNase1*$^{-/-}$ animals and it has been postulated that patrolling monocytes give rise to non-classical lung monocytes that have the capacity to produce IL10, it is conceivable that DNase1-deficiency promotes the generation of IL10-producing non-classical monocytes. Therefore, measurements of IL10 levels in bronchoalveolar lavage from pristane-treated *DNase1*$^{-/-}$ and wild-type mice might provide a clue as to why *DNase1*$^{-/-}$ mice are protected and whether *DNase1*$^{-/-}$ monocytes are polarized toward an anti-inflammatory phenotype. Besides, further investigations of pulmonary monocyte populations might be enlightening. For example, expression profiles of a broad spectrum of markers and cytokines/chemokines could be analyzed by flow cytometry. Gained information could be used for fluorescence-activated cell sorting of individual populations combined with next-generation sequencing or even single-cell and spatial transcriptomics could be considered.

4.2.1.4 Targeting the coagulation system as potential therapy

The generation of phagocytic macrophages with anti-inflammatory phenotype that remove apoptotic cells from tissues is perturbed in SLE. Attempts have already been made to change the polarization of macrophages to an anti-inflammatory state. Administration of LXR agonist T0901317 induced an alternative macrophage phenotype *in vivo* and protected mice from DAH (Han et al. 2018). In human patients with DAH, corticosteroids and immunosuppressive agents remain the gold standard, and

recombinant-activated human factor VII (rFVII) has successfully been used as new therapy (Heslet et al. 2006, Park 2013). Initially, recombinant FVII was developed to treat bleeding in hemophilia patients with autoantibodies against factors VIII or IX because rFVII activates the coagulation cascade by binding to tissue factor at the site of injury and initiating the formation of thrombin that stimulates platelets and triggers coagulation (Jurlander et al. 2001). In addition, serine protease inhibitors called serpins regulate thrombotic and thrombolytic protease cascades and were successfully used to reduce DAH in pristane-treated mice (Guo et al. 2021, Zhuang et al. 2021). These observations are in line with results from a large case-control study of lupus DAH patients which revealed that patient's history of thrombocytopenia is strongly predictive of DAH (Kazzaz et al. 2015). Consequently, these data suggest that therapeutically targeting the coagulation system could be a promising strategy to prevent severe DAH. Interestingly, Carminita and colleagues discovered a DNase-dependent pathway of thrombus formation *in vivo* (Carminita et al. 2021). Following endothelial injury, neutrophils are recruited to the damaged vessel wall, become activated by ATP and bind to endothelial cells where they initiate the tissue factor dependent coagulation cascade (Darbousset et al. 2012, Darbousset et al. 2014). *In vivo*, administration of DNase1 significantly reduced the accumulation of neutrophils and platelet thrombus formation at the site of injury. This result would not be surprising if NETosis occurred during thrombus formation since DNase1 can be used to degrade NETs. However, electron microscopy of the thrombus at the site of injury revealed that neutrophils did not release NETs. Instead, DNase1 hydrolyzes ATP and ADP, leading to the generation of adenosine and thereby the inhibition of ATP-dependent neutrophil activation, ADP-dependent human as well as mouse platelet aggregation and ultimately thrombus formation *in vivo* (Carminita et al. 2021). This in turn could mean that the absence of DNase1 supports the formation of thrombi and suppresses bleeding which could be a possible explanation why *DNase1*$^{-/-}$ mice are protected from severe DAH. Potentially, more efficient closure of initial blood-airway barrier disruptions could prevent a massive recruitment of inflammatory granulocytes and monocytes that contribute to tissue damage.

4.2.2 Involvement of DNase1l3 in DAH

Loss of DNase1l3 activity seems to play a crucial role in human and murine SLE-like disorders. In humans, null mutations and hypomorphic variants leading to dysfunctional DNASE1l3 are linked to familial and sporadic systemic lupus erythematosus, respectively (Al-Mayouf et al. 2011, Belot et al. 2020, Carbonella et al. 2017). In addition, *DNase1l3*$^{-/-}$ mice are prone to develop SLE-like syndromes but pathological manifestations develop progressively, and complications are rather mild in B6 mice compared to other murine models of spontaneously occurring lupus (Sisirak et al. 2016). Therefore, it is conceivable that the loss of DNase1l3 in B6 mice treated with pristane at 2 months of age did not have a major impact on the development of diffuse alveolar hemorrhage. Indeed, *DNase1l3*$^{-/-}$ mice responded similarly to wild-type controls when challenged with pristane. A comparable increase in lung weight was detected in both groups and severe cases of hemorrhage affecting the complete organ were also observed. Notably, the expression of DNase1l3 is mainly restricted to the spleen, suggesting that other organs might be less affected by the lack of the deoxyribonuclease. In addition, in contrast to DNase1, DNase1l3 is sensitive to proteolysis by plasmin activated by the plasminogen system (Napirei et al. 2009), which is presumably initiated during small-vessel inflammation.

4.2.3 Pld3-deficiency exacerbates lung damage

The dual loss of Pld3 and Pld4 is lethal due to severe liver inflammation accompanied by excessive activation of macrophages (Gavin et al. 2018). Pld3 is highly expressed by macrophages residing in various organs including the respiratory tract. If macrophages are challenged in the lung, one might expect that Pld3-deficient individuals show stronger proinflammatory responses than wild-type controls. As speculated, *Pld3*$^{-/-}$ mice developed severe alveolar bleedings accompanied by significantly increased tissue swelling after pristane-treatment. Further experiments focusing on phenotype and expression profiles of wild-type, *DNase1*$^{-/-}$ and *Pld3*$^{-/-}$ monocytes/macrophages may provide insights into the development of DAH or other disorders involving monocyte-derived cells and vessel inflammation.

4.2.4 Different roles of extracellular and lysosomal waste-management nucleases in pristane-induced DAH

Although both DNase1 and DNase1l3 are present in the circulation, only the loss of DNase1 attenuates the manifestation of DAH, whereas the lack of lysosomal Pld3 exacerbated tissue damage. But all three enzymes could be considered as waste-management nucleases. So, what makes them different and could explain the contrary phenotypes?

Fragmentation patterns of circulating plasma DNA might provide interesting indications. Plasma cell-free DNA (cfDNA) has a peak fragment size frequency at 166 bp which is reminiscent of a nucleosome (146 bp) including linker sequence (~ 20 bp). In addition, smaller fractions of short fragments (20-120 bp) and long fragments > 250 bp occur. In DNase1-deficient mice, cfDNA fragmentation can be altered and shows a reduction in short DNA pieces, an increase in the frequency of 166 bp fragments, unaltered frequencies of plasma DNA molecules above 250 bp, and sequences are hypermethylated compared with wild-type mice. In contrast, cfDNA in *DNase1l3*$^{-/-}$ mice exhibit an increase in short DNA molecules, decrease in 166 bp fragments, slight increase in pieces > 250 bp with peak values corresponding to di-, tri-, and tetra-nucleosome sizes as well as hypomethylation due to increased representation of open chromatin regions and CpG islands. Thus, loss of DNase1l3 revealed that DNase1 elevated the representation of open chromatin regions and CpG islands, especially in shorter fragments (≤ 80 bp), resulting in the relative hypomethylation of cfDNA (Han et al. 2020, Lo et al. 2010, Snyder et al. 2016).

Interestingly, plasma DNA of SLE patients showed skewed cfDNA fragmentation profiles with a significantly elevated fraction of short DNA molecules. The increase in the proportion of short fragments in SLE patients correlated with the disease activity and anti-dsDNA antibody level. Additionally, SLE patients' plasma DNA showed decreased methylation densities. Compared with healthy controls, patients had higher concentrations of IgG-bound plasma DNA and short DNA fragments were enriched in the IgG-bound fraction, suggesting that the preferential binding of anti-DNA antibodies to short DNA molecules hinders their removal from the circulation (Chan et al. 2014). Thus, characteristics of circulating cfDNA in DNase1l3-deficient mice resemble plasma DNA

fragmentation profiles found in SLE patients, while DNase1 activity seems to increase the occurrence of potentially harmful short DNA molecules.

Since Tlr9 is primarily activated by ligands with unmethylated CpG motifs (Coch et al. 2009, Hartmann and Krieg 2000, Krieg et al. 1995) and DNase1 contributes to the generation of short hypomethylated plasma DNA fragments originating from open chromatin regions and CpG islands, questioning a possible link might be reasonable. One could also ask what function a certain DNA fragmentation profile has *in vivo*, and why circulating DNA is not completely degraded, although DNase1 certainly has the ability *in vitro*. Crystal structures of Tlr9 with agonistic and inhibiting ligands revealed sequence-dependent mechanisms regulating different conformations of the endosomal DNA sensor. For example, ODN 1668 and iDNA4084 are both 12-mers but while the stimulatory ligand (1668) initiates dimerization, the inhibitory molecule (iDNA4084) keeps Tlr9 in its monomeric conformation. This inhibitory effect is dependent on the sequence of iDNA4084 which facilitates intramolecular base pair binding resulting in a secondary structure that prevents dimerization (Ohto et al. 2015).

Based on these results, one could conclude that the absence of DNase1 in *DNase1*$^{-/-}$ mice leads to the reduction of circulating DNA fragments that are potentially able to activate Tlr9 signaling. This could be another possible explanation for the protection of *DNase1*$^{-/-}$ animals against severe DAH. In line with this, *Tlr9*$^{-/-}$ mice were partially protected from severe DAH after pristane challenge.

In contrast to DNase1 and DNase1l3, Pld3 is located intracellularly in endolysosomal compartments where it only degrades ssDNA without 5’-phosphate (5’-PO) terminus and secondary structures (Gavin et al. 2018). However, incoming endosomal DNAs are predominantly double-stranded and have a 5’-PO since upstream nucleases including DNase1, Trex1 and CAD perform 5’-PO and 3’-OH substrate cleavage which renders it resistant to Pld3/4. In contrast, DNase2a is a lysosomal endonuclease which cleaves dsDNA and ssDNA leaving DNA fragments with 5’-OH and 3’-PO which renders them accessible to Pld3 and -4 (Bartok and Hartmann 2020, Chan et al. 2015). Thus, Pld3 and Pld4 probably act downstream of DNase2a and inhibit excessive Tlr9 activation by degrading its agonists. Interestingly, Pld3 and Pld4 are proposed to digest ssRNA in addition to ssDNA and limit autoinflammatory triggering by multiple NA sensors including

Tlr9, Tlr7 and Sting (Gavin et al. 2021). Although signaling through Tlr9 makes a major contribution to pathological manifestation in *Pld3*$^{-/-}$ *Pld4*$^{-/-}$ mice, certain abnormalities including a type I IFN signature remain in the absence of endosomal Tlr signaling. In more detail, a Sting-dependent type I IFN signature remain in *Unc93b1*$^{3d/3d}$ *Pld3*$^{-/-}$ *Pld4*$^{-/-}$ mice. These observations could explain why Pld3-deficient mice were more severely affected by pristane since type I IFNs are involved in the pathogenesis of SLE. For example, IFNα is elevated in a fraction of SLE patients (Lichtman et al. 2012, Niewold 2011) and has been implicated in pathological manifestations in several murine lupus models (Agrawal et al. 2009, Braun et al. 2003, Jørgensen et al. 2007, Nacionales et al. 2007, Santiago-Raber et al. 2003, Thibault et al. 2009). Additionally, *in vivo* adenoviral-mediated delivery of murine IFNα results in accelerated onset of SLE in *DNase1l3*$^{-/-}$ mice or induces early lethal lupus in autoimmune-prone (NZBxNZW)F1 animals (Mathian et al. 2005, Sisirak et al. 2016). Consistently, autoreactivity and autoimmune renal manifestations are facilitated by Ifnar1 (a subunit of the receptor of type I IFNs) signaling in *DNase1l3*$^{-/-}$ mice and MRL.Faslpr mice (Nickerson et al. 2013, Soni et al. 2020).

4.3 Role of endosomal and cytoplasmic DNA sensors

Organs that rely on accurate and delicate tissue architecture are particularly vulnerable to damage induced by cell death and excessive repair processes. Failure to properly clear cellular debris, including DNA, can initiate inflammatory responses, contributing to further damage. Especially in organs that are in constant contact with pollutants, allergens and pathogens immune responses must be tightly regulated. Various triggers including silica particle and cigarette smoke induce lung cell death and cause the release of mitochondrial and/or nuclear self-DNA that drive airway inflammation and excessive repair responses, often leading to fibrosis (Benmerzoug et al. 2018, Benmerzoug et al. 2019, Nascimento et al. 2019). Here, the cytotoxic compound pristane was used to initiate lung damage in wild-type, *Tlr9*$^{-/-}$ and *Sting*$^{-/-}$ mice which in some cases resulted in disrupted integrity of the blood-air barrier and lead to respiratory failure due to widespread hemorrhages. Sting-deficiency significantly reduced lung swelling and pulmonary inflammation after pristane challenge, which is in line with previous results showing that the lack of Sting prevents fatal pristane-induced alveolar hemorrhage in *Tank*$^{-/-}$ mice. Tank is a negative regulator of NF-κB signaling and

suppresses DNA-mediated induction of IFN-stimulated genes in macrophages by inhibiting cGas-Sting-signaling. Thus, loss of Tank results in an excessive Sting-dependent IFN response. Consequently, *Sting*$^{-/-}$ *Tank*$^{-/-}$ mice have significantly increased survival rates compared to *Tank*$^{-/-}$ controls (Wakabayashi et al. 2021). But the question remains how the cGas-Sting pathway might be activated by pristane. *In vitro* and *in vivo*, the administration of pristane leads to cell death. Features of apoptosis via the mitochondrial pathway including increased expression of pro-apoptotic Bax, decreased protein levels of anti-apoptotic Bcl-2 and Bcl-xl are detected in lung sections and in *in vitro* cultures of alveolar epithelial cells (Chen et al. 2021, Yang et al. 2021). Besides, cytochrome c is released and caspase-3 and -9 are activated in pristane-mediated apoptosis (Calvani et al. 2005). During intrinsic apoptosis, Bax and Bak are activated forming multimers that generate pores within the outer mitochondrial membrane causing mitochondrial outer membrane permeabilization (MOMP); this leads to the release of intermembrane space proteins including cytochrome c. Over time, Bax/Bak-mediated pores expand and enable inner mitochondrial membrane extrusion and rupture allowing the release of mitochondrial DNA into the cytosol whereupon it can initiate cGas-Sting-signaling, leading to pro-inflammatory interferon signaling. Although multiple results indicate that pristane induces apoptotic cell death, cytosolic release of mitochondrial DNA leading to Sting signaling can also occur in other forms of cell death including necroptosis which is a regulated form of necrotic cell death orchestrated by RIPK1/RIPK3-mediated activation of MLKL (Bock and Tait 2020, Ketelut-Carneiro and Fitzgerald 2022). However, RIPK3-deficiency did not impact the development or progression of renal damage in several murine models of lupus including pristane-induced lupus, suggesting that RIPK3 is dispensable at least for renal complications (Corradetti et al. 2016).

In addition to detecting intracellularly released mtDNA, cGas recognizes phagocytosed neutrophil extracellular traps that escape phagosomes and translocate to the cytosol resulting in the production of type I IFNs by macrophages and other myeloid cells (Apel et al. 2021). In parallel, ingested NETs might also activate Tlr9 which triggers NF-κB signaling, leading to the release of proinflammatory cytokines. In line with this, Tlr9-deficiency positively influenced the outcome of pristane-induced lung hemorrhage progression but showed less severe effects compared to Sting-deficiency. Notably, only

NETs of certain size activated cGas *in vitro*. NETs digested with DNase1 led to fragments larger than 150 bp under certain conditions which activated recombinant cGas, whereas undigested structures and DNA molecules of nucleosome size (~ 150 bp) had no stimulatory effect, suggesting that the cleavage of NETs by DNase1 initially enforces cGas activation, whereas further digestion hampers it (Apel et al. 2021). These indications support the hypothesis that DNase1 might be required to cleave released self-DNA into fragments that are harmful and could drive Tlr9-dependent proinflammatory cytokine release as well as Sting-dependent type I IFN response and lung cell death.

Exposure of human SLE neutrophils to agonistic autoantibodies resulted in the release of oxidized DNA of mitochondrial origin (Caielli et al. 2016). Oxidized DNA, containing 8-OH-deoxyguanosine (8-OH-dG), initiates cGas-Sting-signaling, and dysfunction of the DNA repair enzyme that patches 8-OH-dG lesions, termed Ogg1 (oxoguanisine glycolase 1), is associated with the development of lupus nephritis (Lee et al. 2015). However, in Ogg1-deficient mice pristane-induced lupus resulted in cutaneous complications rather than increased kidney pathology, (Tumurkhuu et al. 2020). In line with this, cGas- or Sting-deficiency failed to rescue renal complications including autoantibody production and kidney damage in pristane-induced SLE and lupus-prone mouse models (Motwani et al. 2021, Sharma et al. 2015). In contrast, gain-of-function mutations in STING were identified in human patients suffering from an inflammatory syndrome with lupus-like manifestations, familial chilblain lupus and so-called SAVI (Sting-associated vasculopathy with onset in infancy) which leads to severe small-vessel damage (Jeremiah et al. 2014, König et al. 2017, Liu et al. 2014). Taken together, the clinical heterogeneity of SLE manifestations might be influenced by the involvement of multiple DNA sensors. While renal complications might be primarily driven by endosomal TLRs, activation of cytoplasmic DNA sensors seems to be critical for the development of vessel inflammation and severe, life-threatening pulmonary hemorrhage. Since NA-sensor pathways are intertwined and influence each other, it would be advisable to elucidate their functions in great detail in order to avoid possible side effects of therapies that primarily target one receptor.

5 Abstract

In healthy and diseased individuals, endogenous nucleic acids are present in various forms and need to be processed and cleared. Failed clearance of DNA is associated with an autoimmune disease termed systemic lupus erythematosus (SLE), which is characterized by systemic inflammation affecting multiple organs including kidney and lung. In SLE patients and lupus-prone mouse models, myeloid cells contribute to the immune-mediated pathology and recognition of DNA-derived products drives their activation. In contrast, detection of DNA-derived products can contribute to the survival, proliferation and differentiation of myeloid cells resulting in cancer-like cell expansion also termed histiocytosis.

The aim of this thesis was to investigate how the loss of DNA-degrading enzymes influences myeloid cell populations under homeostatic conditions and what effects these changes have under inflammatory conditions. Therefore, multiple deoxyribonuclease-deficient mice including *DNase1*$^{-/-}$, *DNase1l1*$^{-/-}$, *Dnase1l2*$^{-/-}$, *DNase1l3*$^{-/-}$ and *Pld3*$^{-/-}$ mice were generated. While in *DNase1*$^{-/-}$ and *DNase1l2*$^{-/-}$ mice elevated numbers of patrolling monocytes were found, loss of Dnase1l1 and DNase1l3 led to the expansion of monocyte-derived cells expressing MHC class II. *Pld3*$^{-/-}$ mice developed splenomegaly accompanied by an expansion of diverse monocyte populations. But apart from enlarged spleens, no gross pathological manifestations could be observed. Since the effects of the cellular alterations were not apparent, deoxyribonuclease-deficient individuals were treated with a compound termed pristane that induces cell death and boosts the release of self-DNA. Besides, pristane is known to induce renal and pulmonary SLE-like complications. Surprisingly, it has been discovered that the loss of DNase1 protects against the development of severe pulmonary hemorrhages after pristane challenge, whereas deficiency of DNase1l1, Dnase1l2 and DNase1l3 did not affect disease progression. In contrast, Pld3-deficiency aggravated pathological manifestations. Since myeloid cells contribute significantly to the development of pristane-induced pulmonary hemorrhages, diverse populations in the peritoneum – the initial site of inflammation – and lung – the site of bleeding – were examined. In addition, the involvement of two DNA sensors, which are associated with the manifestation of SLE-linked complications, was investigated. Pristane-challenged *Tlr9*$^{-/-}$ mice were partially while *Sting*$^{-/-}$ mice were

primarily protected from severe lung injuries, suggesting that both DNA sensors are involved in the development of alveolar hemorrhage.

6 List of figures

7 List of tables

8 References

Abe T, and Barber. Cytosolic-DNA-Mediated, STING-Dependent Proinflammatory Gene Induction Necessitates Canonical NF-κB Activation through TBK1. *J Virol* 2014; *88*(10), 5328–5341. DOI: 10.1128/jvi.00037-14

Ablasser A, Goldeck M, Cavlar T, Deimling T, Witte G, Röhl I, Hopfner K-P, Ludwig J, Hornung V. cGAS produces a 2'-5'-linked cyclic dinucleotide second messenger that activates STING. *Nature* 2013; 498 (7454), 380–384. DOI: 10.1038/nature12306

Aglietti RA, Estevez A, Gupta A, Ramirez MG, Liu PS, Kayagaki N, Ciferri C, Dixit VM, Dueber EC. GsdmD p30 elicited by caspase-11 during pyroptosis forms pores in membranes. *Proc Natl Acad Sci USA* 2016; *113*(28), 7858–7863. DOI: 10.1073/pnas.1607769113

Agrawal H, Jacob N, Carreras E, Bajana S, Putterman C, Turner S, Neas B, Mathian A, Koss MN, Stohl W, Kovats S, Jacob CO. Deficiency of Type I IFN Receptor in Lupus-Prone New Zealand Mixed 2328 Mice Decreases Dendritic Cell Numbers and Activation and Protects from Disease. *J Immunology* 2009; *183*(9), 6021–6029. DOI: 10.4049/jimmunol.0803872

Ahn J, Gutman D, Saijo S, Barber GN. STING manifests self DNA-dependent inflammatory disease. *Proc Natl Acad Sci USA* 2012; 109(47), 19386–19391. DOI: 10.1073/pnas.1215006109

Akilesh HM, Buechler MB, Duggan JM, Hahn WO, Matta B, Sun X, Gessay G, Whalen E, Mason M, Presnell SR, Elkon KB, Lacy-Hulbert A, Barnes BJ, Pepper M, Hamerman JA. Chronic TLR7 and TLR9 signaling drives anemia via differentiation of specialized hemophagocytes. *Science* 2019; *363*(6423), eaao5213. DOI: 10.1126/science.aao5213

Alexopoulou L, Holt AC, Medzhitov R, Flavell RA. Recognition of double-stranded RNA and activation of NF-kappaB by Toll-like receptor 3. *Nature* 2001; 413, 732–738. DOI: 10.1038/35099560

Al-Mayouf SM, Sunker A, Abdwani R, Abrawi SA, Almurshedi F, Alhashmi N, Al Sonbul A, Sewairi W, Qari A, Abdallah E, Al-Owain M, All Motywee S, Al-Rayes H, Hashem M, Khalak H, Al-Jebali L, Alkuraya FS. Loss-of-function variant in DNASE1L3 causes a familial form of systemic lupus erythematosus. *Nat Genet* 2011; 43, 1186–1188. DOI: 10.1038/ng.975

Amano H, Amano E, Santiago-Raber ML, Moll T, Martinez-Soria E, Fossati-Jimack L, Iwamoto M, Rozzo SJ, Kotzin BL, Izui S. Selective Expansion of a Monocyte Subset Expressing the CD11c Dendritic Cell Marker in the Yaa Model of Systemic Lupus Erythematosus. *Arthritis Rheum* 2005; 52(9), 2790–2798. DOI: 10.1002/art.21365

Andrade C, Mendonça T, Farinha F, Correia J, Marinho A, Almeida I, Vasconcelos C. Alveolar hemorrhage in systemic lupus erythematosus: a cohort review. *Lupus.* 2016; 25(1), 75-80. DOI: 10.1177/0961203315605365

Andreeva L, Hiller B, Kostrewa D, Lässig C, de Oliveira Mann CC, Drexler DJ, Maiser A, Gaidt M, Leonhardt H, Hornung V, Hopfner K-P. cGAS senses long and HMGB/TFAM-bound U-turn DNA by forming protein-DNA ladders. *Nature* 2017; 549(7672), 394–398. DOI: 10.1038/nature23890

Andrejeva J, Childs KS, Young DF, Carlos TS, Stock N, Goodbourn S, Randall RE. The V proteins of paramyxoviruses bind the IFN-inducible RNA helicase, mda-5, and inhibit its activation of the IFN-β promoter. *Proc Natl Acad Sci USA* 2004*;* 101(49), 17264–17269. DOI: 10.1038/nature23890

Apel F, Andreeva L, Knackstedt LS, Streeck R, Frese CK, Goosmann C, Hopfner KP, Zychlinsky A. The cytosolic DNA sensor cGAS recognizes neutrophil extracellular traps. *Sci Signal* 2021; 14(673), eaax7942. DOI: 10.1126/scisignal.aax7942.

Badsha H, 112mm CL, Kong KO, Lian TY, Chng HH. Pulmonary hemorrhage in systemic lupus erythematosus. *Semin Arthritis Rheum* 2004; 33(6), 414–421. DOI: 10.1016/j.semarthrit.2003.09.006

Balada E, Ordi-Ros J, Hernanz S, Villarreal J, Cortés F, Vilardell-Tarrés M, Cortés F, Vilardell-Tarrés M, Labrador M. DNASE I mutation and systemic lupus erythematosus in a Spanish population: comment on the article by Tew et al. *Arthritis Rheum* 2002; 46(7), 1974–1976. DOI: 10.1002/art.10349

Baldwin SA, Yao SYM, Hyde RJ, Ng AML, Foppolo S, Barnes K, Ritzel MWL, Cass CE, Young JD. Functional characterization of novel human and mouse equilibrative nucleoside transporters (hENT3 and mENT3) located in intracellular membranes. *J Biol Chem* 2005; *280*(16), 15880–15887. DOI: 10.1074/jbc.M414337200

Baranovskii AG, Buneva VN, Nevinsky GA. Human Deoxyribonucleases. *Biochemistry (Mosc)* 2004; 69(6), 587-601. DOI: 10.1023/b:biry.0000033731.50496.01

Barker TT, Lee PY, Kelly-Scumpia KM, Weinstein JS, Nacionales DC, Kumagai Y, Akira S, Croker BP, Sobel ES, Reeves WH, Satoh M. Pathogenic role of B cells in the development of diffuse alveolar hemorrhage induced by pristane. *Lab Invest* 2011; 91(10), 1540–1550. DOI: 10.1038/labinvest.2011.108

Barrat FJ, Meeker T, Gregorio J, Chan JH, Uematsu S, Akira S, Chang B, Duramad O, Coffman RL. Nucleic acids of mammalian origin can act as endogenous ligands for Toll-like receptors and may promote systemic lupus erythematosus. *J Exp Med* 2005*;* 202(8), 1131–1139. DOI: 10.1084/jem.20050914

Bartok E, Hartmann G. Immune Sensing Mechanisms that Discriminate Self from Altered Self and Foreign Nucleic Acids. *Immunity* 2020; 53(1), 54–77. DOI: 10.1016/j.immuni.2020.06.014

Baum R, Sharma S, Carpenter S, Li QZ, Busto P, Fitzgerald KA, Marshak-Rothstein A, Gravallese EM. Cutting edge: AIM2 and endosomal TLRs differentially regulate arthritis and autoantibody production in DNase II-deficient mice. *J Immunol* 2015; 194(3), 873–877. DOI: 10.4049/jimmunol.1402573

Bedoui S, Herold MJ, Strasser A. Emerging connectivity of programmed cell death pathways and its physiological implications. *Nat Rev Mol Cell Biol* 2020; 21(11), 678–695. DOI: 10.1038/s41580-020-0270-8

Belot A, Rice GI, Omarjee SO, Rouchon Q, Smith EMD, Moreews M, Tusseau M, Frachette C, Bournhonesque R, Thielens N, Gaboriaud C, Rouvet I, Chopin E, Hoshino A, Latour S, Ranchin B, Cimaz R, Romagnani P, Malcus C, Fabien N, Sarda M-N, Kassai B, Lega J-C, Decramer S, Abou-Jaoude P, Bruce IN, Simonet T, Bardel C, Rollat-Farnier PA, Viel S, Reumaux H, O'Sullivan J, Walzer T, Mathieu A-L, Marenne G,

Ludwig T, Genin E, Ellingford J, Bader-Meunier B, Briggs TA, Beresford MW, Crow YJ. Contribution of rare and predicted pathogenic gene variants to childhoodonset lupus: a large, genetic panel analysis of British and French cohorts. *Lancet Rheumatol* 2020; 2(2), e99–109. DOI: 10.1016/S2665-9913(19)30142-0

Benmerzoug S, Rose S, Bounab B, Gosset D, Duneau L, Chenuet P, Mollet L, le Bert M, Lambers C, Geleff S, Roth M, Fauconnier L, Sedda D, Carvalho C, Perche O, Laurenceau D, Ryffel B, Apetoh L, Kiziltunc A, Uslu H, Albez FS, Akgun M, Togbe D, Quesniaux VFJ. STING-dependent sensing of self-DNA drives silica-induced lung inflammation. *Nat Commun* 2018; 9, 5226. DOI: 10.1038/s41467-018-07425-1

Benmerzoug S, Ryffel B, Togbe D, Quesniaux VFJ. Self-DNA sensing in lung inflammatory disease. *Trends Immunol* 2019, 40(8), 719-734. DOI: 10.1016/j.it.2019.06.001

Bessis MC, Breton-Goriijs J. Iron Metabolism in the Bone Marrow as Seen by Electron Microscopy: A Critical Review*. Blood* 1962; 19, 635-663. http://ashpublications.org/blood/article-pdf/19/6/635/751868/635.pdf

Bethunaickan R, Berthier CC, Ramanujam M, Sahu R, Zhang W, Sun Y, Bottinger EP, Ivashkiv L, Kretzler M, Davidson A. A unique hybrid renal mononuclear phagocyte activation phenotype in murine systemic lupus erythematosus nephritis. *J Immunol* 2011; 186(8), 4994-5003. DOI: 10.4049/jimmunol.1003010

Billen LP, Shamas-Din A, Andrews DW. Bid: a Bax-like BH3 protein. *Oncogene* 2008; 27, S93–S104. DOI: 10.1038/onc.2009.47

Boatright KM, Salvesen GS. Mechanisms of caspase activation. *Curr. Opin. Cell Biol* 2003; 15(6), 725–731. DOI: 10.1016/j.ceb.2003.10.009

Bock FJ, Tait SWG. Mitochondria as multifaceted regulators of cell death. *Nat Rev Mol Cell Biol* 2020; 21, 85–100. DOI: 10.1038/s41580-019-0173-8

Bodaño A, González A, Balada E, Ordi J, Carreira P, Gómez-Reino JJ, Conde C. Study of DNASE I gene polymorphisms in systemic lupus erythematosus susceptibility. *Ann Rheum Dis* 2007; 66(4), 560–561.

Doi: 10.1136/ard.2006.067140

Bohnhorst J, Rasmussen T, Moen SH, Flottum M, Knudsen L, Børset M, Espevik T, Sundan A. Toll-like receptors mediate proliferation and survival of multiple myeloma cells. *Leukemia* 2006; 20(6), 1138–1144. DOI: 10.1038/sj.leu.2404225

Bossaller L, Christ A, Pelka K, Nündel K, Chiang PI, Pang C, Mishra N, Busto P, Bonegio RG, Schmidt RE, Latz E, Marshak-Rothstein A. TLR9 Deficiency Leads to Accelerated Renal Disease and Myeloid Lineage Abnormalities in Pristane-Induced Murine Lupus. *J Immunol* 2016; 197(4), 1044-1053. DOI: 10.4049/jimmunol.1501943

Boucher D, Monteleone M, Coll RC, Chen KW, Ross CM, Teo JL, Gomez GA, Holley CL, Bierschenk D, Stacey KJ, Yap AS, Bezbradica, JS, Schroder K. Caspase-1 self-cleavage is an intrinsic mechanism to terminate inflammasome activity. *J Exp Med* 2018; 215(3), 827–840. DOI: 10.1084/jem.20172222

Braun D, Geraldes P, Demengeot J. Type I Interferon controls the onset and severity of autoimmune manifestations in lpr mice. *J Autoimmun* 2003, 20(1), 15–25. DOI:

10.1016/S0896-8411(02)00109-9

Brinkmann V, Reichard U, Goosmann C, Fauler B, Uhlemann Y, Weiss DS, Weinrauch Y, Zychlinsky A. Neutrophil extracellular traps kill bacteria. *Science* 2004; 303(5663), 1532–1535. DOI: 10.1126/science.1092385

Brumpton BM, Ferreira MAR. Multivariate eQTL mapping uncovers functional variation on the X-chromosome associated with complex disease traits. *Hum Genet* 2016; 135(7), 827–839. DOI: 10.1007/s00439-016-1674-6

Burnham P, Kim MS, Agbor-Enoh S, Luikart H, Valantine HA, Khush KK, de Vlaminck I. Single-stranded DNA library preparation uncovers the origin and diversity of ultrashort cell-free DNA in plasma. *Sci Rep* 2016; 6, 27859. DOI: 10.1038/srep27859

Burdette DL, Monroe KM, Sotelo-Troha K, Iwig JS, Eckert B, Hyodo M, Hayakawa Y, Vance RE. STING is a direct innate immune sensor of cyclic di-GMP. *Nature* 2011; 478, 515–518. DOI: 10.1038/nature10429

Bürckstümmer T, Baumann C, Blüml S, Dixit E, Dürnberger G, Jahn H, Planyavsky M, Bilban M, Colinge J, Bennett KL, Superti-Furga G. An orthogonal proteomic-genomic screen identifies AIM2 as a cytoplasmic DNA sensor for the inflammasome. *Nat Immunol* 2009; 10(3), 266–272. DOI: 10.1038/ni.1702

Bygrave AE, Rose KL, Cortes-Hernandez J, Warren J, Rigby RJ, Cook TH, Walport MJ, Vyse TJ, Botto M. Spontaneous autoimmunity in 129 and C57BL/6 mice-implications for autoimmunity described in gene-targeted mice. *PloS Biol* 2004; 2(8), E243. DOI: 10.1371/journal.pbio.0020243

Cai Y, Shi Z, Bai Y. Review of Rosai-Dorfman Disease: New Insights into the Pathogenesis of This Rare Disorder. *Acta Haematol* 2017; 138(1), 14–23. DOI: 10.1159/000475588

Caielli S, Athale S, Domic B, Murat E, Chandra M, Banchereau R, Baisch J, Phelps K, Clayton S, Gong M, Wright T, Punaro M, Palucka K, Guiducci C, Banchereau J, Pascual V. Oxidized mitochondrial nucleoids released by neutrophils drive type I interferon production in human lupus. *J Exp Med* 2016; 213(5), 697–713. DOI: 10.1084/jem.20151876

Calvani N, Caricchio R, Tucci M, Sobel ES, Silvestris F, Tartaglia P, Richards HB. Induction of Apoptosis by the Hydrocarbon Oil Pristane: Implications for Pristane-Induced Lupus. *J Immunol* 2005; 175(7), 4777–4782. DOI: 10.4049/jimmunol.175.7.4777

Carbonella A, Mancano G, Gremese E, Alkuraya FS, Patel N, Gurrieri F, Ferraccioli G. An autosomal recessive DNASE1L3 -related autoimmune disease with unusual clinical presentation mimicking systemic lupus erythematosus. *Lupus* 2017; 26(7), 768–772. DOI: 10.1177/0961203316676382

Carminita E, Crescence L, Brouilly N, Altié A, Panicot-Dubois L, Dubois C. DNAse-dependent, NET-independent pathway of thrombus formation in vivo. *PNAS* 2021; 118(28), DOI: 10.1073/pnas.2100561118

Chakraborty P, Kacem HH, Makni-Karray K, Jarraya F, Hachicha J, Ayadi H. The A/T mutation in exon 2 of the DNASE1 gene is not present in Tunisian patients with systemic lupus erythematosus or in healthy subjects. *Arthritis Rheum* 2003; 48(11), 3297–3298.

DOI: 10.1002/art.11318

Chan RWY, Jiang P, Peng X, Tamc LS, Liao GJW, Li EKM, Wong PCH, Sun H, Chan KCA, Chiu RWK, Dennis Lo YM. Plasma DNA aberrations in systemic lupus erythematosus revealed by genomic and methylomic sequencing. *Proc Natl Acad Sci USA* 2014; 111(49), E5302–E5311. DOI: 10.1073/pnas.1421126111

Chan MP, Onji M, Fukui R, Kawane K, Shibata T, Saitoh S-I, Ohto U, Shimizu T, Barber GN, Miyake K.. DNase II-dependent DNA digestion is required for DNA sensing by TLR9. *Nat Commun* 2015; 6, 5853. DOI: 10.1038/ncomms6853

Chen W-C, Wang W-C, Lu H-F, Okada Y, Chang W-P, Chou Y-H, Chang H-H, Huang J-D, Chen D-Y, Chang W-C. rs2841277 (PLD4) is associated with susceptibility and rs4672495 isassociated with disease activity in rheumatoid arthritis. *Oncotarget* 2017; 8(38), 64180–64190. DOI: 10.18632/oncotarget.19419

Chen YC, Chou YC, Hsieh YT, Kuo PY, Yang ML, Chong HE, Wu CL, Shiau AL, Wang CR. Targeting intra-pulmonary P53-dependent long non-coding RNA expression as a therapeutic intervention for systemic lupus erythematosus-associated diffuse alveolar hemorrhage. *Int J Mol Sci* 2021; *22*(13), 6948. DOI: 10.3390/ijms22136948

Chitrabamrung S, Rubin RL, Tan EM. Serum Deoxyribonuclease I and Clinical Activity in Systemic Lupus Erythematosus. *Rheumatol Int* 1981; 1(2), 55-60. DOI: 10.1007/BF00541153

Chiu RWK, Chan LYS, Lam NYL, Tsui NBY, Ng EKO, Rainer TH, Dennis Lo YM. Quantitative Analysis of Circulating Mitochondrial DNA in Plasma. *Clin Chem* 2003; 49(5), 719-726. DOI: 10.1373/49.5.719

Chowdhary VR, Grande JP, Luthra HS, David CS. Characterization of haemorrhagic pulmonary capillaritis: Another manifestation of Pristane-induced lupus. *Rheumatology* 2007, 46(9), 1405–1410. DOI: 10.1093/rheumatology/kem117

Coch C, Busch N, Wimmenauer V, Hartmann E, Janke M, Abdel-Mottaleb MMA, Lamprecht A, Ludwig J, Barchet W, Schlee M, Hartmann G. Higher activation of TLR9 in plasmacytoid dendritic cells by microbial DNA compared with self-DNA based on CpG-specific recognition of phosphodiester DNA. *J Leukoc Biol* 2009; 86(3), 663–670. DOI: 10.1189/jlb.0509314

Cohen D, Melamed S, Millman A, Shulman G, Oppenheimer-Shaanan Y, Kacen A, Doron S, Amitai G, Sorek R. Cyclic GMP-AMP signalling protects bacteria against viral infection. *Nature* 2019; 574, 691–695. DOI: 10.1038/s41586-019-1605-5

Cordonnier C, Bernardi G. A comparative study of acid deoxyribonucleases extracted from different tissues and species. *Can J Biochem* 1968; 46(8), 989–995. DOI: 10.1139/o68-148

Corradetti C, Jog NR, Gallucci S, Madaio M, Balachandran S, Caricchio R. Immune-mediated nephropathy and systemic autoimmunity in mice does not require receptor interacting protein Kinase 3 (RIPK3). *PloS ONE* 2016; 11(9). DOI: 10.1371/journal.pone.0163611

Cosentino K, Garcia-Saez AJ. Bax and Bak pores: Are we closing the circle? *Trends Cell Biol* 2017; 27(4), 266–275. DOI: 10.1016/j.tcb.2016.11.004

Crow YJ, Hayward BE, Parmar R, Robins P, Leitch A, Ali M, Black DN, van Bokhoven H, Brunner HG, Hamel BC, Corry PC, Cowan FM, Frints SG, Klepper J, Livingston JH, Lynch SA, Massey RF, Meritet JF, Michaud JL, Ponsot G, Voit T, Lebon P, Bonthron DT, Jackson AP, Barnes DE, Lindahl T. Mutations in the gene encoding the 3′-5′ DNA exonuclease TREX1 cause Aicardi-Goutières syndrome at the AGS1 locus. *Nat Genet* 2006; 38(8), 917–920. DOI: 10.1038/ng1845

Cruchaga C, Karch CM, Jin SC, Benitez BA, Cai Y, Guerreiro R, Harari O, Norton J, Budde J, Bertelsen S, Jeng AT, Cooper B, Skorupa T, Carrell D, Levitch D, Hsu S, Choi J, Ryten M, Sassi C, Bras J, Gibbs RJ, Hernandez DG, Lupton MK, Powell J, Forabosco P, Ridge PG, Corcoran CD, Tschanz JT, Norton MC, Munger RG, Schmutz C, Leary M, Demirci FY, Bamne MN, Wang X, Lopez OL, Ganguli M, Medway C, Turton J, Lord J, Braae A, Barber I, Brown K; Alzheimer's Research UK (ARUK) Consortium, Pastor P, Lorenzo-Betancor O, Brkanac Z, Scott E, Topol E, Morgan K, Rogaeva E, Singleton A, Hardy J, Kamboh MI, George-Hyslop PS, Cairns N, Morris JC, Kauwe JSK, Goate AM. Rare coding variants in the phospholipase D3 gene confer risk for Alzheimer's disease. *Nature* 2014; 505(7484), 550-554. DOI: 10.1038/nature12825

Cymerman IA, Meiss G, Bujnicki JM. DNase II is a member of the phospholipase D superfamily. *Bioinformatics* 2005; 21(21), 3959–3962. DOI: 10.1093/bioinformatics/bti659

Czabotar PE, Lessene G, Strasser A, Adams JM. Control of apoptosis by the BCL-2 protein family: implications for physiology and therapy. *Nat Rev Mol Cell Biol* 2014; 15(1), 49–63. DOI: 10.1038/nrm3722

Dang EV, McDonald JG, Russell DW, Cyster JG. Oxysterol Restraint of Cholesterol Synthesis Prevents AIM2 Inflammasome Activation. *Cell* 2017; 171(5), 1057–1071.e11. DOI: 10.1016/j.cell.2017.09.029

Darbousset R, Thomas GM, Mezouar S, Frère C, Bonier R, Mackman N, Renné T, Dignat-George F, Dubois C, Panicot-Dubois L. Tissue factor-positive neutrophils bind to injured endothelial wall and initiate thrombus formation. *Blood* 2012, 120(10), 2133–2143. DOI: 10.1182/blood-2012-06-437772

Darbousset R, Delierneux C, Mezouar S, Hego A, Lecut C, Guillaumat I, Riederer MA, Evans RJ, Dignat-George F, Panicot-Dubois L, Oury C, Dubois C. P2X1 expressed on polymorphonuclear neutrophils and platelets is required for thrombosis in mice. *Blood* 2014; 124(16), 2575–2585. DOI: 10.1182/blood-2014-04

Davenne T, Bridgeman A, Rigby RE, Rehwinkel J. Deoxyguanosine is a TLR7 agonist. *Eur J Immunol* 2020; 50(1), 56–62. DOI: 10.1002/eji.201948151

Davis JC, Manzi S, Yarboro C, Rairie J, Mcinnes I, Averthelyi D, Sinicropi D, Hale VG, Balow J, Austin H, Boumpas DT, Klippel JH. Recombinant human Dnase I (rhDNase) in patients with lupus nephritis. *Lupus* 1999; 8(1), 68–76. DOI: 10.1191/096120399678847380

Delgado-Rizo V, Martínez-Guzmán MA, Iñiguez-Gutierrez L, García-Orozco A, Alvarado-Navarro A, Fafutis-Morris M. Neutrophil extracellular traps and its implications in inflammation: An overview. *Front Immunol* 2017; 8(81). DOI: 10.3389/fimmu.2017.00081

de Prost N, Parrot A, Picard C, Ancel P-Y, Mayaud C, Fartoukh M, Cadranel J. Diffuse alveolar haemorrhage: factors associated with in-hospital and long-term mortality. *Eur Respir J* 2010; 35(6), 1303–1311. DOI: 10.1183/09031936.00075309

Diebold SS, Kaisho T, Hemmi H, Akira S, Reis e Sousa C. Innate antiviral responses by means of TLR7-mediated recognition of single-stranded RNA. *Science* 2004; 303(5663), 1529-1531. DOI: 10.1126/science.1093616

Ding J, Wang K, Liu W, She Y, Sun Q, Shi J, Sun H, Wang DC, Shao F. Pore-forming activity and structural autoinhibition of the gasdermin family. *Nature* 2016; *535*(7610), 111–116. DOI: 10.1038/nature18590

Doron S, Melamed S, Ofir G, Leavitt A, Lopatina A, Keren M, Amitai G, Sorek R. Systematic discovery of antiphage defense systems in the microbial pangenome. *Science* 2018; 359(6379), eaar4120. DOI: 10.1126/science.aar4120

Drew HR. Structural Specificities of Five Commonly Used DNA Nucleases. *J Mol Biol* 1984; 176(4), 553-557. DOI: 10.1016/0022-2836(84)90176-1

Enari M, Sakahira H, Yokoyama H, Okawa K, Iwamatsu A, Nagata S. A caspase-activated DNase that degrades DNA during apoptosis, and its inhibitor ICAD. *Nature* 1998*;* 391(6662), 43–50. DOI: 10.1038/34112

Fernandes-Alnemri T, Yu JW, Datta P, Wu J, Alnemri ES. AIM2 activates the inflammasome and cell death in response to cytoplasmic DNA. *Nature* 2009; 458(7237), 509–513. DOI: 10.1038/nature07710

Fischer H, Eckhart L, Mildner M, Jaeger K, Buchberger M, Ghannadan M, Tschachler E. DNase1L2 degrades nuclear DNA during corneocyte formation. *J Invest Dermatol* 2007, 127(1), 24–30. DOI: 10.1038/sj.jid.5700503

Fischer H, Szabo S, Scherz J, Jaeger K, Rossiter H, Buchberger M, Ghannadan M, Hermann M, Theussl HC, Tobin DJ, Wagner EF, Tschachler E, Eckhart L. Essential role of the keratinocyte-specific endonuclease DNase1L2 in the removal of nuclear DNA from hair and nails. *J Invest Dermatol* 2011; 131(6), 1208–1215. DOI: 10.1038/jid.2011.13

Fischer H, Buchberger M, Napirei M, Tschachler E, Eckhart L. Inactivation of DNase1L2 and DNase2 in keratinocytes suppresses DNA degradation during epidermal cornification and results in constitutive parakeratosis. *Sci Rep* 2017; *7*(6433). DOI: 10.1038/s41598-017-06652-8

Fukui R, Saitoh S, Matsumoto F, Kozuka-Hata H, Oyama M, Tabeta K, Beutler B, Miyake K. Unc93B1 biases Toll-like receptor responses to nucleic acid in dendritic cells toward DNA- but against RNA-sensing. *J Exp Med* 2009; 206(6), 1339-1350. DOI: 10.1084/jem.20082316

Fukui R, Saitoh S, Kanno A, Onji M, Shibata T, Ito A, Onji M, Matsumoto M, Akira S, Yoshida N, Miyake K. Unc93B1 restricts systemic lethal inflammation by orchestrating Toll-like receptor 7 and 9 trafficking. *Immunity* 2011; 35(1), 69-81. DOI: 10.1016/j.immuni.2011.05.010.

Gabrilovich DI, Nagaraj S. Myeloid-derived suppressor cells as regulators of the immune system. *Nat Rev Immunol* 2009; 9, 162-174. DOI: 10.1038/nri2506

Gall A, Treuting P, Elkon KB, Loo Y-M, Gale M, Barber GN, Stetson DB. Autoimmunity initiates in nonhematopoietic cells and progresses via lymphocytes in an interferon-dependent autoimmune disease. *Immunity* 2012; 36(1), 120–131. DOI: 10.1016/j.immuni.2011.11.018

Gao D, Wu J, Wu YT, Du F, Aroh C, Yan N, et al. Cyclic GMP-AMP synthase is an innate immune sensor of HIV and other retroviruses. *Science* 2013a; 341(6148), 903–906. DOI: 10.1126/science.1240933

Gao P, Ascano M, Wu Y, Barchet W, Gaffney BL, Zillinger T, Serganov AA, Liu Y, Jones RA, Hartmann G, Tuschl T, Patel DJ. Cyclic [G(2',5')pA(3',5')p] is the metazoan second messenger produced by DNA-activated cyclic GMP-AMP synthase. *Cell* 2013b; 153(5), 1094–1107. DOI: 10.1016/j.cell.2013.04.046

Gao P, Ascano M, Zillinger T, Wang W, Dai P, Serganov AA, Gaffney BL, Shuman S, Jones RA, Deng L, Hartmann G, Barchet W, Tuschl T, Patel DJ. Structure-function analysis of STING activation by c[G(2',5')pA(3',5')p] and targeting by antiviral DMXAA. *Cell* 2013c; 154(4), 748–762. DOI: 10.1016/j.cell.2013.07.023

Gao D, Li T, Li XD, Chen X, Li QZ, Wight-Carter M, Chen ZJ. Activation of cyclic GMP-AMP synthase by self-DNA causes autoimmune diseases. *Proc Natl Acad Sci USA* 2015; 112(42), E5699–705. DOI: 10.1073/pnas.1516465112

Garcia-Romo GS, Caielli S, Vega B, Connolly J, Allantaz F, Xu Z, Punaro M, Baisch J, Guiducci C, Coffman RL, Barrat FJ, Banchereau J, Pascual V. Netting neutrophils are major inducers of type I IFN production in pediatric systemic lupus erythematosus. *Sci Transl Med* 2011; *3*(73), 73ra20. DOI: 10.1126/scitranslmed.3001201

Gavin AL, Huang D, Huber C, Mårtensson A, Tardif V, Skog PD, Blane TR, Thinnes TC, Osborn K, Chong HS, Kargaran F, Kimm P, Zeitjian A, Sielski RL, Briggs M, Schulz SR, Zarpellon A, Cravatt B, Pang ES, Teijaro J, de la Torre JC, O'Keeffe M, Hochrein H, Damme M, Teyton L, Lawson BR, Nemazee D. PLD3 and PLD4 are single-stranded acid exonucleases that regulate endosomal nucleic-acid sensing. *Nat Immunol* 2018; 19(9), 942-953. DOI: 10.1038/s41590-018-0179-y

Gavin AL, Huang D, Blane TR, Thinnes TC, Murakami Y, Fukui R, Miyake K, Nemazee D. Cleavage of DNA and RNA by PLD3 and PLD4 limits autoinflammatory triggering by multiple sensors. *Nat Commun* 2021; 12(1), 5874. DOI: 10.1038/s41467-021-26150-w.

Gehrke N, Mertens C, Zillinger T, Wenzel J, Bald T, Zahn S, Tüting T, Hartmann G, Barchet W. Oxidative damage of DNA confers resistance to cytosolic nuclease TREX1 degradation and potentiates STING-dependent immune sensing. *Immunity* 2013; 39(3), 482-495. DOI: 10.1016/j.immuni.2013.08.004

GeurtsvanKessel C, Lambrecht B. Division of labor between dendritic cell subsets of the lung. *Mucosal Immunol* 2008; 1(6), 442–450. DOI: 10.1038/mi.2008.39

Giacona MB, Ruben GC, Iczkowski KA, Roos TB, Porter DM, Sorenson GD. Cell-Free DNA in Human Blood Plasma: Length Measurements in Patients with Pancreatic Cancer and Healthy Controls. *Pancreas* 1998; 17(1), 89-97. DOI: 10.1097/00006676-199807000-00012

Gitlin L, Barchet W, Gilfillan S, Cella M, Beutler B, Flavell RA, Diamond MS, Colonna M. Essential role of mda-5 in type I IFN responses to polyriboinosinic:polyribocytidylic acid

and encephalomyocarditis picornavirus. Proc Natl Acad Sci USA 2006; 103(22), 8459–8464. DOI: 10.1073/pnas.0603082103

Gonzalez AC, SchweizerM, Jagdmann S, Bernreuther C, Reinheckel T, Saftig P, Damme M. Unconventional trafficking of mammalian phospholipase D3 to lysosomes. *Cell Rep* 2018; 22(4), 1040–1053. DOI: 10.1016/j.celrep.2017.12.100

Gray EE, Treuting PM, Woodward JJ, Stetson DB. Cutting Edge: cGAS Is Required for Lethal Autoimmune Disease in the Trex1-Deficient Mouse Model of Aicardi-Goutières Syndrome. *J Immunol* 2015; 195(5), 1939-1943. DOI: 10.4049/jimmunol.1500969.

Green DR. The Coming Decade of Cell Death Research: Five Riddles. *Cell* 2019; 177(5), 1094-1107. DOI: 10.1016/j.cell.2019.04.024

Guo Q, Yaron JR, Wallen JW 3rd, Browder KF, Boyd R, Olson TL, Burgin M, Ulrich P, Aliskevich E, Schutz LN, Fromme P, Zhang L, Lucas AR. PEGylated Serp-1 Markedly Reduces Pristane-Induced Experimental Diffuse Alveolar Hemorrhage, Altering uPAR Distribution, and Macrophage Invasion. *Front Cardiovasc Med* 2021; 8, 633212. DOI: 10.3389/fcvm.2021.633212

Hakkim A, Fürnrohr BG, Amann K, Laube B, Abed UA, Brinkmann V, Herrmann M, Voll RE, Zychlinsky A. Impairment of neutrophil extracellular trap degradation is associated with lupus nephritis. *Proc Natl Acad Sci USA* 2010; 107(21), 9813-9818. DOI: 10.1073/pnas.0909927107

Han S, Zhuang H, Shumyak S, Wu J, Xie C, Li H, Yang LJ, Reeves WH. Liver X Receptor Agonist Therapy Prevents Diffuse Alveolar Hemorrhage in Murine Lupus by Repolarizing Macrophages. *Front Immunol* 2018; 9, 135. DOI: 10.3389/fimmu.2018.00135

Han DSC, Ni M, Chan RWY, Chan VWH, Lui KO, Chiu RWK, Lo YMD. The Biology of Cell-free DNA Fragmentation and the Roles of DNASE1, DNASE1L3, and DFFB. *Am J Hum Genet* 2020; 106(2), 202-214. DOI: 10.1016/j.ajhg.2020.01.008

Haroche J, Cohen-Aubart F, Rollins BJ, Donadieu J, Charlotte F, Idbaih A, Vaglio A, Abdel-Wahab O, Emile JF, Amoura Z. Histiocytoses: emerging neoplasia behind inflammation. *Lancet Oncol* 2017; 18(2), e113-e125. DOI: 10.1016/S1470-2045(17)30031-1

Hartmann G, Krieg AM. Mechanism and function of a newly identified CpG DNA motif in human primary B cells. *J Immunol* 2000; 164(2), 944-953. DOI: 10.4049/jimmunol.164.2.944

Hasan UA, Trinchieri G, Vlach J. Toll-like receptor signaling stimulates cell cycle entry and progression in fibroblasts. *J.Biol.Chem* 2005; 280(21), 20620–20627. DOI: 10.1074/jbc.M500877200

Hasan M, Koch J, Rakheja D, Pattnaik AK, Brugarolas J, Dozmorov I, Levine B, Wakeland EK, Lee-Kirsch MA, Yan N. Trex1 regulates lysosomal biogenesis and interferon-independent activation of antiviral genes. *Nat Immunol* 2013; 14(1), 61-71. DOI: 10.1038/ni.2475

Heil F, Hemmi H, Hochrein H, Ampenberger F, Kirschning C, Akira S, Lipford G, Wagner H, Bauer S. Species-specific recognition of single-stranded RNA via toll-like receptor 7

and 8. *Science* 2004; 303(5663), 1526-1529. DOI: 10.1126/science.1093620

Heinz LX, Lee J, Kapoor U, Kartnig F, Sedlyarov V, Papakostas K, César-Razquin A, Essletzbichler P, Goldmann U, Stefanovic A, Bigenzahn JW, Scorzoni S, Pizzagalli MD, Bensimon A, Müller AC, King FJ, Li J, Girardi E, Mbow ML, Whitehurst CE, Rebsamen M, Superti-Furga G. TASL is the SLC15A4-associated adaptor for IRF5 activation by TLR7-9. *Nature* 2020; 581, 316-322. DOI: 10.1038/s41586-020-2282-0

Hemmi H, Takeuchi O, Kawai T, Kaisho T, Sato S, Sanjo H, Matsumoto M, Hoshino K, Wagner H, Takeda K, Akira S. A Toll-like receptor recognizes bacterial DNA. *Nature* 2000; 408(6813), 740-745. DOI: 10.1038/35047123

Heslet L, Nielsen JD, Levi M, Sengeløv H, Johansson PI. Successful pulmonary administration of activated recombinant factor VII in diffuse alveolar hemorrhage. *Crit Care* 2006; 10(6), R177. Doi: 10.1186/cc5132

Hornung V, Ablasser A, Charrel-Dennis M, Bauernfeind F, Horvath G, Caffrey DR, Latz E, Fitzgerald KA. AIM2 recognizes cytosolic dsDNA and forms a caspase-1-activating inflammasome with ASC. *Nature* 2009; 458(7237), 514–518. DOI: 10.1038/nature07725

Hsu CL, Lin W, Seshasayee D, Chen YH, Ding X, Lin Z, Suto E, Huang Z, Lee WP, Park H, Xu M, Sun M, Rangell L, Lutman JL, Ulufatu S, Stefanich E, Chalouni C, Sagolla M, Diehl L, Fielder P, Dean B, Balazs M, Martin F. Equilibrative nucleoside transporter 3 deficiency perturbs lysosome function and macrophage homeostasis. *Science* 2012; 335(6064), 89-92. DOI: 10.1126/science.1213682

Huang B, Zhao J, Unkeless JC, Feng ZH, Xiong H. TLR signaling by tumor and immune cells: a double-edged sword. *Oncogene* 2008; 27(2), 218-224. DOI: 10.1038/sj.onc.1210904

Itoh N, Yonehara S, Ishii A, Yonehara M, Mizushima S, Sameshima M, Hase A, Seto Y, Nagata S. The polypeptide encoded by the cDNA for human cell surface antigen Fas can mediate apoptosis. *Cell* 1991; 66(2), 233-243. DOI: 10.1016/0092-8674(91)90614-5

Janz S, Shacter E. A new method for delivering alkanes to mammalian cells: preparation and preliminary characterization of an inclusion complex between beta-cyclodextrin and pristane (2,6,10,14-tetramethylpentadecane). *Toxicology* 1991; 69(3), 301-315. DOI: 10.1016/0300-483x(91)90189-8

Jarrot PA, Tellier E, Plantureux L, Crescence L, Robert S, Chareyre C, Daniel L, Secq V, Garcia S, Dignat-George F, Panicot-Dubois L, Dubois C, Kaplanski G. Neutrophil extracellular traps are associated with the pathogenesis of diffuse alveolar hemorrhage in murine lupus. *J Autoimmun* 2019; 100, 120-130. DOI: 10.1016/j.jaut.2019.03.009

Jego G, Bataille R, Geffroy-Luseau A, Descamps G, Pellat-Deceunynck C. Pathogen-associated molecular patterns are growth and survival factors for human myeloma cells through Toll-like receptors. *Leukemia* 2006; 20(6), 1130–1137. DOI: 10.1038/sj.leu.2404226

Jeremiah N, Neven B, Gentili M, Callebaut I, Maschalidi S, Stolzenberg MC, Goudin N, Frémond ML, Nitschke P, Molina TJ, Blanche S, Picard C, Rice GI, Crow YJ, Manel N, Fischer A, Bader-Meunier B, Rieux-Laucat F. Inherited STING-activating mutation underlies a familial inflammatory syndrome with lupus-like manifestations. *J Clin Invest* 2014; 124(12), 5516-5520. DOI: 10.1172/JCI79100

Jiang D, Liang J, Fan J, Yu S, Chen S, Luo Y, Prestwich GD, Mascarenhas MM, Garg HG, Quinn DA, Homer RJ, Goldstein DR, Bucala R, Lee PJ, Medzhitov R, Noble PW. Regulation of lung injury and repair by Toll-like receptors and hyaluronan. *Nat Med* 2005; 11(11), 1173-1179. DOI: 10.1038/nm1315

Jiménez-Alcázar M, Rangaswamy C, Panda R, Bitterling J, Simsek YJ, Long AT, Bilyy R, Krenn V, Renné C, Renné T, Kluge S, Panzer U, Mizuta R, Mannherz HG, Kitamura D, Herrmann M, Napirei M, Fuchs TA. Host Dnases prevent vascular occlusion by neutrophil extracellular traps. *Science* 2017; 358(6367), 1202-1206. DOI: 10.1126/science.aam8897

Jin T, Perry A, Jiang J, Smith P, Curry JA, Unterholzner L, Jiang Z, Horvath G, Rathinam VA, Johnstone RW, Hornung V, Latz E, Bowie AG, Fitzgerald KA, Xiao TS. Structures of the HIN domain:DNA complexes reveal ligand binding and activation mechanisms of the AIM2 inflammasome and IFI16 receptor. *Immunity* 2012; 36(4), 561-571. DOI: 10.1016/j.immuni.2012.02.014

Jørgensen TN, Roper E, Thurman JM, Marrack P, Kotzin BL. Type I interferon signaling is involved in the spontaneous development of lupus-like disease in B6.Nba2 and (B6.Nba2 x NZW)F(1) mice. *Genes Immun* 2007; 8(8), 653-662. DOI: 10.1038/sj.gene.6364430

Judge AD, Sood V, Shaw JR, Fang D, McClintock K, MacLachlan I. Sequence-dependent stimulation of the mammalian innate immune response by synthetic siRNA. *Nat Biotechnol* 2005; 23(4), 457-462. DOI: 10.1038/nbt1081

Julian MW, Shao G, Bao S, Knoell DL, Papenfuss TL, VanGundy ZC, Crouser ED. Mitochondrial transcription factor A serves as a danger signal by augmenting plasmacytoid dendritic cell responses to DNA. *J Immunol* 2012; 189(1), 433-443. DOI: 10.4049/jimmunol.1101375

Jurk M, Heil F, Vollmer J, Schetter C, Krieg AM, Wagner H, Lipford G, Bauer S. Human TLR7 or TLR8 independently confer responsiveness to the antiviral compound R-848. *Nat Immunol* 2002; 3(6), 499. DOI: 10.1038/ni0602-499

Jurlander B, Thim L, Klausen NK, Persson E, Kjalke M, Rexen P, Jørgensen TB, Østergaard PB, Erhardtsen E, Bjørn SE. Recombinant activated factor VII (rFVIIa): characterization, manufacturing, and clinical development. Semin *Thromb Hemost* 2001; 27(4), 373-384. DOI: 10.1055/s-2001-16971

Kalluri R, LeBleu VS. The biology, function, and biomedical applications of exosomes. *Science* 2020; 367(6478), eaau6977. DOI: 10.1126/science.aau6977

Kamen DL, Strange C. Pulmonary manifestations of systemic lupus erythematosus. *Clin Chest Med* 2010; 31(3), 479-488. DOI: 10.1016/j.ccm.2010.05.001

Kaplan MJ. Neutrophils in the pathogenesis and manifestations of SLE. *Nat Rev Rheumatol* 2011; 7(12), 691-699. DOI: 10.1038/nrrheum.2011.132

Kaul, A., Gordon, C., Crow, M. Touma Z, Urowitz MB, van Vollenhoven R, Ruiz-Irastorza G, Hughes G. Systemic lupus erythematosus. *Nat Rev Dis Primers* 2016; 2, 16039. DOI: 10.1038/nrdp.2016.39

Kawane K, Fukuyama H, Kondoh G, Takeda J, Ohsawa Y, Uchiyama Y, Nagata S. Requirement of DNase II for definitive erythropoiesis in the mouse fetal liver. *Science*

2001; 292(5521), 1546-1549. DOI: 10.1126/science.292.5521.1546

Kawane K, Fukuyama H, Yoshida H, Nagase H, Ohsawa Y, Uchiyama Y, Okada K, Iida T, Nagata S. Impaired thymic development in mouse embryos deficient in apoptotic DNA degradation. *Nat Immunol* 2003; 4, 138–144. DOI: 10.1038/ni881

Kawane K, Ohtani M, Miwa K, Kizawa T, Kanbara Y, Yoshioka Y, Yoshikawa H, Nagata S. Chronic polyarthritis caused by mammalian DNA that escapes from degradation in macrophages. *Nature* 2006; 443(7114), 998-1002. DOI: 10.1038/nature05245.

Kawane K, Tanaka H, Kitahara Y, Shimaoka S, Nagata S. Cytokine-dependent but acquired immunity-independent arthritis caused by DNA escaped from degradation. *Proc Natl Acad Sci USA* 2010; 107(45), 19432-19437. DOI: 10.1073/pnas.1010603107

Kazzaz NM, Coit P, Lewis EE, McCune WJ, Sawalha AH, Knight JS. Systemic lupus erythematosus complicated by diffuse alveolar haemorrhage: risk factors, therapy and survival. *Lupus Sci Med* 2015; 2(1), e000117. DOI: 10.1136/lupus-2015-000117

Kerr JF, Wyllie AH, Currie AR. Apoptosis: a basic biological phenomenon with wide-ranging implications in tissue kinetics. *Br J Cancer* 1972; 26(4), 239-257. DOI: 10.1038/bjc.1972.33

Kessenbrock K, Krumbholz M, Schönermarck U, Back W, Gross WL, Werb Z, Gröne HJ, Brinkmann V, Jenne DE. Netting neutrophils in autoimmune small-vessel vasculitis. *Nat Med* 2009; 15(6), 623-625. DOI: 10.1038/nm.1959

Ketelut-Carneiro N, Fitzgerald KA. Apoptosis, Pyroptosis, and Necroptosis—Oh My! The Many Ways a Cell Can Die. *J Mol Biol* 2022; 434(4), 167378. DOI: 10.1016/j.jmb.2021.167378

Keyel PA. Dnases in health and disease. *Dev Biol* 2017; 429(1), 1-11. DOI: 10.1016/j.ydbio.2017.06.028

Khan N, Lawlor KE, Murphy JM, Vince JE. More to life than death: molecular determinants of necroptotic and non-necroptotic RIP3 kinase signaling. *Curr Opin Immunol* 2014; 26, 76-89. DOI: 10.1016/j.coi.2013.10.017

Kim EJ, Collard HR, King TE Jr. Rheumatoid arthritis-associated interstitial lung disease: the relevance of histopathologic and radiographic pattern. *Chest* 2009; 136(5), 1397-1405. DOI: 10.1378/chest.09-0444

Kischkel FC, Hellbardt S, Behrmann I, Germer M, Pawlita M, Krammer PH, Peter ME. Cytotoxicity-dependent APO-1 (Fas/CD95)-associated proteins form a death-inducing signaling complex (DISC) with the receptor. *EMBO J* 1995; 14(22), 5579-5588. DOI: 10.1002/j.1460-2075.1995.tb00245.x

König N, Fiehn C, Wolf C, Schuster M, Cura Costa E, Tüngler V, Alvarez HA, Chara O, Engel K, Goldbach-Mansky R, Günther C, Lee-Kirsch MA. Familial chilblain lupus due to a gain-of-function mutation in STING. *Ann Rheum Dis* 2017, *76*(2), 468–472. DOI: 10.1136/annrheumdis-2016-209841

Krieg AM, Yi AK, Matson S, Waldschmidt TJ, Bishop GA, Teasdale R, Koretzky GA, Klinman DM. CpG motifs in bacterial DNA trigger direct B-cell activation. *Nature* 1995; 374(6522), 546-549. DOI: 10.1038/374546a0

Krieser RJ, MacLea KS, Park JP, Eastman A. The cloning, genomic structure,

localization, and expression of human deoxyribonuclease Iibeta. *Gene* 2001; 269(1-2), 205-216. Doi: 10.1016/s0378-1119(01)00434-6

Krieser RJ, MacLea KS, Longnecker DS, Fields JL, Fiering S, Eastman A. Deoxyribonuclease Iialpha is required during the phagocytic phase of apoptosis and its loss causes perinatal lethality. *Cell Death Differ* 2002; 9(9), 956-962. DOI: 10.1038/sj.cdd.4401056

Kuriakose J, Redecke V, Guy C, Zhou J, Wu R, Ippagunta SK, Tillman H, Walker PD, Vogel P, Häcker H. Patrolling monocytes promote the pathogenesis of early lupus-like glomerulonephritis. *J Clin Invest* 2019; 129(6), 2251-2265. DOI: 10.1172/JCI125116

Lahm A, Suck D. DNase I-induced DNA conformation. 2 A structure of a DNase I-octamer complex. *J Mol Biol* 1991; 222(3), 645-667. DOI: 10.1016/0022-2836(91)90502-w

Lande R, Gregorio J, Facchinetti V, Chatterjee B, Wang YH, Homey B, Cao W, Wang YH, Su B, Nestle FO, Zal T, Mellman I, Schröder JM, Liu YJ, Gilliet M. Plasmacytoid dendritic cells sense self-DNA coupled with antimicrobial peptide. *Nature* 2007; 449(7162), 564-569. DOI: 10.1038/nature06116

Lande R, Ganguly D, Facchinetti V, Frasca L, Conrad C, Gregorio J, Meller S, Chamilos G, Sebasigari R, Riccieri V, Bassett R, Amuro H, Fukuhara S, Ito T, Liu YJ, Gilliet M. Neutrophils activate plasmacytoid dendritic cells by releasing self-DNA-peptide complexes in systemic lupus erythematosus. *Sci Transl Med* 2011; 3(73), 73ra19. DOI: 10.1126/scitranslmed.3001180

Latz E, Xiao TS, Stutz A. Activation and regulation of the inflammasomes. *Nat Rev Immunol* 2013; 13(6), 397-411. DOI: 10.1038/nri3452

Lechardeur D, Xu M, Lukacs GL. Contrasting nuclear dynamics of the caspase-activated DNase (CAD) in dividing and apoptotic cells. *J Cell Biol* 2004; 167(5), 851-862. DOI: 10.1083/jcb.200404105.

Lee PY, Kumagai Y, Li Y, Takeuchi O, Yoshida H, Weinstein J, Kellner ES, Nacionales D, Barker T, Kelly-Scumpia K, van Rooijen N, Kumar H, Kawai T, Satoh M, Akira S, Reeves WH. TLR7-dependent and FcgammaR-independent production of type I interferon in experimental mouse lupus. *J Exp Med* 2008a; 205(13), 2995-3006. DOI: 10.1084/jem.20080462.

Lee PY, Weinstein JS, Nacionales DC, Scumpia PO, Li Y, Butfiloski E, van Rooijen N, Moldawer L, Satoh M, Reeves WH. A novel type I IFN-producing cell subset in murine lupus. *J Immunol* 2008b; 180(7), 5101-5108. DOI: 10.4049/jimmunol.180.7.5101

Lee PY, Li Y, Kumagai Y, Xu Y, Weinstein JS, Kellner ES, Nacionales DC, Butfiloski EJ, van Rooijen N, Akira S, Sobel ES, Satoh M, Reeves WH. Type I interferon modulates monocyte recruitment and maturation in chronic inflammation. *Am J Pathol* 2009; 175(5), 2023-2033. DOI: 10.2353/ajpath.2009.090328

Lee HT, Lin CS, Lee CS, Tsai CY, Wei YH. The role of hOGG1 C1245G polymorphism in the susceptibility to lupus nephritis and modulation of the plasma 8-OhdG in patients with systemic lupus erythematosus. *Int J Mol Sci* 2015; 16(2), 3757-3768. DOI: 10.3390/ijms16023757

Lee PY, Nelson-Maney N, Huang Y, Levescot A, Wang Q, Wei K, Cunin P, Li Y, Lederer

JA, Zhuang H, Han S, Kim EY, Reeves WH, Nigrovic PA. High-dimensional analysis reveals a pathogenic role of inflammatory monocytes in experimental diffuse alveolar hemorrhage. *JCI Insight* 2019; 4(15), e129703. DOI: 10.1172/jci.insight.129703

Lee-Kirsch MA, Gong M, Chowdhury D, Senenko L, Engel K, Lee YA, de Silva U, Bailey SL, Witte T, Vyse TJ, Kere J, Pfeiffer C, Harvey S, Wong A, Koskenmies S, Hummel O, Rohde K, Schmidt RE, Dominiczak AF, Gahr M, Hollis T, Perrino FW, Lieberman J, Hübner N. Mutations in the gene encoding the 3'-5' DNA exonuclease TREX1 are associated with systemic lupus erythematosus. *Nat Genet* 2007a; 39(9), 1065-1067. DOI: 10.1038/ng2091

Lee-Kirsch MA, Chowdhury D, Harvey S, Gong M, Senenko L, Engel K, Pfeiffer C, Hollis T, Gahr M, Perrino FW, Lieberman J, Hubner N. A mutation in TREX1 that impairs susceptibility to granzyme A-mediated cell death underlies familial chilblain lupus. *J Mol Med (Berl)* 2007b; 85(5), 531-537. DOI: 10.1007/s00109-007-0199-9

Leffler J, Gullstrand B, Jonsen A, Nilsson JA, Martin M, Blom AM, Bengtsson AA. Degradation of neutrophil extracellular traps co-varies with disease activity in patients with systemic lupus erythematosus. *Arthritis Res Ther* 2013; 15, R84. DOI: 10.1186/ar4264

Leffler J, Ciacma K, Gullstrand B, Bengtsson AA, Martin M, Blom AM. A subset of patients with systemic lupus erythematosus fails to degrade DNA from multiple clinically relevant sources. *Arthritis Res Ther* 2015; 17(1), 205. DOI: 10.1186/s13075-015-0726-y

Leonard JN, Ghirlando R, Askins J, Bell JK, Margulies DH, Davies DR, Segal DM. The TLR3 signaling complex forms by cooperative receptor dimerization. *Proc Natl Acad Sci USA* 2008; 105(1), 258-263. DOI: 10.1073/pnas.0710779105

Li X, Jiang S, Tapping RI. Toll-like receptor signaling in cell proliferation and survival. *Cytokine* 2010; 49(1), 1-9. DOI: 10.1016/j.cyto.2009.08.010

Li XD, Chen ZJ. Sequence specific detection of bacterial 23S ribosomal RNA by TLR13. *Elife* 2012; 1, e00102. DOI: 10.7554/eLife.00102

Li XD, Wu J, Gao D, Wang H, Sun L, Chen ZJ. Pivotal roles of cGAS-cGAMP signaling in antiviral defense and immune adjuvant effects. *Science* 2013a; 341(6152), 1390–1394. DOI: 10.1126/science.1244040

Li X, Shu C, Yi G, Chaton CT, Shelton CL, Diao J, Zuo X, Kao CC, Herr AB, Li P. Cyclic GMP-AMP synthase is activated by double-stranded DNA-induced oligomerization. *Immunity* 2013b; 39(6), 1019-1031. DOI: 10.1016/j.immuni.2013.10.019

Li Y, Wu J, Xu L, Wu Q, Wan Z, Li L, Yu H, Li X, Li K, Zhang Q, Hou Z, Sun X, Chen H. Regulation of Leukocyte Recruitment to the Spleen and Peritoneal Cavity during Pristane-Induced Inflammation. *J Immunol Res* 2017; 2017, 9891348. DOI: 10.1155/2017/9891348

Lichtenbelt KD, Kroos MA, Sinke RJ, Wokke JJH, Reuser AJJ, Ausems MGEM. Frequency of the deletion polymorphism of DNASE1L1 in 137 patients with acid maltase deficiency (Pompe disease). *Exp Mol Pathol* 2006; 80, 308–309. DOI: 10.1016/j.yexmp.2006.02.003

Lichtman EI, Helfgott SM, Kriegel MA. Emerging therapies for systemic lupus erythematosus—focus on targeting interferon-alpha. *Clin Immunol* 2012; 143(3), 210-

221. DOI: 10.1016/j.clim.2012.03.005

Lim SS, Bayakly AR, Helmick CG, Gordon C, Easley KA, Drenkard C. The incidence and prevalence of systemic lupus erythematosus, 2002-2004: The Georgia Lupus Registry. *Arthritis Rheumatol* 2014; 66(2), 357-368. DOI: 10.1002/art.38239

Lindahl T, Gally JA, Edelman GM. Properties of deoxyribonuclease 3 from mammalian tissues. *J Biol Chem* 1969; 244(18), 5014-5019. DOI: 10.1016/S0021-9258(18)94303-6

Lindahl T, Barnes DE, Yang Y-G, Robins P. Biochemical properties of mammalian TREX1 and its association with DNA replication and inherited inflammatory disease. *Biochem Soc Trans* 2009; 37,535–538. DOI: 10.1042/BST0370535

Liu X, Zou H, Slaughter C, Wang X. DFF, a heterodimeric protein that functions downstream of caspase-3 to trigger DNA fragmentation during apoptosis. *Cell* 1997; 89(2), 175-184. DOI: 10.1016/s0092-8674(00)80197-x

Liu L, Botos I, Wang Y, Leonard JN, Shiloach J, Segal DM, Davies DR. Structural basis of toll-like receptor 3 signaling with double-stranded RNA. *Science* 2008; 320(5874), 379-381. Doi: 10.1126/science.1155406

Liu Y, Jesus AA, Marrero B, Yang D, Ramsey SE, Sanchez GAM, Tenbrock K, Wittkowski H, Jones OY, Kuehn HS, Lee CR, DiMattia MA, Cowen EW, Gonzalez B, Palmer I, DiGiovanna JJ, Biancotto A, Kim H, Tsai WL, Trier AM, Huang Y, Stone DL, Hill S, Kim HJ, St Hilaire C, Gurprasad S, Plass N, Chapelle D, Horkayne-Szakaly I, Foell D, Barysenka A, Candotti F, Holland SM, Hughes JD, Mehmet H, Issekutz AC, Raffeld M, McElwee J, Fontana JR, Minniti CP, Moir S, Kastner DL, Gadina M, Steven AC, Wingfield PT, Brooks SR, Rosenzweig SD, Fleisher TA, Deng Z, Boehm M, Paller AS, Goldbach-Mansky R. Activated STING in a vascular and pulmonary syndrome. *N Engl J Med* 2014; 371(6), 507-518. DOI: 10.1056/NEJMoa1312625

Liu X, Zhang Z, Ruan J, Pan Y, Magupalli VG, Wu H, Lieberman J. Inflammasome-activated gasdermin D causes pyroptosis by forming membrane pores. *Nature* 2016; 535(7610), 153-158. DOI: 10.1038/nature18629

Liu J, Wei Y, Lu Y, Li Y, Chen Q, Li Y. The discovery of potent immunostimulatory CpG-ODNs widely distributed in bacterial genomes. *J Microbiol* 2020; 58(2), 153-162. DOI: 10.1007/s12275-020-9289-y

Lo YM, Chan KC, Sun H, Chen EZ, Jiang P, Lun FM, Zheng YW, Leung TY, Lau TK, Cantor CR, Chiu RW. Maternal plasma DNA sequencing reveals the genome-wide genetic and mutational profile of the fetus. *Sci Transl Med* 2010; 2(61), 61ra91. DIO: 10.1126/scitranslmed.3001720

Lood C, Blanco LP, Purmalek MM, Carmona-Rivera C, De Ravin SS, Smith CK, Malech HL, Ledbetter JA, Elkon KB, Kaplan MJ. Neutrophil extracellular traps enriched in oxidized mitochondrial DNA are interferogenic and contribute to lupus-like disease. *Nat Med* 2016; 22(2), 146-153. DOI: 10.1038/nm.4027

Lövgren T, Eloranta ML, Båve U, Alm GV, Rönnblom L. Induction of interferon-alpha production in plasmacytoid dendritic cells by immune complexes containing nucleic acid released by necrotic or late apoptotic cells and lupus IgG. *Arthritis Rheum* 2004; 50(6), 1861-1872. DOI: 10.1002/art.20254

Lu A, Magupalli VG, Ruan J, Yin Q, Atianand MK, Vos MR, Schröder GF, Fitzgerald KA,

Wu H, Egelman EH. Unified polymerization mechanism for the assembly of ASC-dependent inflammasomes. *Cell* 2014; 156(6), 1193-1206. DOI: 10.1016/j.cell.2014.02.008

Lugrin J, Martinon F. The AIM2 inflammasome: Sensor of pathogens and cellular

perturbations. *Immunol Rev* 2018; 281(1), 99–114. DOI: 10.1111/imr.12618

Lui YYN, Chik KW, Chiu RWK, Ho CY, Lam CWK, Lo DYM. Predominant hematopoietic origin of cell-free DNA in plasma and serum after sex-mismatched bone marrow transplantation. *Clin Chem* 2002; 48(3), 421-427. DOI: 10.1093/clinchem/48.3.421

Malferrari G, Mirabella M, D'Alessandra Y, Servidei S, Biunno I. Deletion polymorphism of DNASE1L1, an X-Linked DNase I-like gene, in acid maltase deficiency disorders. *Exp Mol Pathol* 2001; 70(2), 173–174. DOI: 10.1006/exmp.2001.2374

Manils J, Fischer H, Climent J, Casas E, García-Martínez C, Bas J, Sukseree S, Vavouri T, Ciruela F, de Anta JM, Tschachler E, Eckhart L, Soler C. Double deficiency of Trex2 and DNase1L2 nucleases leads to accumulation of DNA in lingual cornifying keratinocytes without activating inflammatory responses. *Sci Rep* 2017; 7(1), 11902. DOI: 10.1038/s41598-017-12308-4

Mathian A, Weinberg A, Gallegos M, Banchereau J, Koutouzov S. IFN-alpha induces early lethal lupus in preautoimmune (New Zealand Black x New Zealand White) F1 but not in BALB/c mice. *J Immunol* 2005; 174(5), 2499-2506. DOI: 10.4049/jimmunol.174.5.2499

Matyszewski M, Morrone SR, Sohn J. Digital signaling network drives the assembly of the AIM2-ASC inflammasome. *Proc Natl Acad Sci* 2018; 115(9), E1963–1972. DOI: 10.1073/pnas.1712860115

Mazur DJ, Perrino FW. Identification and Expression of the TREX1 and TREX2 cDNA sequences encoding mammalian 3′→ 5′ exonucleases. *J Biol Chem* 1999; 274, 19655–11660. DOI: 10.1074/jbc.274.28.19655

McIlroy D, Tanaka M, Sakahira H, Fukuyama H, Suzuki M, Yamamura K, Ohsawa Y, Uchiyama Y, Nagata S. An auxiliary mode of apoptotic DNA fragmentation provided by phagocytes. *Genes Dev* 2000; 14(5), 549-558. DOI: 10.1101/gad.14.5.549

Mohammadoo-Khorasani M, Musavi M, Mousavi M, Moossavi M, Khoddamian M, Sandoughi M, Zakeri Z. Deoxyribonuclease I gene polymorphism and susceptibility to systemic lupus erythematosus. *Clin Rheumatol* 2016; 35(1), 101-105. DOI: 10.1007/s10067-015-3111-y

Mohan Kumar D, Yamaguchi M, Miura K, Lin M, Los M, Coy JF, Rikihisa Y. Ehrlichia chaffeensis uses its surface protein EtpE to bind GPI-anchored protein DNase X and trigger entry into mammalian cells. *PloS Pathog* 2013; 9(10), e1003666. DOI: 10.1371/journal.ppat.1003666

Molho-Pessach V, Lerer I, Abeliovich D, Agha Z, Abu Libdeh A, Broshtilova V, Elpeleg O, Zlotogorski A. The H syndrome is caused by mutations in the nucleoside transporter hENT3. *Am J Hum Genet* 2008; 83(4), 529-534. DOI: 10.1016/j.ajhg.2008.09.013

Morgan NV, Morris MR, Cangul H, Gleeson D, Straatman-Iwanowska A, Davies N, Keenan S, Pasha S, Rahman F, Gentle D, Vreeswijk MP, Devilee P, Knowles MA,

Ceylaner S, Trembath RC, Dalence C, Kismet E, Köseoğlu V, Rossbach HC, Gissen P, Tannahill D, Maher ER. Mutations in SLC29A3, encoding an equilibrative nucleoside transporter ENT3, cause a familial histiocytosis syndrome (Faisalabad histiocytosis) and familial Rosai-Dorfman disease. *PloS Genet* 2010; 6(2), e1000833. DOI: 10.1371/journal.pgen.1000833

Morrone SR, Matyszewski M, Yu X, Delannoy M, Egelman EH, Sohn J. Assembly-driven activation of the AIM2 foreign-dsDNA sensor provides a polymerization template for downstream ASC. *Nat Commun* 2015; 6(1), 7827. DOI: 10.1038/ncomms8827

Moss J, Magenheim J, Neiman D, Zemmour H, Loyfer N, Korach A, Samet Y, Maoz M, Druid H, Arner P, Fu KY, Kiss E, Spalding KL, Landesberg G, Zick A, Grinshpun A, Shapiro AMJ, Grompe M, Wittenberg A D, Glaser B, Shemer R, Kaplan T, Dor Y. Comprehensive human cell-type methylation atlas reveals origins of circulating cell-free DNA in health and disease. *Nat Commun* 2018; 9, 5068. DOI: 10.1038/s41467-018-07466-6

Motwani M, Pesiridis S, Fitzgerald KA. DNA sensing by the cGAS-STING pathway in health and disease. *Nat Rev Genet* 2019; 20(11), 657-674. DOI: 10.1038/s41576-019-0151-1

Motwani M, McGowan J, Antonovitch J, Gao KM, Jiang Z, Sharma S, Baltus GA, Nickerson KM, Marshak-Rothstein A, Fitzgerald KA. cGAS-STING Pathway Does Not Promote Autoimmunity in Murine Models of SLE. *Front Immunol* 2021; 12, 605930. DOI: 10.3389/fimmu.2021.605930

Murakami Y, Fukui R, Tanaka R, Motoi Y, Kanno A, Sato R, Yamaguchi K, Amano H, Furukawa Y, Suzuki H, Suzuki Y, Tamura N, Yamashita N, Miyake K. Anti-TLR7 Antibody Protects Against Lupus Nephritis in NZBWF1 Mice by Targeting B Cells and Patrolling Monocytes. *Front Immunol* 2021; 12, 777197. DOI: 10.3389/fimmu.2021.777197

Nacionales DC, Kelly KM, Lee PY, Zhuang H, Li Y, Weinstein JS, Sobel E, Kuroda Y, Akaogi J, Satoh M, Reeves WH. Type I interferon production by tertiary lymphoid tissue developing in response to 2,6,10,14-tetramethyl-pentadecane (pristane). *Am J Pathol* 2006; 168(4), 1227-1240. DOI: 10.2353/ajpath.2006.050125

Nacionales DC, Kelly-Scumpia KM, Lee PY, Weinstein JS, Lyons R, Sobel E, Satoh M, Reeves WH. Deficiency of the type I interferon receptor protects mice from experimental lupus. *Arthritis Rheum* 2007; 56(11), 3770-3783. DOI: 10.1002/art.23023

Naeem AS, Zhu Y, Di WL, Marmiroli S, O'Shaughnessy RF. AKT1-mediated Lamin A/C degradation is required for nuclear degradation and normal epidermal terminal differentiation. *Cell Death Differ* 2015; 22(12), 2123-2132. DOI: 10.1038/cdd.2015.62

Nagai Y, Garrett KP, Ohta S, Bahrun U, Kouro T, Akira S, Takatsu K, Kincade PW. Toll-like receptors on hematopoietic progenitor cells stimulate innate immune system replenishment. *Immunity* 2006; 24(6), 801-812. DOI: 10.1016/j.immuni.2006.04.008

Naito Y, Hino K, Bono H, Ui-Tei K. CRISPRdirect: software for designing CRISPR/Cas guide RNA with reduced off-target sites. *Bioinformatics* 2015; 31(7), 1120-1123. DOI: 10.1093/bioinformatics/btu743

Nakahara M, Nagasaka A, Koike M, Uchida K, Kawane K, Uchiyama Y, Nagata S.

Degradation of nuclear DNA by DNase II-like acid DNase in cortical fiber cells of mouse eye lens. *FEBS J* 2007; 274(12), 3055-3064. DOI: 10.1111/j.1742-4658.2007.05836.x

Namjou B, Kothari PH, Kelly JA, Glenn SB, Ojwang JO, Adler A, Alarcón-Riquelme ME, Gallant CJ, Boackle SA, Criswell LA, Kimberly RP, Brown E, Edberg J, Stevens AM, Jacob CO, Tsao BP, Gilkeson GS, Kamen DL, Merrill JT, Petri M, Goldman RR, Vila LM, Anaya JM, Niewold TB, Martin J, Pons-Estel BA, Sabio JM, Callejas JL, Vyse TJ, Bae SC, Perrino FW, Freedman BI, Scofield RH, Moser KL, Gaffney PM, James JA, Langefeld CD, Kaufman KM, Harley JB, Atkinson JP. Evaluation of the TREX1 gene in a large multi-ancestral lupus cohort. *Genes Immun* 2011; 12(4), 270-279. DOI: 10.1038/gene.2010.73

Napirei M, Karsunky H, Zevnik B, Stephan H, Mannherz HG, Möröy T. Features of systemic lupus erythematosus in Dnase1-deficient mice. *Nat Genet* 2000; 25(2), 177-181. DOI: 10.1038/76032

Napirei M, Wulf S, Mannherz HG. Chromatin breakdown during necrosis by serum Dnase1 and the plasminogen system. *Arthritis Rheum* 2004a; 50(6), 1873-1883. DOI: 10.1002/art.20267

Napirei M, Ricken A, Eulitz D, Knoop H, Mannherz HG. Expression pattern of the deoxyribonuclease 1 gene: lessons from the Dnase1 knockout mouse. *Biochem J* 2004b; 380(Pt3), 929-937. DOI: 10.1042/BJ20040046

Napirei M, Wulf S, Eulitz D, Mannherz HG, Kloeckl T. Comparative characterization of rat deoxyribonuclease 1 (Dnase1) and murine deoxyribonuclease 1-like 3 (Dnase1l3). *Biochem J* 2005; 389(Pt2), 355-364. DOI: 10.1042/BJ20042124

Napirei M, Ludwig S, Mezrhab J, Klöckl T, Mannherz HG. Murine serum nucleases—contrasting effects of plasmin and heparin on the activities of DNase1 and DNase1-like 3 (DNase1l3). *FEBS J* 2009; 276(4), 1059-1073. DOI: 10.1111/j.1742-4658.2008.06849.x

Nascimento M, Gombault A, Lacerda-Queiroz N, Panek C, Savigny F, Sbeity M, Bourinet M, Le Bert M, Riteau N, Ryffel B, Quesniaux VFJ, Couillin I. Self-DNA release and STING-dependent sensing drives inflammation to cigarette smoke in mice. *Sci Rep* 2019; 9(1), 14848. DOI: 10.1038/s41598-019-51427-y

Naugler WE, Sakurai T, Kim S, Maeda S, Kim K, Elsharkawy AM, Karin M. Gender disparity in liver cancer due to sex differences in MyD88-dependent IL-6 production. *Science* 2007; 317(5834), 121-124. DOI: 10.1126/science.1140485

Newton K, Manning G. Necroptosis and Inflammation. *Annu Rev Biochem* 2016; 85, 743-763. DOI: 10.1146/annurev-biochem-060815-014830

Nickerson KM, Cullen JL, Kashgarian M, Shlomchik MJ. Exacerbated autoimmunity in the absence of TLR9 in MRL.Fas(lpr) mice depends on Ifnar1. *J Immunol* 2013; 190(8), 3889-3894. DOI: 10.4049/jimmunol.1203525

Niewold TB. Interferon alpha as a primary pathogenic factor in human lupus. *J Interferon Cytokine Res* 2011; 31(12), 887-892. DOI: 10.1089/jir.2011.0071

Nishimoto S, Kawane K, Watanabe-Fukunaga R, Fukuyama H, Ohsawa Y, Uchiyama Y, Hashida N, Ohguro N, Tano Y, Morimoto T, Fukuda Y, Nagata S. Nuclear cataract caused by a lack of DNA degradation in the mouse eye lens. *Nature* 2003; 424(6952),

1071-1074. DOI: 10.1038/nature01895

O'Neill KL, Huang K, Zhang J, Chen Y, Luo X. Inactivation of prosurvival Bcl-2 proteins activates Bax/Bak through the outer mitochondrial membrane. *Genes Dev* 2016; 30(8), 973-988. DOI: 10.1101/gad.276725.115

Ohto U, Shibata T, Tanji H, Ishida H, Krayukhina E, Uchiyama S, Miyake K, Shimizu T. Structural basis of CpG and inhibitory DNA recognition by Toll-like receptor 9. *Nature* 2015; 520(7549), 702-705. DOI: 10.1038/nature14138

Ohto U, Ishida H, Shibata T, Sato R, Miyake K, Shimizu T. Toll-like Receptor 9 Contains Two DNA Binding Sites that Function Cooperatively to Promote Receptor Dimerization and Activation. *Immunity* 2018; 48(4), 649-658.e4. DOI: 10.1016/j.immuni.2018.03.013

Oka T, Hikoso S, Yamaguchi O, Taneike M, Takeda T, Tamai T, Oyabu J, Murakawa T, Nakayama H, Nishida K, Akira S, Yamamoto A, Komuro I, Otsu K. Mitochondrial DNA that escapes from autophagy causes inflammation and heart failure. *Nature* 2012; 485(7397), 251-255. DOI: 10.1038/nature10992

Okabe Y, Kawane K, Akira S, Taniguchi T, Nagata S. Toll-like receptor-independent gene induction program activated by mammalian DNA escaped from apoptotic DNA degradation. *J Exp Med* 2005; 202(10), 1333–1339. DOI: 10.1084/jem.20051654

Okada Y, Terao C, Ikari K, Kochi Y, Ohmura K, Suzuki A, Kawaguchi T, Stahl EA, Kurreeman FA, Nishida N, Ohmiya H, Myouzen K, Takahashi M, Sawada T, Nishioka Y, Yukioka M, Matsubara T, Wakitani S, Teshima R, Tohma S, Takasugi K, Shimada K, Murasawa A, Honjo S, Matsuo K, Tanaka H, Tajima K, Suzuki T, Iwamoto T, Kawamura Y, Tanii H, Okazaki Y, Sasaki T, Gregersen PK, Padyukov L, Worthington J, Siminovitch KA, Lathrop M, Taniguchi A, Takahashi A, Tokunaga K, Kubo M, Nakamura Y, Kamatani N, Mimori T, Plenge RM, Yamanaka H, Momohara S, Yamada R, Matsuda F, Yamamoto K. Meta-analysis identifies nine new loci associated with rheumatoid arthritis in the Japanese population. *Nat Genet* 2012; 44(5), 511-516. DOI: 10.1038/ng.2231

Oldenburg M, Krüger A, Ferstl R, Kaufmann A, Nees G, Sigmund A, Bathke B, Lauterbach H, Suter M, Dreher S, Koedel U, Akira S, Kawai T, Buer J, Wagner H, Bauer S, Hochrein H, Kirschning CJ. TLR13 recognizes bacterial 23S rRNA devoid of erythromycin resistance-forming modification. *Science* 2012; 337(6098), 1111-1115. DOI: 10.1126/science.1220363

Orebaugh CD, Fye JM, Harvey S, Hollis T, Wilkinson JC, Perrino FW. The TREX1 C-terminal region controls cellular localization through ubiquitination. *J Biol Chem* 2013; 288(40), 28881–28892. DOI: 10.1074/jbc.M113.503391

Otani Y, Yamaguchi Y, Sato Y, Furuichi T, Ikenaka K, Kitani H, Hiroko B. PLD4 is involved in phagocytosis of microglia: expression and localization changes of PLD4 are correlated with activation State of Microglia. *PloS ONE* 2011; 6(11), e27544. DOI: 10.1371/journal.pone.0027544

Padron-Barthe L, Leprêtre C, Martin E, Counis MF, Torriglia A. Conformational modification of serpins transforms leukocyte elastase inhibitor into an endonuclease involved in apoptosis. *Mol Cell Biol* 2007; 27(11), 4028-4036. DOI: 10.1128/MCB.01959-06

Pal K, Zhao Y, Wang Y, Wang X. Ubiquitous membrane-bound DNase activity in

podosomes and invadopodia. *J Cell Biol* 2021; 220(7), e202008079. DOI: 10.1083/jcb.202008079

Park MS. Diffuse alveolar hemorrhage. *Tuberc Respir Dis (Seoul)* 2013; 74(4), 151–162. DOI: 10.4046/trd.2013.74.4.151

Pisitkun P, Deane JA, Difilippantonio MJ, Tarasenko T, Satterthwaite AB, Bolland S. Autoreactive B Cell Responses to RNA-Related Antigens Due to TLR7 Gene Duplication. *Science* 2006; 312(5780), 1669-1672. DOI: 10.1126/science.1124978

Rakoff-Nahoum S, Paglino J, Eslami-Varzaneh F, Edberg S, Medzhitov R. Recognition of commensal microflora by toll-like receptors is required for intestinal homeostasis. *Cell* 2004; 118(2), 229-241. DOI: 10.1016/j.cell.2004.07.002

Rakoff-Nahoum S, Medzhitov R. Regulation of spontaneous intestinal tumorigenesis through the adaptor protein MyD88. *Science* 2007; 317(5834), 124-127. DOI: 10.1126/science.1140488

Rashedi I. The role of DNase X in skeletal muscle addressed by targeted disruption of the gene in a mouse model. University of Manitoba, Winnipeg 2008, 122 p.

Rice G, Newman WG, Dean J, Patrick T, Parmar R, Flintoff K, Robins P, Harvey S, Hollis T, O'Hara A, Herrick AL, Bowden AP, Perrino FW, Lindahl T, Barnes DE, Crow YJ. Heterozygous mutations in TREX1 cause familial chilblain lupus and dominant Aicardi-Goutieres syndrome. *Am J Hum Genet* 2007; 80(4), 811-815. DOI: 10.1086/513443

Robinson A, Han CZ, Glass CK, Pollard JW. Monocyte Regulation in Homeostasis and Malignancy. *Trends Immunol* 2021; 42(2), 104-119. DOI: 10.1016/j.it.2020.12.001

Rock KL, Kono H. The inflammatory response to cell death. *Annu Rev Pathol* 2008; 3, 99-126. DOI: 10.1146/annurev.pathmechdis.3.121806.151456

Rodero MP, Tesser A, Bartok E, Rice GI, Della Mina E, Depp M, Beitz B, Bondet V, Cagnard N, Duffy D, Dussiot M, Frémond ML, Gattorno M, Guillem F, Kitabayashi N, Porcheray F, Rieux-Laucat F, Seabra L, Uggenti C, Volpi S, Zeef LAH, Alyanakian MA, Beltrand J, Bianco AM, Boddaert N, Brouzes C, Candon S, Caorsi R, Charbit M, Fabre M, Faletra F, Girard M, Harroche A, Hartmann E, Lasne D, Marcuzzi A, Neven B, Nitschke P, Pascreau T, Pastore S, Picard C, Picco P, Piscianz E, Polak M, Quartier P, Rabant M, Stocco G, Taddio A, Uettwiller F, Valencic E, Vozzi D, Hartmann G, Barchet W, Hermine O, Bader-Meunier B, Tommasini A, Crow YJ. Type I interferon-mediated autoinflammation due to DNase II deficiency. *Nat Commun* 2017; 8(1), 2176. DOI: 10.1038/s41467-017-01932-3

Rongvaux A, Jackson R, Harman CC, Li T, West AP, de Zoete MR, Wu Y, Yordy B, Lakhani SA, Kuan CY, Taniguchi T, Shadel GS, Chen ZJ, Iwasaki A, Flavell RA. Apoptotic caspases prevent the induction of type I interferons by mitochondrial DNA. *Cell* 2014; 159(7), 1563-1577. DOI: 10.1016/j.cell.2014.11.037

Rossol M, Pierer M, Arnold S, Keysser G, Burkhardt H, Baerwald C, Wagner U. Homozygosity for DNASE2 single nucleotide polymorphisms in the 5'-regulatory region is associated with rheumatoid arthritis. *Ann Rheum Dis* 2009; 68(9), 1498-1503. DOI: 10.1136/ard.2008.092239

Sabatel C, Radermecker C, Fievez L, Paulissen G, Chakarov S, Fernandes C, Olivier S,

Toussaint M, Pirottin D, Xiao X, Quatresooz P, Sirard JC, Cataldo D, Gillet L, Bouabe H, Desmet CJ, Ginhoux F, Marichal T, Bureau F. Exposure to Bacterial CpG DNA Protects from Airway Allergic Inflammation by Expanding Regulatory Lung Interstitial Macrophages. *Immunity* 2017; 46(3), 457-473. DOI: 10.1016/j.immuni.2017.02.016

Sakahira H, Enari M, Nagata S. Cleavage of CAD inhibitor in CAD activation and DNA degradation during apoptosis. *Nature* 1998; 391(6662), 96-99. DOI: 10.1038/34214

Sallai K, Nagy E, Derfalvy B, Müzes G, Gergely P. Antinucleosome antibodies and decreased deoxyribonuclease activity in sera of patients with systemic lupus erythematosus. *Clin Diagn Lab Immunol* 2005; 12(1), 56–59. DOI: 10.1128/CDLI.12.1.56-59.2005

Salvesen GS, Dixit VM. Caspase activation: the induced- proximity model. *Proc Natl Acad Sci USA* 1999; 96(20), 10964–10967. DOI: 10.1073/pnas.96.20.1096

Samejima K, Tone S, Earnshaw WC. CAD/DFF40 nuclease is dispensable for high molecular weight DNA cleavage and stage I chromatin condensation in apoptosis. *J Biol Chem* 2001; 276(48), 45427-45432. DOI: 10.1074/jbc.M108844200

Samejima K, Earnshaw WC. Trashing the genome: the role of nucleases during apoptosis. *Nat Rev Mol Cell Biol* 2005; 6(9), 677-688. DOI: 10.1038/nrm1715

Santa P, Garreau A, Serpas L, Ferriere A, Blanco P, Soni C, Sisirak V. The Role of Nucleases and Nucleic Acid Editing Enzymes in the Regulation of Self-Nucleic Acid Sensing. *Front Immunol* 2021; 12, 629922. DOI: 10.3389/fimmu.2021.629922

Santiago-Raber ML, Baccala R, Haraldsson KM, Choubey D, Stewart TA, Kono DH, Theofilopoulos AN. Type-I interferon receptor deficiency reduces lupus-like disease in NZB mice. *J Exp Med* 2003; 197(6), 777-788. DOI: 10.1084/jem.20021996

Sato R, Reuter T, Hiranuma R, Shibata T, Fukui R, Motoi Y, Murakami Y, Tsukamoto H, Yamazaki S, Liu K, Saitoh SI, Latz E, Miyake K. The impact of cell maturation and tissue microenvironments on the expression of endosomal Toll-like receptors in monocytes and macrophages. *Int Immunol* 2020; 32(12), 785-798. DOI: 10.1093/intimm/dxaa055

Satoh M, Reeves WH. Induction of lupus-associated autoantibodies in BALB/c mice by intraperitoneal injection of pristane. *J Exp Med* 1994; 180(6), 2341-2346. DOI: 10.1084/jem.180.6.2341

Satoh M, Kumar A, Kanwar YS, Reeves WH. Anti-nuclear antibody production and immune-complex glomerulonephritis in BALB/c mice treated with pristane. *Proc Natl Acad Sci USA* 1995; 92(24), 10934-10938. DOI: 10.1073/pnas.92.24.10934

Satoh M, Hamilton KJ, Ajmani AK, Dong X, Wang J, Kanwar YS, Reeves WH. Autoantibodies to ribosomal P antigens with immune complex glomerulonephritis in SJL mice treated with pristane. *J Immunol* 1996; 157(7), 3200-3206.

Satoh M, Weintraub JP, Yoshida H, Shaheen VM, Richards HB, Shaw M, Reeves WH. Fas and Fas ligand mutations inhibit autoantibody production in pristane-induced lupus. *J Immunol* 2000; 165(2), 1036-1043. DOI: 10.4049/jimmunol.165.2.1036

Schäfer P, Cymerman IA, Bujnicki JM, Meiss G. Human lysosomal DNase IIalpha contains two requisite PLD-signature (HxK) motifs: evidence for a pseudodimeric structure of the active enzyme species. *Protein Sci* 2007; 16(1), 82-91. DOI:

10.1110/ps.062535307

Schlee M, Hartmann G. Discriminating self from non-self in nucleic acid sensing. *Nat Rev Immunol* 2016; 16(9), 566-580. DOI: 10.1038/nri.2016.78

Schyns J, Bai Q, Ruscitti C, Radermecker C, de Schepper S, Chakarov S, Farnir F, Pirottin D, Ginhoux F, Boeckxstaens G, Bureau F, Marichal T. Non-classical tissue monocytes and two functionally distinct populations of interstitial macrophages populate the mouse lung. *Nat Commun* 2019, 10, 3964. DOI: 10.1038/s41467-019-11843-0

Segawa K, Kurata S, Yanagihashi Y, Brummelkamp TR, Matsuda F, Nagata S. Caspase-mediated cleavage of phospholipid flippase for apoptotic phosphatidylserine exposure. *Science* 2014; 344(6188), 1164-1168. DOI: 10.1126/science.1252809

Seredkina N, Rekvig OP. Acquired loss of renal nuclease activity is restricted to DNaseI and is an organ-selective feature in murine lupus nephritis. *Am J Pathol* 2011; 179(3), 1120-1128. DOI: 10.1016/j.ajpath.2011.05.011

Serpas L, Chan RWY, Jiang P, Ni M, Sun K, Rashidfarrokhi A, Soni C, Sisirak V, Lee WS, Cheng SH, Peng W, Allen Chan KC, Chiu RWK., Reizis B, Lo YMD. Dnase1l3 deletion causes aberrations in length and end-motif frequencies in plasma DNA. *PNAS* 2019; 116(2), 641–649. DOI: 10.1073/pnas.1815031116

Sharma S, Campbell AM, Chan J, Schattgen SA, Orlowski GM, Nayar R, Huyler AH, Nündel K, Mohan C, Berg LJ, Shlomchik MJ, Marshak-Rothstein A, Fitzgerald KA. Suppression of systemic autoimmunity by the innate immune adaptor STING. *Proc Natl Acad Sci USA* 2015; 112(7), E710-717. DOI: 10.1073/pnas.1420217112

Shibata T, Ohto U, Nomura S, Kibata K, Motoi Y, Zhang Y, Murakami Y, Fukui R, Ishimoto T, Sano S, Ito T, Shimizu T, Miyake K. Guanosine and its modified derivatives are endogenous ligands for TLR7. *Int Immunol* 2016; 28(5), 211-222. DOI: 10.1093/intimm/dxv062

Shibata T, Taoka M, Saitoh S-I, Yamauchi Y, Motoi Y, Komine M, Fujita E, Sato R, Sagara H, Ichinohe T, Kawazoe M, Kato C, Furusho K, Murakami Y, Fukui R, Ohtsuki M, Ohto U, Shimizu T, Yoshida N, Isobe T, Miyake K. Nucleosides drive histiocytosis in SLC29A3 disorders by activating TLR7. 2019 DOI: 10.1101/2019.12.16.877357

Shimada K, Crother TR, Karlin J, Dagvadorj J, Chiba N, Chen S, Ramanujan VK, Wolf AJ, Vergnes L, Ojcius DM, Rentsendorj A, Vargas M, Guerrero C, Wang Y, Fitzgerald KA, Underhill DM, Town T, Arditi M. Oxidized mitochondrial DNA activates the NLRP3 inflammasome during apoptosis. *Immunity* 2012; 36(3), 401-414. DOI: 10.1016/j.immuni.2012.01.009

Shin HD, Park BL, Kim LH, Lee HS, Kim TY, Bae SC. Common DNase I polymorphism associated with autoantibody production among systemic lupus erythematosus patients. *Hum Mol Genet* 2004; 13, 2343–2350. DOI: 10.1093/hmg/ddh275

Shiokawa D, Ohyama H, Yamada T, Tanuma S. Purification and properties of DNase gamma from apoptotic rat thymocytes. *Biochem J* 1997; 326 (Pt 3)(Pt 3), 675-681. DOI: 10.1042/bj3260675

Shiokawa D, Tanuma S. Molecular cloning and expression of a cDNA encoding an apoptotic endonuclease DNase gamma. *Biochem J* 1998; 332 (Pt 3)(Pt 3), 713-720.

DOI: 10.1042/bj3320713

Shiokawa D, Tanuma S. Characterization of human DNase I family endonucleases and activation of DNase gamma during apoptosis. *Biochemistry* 2001; 40(1), 143-152. DOI: 10.1021/bi001041a

Shiokawa D, Kobayashi T, Tanuma S. Involvement of DNase gamma in apoptosis associated with myogenic differentiation of C2C12 cells. *J Biol Chem* 2002; 277(34), 31031-31037. DOI: 10.1074/jbc.M204038200

Shiokawa D, Shika Y, Tanuma S. Identification of two functional nuclear localization signals in DNase gamma and their roles in its apoptotic DNase activity. *Biochem J* 2003; 376(Pt2), 377-381. DOI: 10.1042/BJ20030820

Shiokawa D, Matsushita T, Kobayashi T, Matsumoto Y, Tanuma S. Characterization of the human DNAS1L2 gene and the molecular mechanism for its transcriptional activation induced by inflammatory cytokines. *Genomics* 2004; 84(1), 95-105. DOI: 10.1016/j.ygeno.2004.02.003

Shiokawa D, Shika Y, Saito K, Yamazaki K, Tanuma S. Physical and biochemical properties of mammalian DNase X proteins: non-AUG translation initiation of porcine and bovine mRNAs for DNase X. *Biochem J* 2005; 392(Pt3), 511–517. DOI: 10.1042/BJ20051114

Shiokawa D, Matsushita T, Shika Y, Shimizu M, Maeda M, Tanuma S. DNase X is a glycosylphosphatidylinositol-anchored membrane enzyme that provides a barrier to endocytosis-mediated transfer of a foreign gene. *J Biol Chem* 2007; 282(23), 17132-17140. DOI: 10.1074/jbc.M610428200

Simmonds MJ, Heward JM, Kelly MA, Allahabadia A, Foxall H, Gordon C, Franklyn JA, Gough SC. A nonsense mutation in exon 2 of the DNase I gene is not present in UK subjects with systemic lupus erythematosus and Graves' disease: Comment on the article by Rood et al. *Arthritis Rheum* 2002; 46(11), 3109-3110. DOI: 10.1002/art.10414

Singh R, Letai A, Sarosiek K. Regulation of apoptosis in health and disease: the balancing act of BCL-2 family proteins. *Nat Rev Mol Cell Biol* 2019*;* 20, 175–193. DOI: 10.1038/s41580-018-0089-8

Sisirak V, Sally B, D'Agati V, Martinez-Ortiz W, Özçakar ZB, David J, Rashidfarrokhi A, Yeste A, Panea C, Chida AS, Bogunovic M, Ivanov II, Quintana FJ, Sanz I, Elkon KB, Tekin M, Yalçınkaya F, Cardozo TJ, Clancy RM, Buyon JP, Reizis B. Digestion of Chromatin in Apoptotic Cell Microparticles Prevents Autoimmunity. *Cell* 2016; 166(1), 88-101. DOI: 10.1016/j.cell.2016.05.034

Sleat DE, Zheng H, Qian M, Lobel P. Identification of sites of mannose 6-phosphorylation on lysosomal proteins. *Mol Cell Proteomics* 2006; 5(4), 686-701. DOI: 10.1074/mcp.M500343-MCP200

Snyder MW, Kircher M, Hill AJ, Daza RM, Shendure J. Cell-free DNA Comprises an In Vivo Nucleosome Footprint that Informs Its Tissues-Of-Origin. *Cell* 2016; 164(1-2), 57-68. DOI: 10.1016/j.cell.2015.11.050

Soni C, Perez OA, Voss WN, Pucella JN, Serpas L, Mehl J, Ching KL, Goike J, Georgiou G, Ippolito GC, Sisirak V, Reizis B. Plasmacytoid Dendritic Cells and Type I Interferon Promote Extrafollicular B Cell Responses to Extracellular Self-DNA. *Immunity*

2020; 52(6), 1022-1038.e7. DOI: 10.1016/j.immuni.2020.04.015

Stacey KJ, Young GR, Clark F, Sester DP, Roberts TL, Naik S, Sweet MJ, Hume DA. The molecular basis for the lack of immunostimulatory activity of vertebrate DNA. *J Immunol* 2003; 170(7), 3614-3620. DOI: 10.4049/jimmunol.170.7.3614

Stetson DB, Ko JS, Heidmann T, Medzhitov R. Trex1 prevents cell-intrinsic initiation of autoimmunity. *Cell* 2008; 134, 587–598. DOI: 10.1016/j.cell.2008.06.032

Subramanian S, Tus K, Li QZ, Wang A, Tian XH, Zhou J, Liang C, Bartov G, McDaniel LD, Zhou XJ, Schultz RA, Wakeland EK. A Tlr7 translocation accelerates systemic autoimmunity in murine lupus. *Proc Natl Acad Sci USA* 2006; 103(26), 9970-9975. DOI: 10.1073/pnas.0603912103

Suck D, Oefner C. Structure of DNase I at 2.0 A resolution suggests a mechanism for binding to and cutting DNA. *Nature* 1986; 321(6070), 620-625. DOI: 10.1038/321620a0. PMID: 3713845.

Suck D. DNA recognition by DNase I. *J Mol Recognit* 1994; 7(2), 65-70. DOI: 10.1002/jmr.300070203

Sun L, Wu J, Du F, Chen X, Chen ZJ. Cyclic GMP-AMP synthase is a cytosolic DNA sensor that activates the type I interferon pathway. *Science* 2013; 339(6121), 786-791. DOI: 10.1126/science.1232458

Tanji H, Ohto U, Shibata T, Taoka M, Yamauchi Y, Isobe T, Miyake K, Shimizu T. Toll-like receptor 8 senses degradation products of single-stranded RNA. *Nat Struct Mol Biol* 2015; 22(2), 109-115. DOI: 10.1038/nsmb.2943

Terao C, Ohmura K, Kawaguchi Y, Nishimoto T, Kawasaki A, Takehara K, Furukawa H, Kochi Y, Ota Y, Ikari K, Sato S, Tohma S, Yamada R, Yamamoto K, Kubo M, Yamanaka H, Kuwana M, Tsuchiya N, Matsuda F, Mimori T. PLD4 as a novel susceptibility gene for systemic sclerosis in a Japanese population. *Arthritis Rheum* 2013; 65(2), 472-480. DOI: 10.1002/art.37777

Tew MB, Johnson RW, Reveille JD, Tan FK. A molecular analysis of the low serum deoxyribonuclease activity in lupus patients. *Arthritis Rheum* 2001; 44(10), 2446-2447. DOI: 10.1002/1529-0131(200110)44:10<2446::aid-art409>3.0.co;2-u

Thibault DL, Graham KL, Lee LY, Balboni I, Hertzog PJ, Utz PJ. Type I interferon receptor controls B-cell expression of nucleic acid-sensing Toll-like receptors and autoantibody production in a murine model of lupus. *Arthritis Res Ther* 2009; 11(4), R112. DOI: 10.1186/ar2771

Thomas DA, Du C, Xu M, Wang X, Ley TJ. DFF45/ICAD can be directly processed by granzyme B during the induction of apoptosis. *Immunity* 2000; 12(6), 621-632. DOI: 10.1016/s1074-7613(00)80213-7

Tian J, Avalos AM, Mao SY, Chen B, Senthil K, Wu H, Parroche P, Drabic S, Golenbock D, Sirois C, Hua J, An LL, Audoly L, La Rosa G, Bierhaus A, Naworth P, Marshak-Rothstein A, Crow MK, Fitzgerald KA, Latz E, Kiener PA, Coyle AJ. Toll-like receptor 9-dependent activation by DNA-containing immune complexes is mediated by HMGB1 and RAGE. *Nat Immunol* 2007; 8(5), 487-496. DOI: 10.1038/ni1457

Tumurkhuu G, Chen S, Montano EN, Ercan Laguna D, De Los Santos G, Yu JM, Lane

M, Yamashita M, Markman JL, Blanco LP, Kaplan MJ, Shimada K, Crother TR, Ishimori M, Wallace DJ, Jefferies CA, Arditi M. Oxidative DNA Damage Accelerates Skin Inflammation in Pristane-Induced Lupus Model. *Front Immunol* 2020; 11, 554725. DOI: 10.3389/fimmu.2020.554725

Tumurkhuu G, Laguna DE, Moore RE, Contreras J, Santos GL, Akaveka L, Montano EN, Wang Y, Ishimori M, Venuturupalli S, Forbess LJ, Stripp BR, Wallace DJ, Jefferies CA. Neutrophils Contribute to ER Stress in Lung Epithelial Cells in the Pristane-Induced Diffuse Alveolar Hemorrhage Mouse Model. *Front Immunol* 2022; 13, 790043. DOI: 10.3389/fimmu.2022.790043

Ueki M, Fujihara J, Kimura-Kataoka K, Takeshita H, Iida R, Yasuda T. Five non-synonymous SNPs in the gene encoding human deoxyribonuclease I-like 2 implicated in terminal differentiation of keratinocytes reduce or abolish its activity. *Electrophoresis* 2013; 34(3), 456-462. DOI: 10.1002/elps.201200415

Ueki M, Kimura-Kataoka K, Fujihara J, Takeshita H, Iida R, Yasuda T. Evaluation of all nonsynonymous single-nucleotide polymorphisms in the gene encoding human deoxyribonuclease I-Like 1, possibly implicated in the blocking of endocytosis-mediated foreign gene transfer. *DNA Cell Biol* 2014; 33, 79–87. DOI: 10.1089/dna.2013.2248

Veglia F, Sanseviero E, Gabrilovich DI. Myeloid-derived suppressor cells in the era of increasing myeloid cell diversity. *Nat Rev Immunol* 2021; 21, 485–498. DOI: 10.1038/s41577-020-00490-y

Villanueva E, Yalavarthi S, Berthier CC, Hodgin JB, Khandpur R, Lin AM, Rubin CJ, Zhao W, Olsen SH, Klinker M, Shealy D, Denny MF, Plumas J, Chaperot L, Kretzler M, Bruce AT, Kaplan MJ. Netting neutrophils induce endothelial damage, infiltrate tissues, and expose immunostimulatory molecules in systemic lupus erythematosus. *J Immunol* 2011; 187(1), 538-552. DOI: 10.4049/jimmunol.1100450

Wakabayashi A, Yoshinaga M, Takeuchi O. TANK prevents IFN-dependent fatal diffuse alveolar hemorrhage by suppressing DNA-cGAS aggregation. *Life Sci Alliance* 2021; 5(2), e202101067. DOI: 10.26508/lsa.202101067

Wang B, Yin Q. AIM2 inflammasome activation and regulation: A structural perspective. *J Struct Biol* 2017; 200(3), 279–282. DOI: 10.1016/j.jsb.2017.08.001

Welner RS, Pelayo R, Nagai Y, Garrett KP, Wuest TR, Carr DJ, Borghesi LA, Farrar MA, Kincade PW. Lymphoid precursors are directed to produce dendritic cells as a result of TLR9 ligation during herpes infection. *Blood* 2008; 112(9), 3753-3761. DOI: 10.1182/blood-2008-04-151506

White MJ, McArthur K, Metcalf D, Lane RM, Cambier JC, Herold MJ, van Delft MF, Bedoui S, Lessene G, Ritchie ME, Huang DC, Kile BT. Apoptotic caspases suppress mtDNA-induced STING-mediated type I IFN production. *Cell* 2014; 159(7), 1549-1562. DOI: 10.1016/j.cell.2014.11.036

Widlak P, Li P, Wang X, Garrard WT. Cleavage preferences of the apoptotic endonuclease DFF40 (caspase-activated DNase or nuclease) on naked DNA and chromatin substrates. *J Biol Chem* 2000; 275(11), 8226-8232. DOI: 10.1074/jbc.275.11.8226

Widlak P, Garrard WT. Discovery, regulation, and action of the major apoptotic

nucleases DFF40/CAD and endonuclease G. *J Cell Biochem* 2005; 94(6), 1078-1087. DOI: 10.1002/jcb.20409

Wilber A, Lu M, Schneider MC. Deoxyribonuclease I-like III is an inducible macrophage barrier to liposomal transfection. *Mol Ther* 2002; 6(1), 35-42. DOI: 10.1006/mthe.2002.0625

Wilber A, O'Connor TP, Lu ML, Karimi A, Schneider MC. Dnase1l3 deficiency in lupus-prone MRL and NZB/W F1 mice. *Clin Exp Immunol* 2003; 134(1), 46-52. DOI: 10.1046/j.1365-2249.2003.02267.x

Wolf BB, Schuler M, Echeverri F, Green DR. Caspase-3 is the primary activator of apoptotic DNA fragmentation via DNA fragmentation factor-45/inhibitor of caspase-activated DNase inactivation. *J Biol Chem* 1999; 274(43), 30651-30656. DOI: 10.1074/jbc.274.43.30651

Woo EJ, Kim YG, Kim MS, Han WD, Shin S, Robinson H, Park SY, Oh BH. Structural mechanism for inactivation and activation of CAD/DFF40 in the apoptotic pathway. *Mol Cell* 2004; 14(4), 531-539. DOI: 10.1016/s1097-2765(04)00258-8

Wu J, Sun L, Chen X, Du F, Shi H, Chen C, Chen ZJ. Cyclic GMP-AMP is an endogenous second messenger in innate immune signaling by cytosolic DNA. *Science* 2013; 339(6121), 826-830. DOI: 10.1126/science.1229963

Yakovlev AG, Wang G, Stoica BA, Boulares HA, Spoonde AY, Yoshihara K, Smulson ME. A role of the Ca2+/Mg2+-dependent endonuclease in apoptosis and its inhibition by Poly(ADP-ribose) polymerase. *J Biol Chem* 2000; 275(28), 21302-21308. DOI: 10.1074/jbc.M001087200

Yang Z, Yan L, Cao H, Gu Y, Zhou P, Shi M, Li G, Jiao X, Li N, Li X, Sun K, Shao F. Erythropoietin Protects against Diffuse Alveolar Hemorrhage in Mice by Regulating Macrophage Polarization through the EPOR/JAK2/STAT3 Axis. *J Immunol* 2021; 206(8), 1752-1764. DOI: 10.4049/jimmunol.1901312

Yasutomo K, Horiuchi T, Kagami S, Tsukamoto H, Hashimura C, Urushihara M, Kuroda Y. Mutation of DNASE1 in people with systemic lupus erythematosus. *Nat Genet* 2001; 28(4), 313-314. DOI: 10.1038/91070

Yee CS, Su L, Toescu V, Hickman R, Situnayake D, Bowman S, Farewell V, Gordon C. Birmingham SLE cohort: outcomes of a large inception cohort followed for up to 21 years. *Rheumatology (Oxford)* 2015; 54(5), 836-843. DOI: 10.1093/rheumatology/keu412

Yoneyama M, Kikuchi M, Natsukawa T, Shinobu N, Imaizumi T, Miyagishi M, Taira K, Akira S, Fujita T. The RNA helicase RIG-I has an essential function in double-stranded RNA-induced innate antiviral responses. *Nat Immunol* 2004; 5(7), 730-737. DOI: 10.1038/ni1087

Yoshida H, Okabe Y, Kawane K, Fukuyama H, Nagata S. Lethal anemia caused by interferon-beta produced in mouse embryos carrying undigested DNA. *Nat Immunol* 2005; 6(1), 49-56. DOI: 10.1038/ni1146

Zamora MR, Warner ML, Tuder R, Schwarz MI. Diffuse alveolar hemorrhage and systemic lupus erythematosus. Clinical presentation, histology, survival, and outcome.

Medicine (Baltimore) 1997; 76(3), 192-202. DOI: 10.1097/00005792-199705000-00005

Zhang J, Liu X, Scherer DC, van Kaer L, Wang X, Xu M. Resistance to DNA fragmentation and chromatin condensation in mice lacking the DNA fragmentation factor 45. *Proc Natl Acad Sci USA* 1998; 95(21), 12480-12485. DOI: 10.1073/pnas.95.21.12480

Zhang J, Wang X, Bove KE, Xu M. DNA fragmentation factor 45-deficient cells are more resistant to apoptosis and exhibit different dying morphology than wild-type control cells. *J Biol Chem* 1999; 274(52), 37450-37454. DOI: 10.1074/jbc.274.52.37450

Zhang Q, Raoof M, Chen Y, Sumi Y, Sursal T, Junger W, Brohi K, Itagaki K, Hauser CJ. Circulating mitochondrial DAMPs cause inflammatory responses to injury. *Nature* 2010; 464(7285), 104-107. DOI: 10.1038/nature08780

Zhang X, Wu J, Du F, Xu H, Sun L, Chen Z, Brautigam CA, Zhang X, Chen ZJ. The cytosolic DNA sensor cGAS forms an oligomeric complex with DNA and undergoes switch-like conformational changes in the activation loop. *Cell Rep* 2014; 6(3), 421-430. DOI: 10.1016/j.celrep.2014.01.003

Zhang Z, Ohto U, Shibata T, Krayukhina E, Taoka M, Yamauchi Y, Tanji H, Isobe T, Uchiyama S, Miyake K, Shimizu T. Structural Analysis Reveals that Toll-like Receptor 7 Is a Dual Receptor for Guanosine and Single-Stranded RNA. *Immunity* 2016a; 45(4), 737-748. DOI: 10.1016/j.immuni.2016.09.011

Zhang DF, Fan Y, Wang D, Bi R, Zhang C, Fang Y, Yao YG. PLD3 in Alzheimer's Disease: a Modest Effect as Revealed by Updated Association and Expression Analyses. *Mol Neurobiol* 2016b; 53(6), 4034-4045. DOI: 10.1007/s12035-015-9353-5

Zhuang H, Han S, Xu Y, Li Y, Wang H, Yang LJ, Reeves WH. Toll-like receptor 7-stimulated tumor necrosis factor α causes bone marrow damage in systemic lupus erythematosus. *Arthritis Rheumatol*. 2014; 66(1), 140-151. DOI: 10.1002/art.38189

Zhuang H, Han S, Lee PY, Khaybullin R, Shumyak S, Lu L, Chatha A, Afaneh A, Zhang Y, Xie C, Nacionales D, Moldawer L, Qi X, Yang LJ, Reeves WH. Pathogenesis of Diffuse Alveolar Hemorrhage in Murine Lupus. *Arthritis Rheumatol* 2017; 69(6), 1280-1293. DOI: 10.1002/art.40077

Zhuang H, Han S, Lu L, Reeves WH. Myxomavirus serpin alters macrophage function and prevents diffuse alveolar hemorrhage in pristane-induced lupus. *Clin Immunol* 2021; 229, 108764. DOI: 10.1016/j.clim.2021.108764

Zykova SN, Tveita AA, Rekvig OP. Renal Dnase1 enzyme activity and protein expression is selectively shut down in murine and human membranoproliferative lupus nephritis. *PLoS ONE* 2010; 5(8), e12096. DOI: 10.1371/journal.pone.0012096

9 Acknowledgments

First and foremost, I would like to thank my “Doktorvater” Professor Eicke Latz for his mentorship and trust. He creates an environment in which it is possible to pursue bold ideas, evolve and grow. Thanks to his continuous support I had an unforgettable time both in Bonn and Tokyo.

I would like to thank Professor Kensuke Miyake for taking me in, including me in his incredibly welcoming, affectionate team and innumerable opportunities to gain new insights into science as well as cultural perspectives. He is an exceptional sensei.

I am also particularly grateful to Professor Günter Mayer for agreeing to be the second referee of my thesis, as well as Professor Martin Schlee and Professor Matthias Geyer for supporting my studies as third and fourth referee.

A great thank you goes out to all members of Professor Miyake’s workgroup and all present and past Latzis for their advice and all the great after-work events. In particular, I would like to thank Dr. Ryota Sato, who trained me at the beginning of this project and taught me the necessary skills, Dr. Kaiwen Liu, Dr. Takuma Shibata, Dr. Yuji Motoi and Dr. Ryutaro Fukui for their support and exciting discussions. Furthermore, I would like to thank Haruyo Moriya for taking care and helping me with so many administrative challenges.

Special thanks go to Jule, Carsten, Ryan, Katsuki, Haibing, Anette and Pia for their friendship, encouragement and soulfulness, and my office folks Marta, Fraser, Tobi and Lena who openly welcomed me back to Bonn and made the transition so easy and fun.

Finally, I would like to thank my most loved ones: Ines, Hans-Michael and Matthias for supporting me unconditionally, and especially my life partner Lena for her care, affection, recognition, respect, commitment, and trust. This journey would not have been possible without you.

Publications

K. Liu, R. Sato, T. Shibata, R. Hiranuma, T. Reuter, R. Fukui, Y. Zhang, T. Ichinohe, M. Ozawa, N. Yoshida, E. Latz, K. Miyake, Skewed endosomal RNA responses from TLR7 to TLR3 in RNase T2-deficient macrophages, *Int. Immunol.* **33** (9), 479-490 (2021), DOI: 10.1093/intimm/dxab033

R. Sato, T. Reuter, R. Hiranuma, T. Shibata, R. Fukui, Y. Motoi, Y. Murakami, H. Tsukamoto, S. Yamazaki, K. Liu, S.-I. Saitoh, E. Latz, K. Miyake, The impact of cell maturation and tissue microenvironments on the expression of endosomal Toll-like receptors in monocytes and macrophages, *Int. Immunol.* **32** (12), 785-798 (2020), DOI: 10.1093/intimm/dxaa055

M. Crüsemann, R. Reher, I. Schamari, A. O. Brachmann, T. Ohbayashi, M. Kuschak, D. Malfacini, A. Seidinger, M. Pinto-Carbó, R. Richarz, T. Reuter, S. Kehraus, A. Hallab, M. Attwood, H. B. Schiöth, P. Mergaert, Y. Kikuchi, T. F. Schäberle, E. Kostenis, D. Wenzel, C. E. Müller, J. Piel, A. Carlier, L. Eberl, G. M. König, Heterologous Expression, Biosynthetic Studies, and Ecological Function of the Selective Gq-Signaling Inhibitor FR900359. *Angew. Chem. Int. Ed. Engl.* **57** (3), 836-840 (2018), DOI: 10.1002/anie.201707996